Chapter 4

IFSAR Table of Contents

IFSAR Formatting Legend

Color	Description
	Original Westinghouse AP1000 DCD Revision 19 content (part of plant-specific DCD)
	Departures from AP1000 DCD Revision 19 content (part of plant-specific DCD)
	Standard FSAR content
	Site-specific FSAR content
	Linked cross-references (chapters, appendices, sections, subsections, tables, figures, and references)

TABLE OF CONTENTS

TABLE OF CONTENTS (CONTINUED)

TABLE OF CONTENTS (CONTINUED)

LIST OF TABLES

LIST OF FIGURES

LIST OF FIGURES (CONTINUED)

Chapter 4 Reactor

4.1 Summary Description

This chapter describes the mechanical components of the reactor and reactor core, including the fuel rods and fuel assemblies, the nuclear design, and the thermal-hydraulic design.

The reactor contains a matrix of fuel rods assembled into mechanically identical fuel assemblies along with control and structural elements. The assemblies, containing various fuel enrichments, are configured into the core arrangement located and supported by the reactor internals. The reactor internals also direct the flow of the coolant past the fuel rods. The coolant and moderator are light water at a normal operating pressure of 2250 psia. The fuel, internals, and coolant are contained within a heavy walled reactor pressure vessel. An AP1000 fuel assembly consists of 264 fuel rods in a 17x17 square array. The center position in the fuel assembly has a guide thimble that is reserved for in-core instrumentation. The remaining 24 positions in the fuel assembly have guide thimbles. The guide thimbles are joined to the top and bottom nozzles of the fuel assembly and provide the supporting structure for the fuel grids.

The fuel grids consist of an egg-crate arrangement of interlocked straps that maintain lateral spacing between the rods. The grid straps have spring fingers and dimples that grip and support the fuel rods. The intermediate mixing vane grids also have coolant mixing vanes. In addition, there are four intermediate flow mixing (IFM) grids. The IFM grid straps contain support dimples and coolant mixing vanes only. The top and bottom grids and protective grid do not contain mixing vanes.

The AP1000 fuel assemblies are similar to the 17x17 Robust and 17x17 XL Robust fuel assemblies. The 17x17 Robust fuel assemblies have an active fuel length of 12 feet and three intermediate flow mixing grids in the top mixing vane grid spans. The 17x17 XL Robust fuel assemblies have an active fuel length of 14 feet with no intermediate flow mixing grids. The AP1000 fuel assemblies are the same as the 17x17 XL Robust fuel assemblies except that they have four intermediate flow mixing grids in the top mixing vane grid spans.

There is substantial operating experience with the 17x17 Robust and 17x17 XL Robust fuel assemblies. The 17x17 Robust fuel assemblies are described in References 1, 2 and 3. The 17x17 XL Robust fuel assemblies are described in References 4 and 5.

The XL Robust fuel assembly evolved from the previous VANTAGE+, VANTAGE 5 and VANTAGE 5 HYBRID designs. The XL Robust fuel assembly is based on the substantial design and operating experience with those designs. The design is described and evaluated in References 2, 3, 6 through 10.

A number of proven design features have been incorporated in the AP1000 fuel assembly design. The AP1000 fuel assembly design includes: low pressure drop intermediate grids, four intermediate flow mixing (IFM) grids, a reconstitutable Westinghouse integral nozzle (WIN), and extended burnup capability. The bottom nozzle is a debris filter bottom nozzle (DFBN) that minimizes the potential for fuel damage due to debris in the reactor coolant. The AP1000 fuel assembly design also includes a protective grid for enhanced debris resistance.

The fuel rods consist of enriched uranium, in the form of cylindrical pellets of uranium dioxide, contained in ZIRLO™ (Reference 8) tubing. The tubing is plugged and seal welded at the ends to encapsulate the fuel. An axial blanket comprised of fuel pellets with reduced enrichment may be placed at each end of the enriched fuel pellet stack to reduce the neutron leakage and to improve fuel utilization.

Other types of fuel rods may be used to varying degrees within some fuel assemblies. One type uses an integral fuel burnable absorber (IFBA) containing a thin boride coating on the surface of the fuel pellets. Another type uses fuel pellets containing gadolinium oxide mixed with uranium oxide. The boride-coated fuel pellets and gadolinium oxide/uranium oxide fuel pellets provide a burnable absorber integral to the fuel.

Fuel rods are pressurized internally with helium during fabrication to reduce clad creepdown during operation and thereby prevent clad flattening. The fuel rods in the AP1000 fuel assemblies contain additional gas space below the fuel pellets, compared to the 17x17 Robust, 17x17 XL Robust and other previous fuel assembly designs to allow for increased fission gas production due to high fuel burnups.

Depending on the position of the assembly in the core, the guide thimbles are used for rod cluster control assemblies (RCCAs), gray rod cluster assemblies (GRCAs), neutron source assemblies, non-integral discrete burnable absorber (BA) assemblies, or thimble plugs.

For the initial core design, discrete burnable absorbers (BAs) and integral fuel burnable absorbers are used. Discrete burnable absorber designs, integral fuel burnable absorber designs (including both IFBAs and gadolinium oxide/uranium oxide BAs) or combinations may be used in subsequent reloads.

The bottom nozzle is a box-like structure that serves as the lower structural element of the fuel assembly and directs the coolant flow distribution to the assembly. The size of flow passages through the bottom nozzle limits the size of debris that can enter the fuel assembly. The top nozzle assembly serves as the upper structural element of the fuel assembly and provides a partial protective housing for the rod cluster control assembly or other components.

The rod cluster control assemblies consist of 24 absorber rods fastened at the top end to a common hub, or spider assembly. Each absorber rod consists of an alloy of silver-indium-cadmium, which is clad in stainless steel. The rod cluster control assemblies are used to control relatively rapid changes in reactivity and to control the axial power distribution.

The gray rod cluster assemblies consist of 24 rodlets fastened at the top end to a common hub or spider. Geometrically, the gray rod cluster assembly is the same as a rod cluster control assembly except that 12 of the 24 rodlets are fabricated of stainless steel, while the remaining 12 are silver-indium-cadmium (of a reduced diameter as compared to the RCCA absorber) with stainless steel clad.

The gray rod cluster assemblies are used in load follow maneuvering. The assemblies provide a mechanical shim reactivity mechanism to minimize the need for changes to the concentration of soluble boron.

The reactor core is cooled and moderated by light water at a pressure of 2250 psia. Soluble boron in the moderator/coolant serves as a neutron absorber. The concentration of boron is varied to control reactivity changes that occur relatively slowly, including the effects of fuel burnup. Burnable absorbers are also employed in the initial cycle to limit the amount of soluble boron required and, thereby maintain the desired negative reactivity coefficients.

The nuclear design analyses establish the core locations for control rods and burnable absorbers. The analyses define design parameters, such as fuel enrichments and boron concentration in the coolant.

The nuclear design establishes that the reactor core and the reactor control system satisfy design criteria, even if the rod cluster control assembly of the highest reactivity worth is in the fully withdrawn position.

The core has inherent stability against diametral and azimuthal power oscillations. Axial power oscillations, which may be induced by load changes, and resultant transient xenon may be suppressed by the use of the rod cluster control assemblies.

The control rod drive mechanisms used to withdraw and insert the rod cluster control assemblies and the gray rod cluster assemblies are described in Subsection 3.9.4.

The thermal-hydraulic design analyses establish that adequate heat transfer is provided between the fuel clad and the reactor coolant. The thermal design takes into account local variations in dimensions, power generation, flow distribution, and mixing. The mixing vanes incorporated in the fuel assembly spacer grid design and the fuel assembly intermediate flow mixers induce additional flow mixing between the various flow channels within a fuel assembly, as well as between adjacent assemblies.

The reactor internals direct the flow of coolant to and from the fuel assemblies and are described in Subsection 3.9.5.

The performance of the core is monitored by fixed neutron detectors outside the core, fixed neutron detectors within the core, and thermocouples at the outlet of selected fuel assemblies. The ex-core nuclear instrumentation provides input to automatic control functions.

Table 4.1-1 presents a summary of the principal nuclear, thermal-hydraulic, and mechanical design parameters of the AP1000 fuel. A comparison is provided to the fuel design used in AP1000, AP600 and in a licensed Westinghouse-designed plant using XL Robust fuel. For the comparison with a plant containing XL Robust fuel, a 193 fuel assembly plant is used, since no domestic, Westinghouse-designed 157 fuel assembly plants use 17x17 XL Robust fuel.

Table 4.1-2 tabulates the analytical techniques employed in the core design. The design basis must be met using these analytical techniques. Enhancements may be made to these techniques provided that the changes are bounded by NRC-approved methods, models, or criteria. In addition, application of the process described in WCAP-12488-A, (Reference 9) allows the Combined License holder to make fuel mechanical changes. Table 4.1-3 tabulates the mechanical loading conditions considered for the core internals and components. Specific or limiting loads considered for design purposes of the various components are listed as follows: fuel assemblies in Subsection 4.2.1.5; control rods (RCCAs and GRCAs), burnable absorber rods, and neutron source rods, in Subsection 4.2.1.6. The dynamic analyses, input forcing functions, and response loadings for the control rod drive system and reactor vessel internals are presented in Subsections 3.9.4 and 3.9.5.

4.1.1 Principal Design Requirements

The fuel and rod control rod mechanism are designed so the performance and safety criteria described in Chapter 4 and Chapter 15 are met. [*The mechanical design and physical arrangement of the reactor components, together with the corrective actions of the reactor control, protection, and emergency cooling systems (when applicable) are designed to achieve these criteria, referred to as Principal Design Requirements:*

- *Fuel damage, defined as penetration of the fuel cladding, is predicted not to occur during normal operation and anticipated operational transients.*

*NRC Staff approval is required prior to implementing a change in this information.

- *Materials used in the fuel assembly and in-core control components are selected to be compatible in a pressurized water reactor environment.*
- *For normal operation and anticipated transient conditions, the minimum DNBR calculated using the WRB-2M correlation is greater than or equal to 1.14.*
- *Fuel melting will not occur at the overpower limit for Condition I or II events.*
- *The maximum fuel rod cladding temperature following a loss-of-coolant accident is calculated to be less than 2200°F.*
- *For normal operation and anticipated transient conditions, the calculated core average linear power, including densification effects, is less than or equal to 5.718 kw/ft for the initial fuel cycle.*
- *For normal operation and anticipated transient conditions, the calculated total heat flux hot channel factor, F_Q, is less than or equal to 2.60 for the initial fuel cycle.*
- *Calculated rod worths provide sufficient reactivity to account for the power defect from full power to zero power and provide the required shutdown margin, with allowance for the worst stuck rod.*
- *Calculations of the accidental withdrawal of two control banks using the maximum reactivity change rate predict that the peak linear heat rate and DNBR limits are met.*
- *The maximum rod control cluster assembly and gray rod speed (or travel rate) is 45 inches per minute.*
- *The control rod drive mechanisms are hydrotested after manufacture at a minimum of 125 percent of system design pressure.*
- *For the initial fuel cycle, the fuel rod temperature coefficient is calculated to be negative for power operating conditions.*
- *For the initial fuel cycle, the moderator temperature coefficient is calculated to be negative for power operating conditions.*]*

4.1.2 Combined License Information

This section contained no requirement for additional information.

4.1.3 References

1. Letter from N. J. Liparulo (Westinghouse) to J. E. Lyons (NRC), “Transmittal of Response to NRC Request for Information on Wolf Creek Fuel Design Modifications,” NSD-NRC-97-5189, June 30, 1997.

2. Letter from N. J. Liparulo (Westinghouse) to R. C. Jones (NRC), “Transmittal of Presentation Material for NRC/Westinghouse Fuel Design Change Meeting on April 15, 1996,” NSD-NRC-96-4964, April 22, 1996.

3. Letter from Westinghouse to NRC, “Fuel Criteria Evaluation Process Notification for the 17x17 Robust Fuel Assembly with IFM Grid Design,” NSD-NRC-98-5796, October 13, 1998.

*NRC Staff approval is required prior to implementing a change in this information.

4. Letter from H. A. Sepp (Westinghouse) to T. E. Collins (NRC), “Notification of FCEP Application for WRB-1 and WRB-2 Applicability to the 17x17 Modified LPD Grid Design for Robust Fuel Assembly Application,” NSD-NRC-98-5618, March 25, 1998.

5. Letter from H. A. Sepp (Westinghouse) to T. E. Collins (NRC), “Fuel Criteria Evaluation Process Notification for the Revised Guide Thimble Dashpot Design for the 17x17 XL Robust Fuel Assembly Design,” NSD-NRC-98-5722, June 23, 1998.

6. Davidson, S. L., and Kramer, W. R., (Ed.), “Reference Core Report Vantage 5 Fuel Assembly,” WCAP-10444-P-A (Proprietary), September 1985 and WCAP-10445-A (Non-Proprietary), December 1983.

7. Davidson, S. L., (Ed.), “VANTAGE 5H Fuel Assembly,” Addendum 2-A, WCAP-10444-P-A (Proprietary) and WCAP-10445-NP-A (Non-Proprietary), February 1989.

8. Davidson, S. L., and Nuhfer, D. L., (Ed.), “VANTAGE+ Fuel Assembly Reference Core Report,” WCAP-12610-P-A (Proprietary) and WCAP-14342-A (Non-Proprietary), April 1995.

9. [*Davidson, S. L. (Ed.), “Fuel Criteria Evaluation Process,” WCAP-12488-A (Proprietary) and WCAP-14204-A (Non-Proprietary), October 1994.*]*

10. Letter, Peralta, J. D. (NRC) to Maurer, B. F. (Westinghouse), “Approval for Increase in Licensing Burnup Limit to 62,000 MWD/MTU (TAC No. MD1486),” May 25, 2006.

*NRC Staff approval is required prior to implementing a change in this information.

Table 4.1-1 (Sheet 1 of 3)
Reactor Design Comparison Table

Thermal and Hydraulic Design Parameters	AP1000	AP600	Typical XL Plant
Reactor core heat output (MWt)	3400	1933	3800
Reactor core heat output (10^6 Btu/hr)	11,601	6596	12,969
Heat generated in fuel (%)	97.4	97.4	97.4
System pressure, nominal (psia)	2250	2250	2250
System pressure, minimum steady-state (psia)	2190	2200	2204
Minimum departure from nuclear boiling (DNBR) for design transients Typical flow channel Thimble (cold wall) flow channel	 >1.25[d], >1.22[d] >1.25[d], >1.21[d]	 >1.23 >1.22	 >1.26 >1.24
Departure from nucleate boiling (DNB) correlation[b]	WRB-2M[b]	WRB-2	WRB-1[a]
Coolant Flow[c]			
Total vessel thermal design flow rate (10^6 lbm/hr) Effective flow rate for heat transfer (10^6 lbm/hr) Effective flow area for heat transfer (ft^2) Average velocity along fuel rods (ft/s) Average mass velocity (10^6 lbm/hr-ft^2)	113.5 106.8 41.8 15.8 2.55	72.9 66.3 38.5 10.6 1.72	145.0 132.7 51.1 16.6 2.60
Coolant Temperature[c][e]			
Nominal inlet (°F) Average rise in vessel (°F) Average rise in core (°F) Average in core (°F) Average in vessel (°F)	535.0 77.2 81.4 578.1 573.6	532.8 69.6 75.8 572.6 567.6	561.2 63.6 68.7 597.8 593.0
Heat Transfer			
Active heat transfer surface area (ft^2) Avg. heat flux (BTU/hr-ft^2) Maximum heat flux for normal operation (BTU/hr-ft^2)[f] Average linear power (kW/ft)[g] Peak linear power for normal operation (kW/ft)[f][g] Peak linear power (kW/ft)[f][h] (Resulting from overpower transients/operator errors, assuming a maximum overpower of 118%)	56,700 199,300 518,200 5.72 14.9 $\leq$22.45	44,884 143,000 372,226 4.11 10.7 22.5	69,700 181,200 489,200 5.20 14.0 $\leq$22.45

Table 4.1-1 (Sheet 2 of 3)
Reactor Design Comparison Table

Thermal and Hydraulic Design Parameters	AP1000	AP600	Typical XL Plant
Heat flux hot channel factor (F_Q)	2.60	2.60	2.70
Peak fuel center line temperature (°F) (For prevention of center-line melt)	4700	4700	4700
Fuel assembly design	17x17 XL Robust Fuel	17x17	17x17 XL Robust Fuel/ No IFM
Number of fuel assemblies	157	145	193
Uranium dioxide rods per assembly	264	264	264
Rod pitch (in.)	0.496	0.496	0.496
Overall dimensions (in.)	8.426 x 8.426	8.426 x 8.426	8.426 x 8.426
Fuel weight, as uranium dioxide (lb)	211,588	167,360	261,000
Clad weight (lb)	43,105	35,555	63,200
Number of grids per assembly Top and bottom - (Ni-Cr-Fe Alloy 718) Intermediate Intermediate flow mixing Protective Grid - (Ni-Cr-Fe Alloy 718)	 2[(i)] 8 ZIRLO™ 4 ZIRLO™ 1	 2[(i)] 7 Zircaloy-4 or 7 ZIRLO™ 4 Zircaloy-4 or 5 ZIRLO™ 1	 2 8 ZIRLO™ 0 1
Loading technique, first cycle	3 region nonuniform	3 region nonuniform	3 region nonuniform
Fuel Rods			
Number	41,448	38,280	50,952
Outside diameter (in.)	0.374	0.374	0.374
Diametral gap (non-IFBA) (in.)	0.0065	0.0065	0.0065
Clad thickness (in.)	0.0225	0.0225	0.0225
Clad material	ZIRLO™	Zircaloy-4 or ZIRLO™	Zircaloy-4/ ZIRLO™
Fuel Pellets			
Material	UO_2 sintered	UO_2 sintered	UO_2 sintered
Density (% of theoretical)	95.5	95	95
Diameter (in.)	0.3225	0.3225	0.3225
Length (in.)	0.387	0.387	0.387

Table 4.1-1 (Sheet 3 of 3)
Reactor Design Comparison Table

Rod Cluster Control Assemblies	AP1000	AP600	Typical XL Plant
Neutron Absorber			
RCCA GRCA	24 Ag-In-Cd rodlets 12 304 SS rodlets 12 Ag-In-Cd rodlets	24 Ag-In-Cd rodlets 20 304 SS rodlets 4 Ag-In-Cd rodlets	24 Hafnium or Ag-In-Cd
Cladding material	Type 304 SS, cold-worked	Type 304 SS, cold-worked	Type 304 SS, cold-worked
Clad thickness, (Ag-In-Cd)	0.0185	0.0185	0.0185
Number of clusters	53 RCCAs 16 GRCAs	45 RCCAs 16 GRCAs	57 RCCAs 0 GRCAs
Core Structure			
Core barrel, ID/OD (in.)	133.75/137.75	133.75/137.75	148.0/152.5
Thermal shield	Neutron Panel	None	Neutron Panel
Baffle thickness (in.)	Core Shroud	Radial reflector	0.875
Structure Characteristics			
Core diameter, equivalent (in.)	119.7	115.0	132.7
Core height, cold, active fuel (in.)	168.0	144.0	168.0
Fuel Enrichment First Cycle (Weight Percent)			
Region 1	2.35	1.90	Typical
Region 2	3.40	2.80	3.8 to 4.4
Region 3	4.45	3.70	(5.0 Max)

Notes:
a. WRB-2M will be used in future reloads.
b. See Subsection 4.4.2.2.1 for the use of the W-3, WRB-2 and WRB-2M correlations.
c. Flow rates and temperatures are based on 10 percent steam generator tube plugging for the AP600 and AP1000 designs.
d. 1.25 applies to core and axial offset limits; 1.22 and 1.21 apply to all other RTDP transients.
e. Coolant temperatures based on thermal design flow (for AP600 and AP1000).
f. Based on F_Q of 2.60 for AP600 and AP1000.
g. Based on densified active fuel length. The value for AP1000 is rounded to 5.72 kW/ft.
h. See Subsection 4.3.2.2.6.
i. The top grid will be fabricated of nickel-chromium-iron Alloy 718.

Table 4.1-2
Analytical Techniques in Core Design

Analysis	Technique	Computer Code	Subsection Referenced
Mechanical design of core internals loads, deflections, and stress analysis	Static and dynamic modeling	BLOWDOWN code, FORCE, finite element structural analysis code, and others	3.7.2.1 3.9.2 3.9.3
Fuel rod design Fuel performance characteristics (such as, temperature, internal pressure, and clad stress)	Semi-empirical thermal model of fuel rod with considerations such as fuel density changes, heat transfer, and fission gas release.	Westinghouse fuel rod design model	4.2.1.1 4.2.3.2 4.2.3.3 4.3.3.1 4.4.2.11
Nuclear design Cross-sections and group constants	Microscopic data; macroscopic constants for homogenized core regions	Modified ENDF/B library with PHOENIX-P	4.3.3.2
X-Y and X-Y-Z power distributions, fuel depletion, critical boron concentrations, X-Y and X-Y-Z xenon distributions, reactivity coefficients	2-group diffusion theory, 2-group nodal theory	ANC (2-D or 3-D)	4.3.3.3
Axial power distributions, control rod worths, and axial xenon distribution	1-D, 2-group diffusion theory	APOLLO	4.3.3.3
Fuel rod power	Integral transport theory	LASER	4.3.3.1
Effective resonance temperature	Monte Carlo weighing function	REPAD	4.3.3.1
Criticality of reactor and fuel assemblies	3-D, Monte Carlo theory	AMPX system of codes, KENO-Va	4.3.2.6
Vessel irradiation	Multigroup spatial dependent transport theory	DOT	4.3.2.8
Thermal-hydraulic design steady state	Subchannel analysis of local fluid conditions in rod bundles, including inertial and cross-flow resistance terms; solution progresses from core-wide to hot assembly to hot channel.	VIPRE-01	4.4.4.5.2
Transient departure from nucleate boiling	Subchannel analysis of local fluid conditions in rod bundles during transients by including accumulation terms in conservation equations; solution progresses from core-wide to hot assembly to hot channel.	VIPRE-01	4.4.4.5.4

Table 4.1-3
Design Loading Conditions for Reactor Core Components

- Fuel assembly weight and core component weights (burnable absorbers, sources, RCCA, GRCA)
- Fuel assembly spring forces and core component spring forces
- Internals weight
- Control rod trip (equivalent static load)
- Differential pressure
- Spring preloads
- Coolant flow forces (static)
- Temperature gradients
- Thermal expansion
- Interference between components
- Vibration (mechanically or hydraulically induced)
- Operational transients listed in Table 3.9.1-1
- Pump overspeed
- Seismic loads (safe shutdown earthquake)
- Blowdown forces (due to pipe rupture)

4.2 Fuel System Design

The plant conditions for design are divided into four categories.

- Condition I - normal operation and operational transients
- Condition II - events of moderate frequency
- Condition III - infrequent incidents
- Condition IV - limiting faults

Chapter 15 describes bases and plant operation and events involving each condition.

The reactor is designed so that its components meet the following performance and safety criteria:

- The mechanical design and physical arrangement of the reactor core components, together with corrective actions of the reactor control, protection, and emergency cooling systems (when applicable) provide that:
  - Fuel damage, that is, breach of fuel rod clad pressure boundary, is not expected during Condition I and Condition II events. A very small amount of fuel damage may occur. This is within the capability of the plant cleanup system and is consistent with the plant design bases.
  - The reactor can be brought to a safe state following a Condition III event with only a small fraction of fuel rods damaged. The fraction of fuel rods damaged must be limited to meet the dose guidelines identified in Chapter 15 although sufficient fuel damage might occur to preclude immediate resumption of operation.
  - The reactor can be brought to a safe state and the core kept subcritical with acceptable heat transfer geometry following transients arising from Condition IV events.
- The fuel assemblies are designed to withstand non-operational loads induced during shipping, handling, and core loading without exceeding the criteria of Subsection 4.2.1.5.1.
- The fuel assemblies are designed to accept control rod insertions to provide the required reactivity control for power operations and reactivity shutdown conditions.
- The fuel assemblies have provisions for the insertion of in-core instrumentation.
- The reactor vessel and internals, in conjunction with the fuel assembly structure, directs reactor coolant through the core. Because of the resulting flow distribution and bypass flow, the heat transfer performance requirements are met for the modes of operation.

The following subsection provides the fuel system design bases and design limits. It is consistent with the criteria of the Standard Review Plan, Section 4.2.

Consistent with the growth in technology, Westinghouse modifies fuel system designs. These modifications utilize NRC approved methods. [*A set of design fuel criteria to be satisfied by new fuel designs was issued to the NRC in WCAP-12488-A and its addendums (Reference 1)*]* and also presented below in Subsection 4.2.1.

*NRC Staff approval is required prior to implementing a change in this information.

4.2.1 Design Basis

The fuel rod and fuel assembly design bases are established to satisfy the general performance and safety criteria presented in Section 4.2 of the Standard Review Plan. [*The design bases and acceptance limits used by Westinghouse are also described in the Westinghouse Fuel Criteria Evaluation Process, WCAP-12488-A and its addendums (Reference 1).*]*

The fuel rods are designed to satisfy the fuel rod design criteria for rod burnup levels up to the design discharge burnup using the extended burnup design methods described in the Extended Burnup Evaluation report, WCAP-10125-P-A (Reference 2).

The AP1000 fuel rod design considers effects such as fuel density changes, fission gas release, clad creep, and other physical properties which vary with burnup. The integrity of the fuel rods is provided by designing to prevent excessive fuel temperatures as discussed in Subsection 4.2.1.2.1; excessive internal rod gas pressures due to fission gas releases as discussed in Subsections 4.2.1.3.1 and 4.2.1.3.2; and excessive cladding stresses, strains, and strain fatigue, as discussed in Subsections 4.2.1.1.2 and 4.2.1.1.3. The fuel rods are designed so that the conservative design bases of the following events envelope the lifetime operating conditions of the fuel. For each design basis, the performance of the limiting fuel rod, with appropriate consideration for uncertainties, does not exceed the limits specified by the design basis. The detailed fuel rod design also establishes such parameters as pellet size and density, clad/pellet diametral gap, gas plenum size, and helium pre-pressurization level.

Integrity of the fuel assembly structure is provided by setting limits on stresses and deformations due to various loads and by preventing the assembly structure from interfering with the functioning of other components. Three types of loads are considered:

- Non-operational loads, such as those due to shipping and handling
- Normal and abnormal loads, which are defined for Conditions I and II
- Abnormal loads, which are defined for Conditions III and IV

The design bases for the in-core control components are described in Subsection 4.2.1.6.

4.2.1.1 Cladding

4.2.1.1.1 Mechanical Properties

The ZIRLO™ cladding material combines neutron economy (low absorption cross-section); high corrosion resistance to coolant, fuel, and fission products; and high strength and ductility at operating temperatures. ZIRLO™ is an advanced zirconium based alloy that has the same or similar properties and advantages as Zircaloy-4 and was developed to support extended fuel burnup. WCAP-12610-P-A (Reference 5) provides a discussion of chemical and mechanical properties of the ZIRLO™ cladding material and a comparison to Zircaloy-4.

4.2.1.1.2 Stress-Strain Limits

Clad Stress

[*The volume average effective stress calculated with the Von Mises equation (considering interference due to uniform cylindrical pellet-clad contact, caused by pellet thermal expansion, pellet swelling and uniform clad creep, and pressure differences) is less than the 0.2 percent offset yield stress with due consideration to temperature and irradiation effects for Condition I and II events, WCAP-12488-A (Reference 1).*]* While the clad has some capability for accommodating plastic

*NRC Staff approval is required prior to implementing a change in this information.

strain, the yield stress has been accepted as a conservative design limit. The allowable stress limits due to Condition III and IV loadings, described in Subsection 4.2.1.5.3, are also applied to the fuel rod.

Clad Strain

[*The total plastic tensile creep strain due to uniform clad creep, and uniform cylindrical fuel pellet expansion associated with fuel swelling and thermal expansion is less than one percent from the unirradiated condition, WCAP-12488-A (Reference 1).*]* The acceptance limit for fuel rod clad strain during Condition II events is that the total tensile strain due to uniform cylindrical pellet thermal expansion is less than one percent from the pre-transient value. These limits are consistent with proven practice.

4.2.1.1.3 Fatigue and Vibration

Fatigue

[*The usage factor due to cycle fatigue is less than 1.0, WCAP-12488-A (Reference 1).*]* That is, for a given strain range, the number of strain fatigue cycles are less than those required for failure. The fatigue curve is based on a safety factor of two on the stress amplitude or a safety factor of 20 on the number of cycles, whichever is more conservative.

Vibration

Potential fretting wear due to vibration is prevented, giving confidence that the stress-strain limits are not exceeded during design life. Fretting of the clad surface can occur due to flow-induced vibration between the fuel rods and fuel assembly grid springs. Vibration and fretting forces may vary during the fuel life due to clad diameter creep down combined with grid spring relaxation.

4.2.1.1.4 Chemical Properties

Chemical properties of the ZIRLO™ cladding are discussed in WCAP-12610 (Reference 5).

4.2.1.2 Fuel Material

4.2.1.2.1 Thermal-Physical Properties

The center temperature of the hottest pellet is below the melting temperature of the uranium dioxide. The melting temperature of unirradiated uranium dioxide, 5080°F, decreases by 58°F per 10,000 megawatt days per metric ton of uranium, as discussed in WCAP-9179 (Reference 4). Fuel melting will not occur at the overpower limit for Condition I or II events. This provides sufficient margin for uncertainties as described in Subsection 4.4.2.9.

The nominal design density of the fuel is approximately 95.5 percent of the theoretical density. Additional information on fuel properties is provided in WCAP-9179 (Reference 4).

4.2.1.2.2 Fuel Densification and Fission Product Swelling

The design bases and models used for fuel densification and swelling are provided in WCAP-10851-P-A (Reference 7), and WCAP-15063-P-A, Revision 1 (Reference 21).

4.2.1.2.3 Chemical Properties

WCAP-9179 (Reference 4) and WCAP-12610 (Reference 5) provide the basis for justifying that no adverse chemical interactions occur between the fuel and its adjacent material.

*NRC Staff approval is required prior to implementing a change in this information.

4.2.1.3 Fuel Rod Performance

4.2.1.3.1 Fuel Rod Models

The basic fuel rod models and the ability to predict fuel rod operating characteristics are given in WCAP-15063-P-A, Revision 1 (Reference 21) and Subsection 4.2.3.

4.2.1.3.2 Mechanical Design Limits

Cladding collapse is precluded during the fuel rod design lifetime. Current generation Westinghouse fuel is sufficiently stable with respect to fuel densification. Significant axial gaps in the pellet stack necessary for clad flattening do not occur and therefore, clad flattening will not occur. Clad flattening methodologies are described in WCAP-13589-A, (Reference 8) and WCAP-8377 (Reference 22).

The rod internal gas pressure remains below the value which causes the fuel/clad diametral gap to increase due to outward cladding creep during steady-state operation. Rod pressure is also limited such that extensive departure from nucleate boiling propagation does not occur as discussed in WCAP-8963-P-A (Reference 9).

4.2.1.4 Spacer Grids

4.2.1.4.1 Mechanical Limits and Materials Properties

The grid component strength criteria are based on experimental tests. The limit is established at the 95-percent confidence level on the true mean crush strength at operating temperature. This limit is sufficient to provide that, under worst-case combined seismic and pipe rupture event, the core will maintain a geometry amenable to cooling. As an integral part of the fuel assembly structure, the grids satisfy the applicable fuel assembly design bases and limits defined in Subsection 4.2.1.5.

The grid material and chemical properties are given in WCAP-9179 (Reference 4) and WCAP-12610 (Reference 5).

4.2.1.4.2 Vibration and Fatigue

The grids provide sufficient fuel rod support to limit fuel rod vibration and maintain clad fretting wear within acceptable limits (defined in Subsection 4.2.1.1).

4.2.1.5 Fuel Assembly Structural Design

As discussed in Subsection 4.2.1, the structural integrity of the fuel assemblies is provided by setting design limits on stresses and deformations due to various non-operational, operational, and accident loads. These limits are applied to the design and evaluation of the top and bottom nozzles, guide thimbles, grids, and thimble joints. [*Design changes to the fuel assembly structure qualify for evaluation in WCAP-12488-A (Reference 1).*]*

The design bases for evaluating the structural integrity of the fuel assemblies are discussed in Subsections 4.2.1.5.1 through 4.2.1.5.3.

4.2.1.5.1 Non-Operational

The non-operational load is a loading of 4 g axial (longitudinal) and 6 g lateral (transverse) with dimensional stability.

*NRC Staff approval is required prior to implementing a change in this information.

4.2.1.5.2 Normal Operation and Operational Transients (Condition I) and Events of Moderate Frequency (Condition II)

For the normal operation (Condition I) and upset (Condition II) conditions, the fuel assembly component structural design criteria are established for the two primary material categories, austenitic steels and zirconium alloys. The stress categories and strength theory presented in the ASME Code, Section III, are used as a general guide. The maximum shear theory (Tresca criterion) for combined stresses is used to determine the stress intensities for the austenitic steel components. The stress intensity is defined as the largest numerical difference between the various principal stresses in a three-dimensional field. The design stress intensity value, S_m, for austenitic steels and zirconium alloys is given by the lowest of the following:

- One-third of the specified minimum tensile strength or two-thirds of the specified minimum yield strength at room temperature
- One-third of the tensile strength or 90 percent of the yield strength at temperature, but not to exceed two-thirds of the specified minimum yield strength at room temperature

The stress limits for the austenitic steel components are given below. Stress nomenclature follows the ASME Code, Section III.

Stress Intensity Limits

Categories	Limit
General primary membrane stress intensity	S_m
Local primary membrane stress intensity	1.5 S_m
Primary membrane plus bending stress intensity	1.5 S_m
Total primary plus secondary stress intensity	3.0 S_m

The zirconium alloy structural components, which consist of guide thimbles and fuel tubes, are in turn subdivided into two categories because of material difference and functional requirements. The fuel tube design criteria are covered separately in Subsection 4.2.1.1. The maximum shear theory is used to evaluate the guide thimble design. For conservative purposes, the zirconium alloy unirradiated properties are used to define the stress limits.

4.2.1.5.3 Infrequent Incidents (Condition III) and Limiting Faults (Condition IV)

Typical worse case abnormal loads during Conditions III and IV are represented by seismic and pipe rupture loadings. The design criteria for this category of loadings are as follows:

- Deflections or excessive deformation of components cannot interfere with capability of insertion of the control rods or emergency cooling of the fuel rods.
- The fuel assembly structural components stresses under faulted conditions are evaluated primarily using the methods outlined in Appendix F of the ASME Code, Section III. Since the current analytical methods use linear elastic analysis, the stress allowables are defined as the smaller value of 2.4 S_m or 0.70 S_u for primary membrane and 3.6 S_m or 1.05 S_u for primary membrane plus primary bending. For the austenitic steel fuel assembly components, the stress intensity is defined in accordance with the rules described in the previous section

for normal operating conditions. For the zirconium alloy components, the stress intensity limits are set at two-thirds of the material yield strength, S_y, at reactor operating temperature. This results in zirconium alloy stress limits being the smaller value of 1.6 S_y or 0.70 S_u for primary membrane and 2.4 S_y or 1.05 S_u for primary membrane plus bending. For conservative purposes, the zirconium alloy unirradiated properties are used to define the stress limits.

The material and chemical properties of the fuel assembly components are given in WCAP-9179 (Reference 4) and WCAP-12610 (Reference 5). Subsection 4.2.3.4 discusses the spacer grid crush testing.

Thermal-hydraulic design is discussed in Section 4.4.

4.2.1.6 In-core Control Components

The in-core control components are subdivided into permanent and temporary devices. The permanent components are the rod cluster control assemblies, gray rod cluster assemblies, and secondary neutron source assemblies. The temporary components are the primary neutron source assemblies (which are normally used only in the initial core), the burnable absorber assemblies, and the thimble plugs. For some reloads, the use of burnable absorbers may be necessary for power distribution control and/or to achieve an acceptable moderator temperature coefficient throughout core life (See Subsection 4.3.1.2.2). [*Design changes to the in-core control components qualify for evaluation using the criteria defined in WCAP-12488-A (Reference 1).*]*

Materials are selected for:

- Compatibility in a pressurized water reactor environment
- Adequate mechanical properties at room and operating temperatures
- Resistance to adverse property changes in a radioactive environment
- Compatibility with interfacing components

Material properties are given in WCAP-9179 (Reference 4).

The design bases for the in-core control components are given in Subsections 4.2.1.6.1 through 4.2.1.6.3.

4.2.1.6.1 Control Rods

For Conditions I and II, the stress categories and strength theory presented in the ASME Code, Section III, are used as a general guide in the design of the RCCA and GRCA structural parts in addition to absorber cladding.

Design conditions considered under the ASME Code, Section III, are as follows:

- External pressure equal to the reactor coolant system operating pressure with appropriate allowance for overpressure transients
- Wear allowance equivalent to 1000 reactor trips
- Bending of the rod due to a misalignment in the guide thimble

*NRC Staff approval is required prior to implementing a change in this information.

- Forces imposed on the rods during rod drop
- Loads imposed by the accelerations of the control rod drive mechanism
- Radiation exposure during maximum core life. The absorber material temperature does not exceed its melting temperature (1454°F for silver-indium-cadmium [Ag-In-Cd]), (see WCAP-9179, Reference 4).
- Temperature effects at operating conditions

4.2.1.6.2 Burnable Absorber Rods

For Conditions I and II, the stress categories and strength theory presented in the ASME Code, Section III, are used as a general guide in the design of the burnable absorber cladding. For abnormal loads during Conditions III and IV, code stresses are not considered limiting. Failures of the burnable absorber rods during these conditions must not interfere with reactor shutdown or emergency cooling of the fuel rods. The burnable absorber material is nonstructural. The structural elements of the burnable absorber rod are designed to maintain the absorber geometry even if the absorber material is fractured.

To reduce the dissolved boron requirement for control of excess reactivity, burnable absorber rods have been incorporated in the core design. In the first core, the burnable absorber rods (Pyrex) consist of borosilicate glass tubes contained within Type 304 stainless steel tubular cladding, which is plugged and seal welded at the ends to encapsulate the glass. The absorber material temperature does not exceed its design limit of 1220°F. Mechanical and thermal design and nuclear evaluation of the burnable absorber rods are described in WCAP-7113 (Reference 23).

An alternative discrete burnable absorber is the wet annular burnable absorber (WABA). The burnable absorber material is boron carbide contained in an alumina matrix. Thermal-physical and gas release properties of alumina-boron carbide are described in WCAP-9179 (Reference 4) and WCAP-10021-P-A (Reference 10). Discrete burnable absorber rods are designed so that the absorber temperature does not exceed 1200°F during normal operation or an overpower transient. The 1200°F maximum temperature helium gas release in a discrete burnable absorber rod will not exceed 30 percent of theoretical. See WCAP-10021-P-A (Reference 10).

4.2.1.6.3 Neutron Source Rods

The neutron source rods are designed to withstand the following:

- The external pressure equal to reactor coolant system operating pressure with appropriate allowance for overpressure transients
- An internal pressure equal to the pressure generated by released gases over the source rod life

4.2.1.7 Surveillance Program

Subsection 4.2.4.6 discusses the testing and fuel surveillance operation experience program that has been and is being conducted to verify the adequacy of the fuel performance and design bases. Fuel surveillance and testing results, as they become available, are used to improve fuel rod design and manufacturing processes and to confirm that the design bases and safety criteria are satisfied.

4.2.2 Description and Design Drawings

The fuel assembly, fuel rod, and in-core control component design data is given in Table 4.3-1.

Each fuel assembly consists of 264 fuel rods, 24 guide thimbles, and 1 instrumentation tube arranged within a supporting structure. The instrumentation thimble is located in the center position and provides a channel for insertion of an in-core neutron detector, if the fuel assembly is located in an instrumented core position. The guide thimbles provide channels for insertion of either a rod cluster control assembly, a gray rod cluster assembly, a neutron source assembly, a burnable absorber assembly, or a thimble plug, depending on the position of the particular fuel assembly in the core. Figure 4.2-1 shows a cross-section of the fuel assembly array, and Figure 4.2-2 shows a fuel assembly full-length view.

The fuel rods are loaded into the fuel assembly structure so that there is clearance between the fuel rod ends and the top and bottom nozzles. The fuel rods are supported within the fuel assembly structure by fourteen structural grids (top grid (1), bottom grid (1), intermediate grids (8) and intermediate flow mixer (IFM) grids (4)), plus one protective grid. The top grid is fabricated from nickel-chromium-iron Alloy 718. The bottom grid is fabricated from nickel-chromium-iron Alloy 718. The intermediate grids and the IFM grids are fabricated from ZIRLO™ (see WCAP-12610-P-A, Reference 5). Top, bottom, and intermediate grids provide axial and lateral support to the fuel rods. In addition, the four IFM grids located near the center of the fuel assembly and between the intermediate grids provide additional fuel rod restraint. The protective grid, in combination with the debris filter bottom nozzle (DFBN), the protective zirconium oxide coated fuel cladding, and the long, solid fuel rod bottom end plug, provide debris failure mitigation.

Fuel assemblies are installed vertically in the reactor vessel and stand upright on the lower core plate, which is fitted with alignment pins to locate and orient each assembly. After the fuel assemblies are set in place, the upper support structure is installed. Alignment pins, built into the upper core plate, engage and locate the upper ends of the fuel assemblies. The upper core plate then bears down against the hold-down springs on the top nozzle of each fuel assembly to hold the fuel assemblies in place.

Improper orientation of fuel assemblies within the core is prevented by the use of an indexing hole in one corner of the top nozzle top plate. The assembly is oriented with respect to the handling tool and the core by means of a pin inserted into this indexing hole. Visual confirmation of proper orientation is also provided by an engraved identification number on the opposite corner clamp.

4.2.2.1 Fuel Rods

The fuel rods consist of uranium dioxide ceramic pellets contained in cold-worked and stress relieved ZIRLO™ tubing, which is plugged and seal-welded at the ends to encapsulate the fuel. ZIRLO™ is an advanced zirconium based alloy selected for its mechanical properties and low neutron absorption cross-section (see WCAP-12610-P-A, Reference 5). Figure 4.2-3 shows a schematic of the fuel rod. The fuel pellets are right circular cylinders consisting of slightly enriched uranium dioxide powder which has been compacted by cold pressing and then sintered to the required density. The ends of each pellet are dished slightly, to allow greater axial expansion at the pellet centerline and to increase the void volume for fission gas release. The ends of each pellet also have a small chamfer at the outer cylindrical surface which improves manufacturability, and mitigates potential pellet damage due to fuel rod handling.

Void volume and clearances are provided within the rods to accommodate fission gases released from the fuel, differential thermal expansion between the clad and the fuel, and fuel density changes during irradiation. To facilitate the extended burnup capability necessitated by longer operating cycles, the fuel rod is designed with two plenums (upper and lower) to accommodate the additional

fission gas release. The upper plenum volume is maintained by a fuel pellet hold-down spring. The lower plenum volume is maintained by a standoff assembly.

Shifting of the fuel within the clad during handling or shipping, prior to core loading, is prevented by a stainless steel helical spring which bears on top of the fuel pellet stack. Assembly consists of plugging and welding the bottom of the cladding, installing the bottom plenum spacer assembly, fuel pellets and top plenum spring, and then plugging and welding the top of the rod. The solid bottom end plug has an internal grip feature and tapered end to facilitate fuel rod loading during fuel assembly fabrication and reconstitution. Additionally, the bottom end plug is designed to be sufficiently long to extend through the protective grid. The bottom section of the fuel rod has a protective zirconium oxide coated surface feature. Use of the protective grid with a longer end plug and the debris filter bottom nozzle, in addition to the coated cladding surface, constitutes a three-level debris protection package, which enhances the fuel reliability performance against trapped debris. This precludes any breach in the fuel rod pressure boundary due to clad fretting wear induced by debris trapped at the bottom section of the fuel assembly.

The fuel rods are internally pressurized with helium during the welding process to minimize compressive clad stresses and prevent clad flattening under reactor coolant operating pressures. The fuel rods are pre-pressurized and designed so that:

- The internal gas pressure mechanical design limit referred to in Subsection 4.2.1.3 is not exceeded
- The cladding stress-strain limits (Subsection 4.2.1.1) are not exceeded for Condition I and II events
- Clad flattening will not occur during the fuel core life

The AP1000 fuel rod design may also include axial blankets. The axial blankets consist of fuel pellets of a reduced enrichment at each end of the fuel rod pellet stack. Axial blankets reduce neutron leakage axially and improve fuel utilization. The axial blankets use chamfered pellets that are longer than the enriched pellets to help prevent accidental mixing during manufacturing. Furthermore, axial blankets have no impact on the source range detector response, since the reduction in power from the axial blanket is limited to the top and bottom 0.67 feet of the core, while the source range detectors are centered typically about three feet from the bottom of the core.

The AP1000 fuel rod design may also include annular fuel pellets in the top and bottom 8 inches of the fuel stack. These pellets can be either fully enriched or partially enriched. The annular fuel pellets provide additional void volume in the fuel rod to accommodate fission gas release.

The AP1000 fuel rods include integral fuel burnable absorbers. The integral fuel burnable absorbers may be boride-coated fuel pellets or fuel pellets containing gadolinium oxide mixed with uranium oxide. The boride-coated fuel pellets are identical to the enriched uranium dioxide pellets except for the addition of a thin boride coating less than 0.001 inch in thickness on the pellet cylindrical surface. Coated pellets occupy the central portion of the fuel column. The number and pattern of integral fuel burnable absorber rods within an assembly may vary depending on specific application. See WCAP-12610-P-A (Reference 5).

4.2.2.2 Fuel Assembly Structure

As shown in Figure 4.2-2, the fuel assembly structure consists of a bottom nozzle, top nozzle, fuel rods, guide thimbles, and grids.

4.2.2.2.1 Bottom Nozzle

The bottom nozzle serves as the bottom structural element of the fuel assembly and directs the coolant flow distribution to the assembly. The nozzle is fabricated from Type 304 stainless steel and consists of a perforated plate, and casting which incorporates a skirt and four angle legs with bearing pads. Figure 4.2-2 illustrates this concept. The legs and skirt form a plenum to direct the inlet coolant flow to the fuel assembly. The perforated plate also prevents accidental downward ejection of the fuel rods from the fuel assembly. The bottom nozzle is fastened to the fuel assembly guide thimbles by locked thimble screws, which penetrate through the nozzle and engage with a threaded plug in each guide thimble.

Coolant flows from the plenum in the bottom nozzle, upward through the penetrations in the plate, to the channels between the fuel rods. The penetrations in the plate are positioned between the rows of the fuel rods.

In addition to serving as the bottom structural element of the fuel assembly, the bottom nozzle also functions as a debris filter. The bottom nozzle perforated plate contains a multiplicity of flow holes which are sized to minimize passage of detrimental debris particles into the active fuel region of the core while maintaining sufficient hydraulic and structural margins. Furthermore, the skirt provides improved bottom nozzle structural stability and increased design margins to reduce damage due to abnormal handling.

Axial loads (from top nozzle hold-down springs) imposed on the fuel assembly and the weight of the fuel assembly are transmitted through the bottom nozzle to the lower core plate. Indexing and positioning of the fuel assembly is controlled by alignment holes in two diagonally opposite bearing pads that mate with locating pins in the lower core plate. Lateral loads on the fuel assembly are transmitted to the lower core plate through the locating pins.

The AP1000 bottom nozzle also has a reconstitution design feature which facilitates the easy removal of the nozzle from the fuel assembly. This design incorporates a thimble screw with a circular locking cup located around the screw head. The locking cup is crimped into a local spherical radius relief on the bottom nozzle. To remove the bottom nozzle, a counterclockwise torque is applied to the thimble screw until the locking cup (detents) is relaxed and the thimble screw is removed. This reconstitutable design permits the remote unlocking, the removal, and the relocking of the thimble screws, as the same or a new bottom nozzle is reattached to the fuel assembly.

4.2.2.2.2 Top Nozzle

The reconstitutable top nozzle functions as the upper structural component of the fuel assembly and, in addition, provides a partial protective housing for the rod cluster control assembly, discrete burnable absorber, or other core components. As shown in Figure 4.2-2, the top nozzle assembly includes four sets of hold-down springs, which are secured to the top nozzle top plate. The springs are made of nickel-chromium-iron Alloy 718. The other top nozzle components are made of Type 304 stainless steel.

The adapter plate is provided with round penetrations and slots (with semicircular ends) to permit the flow of coolant upward through the top nozzle. Other round holes are provided in the adapter plate to accept (guide thimble) inserts which are mechanically locked to the adapter plate using a lock tube. The unique design of the insert joint and lock tube are the key design features of the reconstitutable top nozzle.

The ligaments in the adapter plate cover the top of the fuel rods precluding any upward ejection of the fuel rods from the fuel assembly. The enclosure is a box-like structure which establishes the distance between the adapter plate and the top plate. The top plate has a large square hole in the

center to permit access for the rod cluster control assembly, burnable absorber assembly, or other components. Hold-down springs are mounted on the top plate and are retained by retaining pins located at diagonally opposite corners of the top plate.

The top plate also contains integral pads located on the two remaining top nozzle corners. The pads include alignment holes which, when fully engaged with the reactor internals upper core plate guide pins, provide proper alignment to the fuel assembly, reactor internals, and rod control cluster assembly.

As shown in Figure 4.2-4, to remove the top nozzle assembly a tool is first inserted through a lock tube and expanded radially to engage the bottom edge of the tube. An axial force is then exerted on the tool which overrides local lock tube deformations and withdraws the lock tubes from the inserts. After the lock tubes have been removed, the nozzle assembly is removed by raising it off the upper slotted ends of the nozzle inserts, which deflect inwardly under the axial lift load.

With the top nozzle assembly removed, direct access is provided for fuel rod examination or replacement. Reconstitution is completed by the remounting of the nozzle assembly and the insertion of lock tubes. Details of this design feature, the design bases and evaluation of the reconstitutable top nozzle are given in WCAP-10444-P-A (Reference 11).

4.2.2.2.3 Guide Thimbles and Instrument Tube

The guide thimbles are structural members that provide channels for the neutron absorber rods, burnable absorber rods, neutron source rods, or other assemblies. Each guide thimble is fabricated from Zircaloy-4 or ZIRLO™ with constant OD and ID over the entire length. Separate dashpot tubes, which are made from Zircaloy-4 or ZIRLO™ tubing, are inserted into the bottom portion of the guide thimble tubes. The larger tube diameter at the top section provides a relatively large annular area necessary to permit rapid control rod insertion during a reactor trip, as well as to accommodate the flow of coolant during normal operation. Holes are provided on the guide thimble above the dashpot to reduce the rod drop time. The lower portion of the guide thimble with the dashpot tube results in a dashpot action near the end of the control rod travel during normal trip operation. The dashpot is closed at the bottom by means of an end plug, which is provided with a small flow port to avoid fluid stagnation in the dashpot volume during normal operation.

As stated previously, the AP1000 fuel assembly includes a reconstitutable top nozzle as a standard feature. To accommodate the reconstitutable feature, the top end of the zirconium alloy guide thimble is fastened to a tubular sleeve, or insert, by a three tier expansion bulge joint. An expansion tool is inserted inside the nozzle insert and guide thimble to the proper elevation. The four lobes on the expansion tool force the guide thimble and insert outward locally to a predetermined diameter, therefore joining the two components.

Upon installation of the top nozzle assembly, the bulge near the top of the nozzle insert is captured in a corresponding groove in the hole of the top nozzle adapter plate. As shown in Figure 4.2-4, the mechanical connection between the nozzle insert-guide thimble and top nozzle is made by insertion of a lock tube into the insert. The design of the top grid sleeve-guide thimble and top nozzle insert-guide thimble bulge joint connections have been mechanically tested and found to meet applicable design criteria.

The fuel rod support grids, with exception noted for the bottom nickel-chromium-iron Alloy 718 grid, are secured to the guide thimbles using a similar bulge joint connection to create an integral structure. Attachment of the intermediate mixing vane and intermediate flow mixer (IFM) zirconium alloy grids to the guide thimbles is performed using the fastening technique depicted in Figures 4.2-5 and 4.2-6.

The intermediate mixing vane and intermediate flow mixer grids employ a single tier bulge connection between the grid sleeve and guide thimble as compared to the three tier bulge connection used for the top grid. The design of the single tier bulge joint connection has also been mechanically tested and meets the design requirements.

The bottom nickel-chromium-iron Alloy 718 grid is secured to the guide thimble assembly by a double tier bulge connection between the grid sleeve and guide thimble. The design of the double tier bulge joint connection has also been mechanically tested and meets the design requirements.

The lower end of the guide thimble is fitted with a welded end plug. The nickel-chromium-iron Alloy 718 protective grid is secured to the guide thimble assembly by nickel-chromium-iron Alloy 718 spacers that are spot-welded to the grid. As shown in Figure 4.2-7, the spacer is captured between the guide thimble end plug and the bottom nozzle by means of a (thimble) locking screw.

The described methods of grid fastening are standard and have been used successfully since the introduction of zirconium alloy guide thimbles in 1969.

The central instrumentation tube in each fuel assembly is constrained by seating in counterbores located in both top and bottom nozzles. The instrumentation tube has a constant diameter and provides an unrestricted passageway for the in-core neutron detector which enters the fuel assembly from the top nozzle. Furthermore, the instrumentation tube is secured to the top and mid-grids with bulge joint connections similar to those previously discussed for securing the grids to the guide thimbles.

4.2.2.2.4 Grid Assemblies

As shown in Figure 4.2-2, the fuel rods are supported at intervals along their lengths by grid assemblies which maintain the lateral spacing between the rods throughout the design life of the assembly. Each fuel rod is given support at six contact points within each grid by the combination of support dimples and springs. The grid assembly consists of individual slotted straps assembled and interlocked into an egg-crate type arrangement with the straps permanently joined at their points of intersection. The straps may contain springs, support dimples, and mixing vanes; or any such combination.

Two types of structural grid assemblies are used on the AP1000 fuel assembly. One type, with mixing vanes projecting from the edges of the straps into the coolant stream, is used in the high heat flux region of the fuel assemblies to promote mixing of the coolant. The other type, located at the top and bottom of the assembly, does not contain mixing vanes on the internal straps. The outside straps on the grids contain mixing vanes that, in addition to their mixing function, aid in guiding the grids and fuel assemblies past projecting surfaces during handling or during loading and unloading of the core.

Because of its corrosion resistance and high strength properties, the bottom grid material chosen for the AP1000 fuel assembly design is nickel-chromium-iron Alloy 718. The top grid is fabricated from nickel-chromium-iron Alloy 718. The magnitude of the grid restraining force on the fuel rod is set high enough to minimize possible fretting, without overstressing the cladding at the points of contact between the grids and fuel rods. The grid assemblies are designed to allow axial thermal expansion of the fuel rods without imposing restraint sufficient to develop buckling or distortion of the fuel rods.

The eight intermediate (mixing vane), or structural grids on the AP1000 fuel assembly are made of ZIRLO™. This material was selected to take advantage of the material's inherent low neutron capture cross-section. The zirconium alloy grids have thicker straps than the nickel-chromium-iron alloy grids. The zirconium alloy grid incorporates the same grid cell support configuration as the nickel-chromium-iron alloy grid. The zirconium alloy interlocking strap joints and grid/sleeve joints are fabricated by laser welding, whereas the nickel-chromium-iron alloy grid joints (except the protective

grid) are brazed. The interlocking strap joints for the protective grid are also fabricated by laser welding. The mixing vanes incorporated in the zirconium alloy intermediate grids induce additional flow mixing among the various flow channels in a fuel assembly as well as between adjacent fuel assemblies. This additional flow mixing enhances thermal performance.

As shown in Figure 4.2-2, the intermediate flow mixer grids are located at selected spans between the zirconium alloy mixing vane structural grids and incorporate a similar mixing vane array. Their prime function is mid-span flow mixing in the hotter fuel assembly spans. Each intermediate flow mixer grid cell contains four dimples that are designed to prevent mid-span channel closure in the spans containing intermediate flow mixers and fuel rod contact with the mixing vanes. This simplified cell arrangement allows short grid cells so that the intermediate flow mixer grid can accomplish its flow mixing objective with minimal pressure drop.

The intermediate flow mixer (IFM) grids, like the mixing vane grids, are fabricated from ZIRLO™. The intermediate flow mixer grids are manufactured using the same basic techniques as the zirconium alloy structural grid assemblies and are joined to the guide thimbles via sleeves which are welded at the bottom of appropriate grid cells.

Grid impact testing has been performed on zirconium alloy structural grids and the intermediate flow mixer grids indicative of the AP1000 design. The purpose of the testing was to determine the dynamic buckling, or crush, strength of the grids. The grid impact testing was performed at an elevated temperature of 600°F. This temperature is a conservative value representing the core average temperature at the mid-grid locations.

The intermediate flow mixer grids are not intended to be structural members. The intermediate flow mixer grids do, however, share the loads of the structural grids during faulted loading and, as such, contribute to enhance the load carrying capability of the AP1000 fuel assembly.

The dynamic crush strength of the AP1000 structural grids and intermediate flow mixer grids envelope the calculated grid impact loading during combined seismic and pipe rupture events. A coolable geometry is, therefore, provided at the intermediate flow mixer grid elevations, as well as at the structural grid elevations.

4.2.2.3 In-core Control Components

Reactivity control is provided by neutron absorbing rods, gray rods, burnable absorber rods, and a soluble chemical neutron absorber (boric acid). The boric acid concentration is varied to control long-term reactivity changes such as:

- Fuel depletion and fission product buildup
- Cold to hot, zero power reactivity changes
- Reactivity change produced by intermediate-term fission products such as xenon and samarium
- Burnable absorber depletion

The chemical and volume control system, which is used to adjust the level of boron in the coolant, is discussed in Section 9.3.

The rod cluster control assemblies provide reactivity control for:

- Shutdown

- Reactivity changes due to coolant temperature changes in the power range
- Reactivity changes associated with the power coefficient of reactivity
- Reactivity changes due to void formation

A negative power coefficient is maintained at hot, full-power conditions throughout the entire cycle to reduce possible deleterious effects caused by a positive coefficient during pipe rupture or loss-of-flow accidents. The first fuel cycle needs more excess reactivity than subsequent cycles due to the loading of fresh (unburned) fuel. Since soluble boron alone is insufficient to provide a negative moderator coefficient, burnable absorber assemblies are also used. Use of burnable absorber assemblies during reloads is discussed in Subsection 4.3.1.2.2.

The most effective reactivity control components are the rod cluster control assemblies and the corresponding drive rod assemblies, which along with the gray rod cluster assemblies, are the only kinetic parts in the reactor. Figure 4.2-8 identifies the rod cluster control and drive rod assembly, in addition to the arrangement of these components in the reactor relative to the interfacing fuel assembly, guide thimbles, and control rod drive mechanism. The arrangement for the gray rod cluster assemblies is the same.

As shown in Figure 4.2-8, the guidance system for the rod cluster control assembly is provided by the guide thimbles. The guide thimbles provide two regimes of guidance: first, in the lower section, a continuous guidance system provides support immediately above the core, which protects the rod against excessive deformation and wear caused by hydraulic loading. Second, the region above the continuous section provides support and guidance at uniformly spaced intervals.

As shown in Figure 4.2-9, the envelope of support is determined by the pattern of the control rod cluster. The guide thimbles provide alignment and support of the control rods, spider body, and drive rod while maintaining trip times at or below required limits.

Subsections 4.2.2.3.1 through 4.2.2.3.4 describe each reactivity control component in detail. The control rod drive mechanism assembly is described in Subsection 9.3.4. The neutron source assemblies provide a means of monitoring the core during periods of low neutron activity.

4.2.2.3.1 Rod Cluster Control Assemblies

The rod cluster control assemblies are divided into two categories: control and shutdown. The control groups compensate for reactivity changes due to variations in operating conditions of the reactor, that is, power and temperature variations. Two nuclear design criteria have been employed for selection of the control group. First, the total reactivity worth must be adequate to meet the nuclear requirements of the reactor. Second, in view of the fact that these rods may be partially inserted at power operation, the total power peaking factor should be low enough to confirm that the power capability is met. The control and shutdown groups provide adequate shutdown margin.

As illustrated in Figure 4.2-9, a rod cluster control assembly is comprised of a group of individual neutron absorber rods fastened at the top end to a common spider assembly.

The absorber material used in the control rods is silver-indium-cadmium alloy, which is essentially “black” to thermal neutrons and has sufficient additional resonance absorption to significantly increase worth. As shown in Figure 4.2-10, the absorber material is in the form of solid bars sealed in cold-worked stainless steel tubes. Sufficient diametral and end clearance is provided to accommodate relative thermal expansions.

The control rods have bottom plugs with bullet-like tips to reduce the hydraulic drag during reactor trip and to guide smoothly into the dashpot section of the fuel assembly guide thimbles.

The material used in the absorber rod end plugs is Type 308 stainless steel. The design stresses used for the Type 308 material are the same as those defined in the ASME Code, Section III, for Type 304 stainless steel. At room temperature, the yield and ultimate stresses per ASTM 580 (Reference 12) are exactly the same for the two alloys. In view of the similarity of composition of the alloys, the temperature dependence of strength for the two materials is expected to be the same.

The allowable stresses used as a function of temperature are listed in Table I-1.2 of the ASME Code, Section III. The fatigue strength for the Type 308 material is based on the S-N curve for austenitic stainless steels in Figure I-9.2 of the ASME Code, Section III.

The spider assembly is in the form of a central hub with radial vanes containing cylindrical fingers from which the absorber rods are suspended. Internal groove-like profiles to facilitate handling tool and drive rod assembly connection are machined into the upper end of the hub. Coil springs inside the spider body absorb the impact energy at the end of a trip insertion. The radial vanes are joined to the hub by welding and brazing, and the fingers are joined to the vanes by brazing. A bolt, which holds the springs and retainer, is threaded into the hub within the skirt and welded to prevent loosening while in service.

The components of the spider assembly are made from Types 304 and 308 stainless steel except for the retainer, which is of Type 630 material, and the springs, which are nickel-chromium-iron Alloy 718.

The absorber rods are fastened securely to the spider. The rods are first threaded into the spider fingers and then pinned to maintain joint tightness. The pins are then welded in place. The end plug below the pin position is designed with a reduced section to permit flexing of the rods to correct for small operating or assembly misalignments.

The overall length of the rod cluster control assembly is such that, when the assembly is withdrawn through its full travel, the tips of the absorber rods remain engaged in the guide thimbles so that alignment between rods and thimbles is always maintained. Since the rods are long and slender, they are relatively free to conform to any small misalignments with the guide thimble.

4.2.2.3.2 Gray Rod Cluster Assemblies

The mechanical design of the gray rod cluster assemblies plus the control rod drive mechanism and the interface with the fuel assemblies and guide thimbles are identical to the rod cluster control assembly.

As shown in Figure 4.2-11, the gray rod cluster assemblies consist of 24 rodlets fastened at the top end to a common hub or spider. Geometrically, the gray rod cluster assembly is the same as a rod cluster control assembly except that 12 of the 24 rodlets are stainless steel while the remaining 12 contain the reduced diameter silver-indium-cadmium absorber material clad with stainless steel as the rod cluster control assemblies.

The gray rod cluster assemblies are used in load follow maneuvering and provide a mechanical shim to replace the use of changes in the concentration of soluble boron, that is, a chemical shim, normally used for this purpose. The AP1000 uses 53 rod cluster control assemblies and 16 gray rod cluster assemblies.

4.2.2.3.3 Burnable Absorber Assembly

Each burnable absorber assembly consists of discrete burnable absorber rods attached to a hold-down assembly. Figure 4.2-12 shows the burnable absorber assemblies. When needed for nuclear considerations, burnable absorber assemblies are inserted into selected thimbles within fuel assemblies.

The burnable absorber rods (Pyrex) consist of borosilicate glass tubes contained within Type 304 stainless steel tubular cladding, which is plugged and seal welded at the ends to encapsulate the glass. The burnable absorber assembly is shown in Figure 4.2-13.

The typical discrete burnable absorber rods (WABA) consist of pellets of alumina-boron carbide material contained within zirconium alloy tubes. These zirconium alloy tubes, which form the outer clad for the burnable absorber rod, are plugged, pressurized with helium, and seal-welded at each end to encapsulate the stack of absorber material. The absorber stack length, shown in Figure 4.2-12, is positioned axially within the burnable absorber rod by the use of a zirconium alloy bottom-end spacer.

The burnable absorber rods in each fuel assembly are grouped and attached together at the top end of the rods to a hold-down assembly by a flat, perforated retaining plate, which fits within the fuel assembly top nozzle and rests on the adapter plate.

The retaining plate and the burnable absorber rods are held down and restrained against vertical motion through a spring pack which is attached to the plate and is compressed by the upper core plate when the reactor upper internals assembly is lowered into the reactor. With this arrangement, the burnable absorber rods cannot be ejected from the core by flow forces. Each rod is attached to the baseplate by a nut that is crimped into place.

4.2.2.3.4 Neutron Source Assemblies

The purpose of a neutron source assembly is to provide a base neutron level to give confidence that the detectors are operational and responding to core multiplication neutrons. For the first core, a neutron source is placed in the reactor to provide a positive neutron count of at least two counts per second on the source range detectors attributable to core neutrons. The detectors, called source range detectors, are used primarily during subcritical modes of core operation.

The source assembly also permits detection of changes in the core multiplication factor during core loading, refueling, and approach to criticality. This can be done since the multiplication factor is related to an inverse function of the detector count rate. Changes in the multiplication factor can be detected during addition of fuel assemblies while loading the core, changes in control rod positions, and changes in boron concentration.

Both primary and secondary neutron source rods are used. The primary source rod, containing a radioactive material, spontaneously emits neutrons during initial core loading, reactor startup, and initial operation of the first core. After the primary source rod decays beyond the desired neutron flux level, neutrons are then supplied by the secondary source rod. The secondary source rod contains a stable material, which is activated during reactor operation. The activation results in the subsequent release of neutrons.

Four source assemblies are typically installed in initial load of the reactor core: two primary source assemblies and two secondary source assemblies. Each primary source assembly contains one primary source rod and a number of burnable absorber rods. Each secondary source assembly contains a symmetrical grouping of secondary source rodlets. Figure 4.2-14 shows the primary source assembly. Figure 4.2-15 shows the secondary source assembly.

Neutron source assemblies are employed at opposite sides of the core. The source assemblies are inserted into the rod cluster control guide thimbles in fuel assemblies at selected locations.

As shown in Figures 4.2-14 and 4.2-15, the source assemblies contain a hold-down assembly identical to that of the burnable absorber assembly.

The primary and secondary source rods both use the same cladding material as the absorber rods. The secondary source rods contain antimony-beryllium pellets stacked to a height of approximately 88 inches. The primary source rods contain capsules of californium (plutonium-beryllium possible alternate) source material and alumina spacers to position the source material within the cladding. The rods in each assembly are fastened at the top end to a hold-down assembly.

The other structural members, except for the springs, are constructed of Type 304 stainless steel. The springs exposed to the reactor coolant are nickel-chromium-iron Alloy 718.

4.2.3 Design Evaluation

[*The fuel assemblies, fuel rods, and in-core control components are designed to satisfy the performance and safety criteria of*]* Section 4.2 of the Standard Review Plan, the mechanical design bases of Subsection 4.2.1 and [*the Fuel Criteria Evaluation Process per WCAP-12488-A (Reference 1)*]*, and other interfacing nuclear and thermal and hydraulic design bases specified in Sections 4.3 and 4.4.

Effects of Conditions II, III, IV or anticipated transients without trip on fuel integrity are presented in Chapter 15.

The initial step in fuel rod design evaluation for a region of fuel is to determine the limiting rod(s). Limiting rods are defined as those rods whose predicted performance provides the minimum margin to each of the design criteria. For a number of design criteria, the limiting rod is the lead burnup rod of a fuel region. In other instances, it may be the maximum power or the minimum burnup rod. For the most part, no single rod is limiting with respect to all the design criteria.

After identifying the limiting rod(s), an analysis is performed to consider the effects of rod operating history, model uncertainties, and dimensional variations. To verify adherence to the design criteria, the evaluation considers the effects of postulated transient power changes during operation consistent with Conditions I and II. These transient power increases can affect both rod average and local power levels. Parameters considered include rod internal pressure, fuel temperature, clad stress, and clad strain. In fuel rod design analyses, these performance parameters provide the basis for comparison between expected fuel rod behavior and the corresponding design criteria limits.

Fuel rod and assembly models used for the performance evaluations are documented and maintained under an appropriate control system. Material properties used in the design evaluations are given in WCAP-12610 (Reference 5).

4.2.3.1 Cladding

4.2.3.1.1 Vibration and Wear

Fuel rod vibrations are flow induced. The effect of vibration on the fuel assembly and individual fuel rods is minimal. The cyclic stress range associated with deflections of such small magnitude is insignificant and has no effect on the structural integrity of the fuel rod.

The reaction force on the grid supports, due to rod vibration motions, is also small and is much less than the spring preload. Adequate fuel clad spring contact is maintained. No significant wear of the

*NRC Staff approval is required prior to implementing a change in this information.

clad or grid supports is predicted during the life of the fuel assembly based on out-of-pile flow tests, performance of similarly designed fuel in operating reactors, and design analyses.

Clad fretting and fuel vibration has been experimentally investigated, as shown in WCAP-8278 (Reference 13).

4.2.3.1.2 Fuel Rod Internal Pressure and Cladding Stresses

A burnup-dependent fission gas release model (WCAP-15063-P-A, Revision 1 [Reference 21]) is used in determining the internal gas pressure as a function of irradiation time. The plenum volume of the fuel rod has been designed to provide that the maximum internal pressure of the fuel rod will not exceed the value which would cause:

- The fuel/clad diametral gap to increase during steady-state operation
- Extensive departure from nucleate boiling propagation to occur

The clad stresses at a constant local fuel rod power are low. Compressive stresses are created by the pressure differential between the coolant pressure and the rod internal gas pressure. Because of the pre-pressurization with helium, the volume average effective stresses are always less than approximately 14,000 psi at the pressurization level used in the AP1000 fuel rod design. Stresses due to the temperature gradient are not included in this average effective stress because thermal stresses are, in general, negative at the clad inside diameter and positive at the clad outside diameter, and their contribution to the clad volume average stress is small. Furthermore, the thermal stress decreases with time during steady-state operation due to stress relaxation. The stress due to pressure differential is highest in the minimum power rod at beginning-of-life due to low internal gas pressure and decreases as rod power increases. Thermal stresses are maximum in the maximum power rod due to the larger temperature gradient and decrease as the rod power is decreased.

The internal gas pressure at beginning-of-life ranges from approximately 200 to 750 psi for typical lead burnup fuel rods. The total tangential stress at the clad inside diameter at beginning-of-life is approximately 19,500 psi compressive (approximately 18,500 psi due to ΔP and approximately 1,000 due to ΔT) for a low-power rod operating at four kilowatts/foot. Total tangential stress is approximately 20,500 psi compressive (approximately 18,000 psi due to ΔP and approximately 2,500 psi due to ΔT) for a high-power rod operating at 10 kilowatts/foot. However, the volume average effective stress at beginning-of-life is between approximately 13,500 psi (high-power rod) and approximately 14,000 psi (low-power rod). These stresses are substantially below even the unirradiated clad yield strength (approximately 55,500 psi) at a typical clad mean operating temperature of 700°F.

Tensile stresses could be created once the clad has come in contact with the pellet. These stresses would be induced by the fuel pellet swelling during irradiation. Swelling of the fuel pellet can result in small clad strains (less than one percent) for expected discharge burnups, but the associated clad stresses are very low because of clad creep (thermal- and irradiation-induced creep). The one percent strain criterion is extremely conservative for fuel-swelling driven clad strain because the strain rate associated with solid fission products swelling is very slow. A detailed discussion of fuel rod performance is given in Subsection 4.2.3.3.

4.2.3.1.3 Material and Chemical Evaluation

ZIRLO™ clad has a high corrosion resistance to the coolant, fuel, and fission products. As shown in WCAP-8183 (Reference 3), there is considerable pressurized water reactor operating experience on the capability of Zircaloy-4 as a clad material. ZIRLO™, an advanced zirconium based alloy, has

equal or better corrosion resistance than Zircaloy-4 (see WCAP-12610-P-A, [Reference 5]). Controls on fuel fabrication specify maximum moisture levels to preclude clad hydriding.

Metallographic examination of irradiated commercial fuel rods has shown occurrences of fuel/clad chemical interaction. Reaction layers of less than one mil in thickness have been observed between fuel and clad at limited points around the circumference. Metallographic data indicates that this interface layer remains very thin even at high burnup. Thus, there is no indication of propagation of the layer and eventual clad penetration.

Stress corrosion cracking is another postulated phenomenon related to fuel/clad chemical interaction. Out-of-pile tests have shown that in the presence of high clad tensile stresses, large concentrations of iodine can chemically attack the zirconium alloy tubing and may lead to eventual clad cracking. Extensive post-irradiation examination has produced no evidence that this mechanism has been operative in Westinghouse commercial pressurized water reactor fuel.

4.2.3.1.4 Rod Bowing

WCAP-8691 (Reference 14) presents the model used for evaluation of AP1000 fuel rod bowing. This model has been used for bow assessment in 14x14, 15x15, and 17x17 type cores.

4.2.3.1.5 Consequences of Power Coolant Mismatch

Consequences of power coolant mismatch are discussed in Chapter 15.

4.2.3.1.6 Creep Collapse and Creepdown

This subject and the associated irradiation stability of cladding have been evaluated. In WCAP-13589-A (Reference 8), it is shown that current generation Westinghouse fuel is sufficiently stable with respect to fuel densification. Significant axial gaps do not form in the pellet stack, preventing clad collapse from occurring. The design basis of no clad collapse during planned core life is therefore satisfied. Cladding collapse analyses, if required, would be performed using the methods described in WCAP-8377 (Reference 22).

4.2.3.2 Fuel Materials Considerations

Sintered, high-density uranium dioxide fuel reacts only slightly with the clad at core operating temperatures and pressures. In the event of clad defects, the high resistance of uranium dioxide to attack by water protects against fuel deterioration, although limited fuel erosion can occur. The consequences of defects in the clad are greatly reduced by the ability of uranium dioxide to retain fission products, including those which are gaseous or highly volatile.

Observations from several early Westinghouse pressurized water reactors as discussed in WCAP-8218-P-A (Reference 6) have shown that fuel pellets can densify under irradiation to a density higher than the manufactured values. Fuel densification and subsequent settling of the fuel pellets can result in local and distributed gaps in the fuel rods. The densification process is related to the elimination of very small as-fabricated porosity in the fuel during irradiation. Early fuels were intentionally manufactured to low initial density and were undersintered, which resulted in a large fraction of very small pores. Densification behavior in current fuel is controlled by improved manufacturing process controls and by specifying a nominal 95.5 percent initial fuel density, which results in reduced levels of small, densifying porosity.

The evaluation of fuel densification effects and the treatment of fuel swelling and fission gas release are described in WCAP-13589-A (Reference 8) and WCAP-15063-P-A, Revision 1 (Reference 21).

4.2.3.3 Fuel Rod Performance

In the calculation of the steady-state performance of a nuclear fuel rod, the following interacting factors are considered:

- Clad creep and elastic deflection
- Pellet density changes, thermal expansion, gas release, and thermal properties as a function of temperature and fuel burnup
- Internal pressure as a function of fission gas release, rod geometry, and temperature distribution

These effects are evaluated using fuel rod design models, as discussed in WCAP-15063-P-A, Revision 1 (Reference 21), that include appropriate models for time dependent fuel densification. With these interacting factors considered, the model determines the fuel rod performance characteristics for a given rod geometry, power history, and axial power shape. In particular, internal gas pressure, fuel and clad temperatures, and clad deflections are calculated. The fuel rod is divided into several axial sections and radially into a number of annular zones. Fuel density changes are calculated separately for each segment. The effects are integrated to obtain the internal rod pressure.

The initial rod internal pressure is selected to delay fuel/clad mechanical interaction and to avoid the potential for clad flattening. It is limited, however, by the design criteria for the rod internal pressure, as discussed in Subsection 4.2.1.3.

The gap conductance between the pellet surface and the clad inner diameter is calculated as a function of the composition, temperature and pressure of the gas mixture, and the gap size or contact pressure between the clad and pellet. After computing the fuel temperature for each pellet zone, the fractional fission gas release is assessed using an empirical model derived from experimental data, as detailed in WCAP-15063-P-A, Revision 1 (Reference 21). The total amount of gas released is based on the average fractional release within each axial and radial zone and the gas generation rate, which, in turn, is a function of burnup. Finally, the gas released is summed over the zones, and the pressure is calculated.

The model shows close agreement in fit for a variety of published and proprietary data on fission gas release, fuel temperatures, and clad deflections, as detailed in WCAP-15063-P-A, Revision 1 (Reference 21). These data include variations in power, time, fuel density, and geometry.

4.2.3.3.1 Fuel/Cladding Mechanical Interaction

One factor in fuel element duty is potential mechanical interaction of the fuel and clad. This fuel/clad interaction produces cyclic stresses and strains in the clad, and these, in turn, reduce clad life. The reduction of fuel/clad interaction is therefore a goal of design. The technology for using pre-pressurized fuel rods in Westinghouse pressurized water reactors has been developed to further this objective.

The gap between the fuel and clad is initially sufficient to prevent hard contact between the two. However, during power operation a gradual compressive creep of the clad onto the fuel pellet occurs due to the external pressure exerted on the rod by the coolant. Clad compressive creep eventually results in fuel/clad contact. Once fuel/clad contact occurs, changes in power level result in changes in clad stresses and strains. By using pre-pressurized fuel rods to partially offset the effect of the coolant external pressure, the rate of clad creep toward the surface of the fuel is reduced. Fuel rod pre-pressurization delays the time at which fuel/clad contact occurs and, hence, significantly reduces

the extent of cyclic stresses and strains experienced by the clad both before and after fuel/clad contact. These factors result in an increase in the fatigue life margin of the clad and lead to greater clad reliability.

A two-dimensional (r,θ) finite element model has been established to investigate the effects of radial pellet cracks on stress concentrations in the clad. Stress concentration herein is defined as the difference between the maximum clad stress in the θ direction and the mean clad stress. The first case has the fuel and clad in mechanical equilibrium; and, as a result, the stress in the clad is close to zero. In subsequent cases the pellet power is increased in steps and the resultant fuel thermal expansion imposes tensile stress in the clad.

In addition to uniform clad stresses, stress concentrations develop in the clad adjacent to radial cracks in the pellet. These radial cracks have a tendency to open during a power increase, but the frictional forces between fuel and clad oppose the opening of these cracks and result in localized increases in clad stress. As the power is further increased, large tensile stresses exceed the ultimate tensile strength of uranium dioxide and additional cracks in the fuel pellet are created, limiting the magnitude of the stress concentration in the clad.

As part of the standard fuel rod design analysis, the maximum stress concentration evaluated from finite element calculations is added to the volume-averaged effective stress in the clad as determined from one-dimensional stress/strain calculations. The resultant clad stress is then compared to the temperature-dependent cladding yield stress to confirm that the stress/strain criteria are satisfied.

The transient evaluation method is described in the following paragraphs.

Pellet thermal expansion due to power increases is considered the only mechanism by which significant stresses and strains can be imposed on the clad.

Power increases in commercial reactors can result from fuel shuffling (for example, region 3 positioned near the core center for cycle 2 operation after operating near the periphery during cycle 1), reactor power escalation following extended reduced power operation, and full-length control rod movement. In the mechanical design model, lead rods are depleted using best-estimate power histories as determined by core physics calculations. During burnup, the amount of diametral gap closure is evaluated based upon the pellet expansion cracking model, clad creep model, and fuel swelling model. At various times during the depletion, the power is increased locally in the rod to the burnup-dependent attainable power density as determined by core physics calculations. The radial, tangential, and axial clad stresses resulting from the power increase are combined into a volume average effective clad stress.

The von Mises criterion is used to determine whether the clad yield stress has been exceeded. This criterion states that an isotropic material in multi-axial stress will begin to yield plastically when the effective stress exceeds the yield stress as determined by an axial tensile test. The yield stress correlation is that for irradiated cladding, since fuel/clad interaction occurs at high burnup. In applying this criterion, the effective stress is increased by an allowance which accounts for stress concentrations in the clad adjacent to radial cracks in the pellet, prior to the comparison with the yield stress. This allowance was evaluated using a two-dimensional (r,θ) finite element model.

Slow transient power increases can result in large clad strains without exceeding the clad yield stress because of clad creep and stress relaxation. Therefore, in addition to the yield stress criterion, a criterion on allowable clad strain is necessary. Based upon high strain rate burst and tensile test data on irradiated tubing, one percent strain was determined to be a conservative lower limit on irradiated clad ductility and that was adopted as a design criterion.

In addition to the mechanical design models and design criteria, the AP1000 fuel rod design relies on performance data accumulated through transient power test programs in experimental and commercial reactors, and through normal operation in commercial reactors.

It is recognized that a possible limitation to the satisfactory behavior of the fuel rods in a reactor subjected to daily load follow is the failure of the cladding by low-cycle strain fatigue. During their normal residence time in the reactor, the fuel rods may be subjected to on the order of 1000 load follow cycles, with typical changes in power level from 50 to 100 percent of their steady-state values.

The assessment of the fatigue life of the fuel rod cladding is subjected to considerable uncertainty because of the difficulty of evaluating the strain range which results from the cyclic interaction of the fuel pellets and cladding. This difficulty arises, for example, from such highly unpredictable phenomena as pellet cracking, fragmentation, and relocation. Westinghouse investigated this particular phenomenon both analytically and experimentally. Strain fatigue tests on irradiated and nonirradiated hydrided Zircaloy-4 cladding were performed. These tests permitted the definition of a conservative fatigue-life limit and recommendation of a methodology to treat the strain fatigue evaluation of the Westinghouse-referenced fuel rod designs. (See WCAP-9500-P-A, Reference 15.)

Successful load follow operation has been performed on several reactors. There was no significant coolant activity increase that could be associated with the load follow mode of operation.

The Westinghouse analytical approach to strain fatigue is based on a comprehensive review of the available strain fatigue models. The review included the Langer-O'Donnell model (Reference 16) the Yao-Munse model, and the Manson-Halford model. Upon completion of this review, and using the results of the Westinghouse experimental programs as documented in WCAP-9500-P-A (Reference 15), it was concluded that the approach defined by Langer-O'Donnell would be retained and the empirical factors of their correlation modified to conservatively bound the results of the Westinghouse testing program.

The design equations followed the concept for the fatigue design criterion according to the ASME Code, Section III:

- The calculated pseudo stress amplitude (Sa) has to be multiplied by a factor of two to obtain the allowable number of cycles (Nf).
- The allowable cycles for a given Sa is five percent of Nf or a safety factor of 20 on cycles.

The lesser of the two allowable numbers of cycles is selected. The cumulative fatigue life fraction is then computed as:

$$\sum_{1}^{k} \frac{n_k}{N_{f\,k}} \leq 1$$

where:

n_k = number of diurnal cycles of mode k.

$N_{f\,k}$ = number of allowable cycles.

4.2.3.3.2 Irradiation Experience

Westinghouse fuel operational experience is presented in WCAP-8183 (Reference 3). Additional test assembly and test rod experience is given in WCAP-10125-P-A (Reference 2).

4.2.3.3.3 Fuel and Cladding Temperature

The methods used for evaluation of fuel rod temperatures are presented in Subsection 4.4.2.11.

4.2.3.3.4 Potentially Damaging Temperature Effects During Transients

The fuel rod experiences many operational transients (intentional maneuvers) during its residence in the core. A number of thermal effects must be considered when analyzing the fuel rod performance.

The clad can be in contact with the fuel pellet at some time in the fuel lifetime. Clad/pellet interaction occurs if the fuel pellet temperature is increased after the clad is in contact with the pellet. Clad/pellet interaction is discussed in Subsection 4.2.3.3.1.

Clad flattening has been observed in some operating power reactors. This is no longer a concern because clad flattening is precluded during the fuel residence in the core (Subsection 4.2.3.1) by the use of stable fuel.

Potential differential thermal expansion between the fuel rods and the guide thimbles during a transient is considered in the design. Excessive bowing of the fuel rods is precluded because the grid assemblies allow axial movement of the fuel rods relative to the grids. Specifically, thermal expansion of the fuel rods is considered in the grid design so that axial loads imposed on the fuel rods during a thermal transient will not result in excessively bowed fuel rods.

4.2.3.3.5 Fuel Element Burnout and Potential Energy Release

As discussed in Subsection 4.4.2.2, the core is protected from departure from nucleate boiling over the full range of possible operating conditions. In the extremely unlikely event that departure from nucleate boiling should occur, the clad temperature will rise due to the steam blanketing at the rod surface and the consequent degradation in heat transfer. During this time there is a potential for chemical reaction between the cladding and the coolant. However, because of the relatively good film boiling heat transfer following departure from nucleate boiling, the energy release resulting from this reaction is insignificant compared to the power produced by the fuel.

4.2.3.3.6 Coolant Flow Blockage Effects on Fuel Rods

The coolant flow blockage effects on fuel rods are presented in Subsection 4.4.4.7.

4.2.3.4 Spacer Grids

The coolant flow channels are established and maintained by the structure composed of grids and guide thimbles. The lateral spacing between fuel rods is provided and controlled by the support dimples of adjacent grid cells. Contact of the fuel rods on the dimples is maintained through the clamping force of the grid springs. Lateral motion of the fuel rods is opposed by the spring force and the internal moments generated between the spring and the support dimples. Grid testing is discussed in WCAP-8236 (Reference 17) and WCAP-10444-P-A (Reference 11).

4.2.3.5 Fuel Assembly

4.2.3.5.1 Stresses and Deflections

The fuel assembly component stress levels are limited by the design. For example, stresses in the fuel rod due to thermal expansion and zirconium alloy irradiation growth are limited by the relative motion of the rod as it slips over the grid spring and dimple surfaces. Clearances between the fuel rod ends and nozzles are provided so that zirconium alloy irradiation growth does not result in rod

end interference. Stresses in the fuel assembly caused by tripping of the rod cluster control assembly have little influence on fatigue usage margin because of the small number of events during the life of an assembly. Assembly components and prototype fuel assemblies made from production parts have been subjected to structural tests to verify that the design bases requirements are met.

The fuel assembly design loads for shipping have been established at 4 g axial and 6 g lateral. Accelerometers are permanently placed in the shipping cask to monitor and detect fuel assembly accelerations that would exceed the criteria. Experience indicates that loads that exceed the allowable limits rarely occur. Exceeding the limits requires reinspection of the fuel assembly for damage. Tests on various fuel assembly components, such as the grid assembly, sleeves, inserts, and structure joints, have been performed to confirm that the shipping design limits do not result in impairment of fuel assembly function. Seismic analysis methodology of the fuel assembly is presented in WCAP-8236 (Reference 17), WCAP-9401-P-A (Reference 18), and WCAP-10444-P-A (Reference 11).

To demonstrate that the fuel assemblies will maintain a geometry that is capable of being cooled under the worst-case accident Condition IV event, a plant specific or bounding seismic analysis is performed.

The fuel assembly response resulting from safe shutdown earthquake condition is analyzed using time-history numerical techniques. The vessel motion for this type of event primarily causes lateral loads on the reactor core. Consequently, the methodology and analytical procedures as described in WCAP-8236 (Reference 17) and WCAP-9401-P-A (Reference 18) are used to assess the fuel assembly deflections and impact forces.

The motions of the reactor internals upper and lower core plates and the core barrel at the upper core plate elevation, which are simultaneously applied to simulate the reactor core input motion, are obtained from the time-history analysis of the reactor vessel and internals. The fuel assembly response, namely the displacements and impact forces, is obtained with the reactor core model. Similar dynamic analyses of the core were performed using reactor internals motions indicative of the postulated pipe rupture. Scenarios regarding breaches in the pressure boundary are investigated to determine the most limiting structural loads for the fuel assembly. The application of leak-before-break limits the size of the pipe rupture loads for which the fuel assemblies must be analyzed. The pipe rupture used in the fuel assembly analysis is the largest pipe connected to the reactor coolant system which does not satisfy the leak-before-break criteria. Subsection 3.6.3 discusses mechanistic pipe break.

4.2.3.5.1.1 Grid Analyses

The maximum grid impact force obtained from seismic analyses is less than the allowable grid strength. With respect to the guidelines of Appendix A of the Standard Review Plan, Section 4.2, Westinghouse has demonstrated that a simultaneous safe shutdown earthquake and pipe rupture event is highly unlikely. The fatigue cycles, crack initiation, and crack growth due to normal operating and seismic events will not realistically lead to a pipe rupture. More information is available in WCAP-9283 (Reference 19).

Based on the deterministic fracture mechanics evaluation of small flaws in piping components, Westinghouse has demonstrated that the dynamic affects of a large pipe rupture in the primary coolant piping system for the AP1000 design does not have to be considered.

A design basis for the piping design in the AP1000 is that the reactor coolant loop and surge lines will satisfy the leak-before-break criteria for mechanistic pipe break. In addition, the piping connected to the reactor coolant system that is six inch nominal diameter or larger is evaluated for leak-before-break. The result of a pipe leakage event consistent with the mechanistic pipe break evaluation

would be to impose insignificant asymmetric loadings on the reactor core system. Thus, fuel assembly grid loads due to large pipe ruptures are unrealistic and, as such, are not included in the analysis.

The pressure boundary integrity for numerous branch lines is analyzed to determine the most limiting break of a line not qualified for leak-before-break for the dynamic loading of the reactor core. Grid loads resulting from a combined seismic and pipe rupture event do not cause unacceptable grid deformation as to preclude a core coolable geometry.

4.2.3.5.1.2 Nongrid Analyses

The stresses induced in the various fuel assembly nongrid components are assessed based on the most limiting seismic condition. The fuel assembly axial forces resulting from the hold-down spring load together with its own weight distribution are the primary sources of the stresses in the guide thimbles and fuel assembly nozzles. The fuel rod accident induced stresses, which are generally very small, are caused by bending due to the fuel assembly deflections during a seismic event. The seismic-induced stresses are compared with the allowable stress limits for the fuel assembly major components. The component stresses, which include normal operating stresses, are below the established allowable limits. Consequently, the structural designs of the fuel assembly components are acceptable for the design basis accident conditions for the AP1000.

4.2.3.5.2 Dimensional Stability

Localized yielding and slight deformation in some fuel assembly components are allowed to occur during a Condition III or IV event. The maximum permanent deflection, or deformations, do not result in any violation of the functional requirements of the fuel assembly.

4.2.3.6 Reactivity Control Assemblies and Burnable Absorber Rods

4.2.3.6.1 Internal Pressure and Cladding Stresses during Normal, Transient, and Accident Conditions

The designs of the burnable absorber and source rods provide a sufficient cold void volume to accommodate the internal pressure increase during operation. This is not a concern for the rod cluster control assembly absorber rod or gray rod cluster assembly rodlets because no gas is released by the silver-indium-cadmium absorber material.

For the discrete burnable absorber rod, there is sufficient cold void volume to limit the internal pressure to a value, which satisfies the design criteria. For the source rods, a void volume is provided within the rod to limit the maximum internal pressure increase at end-of-life. Figures 4.2-14 and 4.2-15 detail the primary and secondary source assemblies.

During normal transient and accident conditions, the void volume limits the internal pressures to values that satisfy the criteria in Subsection 4.2.1.6. These limits are established not only to prevent the peak stresses from reaching unacceptable values, but also to limit the amplitude of the oscillatory stress component in consideration of the fatigue characteristics of the materials.

Rod, guide thimble, and dashpot flow analyses indicate that the flow is sufficient to prevent coolant boiling within the guide thimble. Therefore, clad temperatures at which the clad material has adequate strength to resist coolant operating pressures and rod internal pressures are maintained.

4.2.3.6.2 Thermal Stability of the Absorber Material, Including Changes and Thermal Expansion

The radial and axial temperature profiles within the source and absorber rods are determined by considering gap conductance, thermal expansion, neutron or gamma heating of the contained material as well as gamma heating of the clad.

The maximum temperatures of the silver-indium-cadmium control rod absorber material are calculated and found to be significantly less than the material melting point and found to occur axially at only the highest flux region. The mechanical and thermal expansion properties of the silver-indium-cadmium absorber material are discussed in WCAP-9179 (Reference 4).

In the first core, the burnable absorber rods (Pyrex) consist of borosilicate glass tubes contained within Type 304 stainless steel tubular cladding, which is plugged and seal welded at the ends to encapsulate the glass. The absorber material temperature does not exceed its design limit of 1220°F. Mechanical and thermal design and nuclear evaluation of the burnable absorber rods are described in WCAP-7113 (Reference 23).

The maximum temperature of the alumina-boron carbide burnable absorber pellet (WABA) is expected to be less than 1200°F which takes place following the initial power ascent. As the operating cycle proceeds, the burnable absorber pellet temperature decreases due to a reduction in heat generation due to boron depletion and better gap conduction as the helium produced diffuses into the gap.

Sufficient diametral and end clearances have been provided in the neutron absorber, burnable absorber, and source rods to accommodate the relative thermal expansions between the enclosed material and the surrounding clad and end plug.

4.2.3.6.3 Irradiation Stability of the Absorber Material, Taking into Consideration Gas Release and Swelling

The irradiation stability of the silver-indium-cadmium absorber material is discussed in WCAP-9179 (Reference 4). Irradiation produces no deleterious effects in the absorber material.

As mentioned in Subsection 4.2.3.6.1, gas release is not a concern for the control rod material because no gas is produced by the absorber material. Sufficient diametral and end clearances are provided to accommodate any potential expansion and/or swelling of the absorber material.

The alumina-boron carbide burnable absorber pellets are designed such that gross swelling or crumbling of the pellets is not predicted to occur during reactor operation. Some minor cracking of the pellets may occur, but this cracking should not affect the overall absorber and stack integrity.

4.2.3.6.4 Potential for Chemical Interaction, Including Possible Waterlogging Rupture

The structural materials selected have good resistance to irradiation damage and are compatible with the reactor environment.

Corrosion of the materials exposed to the coolant is quite low, and proper control of chloride and oxygen in the coolant minimizes potential for the occurrence of stress corrosion. The potential for the interference with rod cluster control assembly movement due to possible corrosion phenomena is very low.

Waterlogging rupture is not a failure mechanism associated with the AP1000 control rods. Furthermore, a breach of the cladding for any postulated reason does not result in serious consequences.

The silver-indium-cadmium absorber material is relatively inert and will remain inert even when subjected to high coolant velocity regions. Rapid loss of reactivity control material will not occur. Test results detailed in WCAP-9179 (Reference 4) concluded that additions of indium and cadmium to silver, in the amounts to form the silver-indium-cadmium absorber material composition, result in small corrosion rates.

For the discrete burnable absorber, in the unlikely event that the zirconium alloy clad is breached, the boron carbide in the affected rod(s) could be leached out by the coolant water. If this occurred early, in-core instruments could detect large peaking factor changes, and corrective action would be taken, if warranted. A postulated clad breach after substantial irradiation would have no significant effect on peaking factors since the boron will have been depleted. Breaching of the zirconium alloy clad by internal hydriding is not expected due to moisture controls employed during fabrication. Rods of this design have performed very well with no failures observed.

4.2.4 Testing and Inspection Plan

4.2.4.1 Quality Assurance Program

The Quality Assurance Program Plan of the Westinghouse Commercial Nuclear Fuel Division for the AP1000 is summarized in Chapter 17.

The program provides for control over activities affecting product quality, commencing with design and development and continuing through procurement, materials handling, fabrication, testing and inspection, storage, and transportation. The program also provides for the indoctrination and training of personnel and for the auditing of activities affecting product quality through a formal auditing program.

Westinghouse drawings and product, process, and material specifications identify the inspections to be performed.

4.2.4.2 Quality Control

Quality control philosophy is generally based on the following inspections being performed to a 95 percent confidence that at least 95 percent of the product meets specification, unless otherwise noted.

4.2.4.2.1 Fuel System Components and Parts

The characteristics inspected depend on the component parts. The quality control program includes dimensional and visual examinations, check audits of test reports, material certification, and nondestructive examination, such as X-ray and ultrasonic.

The material used in the AP1000 core is accepted and released by Quality Control.

4.2.4.2.2 Pellets

Inspection is performed for dimensional characteristics such as diameter, density, length, and squareness of ends. Additional visual inspections are performed for cracks, chips, and surface conditions according to approved standards.

Density is determined in terms of weight per unit length and is plotted on zone charts used in controlling the process. Chemical analyses are taken on a specified sample basis throughout pellet production.

4.2.4.2.3 Rod Inspection

Fuel rod, rod cluster control rod, discrete burnable absorber rod, and source rod inspections consists of the following nondestructive examination techniques and methods, as applicable:

- Each rod is leak tested using a calibrated mass spectrometer, with helium being the detectable gas.
- Rod welds are inspected by ultrasonic test or X-ray in accordance with a qualified technique and Westinghouse specifications meeting the requirements of ASTM-E-142-86 (Reference 20).
- Rods are dimensionally inspected prior to final release. The requirements include such items as length, camber, and visual appearance.
- Fuel rods are inspected by gamma scanning or other approved methods, as discussed in Subsection 4.2.4.5, to confirm proper plenum dimensions.
- Fuel rods are inspected by gamma scanning, or other approved methods, as discussed in Subsection 4.2.4.5, to confirm that no significant gaps exist between pellets.
- Fuel rods are actively and/or passively gamma scanned to verify enrichment control prior to acceptance for assembly loading.
- Traceability of rods and associated rod components is established by quality control.

4.2.4.2.4 Assemblies

Each fuel rod, control rod, burnable absorber rod and source rod assembly is inspected for compliance with drawing and/or specification requirements. Other in-core control component inspection and specification requirements are given in Subsection 4.2.4.4.

4.2.4.2.5 Other Inspections

The following inspections are performed as part of the routine inspection operation:

- Tool and gauge inspection and control, including standardization to primary and/or secondary working standards. Tool inspection is performed at prescribed intervals on serialized tools. Complete records are kept of calibration and conditions of tools.
- Audits are performed of inspection activities and records to confirm that prescribed methods are followed and that records are correct and properly maintained.
- Surveillance inspection, where appropriate, and audits of outside contractors are performed to confirm conformance with specified requirements.

4.2.4.2.6 Process Control

To prevent the possibility of mixing enrichments during fuel manufacture and assembly, strict enrichment segregation and other process controls are exercised.

The uranium dioxide powder is kept in sealed containers. The contents are fully identified both by descriptive tagging and unique barcode numbers. A quality control identification tag completely describing the contents is affixed to the containers before transfer to powder storage. Isotopic content is confirmed by analysis.

Powder withdrawal from storage can be made by only one authorized group, which directs the powder to the correct pellet production line. The pellet production lines are physically separated from each other, and pellets of only a single nominal enrichment and density are produced in a given production line at any given time.

Finished pellets are placed on trays identified with the same color code as the powder containers and transferred to segregated storage racks within the confines of the pelleting area. Samples from each pellet lot are tested for isotopic content and impurity levels prior to acceptance by quality control. Physical barriers are used to prevent mixing of pellets of different nominal densities and enrichments in the pellet storage area. Unused powder and substandard pellets are returned to storage in the original color-coded containers.

Loading of pellets into the clad is performed in isolated production lines; only one density and enrichment (with possible exception for top and bottom (axial blanket) zones) are loaded on a line at a time.

A serialized traceability code is placed on each fuel tube, which identifies the contract and enrichment. The end plugs are inserted and then welded (in an inert gas atmosphere) to seal the tube. The fuel tube remains coded and traceability identified until just prior to installation in the fuel assembly.

Similar traceability is provided for wet annular burnable absorber, source, and control rods, as required.

4.2.4.3 Letdown Radiation Monitoring

Radiation monitoring of the reactor coolant is made by grab samples and laboratory analysis of the primary coolant. Refer to information presented in Subsections 9.3.3 and 9.3.6, and Table 9.3.3-1.

4.2.4.4 In-core Control Component Testing and Inspection

Tests and inspections are performed on each reactivity control component to verify the mechanical characteristics. In the case of the rod cluster control assembly, prototype testing has been conducted. Manufacturing test/inspections and functional testing at the plant site are both performed.

During the component manufacturing phase, the following requirements apply to the reactivity control components to provide the proper functioning during reactor operation:

- Materials are procured to specifications to attain the desired standard of quality.
- Spider assemblies are proof-tested by applying a 5000-pound load to the spider body, so that approximately 310 pounds is applied to each vane. This proof load provides a bending moment at the spider body approximately equivalent to 1.4 times the load caused by the acceleration imposed by the control rod drive mechanism.
- Rods are checked for integrity by the applicable nondestructive methods described in Subsection 4.2.4.2.3.

- To confirm proper fit with the fuel assembly, the rod cluster control, discrete burnable absorber, and source assemblies are installed in the fuel assembly and checked for binding in the dry condition.

The rod cluster control assemblies and gray rod cluster assemblies are also functionally tested, following core loading but prior to criticality, to demonstrate reliable operation of the assemblies. Each assembly is operated (and tripped) one time at full-flow/hot conditions. In addition, any assembly that has a drop time greater than a two sigma limit from the average rod drop time is subjected to additional rod drops to confirm drop time. Thus, each assembly is sufficiently tested to confirm proper functioning and operation.

To demonstrate continuous free movement of the rod cluster control assemblies, and gray rod cluster assemblies, and to provide acceptable core power distributions during operations, partial movement checks are performed on every assembly as required by the technical specifications. In addition, periodic drop tests of the assemblies are performed at each refueling shutdown to demonstrate continued ability to meet trip time requirements.

If a rod cluster control assembly and/or gray rod cluster assembly cannot be moved by its mechanism, adjustments in the boron concentration of the coolant provide that adequate shutdown margin will be achieved following a trip. Thus, inability to move one assembly can be tolerated until the reactor can be safely taken to Mode 3. More than one inoperable assembly could be tolerated but would impose additional demands on the plant operator. Therefore, the number of inoperable assemblies has been limited to one.

4.2.4.5 Tests and Inspections by Others

For tests and inspections performed by others, Westinghouse reviews and approves the quality control procedures, and inspection plans to be utilized to confirm that they are equivalent to the description provided in Subsections 4.2.4.1 through 4.2.4.4 and are performed properly to meet Westinghouse requirements.

4.2.4.6 Inservice Surveillance

As detailed in WCAP-8183 (Reference 3), significant 17x17 fuel assembly operating experience has been obtained. A surveillance program is expected to be established for the AP1000 for inspection of post-irradiated fuel assemblies. This surveillance program will establish the schedule, guidelines, and inspection criteria for conducting visual inspection of post-irradiated fuel assemblies and/or insert components. The surveillance program includes a quantitative visual examination of some discharged fuel assemblies from each refueling. This program also includes criteria for additional inspection requirements for post-irradiated fuel assemblies if unusual characteristics are noticed in the visual inspection or if plant instrumentation and subsequent laboratory analysis indicates gross failed fuel. The post-irradiated fuel surveillance program will address disposition of fuel assemblies and/or insert components receiving an unsatisfactory visual inspection. Those post-irradiated fuel assemblies receiving an unsatisfactory visual inspection are not reinserted into the core until a more detailed inspection and/or evaluation can be performed. Normally the fuel assemblies are taken to the spent fuel inspection station.

4.2.4.7 Onsite Inspection

Written procedures are used for the post-shipment inspection of the new fuel assemblies in addition to reactivity control and source components. Fuel handling procedures specify the sequence in which handling and inspection take place.

Loaded fuel containers, when received onsite, are externally inspected to confirm that labels and markings are intact and security seals are unbroken. After the containers are opened, the shock indicators attached to the suspended internals are inspected to determine whether movement during transit exceeded design limitations.

Following removal of the fuel assembly from the container in accordance with detailed procedures, the fuel assembly plastic wrapper is examined for evidence of damage. The polyethylene wrapper is then removed, and a visual inspection of the entire fuel assembly is performed.

Control rod, gray rod, secondary source rod and discrete burnable absorber rod assemblies are usually shipped in fuel assemblies. They are inspected prior to removal of the fuel assembly from the container. The control rod assembly is withdrawn a few inches from the fuel assembly to confirm free and unrestricted movement, and the exposed section is visually inspected for mechanical integrity, replaced in the fuel assembly, and stored with the fuel assembly. Control rod, secondary source or discrete burnable absorber assemblies may be stored separately or within fuel assemblies in the new fuel storage area.

4.2.5 Combined License Information

Changes to the reference design of the fuel, burnable absorber rods, rod cluster control assemblies, or initial core design from that presented in the DCD are addressed in APP-GW-GLR-059 (Reference 24).

4.2.6 References

1. [*Davidson, S. L. (Ed.), "Fuel Criteria Evaluation Process," WCAP-12488-A (Proprietary) and WCAP-14204-A (Non-Proprietary), October 1994.*]*

2. Davidson, S. L. (Ed.) et al., "Extended Burnup Evaluation of Westinghouse Fuel," WCAP-10125-P-A (Proprietary) and WCAP-10126-NP-A (Non-Proprietary), December 1985.

3. "Operational Experience with Westinghouse Cores," WCAP-8183, (revised annually).

4. Beaumont, M. D., et al., "Properties of Fuel and Core Component Materials," WCAP-9179, Revision 1 (Proprietary) and WCAP-9224 (Non-Proprietary), July 1978.

5. Davidson, S. L., and Nuhfer, D. L. (Ed.), "VANTAGE+ Fuel Assembly Reference Core Report," WCAP-12610-P-A (Proprietary), June 1990 and WCAP-14342-A (Non-Proprietary), April 1995.

6. Hellman, J. M., Ed, "Fuel Densification Experimental Results and Model for Reactor Application," WCAP-8218-P-A (Proprietary) and WCAP-8219-A (Nonproprietary), March 1975.

7. Weiner, R. A., et al., "Improved Fuel Performance Models for Westinghouse Fuel Rod Design and Safety Evaluations," WCAP-10851-P-A (Proprietary) and WCAP-11873-A (Nonproprietary), August, 1988.

8. Davidson, S. L. (Ed) et al., "Assessment of Clad Flattening and Densification Power Spike Factor Elimination in Westinghouse Nuclear Fuel," WCAP-13589-A (Proprietary) and WCAP-14297-A (Non-Proprietary), March 1995.

*NRC Staff approval is required prior to implementing a change in this information.

9. Risher, D., et al., “Safety Analysis for the Revised Fuel Rod Internal Pressure Design Basis,” WCAP-8963-P-A (Proprietary), November 1976 and WCAP-8964-A (Non-Proprietary), August 1977.

10. Skarita, J., et al., “Westinghouse Wet Annular Burnable Absorber Evaluation Report,” WCAP-10021-P-A, Revision 1 (Proprietary) and WCAP-10377-NP-A, Revision 2 (Non-Proprietary), October 1983.

11. Davidson, S. L. (Ed.) et al., “Reference Core Report VANTAGE 5 Fuel Assembly,” WCAP-10444-P-A (Proprietary) and WCAP-10445-NP-A (Nonproprietary), September 1985.

12. ASTM-A-580-90, Specification for Stainless and Heat-resisting Steel Wire.

13. Demario, E. E., “Hydraulic Flow Test of the 17x17 Fuel Assembly,” WCAP-8278 (Proprietary) and WCAP-8279 (Non-Proprietary), February 1974.

14. Skaritka, J. (Ed.), “Fuel Rod Bow Evaluation,” WCAP-8691, Revision 1 (Proprietary) and WCAP-8692, Revision 1 (Non-Proprietary), July 1979.

15. Davidson, S. L. and Iorii, J. A., “Reference Core Report 17x17 Optimized Fuel Assembly,” WCAP-9500-P-A (Proprietary) and WCAP-9500-A (Nonproprietary), May 1982.

16. O’Donnell, W. J., and Langer, B. F., “Fatigue Design Basis for Zircaloy Components,” Nuclear Science and Engineering 20, pp 1-12, 1964.

17. Gesinski, L., and Chiang, D., “Safety Analysis of the 17x17 Fuel Assembly for Combined Seismic and Loss-of-Coolant Accident,” WCAP-8236 (Proprietary) and WCAP-8288 (Nonproprietary), December 1973.

18. Davidson, S. L., et al., “Verification, Testing, and Analysis of the 17x17 Optimized Fuel Assembly,” WCAP-9401-P-A (Proprietary) and WCAP-9402-A (Nonproprietary), August 1981.

19. Witt, F. J., Bamford, W. H., and Esselman, T. C., “Integrity of the Primary Piping Systems of Westinghouse Nuclear Power Plants During Postulated Seismic Events,” WCAP-9283 (Nonproprietary), March 1978.

20. ASTM-E-142-86, Methods for Controlling Quality of Radiographic Testing.

21. Foster, J. P., et al., “Westinghouse Improved Performance Analysis and Design Model (PAD 4.0),” WCAP-15063-P-A, Revision 1 (Proprietary) and WCAP-15064-NP-A, Revision 1 (Non-Proprietary), July 2000.

22. George, R. A., et al., “Revised Clad Flattening Model,” WCAP-8377 (Proprietary), July 1974.

23. WCAP-7113, “Use of Burnable Poison Rods in Westinghouse Pressurized Water Reactors,” October 1967.

24. APP-GW-GLR-059/WCAP-16652-NP, “AP1000 Core & Fuel Design Technical Report,” Revision 0.

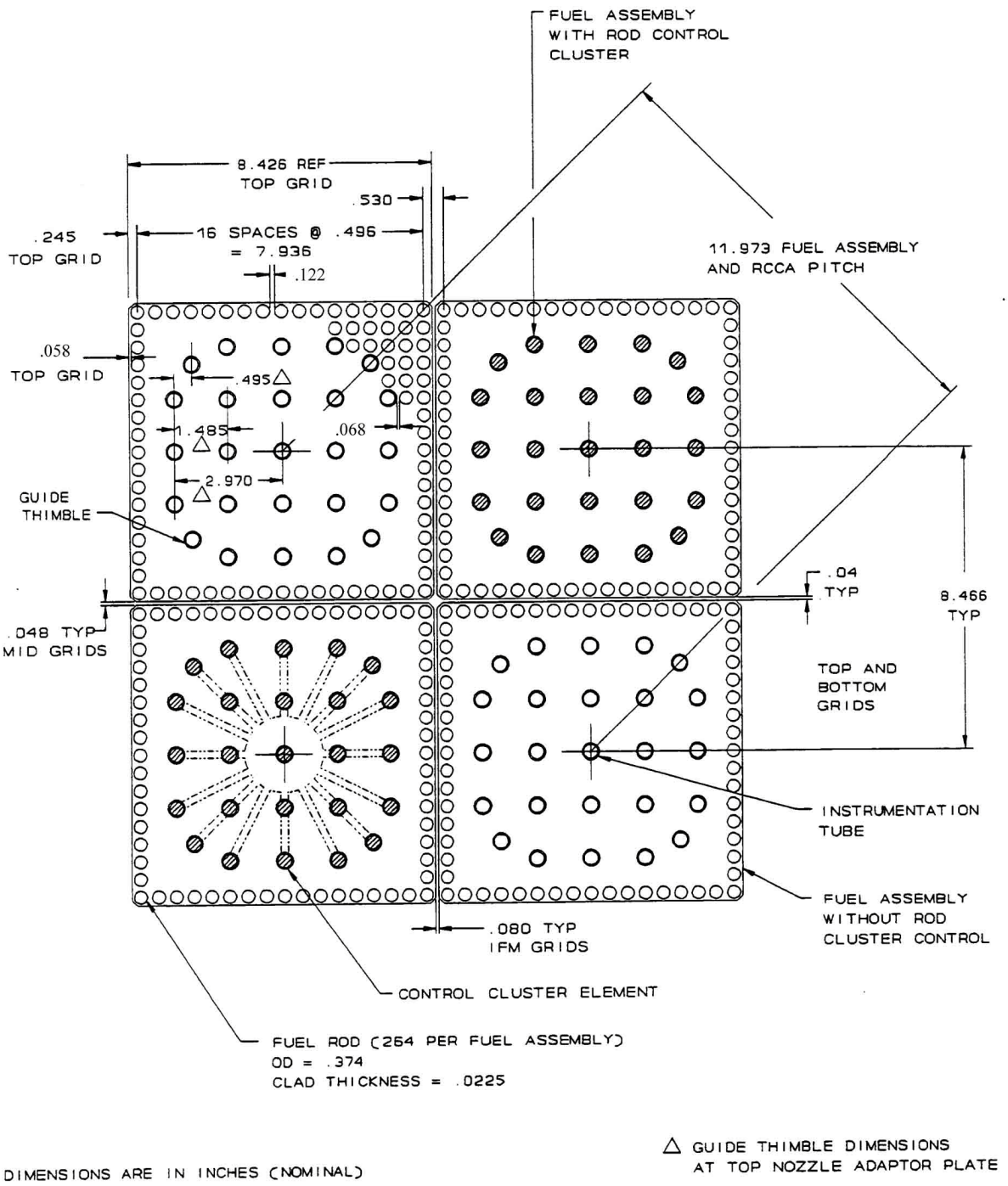

Figure 4.2-1
Fuel Assembly Cross-Section

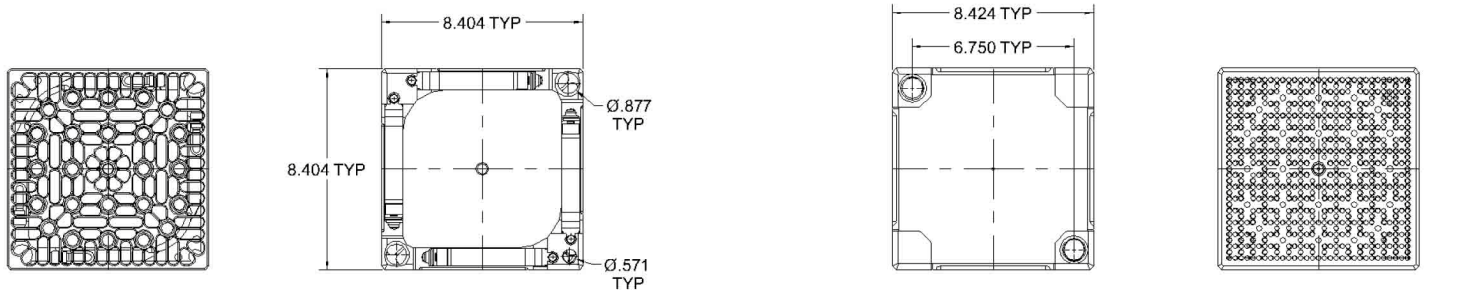

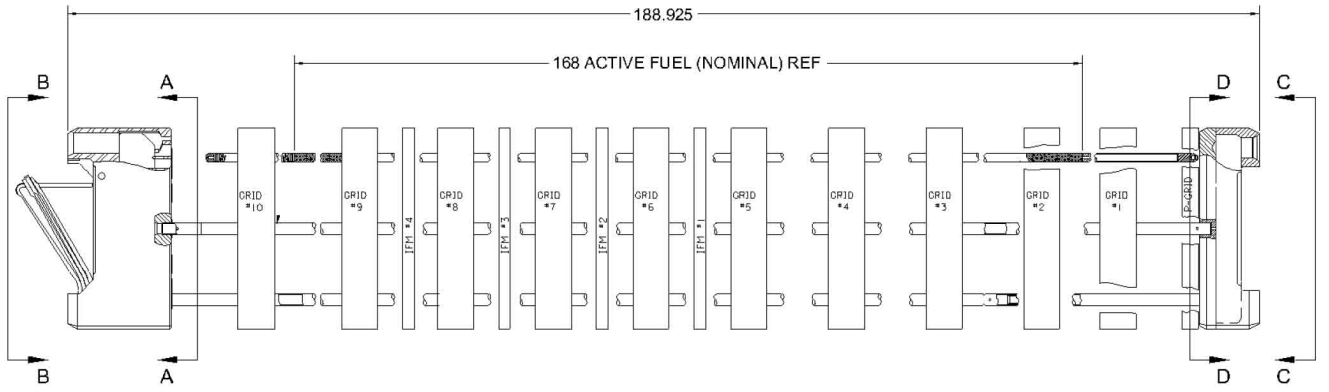

DIMENSIONS ARE IN INCHES (NOMINAL)

Figure 4.2-2
Fuel Assembly Outline

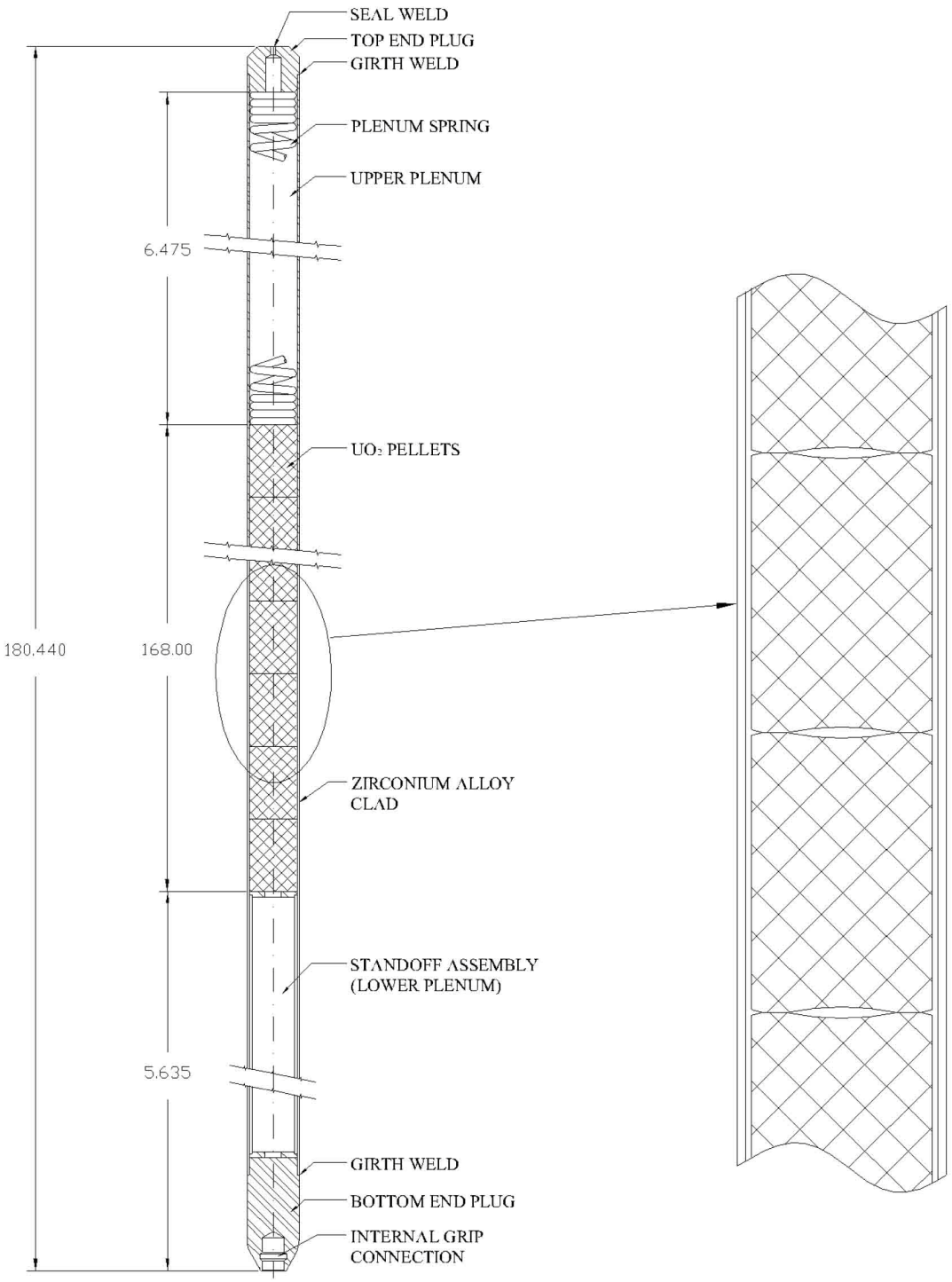

Figure 4.2-3
Fuel Rod Schematic

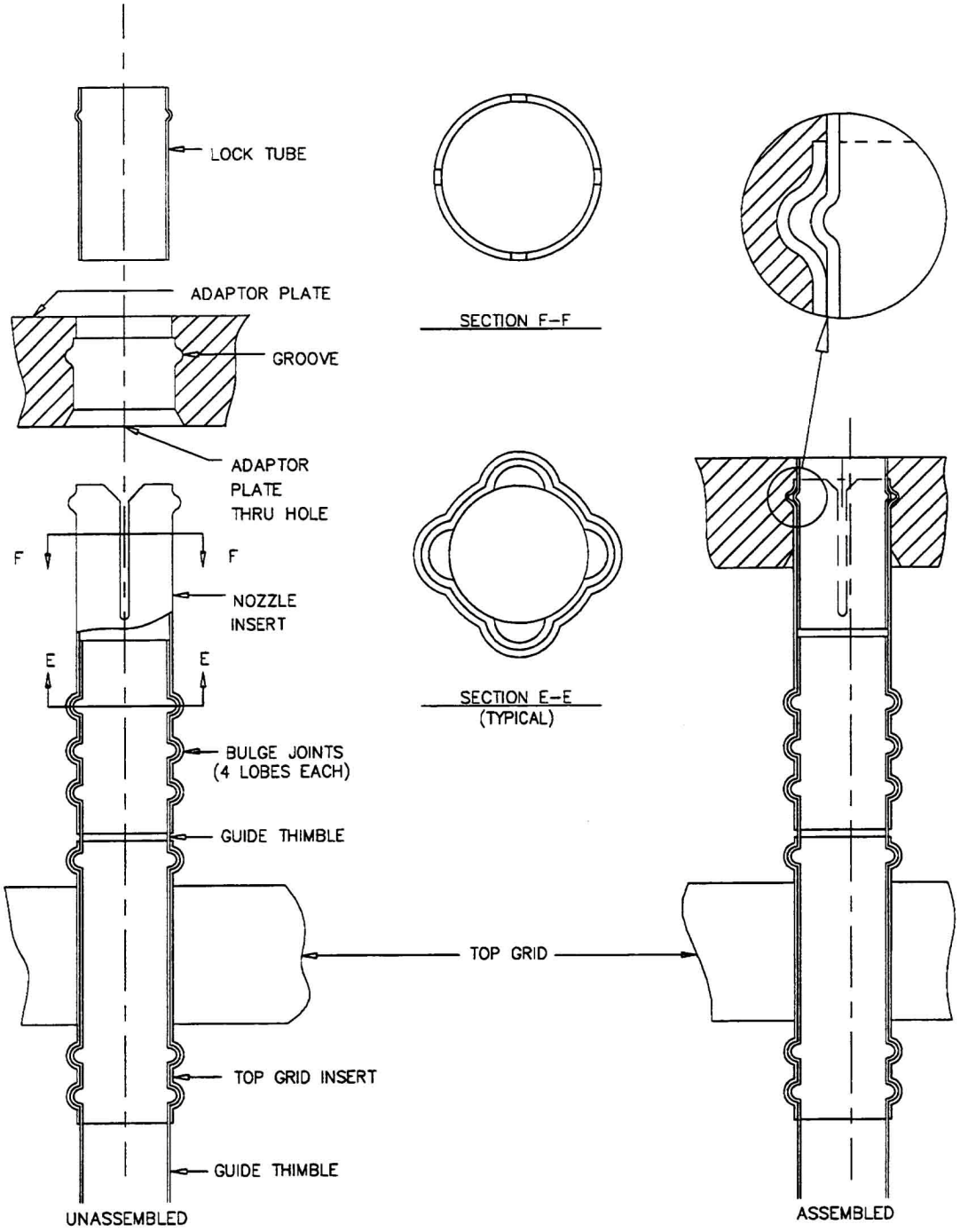

Figure 4.2-4
Top Grid Sleeve Detail

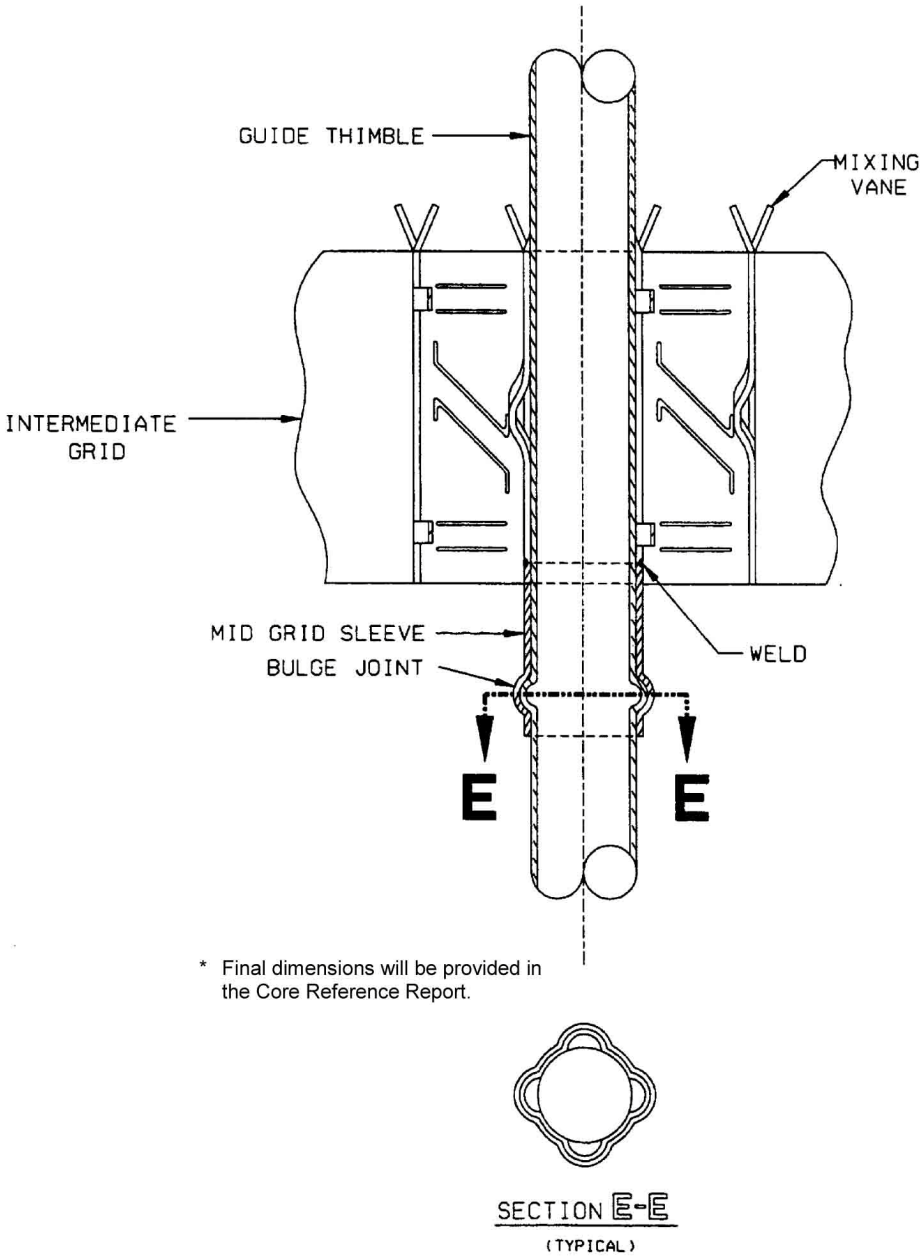

Figure 4.2-5
Intermediate Grid to Thimble Attachment Joint

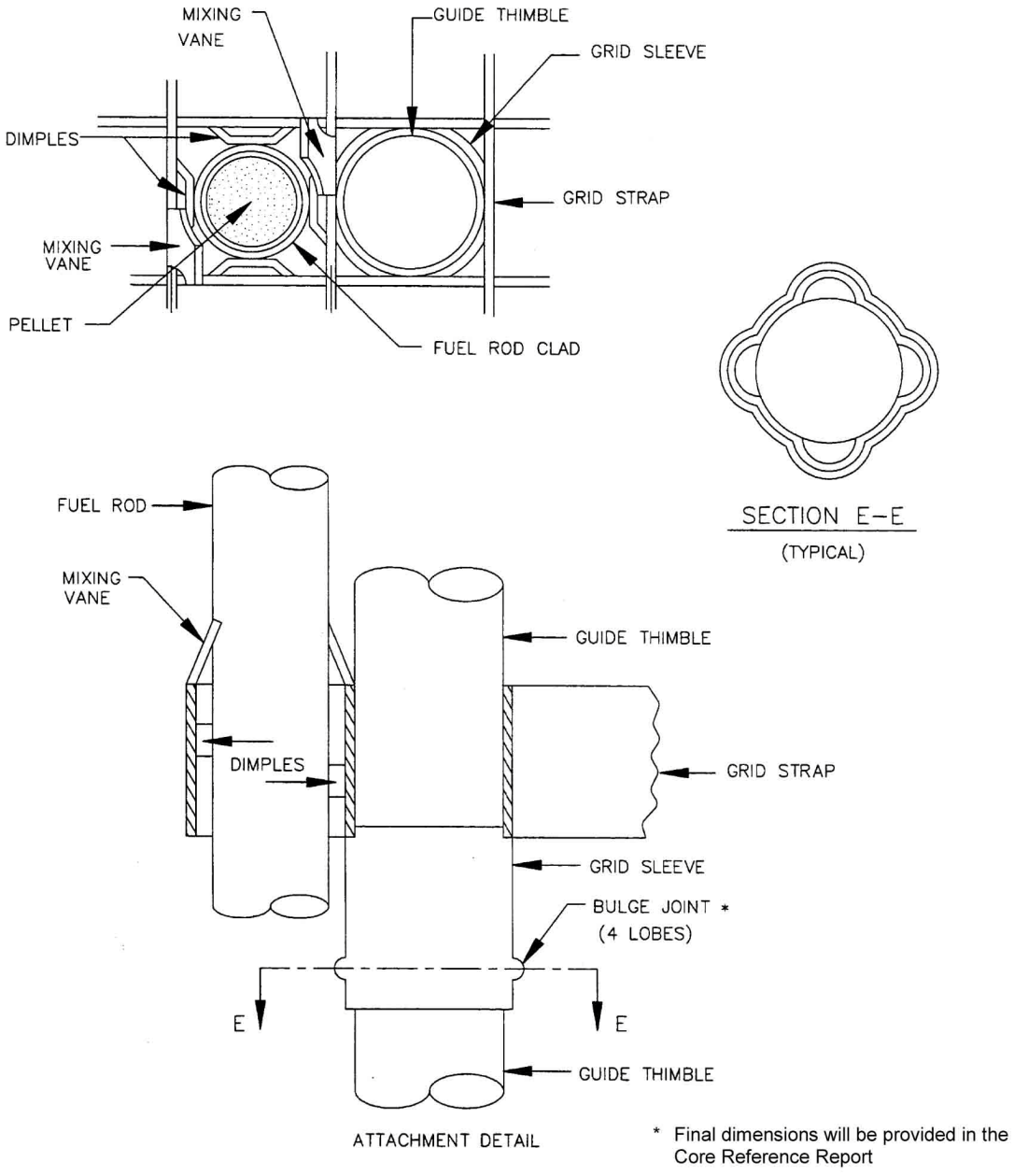

Figure 4.2-6
Intermediate Flow Mixer
Grid to Thimble Attachment

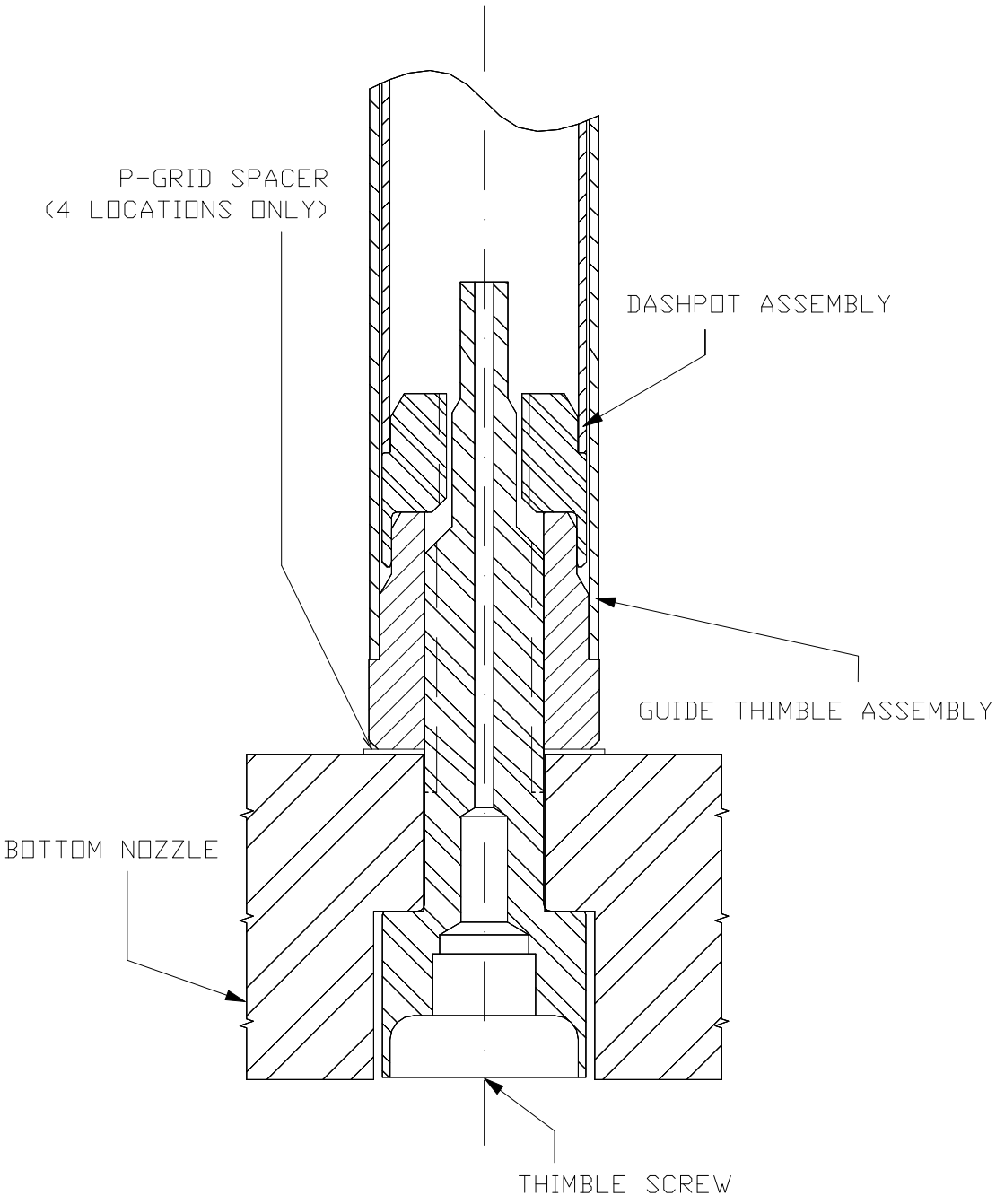

Figure 4.2-7
Grid Thimble to Bottom Nozzle Joint

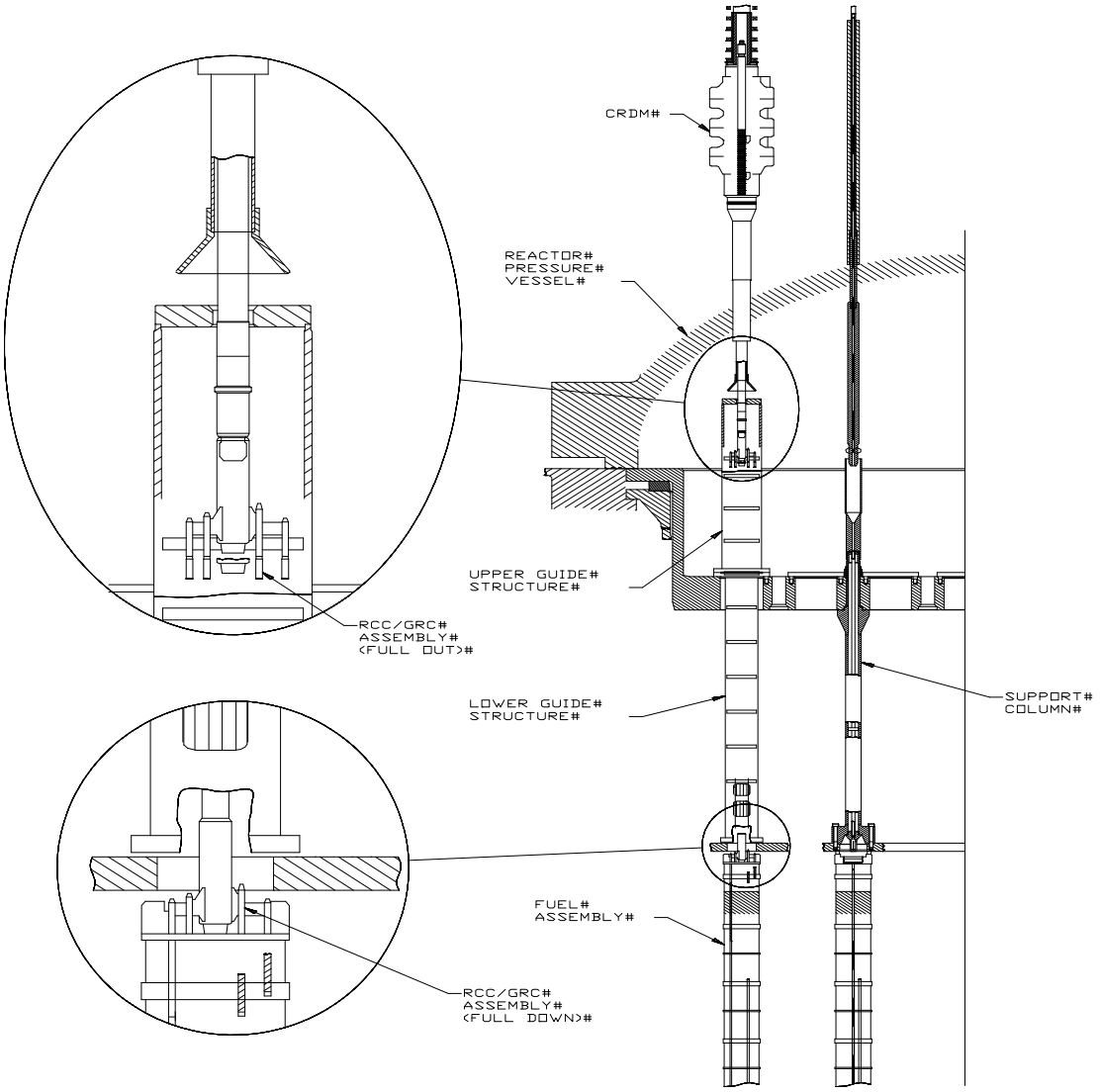

Figure 4.2-8
Rod Cluster Control and Drive Rod
Assembly With Interfacing Components

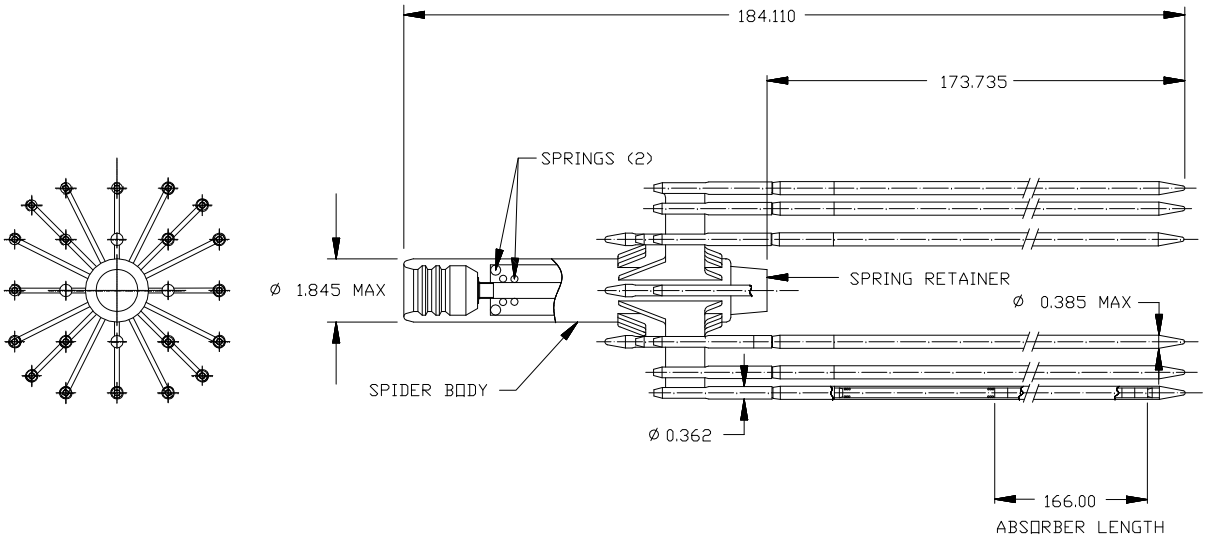

Figure 4.2-9
Rod Cluster Control Assembly

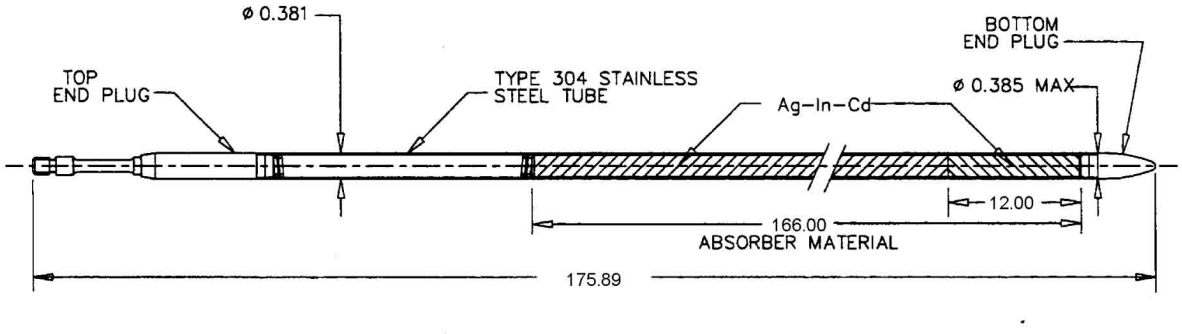

DIMENSIONS ARE IN INCHES (NOMINAL)
UNLESS OTHERWISE NOTED

Figure 4.2-10
Absorber Rod Detail

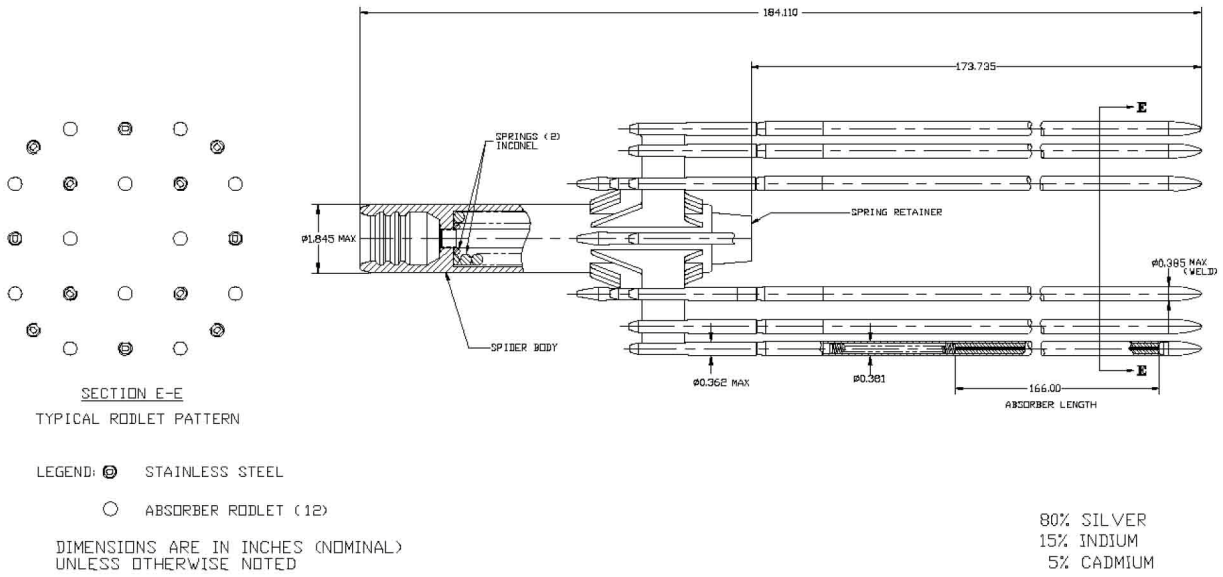

Figure 4.2-11
Gray Rod Cluster Assembly

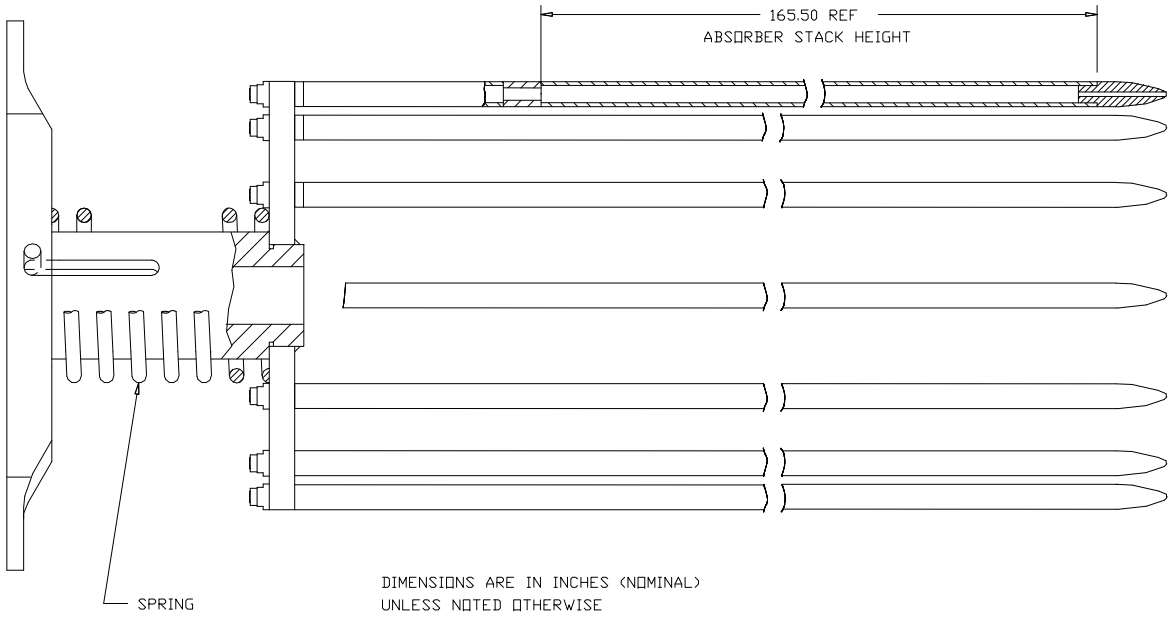

Figure 4.2-12
Discrete Burnable Absorber Assembly

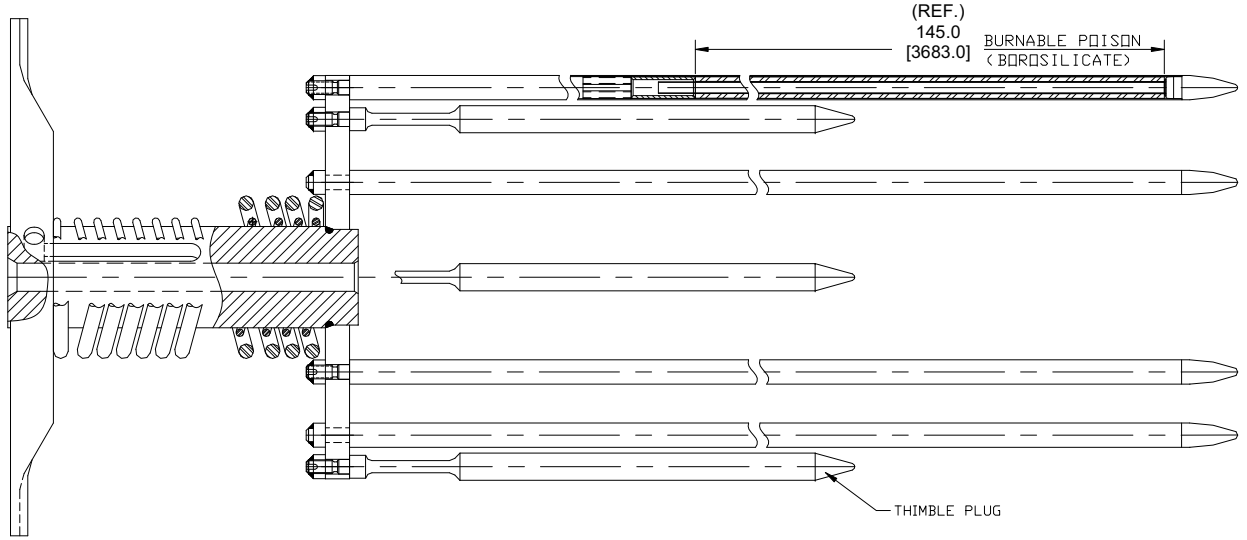

Figure 4.2-13
Burnable Absorber Rod Assembly
(Pyrex) Borosilicate Glass

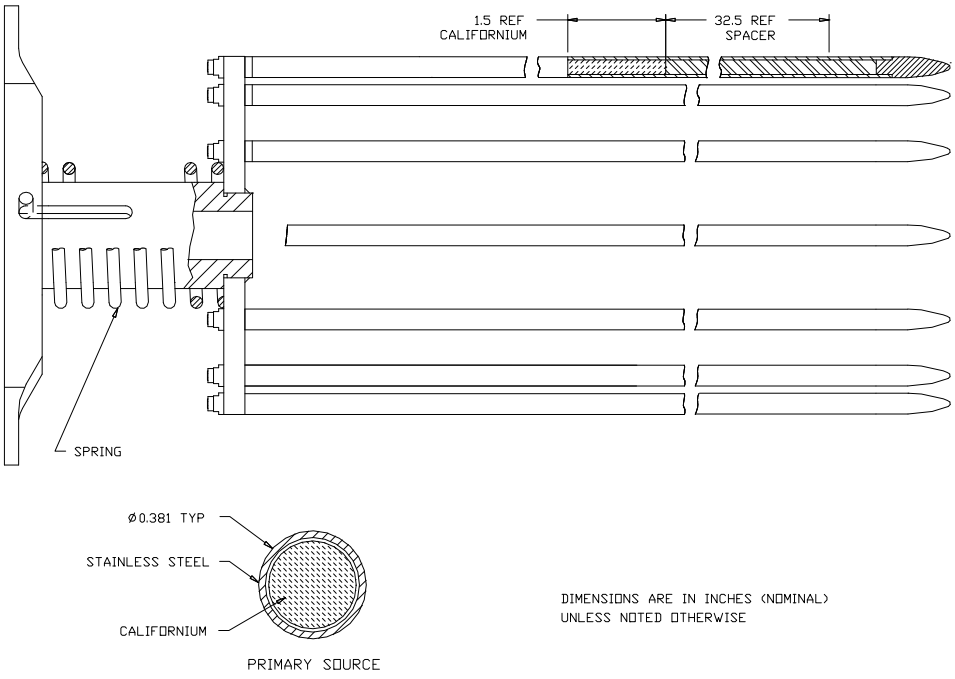

Figure 4.2-14
Primary Source Assembly

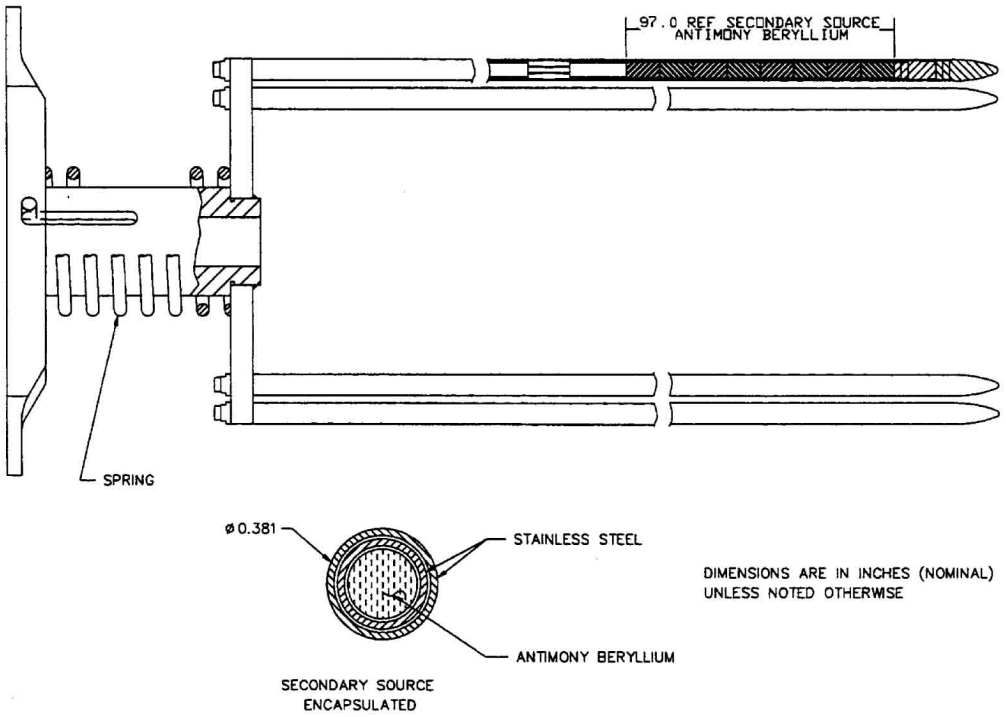

Figure 4.2-15
Secondary Source Assembly

4.3 Nuclear Design

4.3.1 Design Basis

This section describes the design bases and functional requirements used in the nuclear design of the fuel and reactivity control system and relates these design bases to the General Design Criteria (GDC). The design bases are the fundamental criteria that must be met using approved analytical techniques. [*Enhancements to these techniques may be made provided that the changes are founded by NRC approved methodologies as discussed in*]* WCAP-9272-P-A (Reference 1) and [*WCAP-12488-P-A (Reference 2).*]*

The plant conditions for design are divided into four categories:

- Condition I — Normal operation and operational transients
- Condition II — Events of moderate frequency
- Condition III — Infrequent incidents
- Condition IV — Limiting faults

The reactor is designed so that its components meet the following performance and safety criteria:

- In general, Condition I occurrences are accommodated with margin between any plant parameter and the value of that parameter which would require either automatic or manual protective action.
- Condition II occurrences are accommodated with, at most, a shutdown of the reactor with the plant capable of returning to operation after corrective action.
- Fuel damage, that is, breach of fuel rod clad pressure boundary, is not expected during Condition I and Condition II occurrences. A very small amount of fuel damage may occur. This is within the capability of the chemical and volume control system (CVS) and is consistent with the plant design basis.
- Condition III occurrences do not cause more than a small fraction of the fuel elements in the reactor to be damaged, although sufficient fuel element damage might occur to preclude immediate resumption of operation.
- The release of radioactive material due to Condition III occurrences is not sufficient to interrupt or restrict public use of those areas beyond the exclusion area boundary.
- A Condition III occurrence does not by itself generate a Condition IV occurrence or result in a consequential loss of function of the reactor coolant or reactor containment barriers.
- Condition IV faults do not cause a release of radioactive material that results in exceeding the dose limits identified in Chapter 15. Condition IV occurrences are faults that are not expected to occur but are defined as limiting faults which are included in the design.

The core design power distribution limits related to fuel integrity are met for Condition I occurrences through conservative design and are maintained by the action of the control system.

The requirements for Condition II occurrences are met by providing an adequate protection system which monitors reactor parameters.

*NRC Staff approval is required prior to implementing a change in this information.

The control and protection systems are described in Chapter 7.

The consequences of Condition II, III, and IV occurrences are described in Chapter 15.

4.3.1.1 Fuel Burnup

4.3.1.1.1 Basis

A limitation on initial installed excess reactivity or average discharge burnup is not required other than as is quantified in terms of other design bases, such as overall negative power reactivity feedback discussed below. [*The NRC has approved, in WCAP-12488-P-A (Reference 2), maximum fuel rod average burnup of 60,000 MWD/MTU. Extended burnup to 62,000 MWD/MTU has been established in Reference 61.*]*

4.3.1.1.2 Discussion

Fuel burnup is a measure of fuel depletion which represents the integrated energy output of the fuel in megawatt-days per metric ton of uranium (MWD/MTU) and is a useful means for quantifying fuel exposure criteria.

The core design lifetime, or design discharge burnup, is achieved by installing sufficient initial excess reactivity in each fuel region and by following a fuel replacement program (such as that described in Subsection 4.3.2) that meets the safety-related criteria in each cycle of operation.

Initial excess reactivity installed in the fuel, although not a design basis, must be sufficient to maintain core criticality at full-power operating conditions throughout cycle life with equilibrium xenon, samarium, and other fission products present. Burnable absorbers, control rod insertion, and/or chemical shim are used to compensate for the excess reactivity. The end of design cycle life is defined to occur when the chemical shim concentration is essentially zero with control rods present to the degree necessary for operational requirements. In terms of soluble boron concentration, this corresponds to approximately 10 ppm with the control and gray rods essentially withdrawn.

4.3.1.2 Negative Reactivity Feedbacks (Reactivity Coefficients)

4.3.1.2.1 Basis

For the initial fuel cycle, the fuel temperature coefficient will be negative, and the moderator temperature coefficient of reactivity will be negative for power operating conditions, thereby providing negative reactivity feedback characteristics. The design basis meets General Design Criterion 11.

4.3.1.2.2 Discussion

When compensation for a rapid increase in reactivity is considered, there are two major effects. These are the resonance absorption (Doppler) effects associated with changing fuel temperature and the neutron spectrum and reactor composition change effects resulting from changing moderator density. These basic physics characteristics are often identified by reactivity coefficients. The use of slightly enriched uranium results in a Doppler coefficient of reactivity that is negative. This coefficient provides the most rapid reactivity compensation. The initial core is also designed to have an overall negative moderator temperature coefficient of reactivity during power operation so that average coolant temperature changes or void content provides another, slower compensatory effect. For some core designs, if the compensation for excess reactivity is provided only by chemical shim, the moderator temperature coefficient could become positive. Nominal power operation is permitted only in a range of overall negative moderator temperature coefficient. The negative moderator temperature coefficient can be achieved through the use of discrete burnable absorbers (BAs) and/or

*NRC Staff approval is required prior to implementing a change in this information.

integral fuel burnable absorbers and/or control rods by limiting the reactivity controlled by soluble boron.

Burnable absorber content (quantity and distribution) is not stated as a design basis. However, for some reloads, the use of burnable absorbers may be necessary for power distribution control and/or to achieve an acceptable moderator temperature coefficient throughout core life. The required burnable absorber loading is that which is required to meet design criteria.

4.3.1.3 Control of Power Distribution

4.3.1.3.1 Basis

The nuclear design basis is that, with at least a 95 percent confidence level:

- The fuel will not operate with a power distribution that would result in exceeding the departure from nucleate boiling (DNB) design basis (i.e., the departure from nucleate boiling ratio (DNBR) shall be greater than the design limit departure from nucleate boiling ratio as discussed in Subsection 4.4.1) under Condition I and II occurrences, including the maximum overpower condition.

- Under abnormal conditions, including the maximum overpower condition, the peak linear heat rate (PLHR) will not cause fuel melting, as defined in Subsection 4.4.1.2.

- Fuel management will be such as to produce values of fuel rod power and burnup consistent with the assumptions in the fuel rod mechanical integrity analysis of Section 4.2.

- The fuel will not be operated at Peak Linear Heat Rate (PLHR) values greater than those found to be acceptable within the body of the safety analysis under normal operating conditions, including an allowance of one percent for calorimetric error (calorimetric uncertainty calculation will be provided per Subsection 15.0.15.1).

The above basis meets General Design Criterion 10.

4.3.1.3.2 Discussion

Calculation of extreme power shapes which affect fuel design limits are performed with proven methods. The conditions under which limiting power shapes are assumed to occur are chosen conservatively with regard to any permissible operating state. Even though there is close agreement between calculated peak power and measurements, a nuclear uncertainty is applied (Subsection 4.3.2.2.1) to calculated power distribution. Such margins are provided both for the analysis for normal operating states and for anticipated transients.

4.3.1.4 Maximum Controlled Reactivity Insertion Rate

4.3.1.4.1 Basis

The maximum reactivity insertion rate due to withdrawal of rod cluster control assemblies (RCCAs) or gray rod cluster assemblies (GRCAs) or by boron dilution is limited by plant design, hardware, and basic physics. During normal power operation, the maximum controlled reactivity insertion rate is limited. The maximum reactivity change rate for accidental withdrawal of two control banks is set such that PLHR and the departure from nucleate boiling ratio limitations are not challenged. This satisfies General Design Criterion 25.

The maximum reactivity worth of control rods and the maximum rates of reactivity insertion employing control rods are limited to preclude rupture of the coolant pressure boundary or disruption of the core internals to a degree which would impair core cooling capacity due to a rod withdrawal or an ejection accident. (See Chapter 15).

Following any Condition IV occurrence, such as rod ejection or steam line break, the reactor can be brought to the shutdown condition, and the core maintains acceptable heat transfer geometry. This satisfies General Design Criterion 28.

4.3.1.4.2 Discussion

Reactivity addition associated with an accidental withdrawal of a control bank (or banks) is limited by the maximum rod speed (or travel rate) and by the worth of the bank(s). For this reactor, the maximum control and gray rod speed is 45 inches per minute.

The reactivity change rates are conservatively calculated, assuming unfavorable axial power and xenon distributions. The typical peak xenon burnout rate is significantly lower than the maximum reactivity addition rate for normal operation and for accidental withdrawal of two banks.

4.3.1.5 Shutdown Margins

4.3.1.5.1 Basis

Minimum shutdown margin as specified in the technical specifications is required in all operating modes.

In analyses involving reactor trip, the single, highest worth rod cluster control assembly is postulated to remain untripped in its full-out position (stuck rod criterion). This satisfies General Design Criterion 26.

4.3.1.5.2 Discussion

Two independent reactivity control systems are provided: control rods and soluble boron in the coolant. The control rods provide reactivity changes which compensate for the reactivity effects of the fuel and water density changes accompanying power level changes over the range from full load to no load. The control rods provide the minimum shutdown margin under Condition I occurrences and are capable of making the core subcritical rapidly enough to prevent exceeding acceptable fuel damage limits (very small number of rod failures), assuming that the highest worth control rod is stuck out upon trip.

The boron system can compensate for xenon burnout reactivity changes and maintain the reactor in the cold shutdown condition. Thus, backup and emergency shutdown provisions are provided by mechanical and chemical shim control systems which satisfy General Design Criterion 26. Reactivity changes due to fuel depletion are accommodated with the boron system.

4.3.1.5.3 Basis

When fuel assemblies are in the pressure vessel and the vessel head is not in place, keff will be maintained at or below 0.95 with control rods and soluble boron. Further, the fuel will be maintained sufficiently subcritical that removal of the rod cluster control assemblies will not result in criticality.

4.3.1.5.4 Discussion

ANSI N18.2 (Reference 3) specifies a keff not to exceed 0.95 in spent fuel storage racks and transfer equipment flooded with pure water and a keff not to exceed 0.98 in normally dry new fuel storage racks, assuming optimum moderation. No criterion is given for the refueling operation. However, a five percent margin, which is consistent with spent fuel storage and transfer and the new fuel storage, is adequate for the controlled and continuously monitored operations involved.

The boron concentration required to meet the refueling shutdown criteria is specified in the Core Operating Limits Report (COLR). Verification that these shutdown criteria are met, including uncertainties, is achieved using standard design methods. The subcriticality of the core is continuously monitored as described in the technical specifications.

4.3.1.6 Stability

4.3.1.6.1 Basis

The core will be inherently stable to power oscillations at the fundamental mode. This satisfies General Design Criterion 12.

Spatial power oscillations within the core with a constant core power output, should they occur, can be reliably and readily detected and suppressed.

4.3.1.6.2 Discussion

Oscillations of the total power output of the core, from whatever cause, are readily detected by the loop temperature sensors and by the nuclear instrumentation. The core is protected by these systems; a reactor trip occurs if power increases unacceptably, thereby preserving the design margins to fuel design limits. The combined stability of the turbine, steam generator and the reactor power control systems are such that total core power oscillations are not normally possible. The redundancy of the protection circuits results in a low probability of exceeding design power levels.

The core is designed so that diametral and azimuthal oscillations due to spatial xenon effects are self-damping; no operator action or control action is required to suppress them. The stability to diametral oscillations is so great that this excitation is highly improbable. Convergent azimuthal oscillations can be excited by prohibited motion of individual control rods.

Indications of power distribution anomalies are continuously available from an online core monitoring system. The online monitoring system processes information provided by the fixed in-core detectors, in-core thermocouples, and loop temperature measurements. Radial power distributions are therefore continuously monitored, thus power oscillations are readily observable and alarmed. The ex-core long ion chambers also provide surveillance and alarms of anomalous power distributions. In proposed core designs, these horizontal plane oscillations are self-damping by virtue of reactivity feedback effects inherent to the basic core physics.

Axial xenon spatial power oscillations may occur during core life, especially late in the cycle. The online core monitoring system provides continuous surveillance of the axial power distributions. The control rod system provides both manual and automatic control systems for controlling the axial power distributions.

Confidence that fuel design limits are not exceeded is provided by reactor protection system overpower ΔT (OPΔT) and overtemperature ΔT (OTΔT) trip functions, which use the loop temperature sensors, pressurizer pressure indication, and measured axial offset as an input. Detection and suppression of xenon oscillations are discussed in Subsection 4.3.2.7.

4.3.1.7 Anticipated Transients Without Scram (ATWS)

The AP1000 diverse reactor trip actuation system is independent of the reactor trip breakers used by the protection monitoring system. The diverse reactor trip reduces the probability and consequences of a postulated ATWS. The effects of anticipated transients with failure to trip are not considered in the design bases of the plant. Analysis has shown that the likelihood of such a hypothetical event is negligibly small. Furthermore, analysis of the consequences of a hypothetical failure to trip following anticipated transients has shown that no significant core damage would result, system peak pressures should be limited to acceptable values, and no failure of the reactor coolant system would result. (See WCAP-8330, Reference 5). The process used to evaluate the ATWS risk in compliance with 10 CFR 50.62 is described in Section 15.8.

4.3.2 Description

4.3.2.1 Nuclear Design Description

The reactor core consists of a specified number of fuel rods held in bundles by spacer grids and top and bottom fittings. The fuel rods are fabricated from cylindrical tubes made of zirconium based alloy(s) containing uranium dioxide fuel pellets. The bundles, known as fuel assemblies, are arranged in a pattern which approximates a right circular cylinder.

Each fuel assembly contains a 17 x 17 rod array composed nominally of 264 fuel rods, 24 rod cluster control thimbles, and an in-core instrumentation thimble. Figure 4.2-1 shows a cross-sectional view of a 17 x 17 fuel assembly and the related rod cluster control guide thimble locations. Detailed descriptions of the AP1000 fuel assembly design features are given in Section 4.2.

For initial core loading, the fuel rods within a given assembly have the same uranium enrichment in both the radial and axial planes. Fuel assemblies of three different enrichments are used in the initial core loading to establish a favorable radial power distribution. Figure 4.3-1 shows the fuel loading pattern used in the initial cycle. Two regions consisting of the two lower enrichments are interspersed to form a checkerboard pattern in the central portion of the core. The third region is arranged around the periphery of the core and contains the highest enrichment. The enrichments for the initial cycle are shown in Table 4.3-1. Axial blankets consisting of fuel pellets of reduced enrichment placed at the ends of the enriched pellet stack have been considered and may be used in reload cycles. Axial blankets are included in the design basis to reduce neutron leakage and to improve fuel utilization.

Reload core loading patterns can employ various fuel management techniques including “low-leakage” designs where the feed fuel is interspersed checkerboard-style in the core interior and depleted fuel is placed on the periphery. Reload core designs, as well as the initial cycle design, are anticipated to operate approximately 18 months between refueling, accumulating a cycle burnup of approximately 21,000 MWD/MTU. The exact reloading pattern, the initial and final positions of assemblies, and the number of fresh assemblies and their placement are dependent on the energy requirement for the reload cycle and burnup and power histories of the previous cycles.

The core average enrichment is determined by the amount of fissionable material required to provide the desired energy requirements. The physics of the burnout process is such that operation of the reactor depletes the amount of fuel available due to the absorption of neutrons by the U-235 atoms and their subsequent fission. In addition, the fission process results in the formation of fission products, some of which readily absorb neutrons. These effects, the depletion and the buildup of fission products, are partially offset by the buildup of plutonium shown in Figure 4.3-2 for a typical 17 x 17 fuel assembly, which occurs due to the parasitic absorption of neutrons in U-238. Therefore, at the beginning of any cycle a reactivity reserve equal to the depletion of the fissionable fuel and the buildup of fission product poisons less the buildup of fissile fuel over the specified cycle life is built into the reactor. This excess reactivity is controlled by removable neutron-absorbing material in the

form of boron dissolved in the primary coolant, control rod insertion, burnable absorber rods, and/or integral fuel burnable absorbers (IFBA). The stack length of the burnable absorber rods and/or integral absorber bearing fuel may vary for different core designs, with the optimum length determined on a design specific basis. Figure 4.3-3 is a plot of the initial core soluble boron concentration versus core depletion.

The concentration of the soluble neutron absorber is varied to compensate for reactivity changes due to fuel burnup, fission product poisoning including xenon and samarium, burnable absorber depletion, and the cold-to-operating moderator temperature change. Throughout the operating range, the CVS is designed to provide changes in reactor coolant system (RCS) boron concentration to compensate for the reactivity effects of fuel depletion, peak xenon burnout and decay, and cold shutdown boration requirements.

Burnable absorbers are strategically located to provide a favorable radial power distribution and provide for negative reactivity feedback. Figures 4.3-4a and 4.3-4b show the burnable absorber distributions within a fuel assembly for the several patterns used in a 17 x 17 array. The initial core burnable absorber loading pattern is shown in Figure 4.3-5.

Tables 4.3-1 through 4.3-3 contain summaries of reactor core design parameters including reactivity coefficients, delayed neutron fraction, and neutron lifetimes. Sufficient information is included to permit an independent calculation of the nuclear performance characteristics of the core.

4.3.2.2 Power Distribution

The accuracy of power distribution calculations has been confirmed through approximately 1000 flux maps under conditions very similar to those expected. Details of this confirmation are given in WCAP-7308-L-P-A (Reference 7) and in Subsection 4.3.2.2.7.

4.3.2.2.1 Definitions

Relative power distributions within the reactor are quantified in terms of hot channel factors. These hot channel factors are normalized ratios of maximal absolute power generation rates and are a measure of the peak pellet power within the reactor core relative to the average pellet (F_Q) and the energy produced in a coolant channel relative to the core average channel ($F_{\Delta H}$). Absolute power generation rates are expressed in terms of quantities related to the nuclear or thermal design; more specifically, volumetric power density (qvol) is the thermal power produced per unit volume of the core (kW/liter).

Linear heat rate (LHR) is the thermal power produced per unit length of active fuel (kW/ft). Since fuel assembly geometry is standardized, LHR is the unit of absolute power density most commonly used. For practical purposes, LHR differs from qvol by a constant factor which includes geometry effects and the heat flux deposition fraction. The peak linear heat rate (PLHR) is defined as the maximum linear heat rate occurring throughout the reactor. PLHR directly impacts fuel temperatures and decay power levels thus being a significant safety analysis parameter.

Average linear heat rate (ALHR) is the total thermal power produced in the fuel rods expressed as heat flux divided by the total active fuel length of the rods in the core.

Local heat flux is the heat flux at the surface of the cladding (Btu/hr-ft^2). For nominal rod parameters, this differs from linear heat rate by a constant factor.

Rod power is the total power generated in one rod (kW).

Average rod power is the total thermal power produced in the fuel rods divided by the number of fuel rods (assuming the rods have equal length).

The hot channel factors used in the discussion of power distributions in this section are defined as follows:

F_Q , **heat flux hot channel factor**, is defined as the maximum local heat flux on the surface of a fuel rod divided by the average fuel rod heat flux, allowing for manufacturing tolerances on fuel pellets and rods.

F^N_Q , **nuclear heat flux hot channel factor**, is defined as the maximum local fuel rod linear heat rate divided by the average fuel rod linear heat rate, assuming nominal fuel pellet and rod parameters.

F^E_Q , **engineering heat flux hot channel factor**, is the allowance on heat flux required for manufacturing tolerances. The engineering factor allows for local variations in enrichment, pellet density and diameter, burnable absorber content, surface area of the fuel rod, and eccentricity of the gap between pellet and clad. Combined statistically, the net effect is a factor of 1.03 to be applied to the fuel rod surface heat flux.

$F^N_{\Delta H}$, **nuclear enthalpy rise hot channel factor**, is defined as the ratio of the maximum integrated rod power within the core to the average rod power.

Manufacturing tolerances, hot channel power distribution, and surrounding channel power distributions are treated explicitly in the calculation of the departure from nucleate boiling ratio described in Section 4.4.

It is convenient for the purposes of discussion to define subfactors of F_Q . However, design limits are set in terms of the total peaking factor.

F_Q = total peaking factor or heat flux hot channel factor = $\frac{PLHR}{ALHR}$

Without densification effects:

$$F_Q = F^N_Q \times F^E_Q = F^N_{XY} \times F^N_Z \times F^N_U \times F^E_Q$$

where F^N_Q and F^E_Q are defined above and:

F^N_U = factor for calculational uncertainty, assumed to be 1.05.

F^N_{XY} = ratio of peak power density to average power density in the horizontal plane of peak local power.

F^N_Z = ratio of the power per unit core height in the horizontal plane of peak local power to the average value of power per unit core height. If the plane of peak local power coincides with the plane of maximum power per unit core height, then F^N_Z is the core average axial peaking factor.

4.3.2.2.2 Radial Power Distributions

The power shape in horizontal sections of the core at full power is a function of the fuel assembly and burnable absorber loading patterns, the control rod pattern, and the fuel burnup distribution. Thus, at any time in the cycle, a horizontal section of the core can be characterized as unrodded or with control rods. These two situations combined with burnup effects determine the radial power shapes

which can exist in the core at full power. Typical first cycle values of $F_{\Delta H}^{N}$, the nuclear enthalpy rise hot channel factors from beginning of life (BOL) to end of life (EOL) are given in Table 4.3-2. The effects on radial power shapes of power level, xenon, samarium, and moderator density effects are also considered, but these are quite small. The effect of nonuniform flow distribution is negligible. While radial power distributions in various planes of the core are often illustrated, since the moderator density is directly proportional to enthalpy, the core radial enthalpy rise distribution, as determined by the integral of power up each channel, is of greater interest. Figures 4.3-6 through 4.3-11 show typical normalized power density distributions for one-eighth of the core for representative operating conditions. These conditions are as follows:

- Hot full power (HFP) near beginning of life, unrodded, no xenon
- Hot full power near beginning of life, unrodded, equilibrium xenon
- Hot full power near beginning of life, gray bank MA+MB in, equilibrium xenon
- Hot full power near middle of life (MOL), unrodded equilibrium xenon
- Hot full power near end of life, unrodded, equilibrium xenon
- Hot full power near end of life, gray bank MA+MB in, equilibrium xenon

Since the position of the hot channel varies from time to time, a single-reference radial design power distribution is selected for departure from nucleate boiling calculations. This reference power distribution is chosen conservatively to concentrate power in one area of the core, minimizing the benefits of flow redistribution. Assembly powers are normalized to core average power. The radial power distribution within a fuel rod and its variation with burnup as utilized in thermal calculations and fuel rod design are discussed in Section 4.4.

4.3.2.2.3 Assembly Power Distributions

For the purpose of illustration, typical rodwise power distributions from the beginning of life and end of life conditions corresponding to Figures 4.3-7 and 4.3-10, respectively, are given for the same assembly in Figures 4.3-12 and 4.3-13, respectively.

Since the detailed power distribution surrounding the hot channel varies from time to time, a conservatively flat radial assembly power distribution is assumed in the departure from nucleate boiling analysis, described in Section 4.4, with the rod of maximum integrated power artificially raised to the design value of $F_{\Delta H}^{N}$. Care is taken in the nuclear design of the fuel cycles and operating conditions to confirm that a flatter assembly power distribution does not occur with limiting values of $F_{\Delta H}^{N}$.

4.3.2.2.4 Axial Power Distributions

The distribution of power in the axial or vertical direction is largely under the control of the operator through either the manual operation of the control rods or the automatic motion of control rods in conjunction with manual operation of the chemical and volume control system. The automated mode of operation is referred to as mechanical shim (MSHIM) and is discussed in Subsection 4.3.2.4.16. The rod control system automatically modulates the insertion of the axial offset (AO) control bank controlling the axial power distribution simultaneous with the MSHIM gray and control rod banks to maintain programmed coolant temperature. Operation of the chemical and volume control system is initiated manually by the operator to compensate for fuel burnup and maintain the desired MSHIM bank insertion. Nuclear effects which cause variations in the axial power shape include moderator density, Doppler effect on resonance absorption, spatial distribution of xenon, burnup, and axial

distribution of fuel enrichment and burnable absorber. Automatically controlled variations in total power output and rod motion are also important in determining the axial power shape at any time.

The online core monitoring system provides the operator with detailed power distribution information in both the radial and axial sense continuously using signals from the fixed in-core detectors. Signals are also available to the operator from the ex-core ion chambers, which are long ion chambers outside the reactor vessel running parallel to the axis of the core. Separate signals are taken from the each ion chamber. The ion chamber signals are processed and calibrated against in-core measurements such that an indication of the power in the top of the core less the power in the bottom of the core is derived. The calibrated difference in power between the core top and bottom halves, called the flux difference (ΔI), is derived for each of the four channels of ex-core detectors and is displayed on the control panel. The principal use of the flux difference is to provide the shape penalty function to the OTΔT DNB protection and the OPΔT overpower protection.

4.3.2.2.5 Local Power Peaking

Fuel densification occurred early in the evolution of pressurized water reactor fuel manufacture under irradiation in several operating reactors. This caused the fuel pellets to shrink both axially and radially. The pellet shrinkage combined with random hang-up of fuel pellets can result in gaps in the fuel column when the pellets below the hung-up pellet settle in the fuel rod. The gaps vary in length and location in the fuel rod. Because of decreased neutron absorption in the vicinity of the gap, power peaking occurs in the adjacent fuel rods, resulting in an increased power peaking factor. A quantitative measure of this local peaking is given by the power spike factor S(Z), where Z is the axial location in the core. The power spike factor S(z) is discussed in References 8, 9, and 10.

Modern PWR fuel manufacturing practices have essentially eliminated significant fuel densification impacts on reactor design and operation. It has since been concluded and accepted that a densification power spike factor of 1.0 is appropriate for Westinghouse fuel as described in WCAP-13589-A (Reference 59).

4.3.2.2.6 Limiting Power Distributions

According to the ANSI classification of plant conditions (Chapter 15), Condition I occurrences are those expected frequently or regularly in the course of power operation, maintenance, or maneuvering of the plant. As such, Condition I occurrences are accommodated with margin between any plant parameter and the value of that parameter which would require either automatic or manual protective action. Condition I occurrences are considered from the point of view of affecting the consequences of fault conditions (Conditions II, III, and IV). Analysis of each fault condition described is based on a conservative set of corresponding initial conditions.

The list of steady-state and shutdown conditions, permissible deviations, and operational transients is given in Chapter 15. Implicit in the definition of normal operation is proper and timely action by the reactor operator; that is, the operator follows recommended operating procedures for maintaining appropriate power distributions and takes any necessary remedial actions when alerted to do so by the plant instrumentation.

The online monitoring system evaluates the consequences of limiting power distributions based upon the conditions prevalent in the reactor at the current time. Operating space evaluations performed by the online monitoring system include the most limiting power distributions that can be generated by inappropriate operator or control system actions given the current core power level, xenon distribution, MSHIM or AO bank insertion and core burnup. Thus, as stated, the worst or limiting power distribution which can occur during normal operation is considered as the starting point for analysis of Conditions II, III, and IV occurrences.

Improper procedural actions or errors by the operator are assumed in the design as occurrences of moderate frequency (Condition II). Some of the consequences which might result are discussed in Chapter 15. Therefore, the limiting power shapes which result from such Condition II occurrences are those power distributions which deviate from the normal operating condition within the allowable operating space as defined in the core operating limits; e.g., due to lack of proper action by the operator during a xenon transient following a change in power level brought about by control rod motion. Power distributions which fall in this category are used for determination of the reactor protection system setpoints to maintain margin to overpower or departure from nucleate boiling limits.

The means for maintaining power distributions within the required absolute power generation limits are described in the technical specifications. The online core monitoring system provides the operator with the current allowable operating space, detailed current power distribution information, thermal margin assessment and operational recommendations to manage and maintain required thermal margins. As such, the online monitoring system provides the primary means of managing and maintaining required operating thermal margins during normal operation.

In the unlikely event that the online monitoring system is out of service, power distribution controls based on bounding, precalculated analysis are also provided to the operator such that the online monitoring system is not a required element for short term reactor operation. Limits are placed on the axial flux difference so that the heat flux hot channel factor F_Q is maintained within acceptable limits. A discussion of precalculated power distribution control in Westinghouse pressurized water reactors (PWRs) is included in WCAP-7811 (Reference 11). Detailed background information on the design constraints on local power density in a Westinghouse PWR, on the defined operating procedures, and on the measures taken to preclude exceeding design limits is presented in the Westinghouse topical report on power distribution control and load following procedures WCAP-8385 (Reference 12). The following paragraphs summarize these reports and describe the calculations used to establish the upper bound on peaking factors.

The calculations used to establish the upper bound on peaking factors, F_Q and $F_{\Delta H}^N$, include the nuclear effects which influence the radial and axial power distributions throughout core life for various modes of operation, including load follow, reduced power operation, and axial xenon transients.

Power distributions are calculated for the full-power condition. Fuel and moderator temperature feedback effects are included within these calculations in each spatial dimension. The steady-state nuclear design calculations are done for normal flow with the same mass flow in each channel and flow redistribution effects neglected. The effect of flow redistribution is calculated explicitly where it is important in the departure from nucleate boiling analysis of accidents. The effect of xenon on radial power distribution is small (compare Figures 4.3-6 and 4.3-7) but is included as part of the normal design process.

The core axial profile can experience significant changes, which can occur rapidly as a result of rod motion and load changes and more slowly due to xenon distribution. For the study of points of closest approach to thermal margin limits, several thousand cases are examined. Since the properties of the nuclear design dictate what axial shapes can occur, boundaries on the limits of interest can be set in terms of the parameters which are readily observed on the plant. Specifically, the nuclear design parameters significant to the axial power distribution analysis are as follows:

- Core power level
- Core height
- Coolant temperature and flow
- Coolant temperature program as a function of reactor power

- Fuel cycle lifetimes
- Rod bank worth
- Rod bank overlaps

Normal operation of the plant assumes compliance with the following conditions:

- Control rods in a single bank move together with no individual rod insertion differing from the bank demand position by more than the number of steps identified in the technical specifications.
- Control banks are sequenced with overlapping banks.
- The control bank insertion limits are not violated.
- Axial power distribution control procedures, which are given in terms of flux difference control and control bank position, are observed.

The axial power distribution procedures referred to above are part of the required operating procedures followed in normal operation with the online monitoring system out of service. In service, the online core monitoring system provides continuous indication of power distribution, shutdown margin, and margin to design limits.

The relaxed axial offset control (RAOC) procedures described in WCAP-10216-P-A (Reference 13) were developed to provide wide control band widths and consequently, more operating flexibility. These wide operating limits, particularly at lower power levels, increase plant availability by allowing quicker plant startup and increased maneuvering flexibility without trip. This procedure has been modified to accommodate AP1000 MSHIM operation. It is applied to analysis of axial power distributions under MSHIM control for the purpose of defining the allowed normal operating space such that Condition I thermal margin limits are maintained and Condition II occurrences are adequately protected by the reactor protection system when the online monitoring system is out of service.

The purpose of this analysis is to find the widest permissible ΔI versus power operating space by analyzing a wide range of achievable xenon distributions, MSHIM/AO bank insertion, and power level.

The bounding analyses performed off line in anticipation of the online monitoring system being out of service is similar to that based on the relaxed axial offset control analysis, which uses a xenon reconstruction model described in WCAP-10216-P-A (Reference 13). This is a practical method which is used to define the power operating space allowed with AP1000 MSHIM operation. Each resulting power shape is analyzed to determine if loss-of-coolant accident constraints are met or exceeded.

The online monitoring system evaluates the effects of radial xenon distribution changes due to operational parameter changes continuously and therefore eliminates the need for overly conservative bounding evaluations when the online monitoring system is available. A detailed discussion of this effect may be found in WCAP-8385 (Reference 12). The calculated values have been increased by a factor of 1.05 for method uncertainty and a factor of 1.03 for the engineering factor F^{E}_{Q}.

The envelope drawn in Figure 4.3-14 represents an upper bound envelope on local power density versus elevation in the core. This envelope is a conservative representation of the bounding values of local power density.

The online monitoring system measures the core condition continuously and evaluates the thermal margin condition directly in terms of peak linear heat rate and margin to departure from nucleate boiling limitations directly.

Allowing for fuel densification effects, the average linear power at 3400 MW is 5.72 kW/ft. From Figure 4.3-14, the conservative upper bound value of normalized local power density, including uncertainty allowances, is 2.60 corresponding to a peak linear heat rate of 15.0 kW/ft at each core elevation at 101 percent power.

To determine reactor protection system setpoints with respect to power distributions, three categories of events are considered: rod control equipment malfunctions and operator errors of commission or omission. In evaluating these three categories of events, the core is assumed to be operating within the four constraints described above.

The first category comprises uncontrolled rod withdrawal (with rods moving in the normal bank sequence) for both AO and MSHIM banks. Also included are motions of the AO and MSHIM banks below their insertion limits, which could be caused, for example, by uncontrolled dilution or primary coolant cooldown. Power distributions are calculated throughout these occurrences, assuming short-term corrective action; that is, no transient xenon effects are considered to result from the malfunction. The event is assumed to occur from typical normal operating situations, which include normal xenon transients. It is further assumed in determining the power distributions that total core power level would be limited by reactor trip to below the overpower protection setpoint of nominally 118 percent rated thermal power. Since the study is to determine protection limits with respect to power and axial offset, no credit is taken for OTΔT or OPΔT trip setpoint reduction due to flux difference. The peak power density which can occur in such events, assuming reactor trip at or below 118 percent, is less than that required for fuel centerline melt, including uncertainties and densification effects.

The second category assumes that the operator mispositions the AO and/or MSHIM rod banks in violation of the insertion limits and creates short-term conditions not included in normal operating conditions.

The third category assumes that the operator fails to take action to correct a power distribution limit violation (such as boration/dilution transient) assuming automatic operation of the rod control system which will maintain constant reactor power.

For each of the above categories, the trip setpoints are designed so as not to exceed fuel centerline melt criteria as well as fuel mechanical design criteria.

The appropriate hot channel factors F_Q and $F_{\Delta H}^N$ for peak local power density and for DNB analysis at full power are based on analyses of possible operating power shapes and are addressed in the technical specifications.

The maximum allowable F_Q can be increased with decreasing power, as shown in the technical specifications. Increasing $F_{\Delta H}^N$ with decreasing power is permitted by the DNB protection setpoints and allows radial power shape changes with rod insertion to the insertion limits, as described in Subsection 4.4.4.3. The allowance for increased $F_{\Delta H}^N$ permitted is addressed in the technical specifications.

This becomes a design basis criterion which is used for establishing acceptable control rod patterns and control bank sequencing. Likewise, fuel loading patterns for each cycle are selected with consideration of this design criterion. The worst values of $F^N_{\Delta H}$ for possible rod configurations occurring in normal operation are used in verifying that this criterion is met. The worst values generally occur when the rods are assumed to be at their insertion limits. Operation with rod positions above the allowed rod insertion limits provides increased margin to the $F^N_{\Delta H}$ criterion. As discussed in Section 3.2 of WCAP-7912-P-A (Reference 14), it has been determined that the technical specifications limits are met, provided the above conditions are observed. These limits are taken as input to the thermal-hydraulic design basis, as described in Subsection 4.4.4.3.1.

When a situation is possible in normal operation which could result in local power densities in excess of those assumed as the precondition for a subsequent hypothetical accident, but which would not itself cause fuel failure, administrative controls and alarms are provided for returning the core to a safe condition. These alarms are described in Chapter 7.

The independence of the various individual uncertainties constituting the uncertainty factor on F_Q enables the uncertainty (F^U_Q) to be calculated by statistically combining the individual uncertainties on the limiting rod. The standard deviation of the resultant distribution of F^U_Q is determined by taking the square root of the sum of the variances of each of the contributing distributions WCAP-7308-L-P-A (Reference 7). The values for F^E_Q and F^N_U are 1.03 and 1.05, respectively. The value for the rod bow factor, F^B_Q, is 1.056, which accounts for the maximum F_Q penalty as a function of burnup due to rod bow effects.

4.3.2.2.7 Experimental Verification of Power Distribution Analysis

This subject is discussed in WCAP-7308-L-P-A (Reference 7) and WCAP-12472-P-A (Reference 4). A summary of these reports and the extension to include the fixed in-core instrumentation system is given below. Power distribution related measurements are incorporated into the evaluation of calculated power distribution information using the in-core instrumentation processing algorithms contained within the online monitoring system. The processing algorithms contained within the online monitoring system are functionally identical to those historically used for the evaluation of power distribution measurements in Westinghouse PWRs. Advances in technology allow a complete functional integration of reaction rate measurement algorithms and the expected reaction rate predictive capability within the same software package. The predictive software integrated within the online monitoring system supplies accurate, detailed information of current reactor conditions. The historical algorithms are described in detail in WCAP-12472-P-A (Reference 4).

The measured versus calculational comparison is performed continuously by the online monitoring system throughout the core life. The online monitoring system operability requirements are specified in the technical specifications.

In a measurement of the reactor power distribution and the associated thermal margin limiting parameters, with the in-core instrumentation system described in Subsections 7.7.1 and 4.4.6, the following uncertainties must be considered:

A. Reproducibility of the measured signal

B. Errors in the calculated relationship between detector current and local power generation within the fuel bundle

C. Errors in the detector current associated with the depletion of the emitter material, manufacturing tolerances and measured detector depletion

D. Errors due to the inference of power generation some distance from the measurement thimble

The appropriate allowance for category A has been accounted for through the imposition of strict manufacturing tolerances for the individual detectors. This approach is accepted industry practice and has been used in PWRs with fixed in-core instrumentation worldwide. Errors in category B above are quantified by calculation and evaluation of critical experiment data on arrays of rods with simulated guide thimbles, control rods, burnable absorbers, etc. These critical experiments provide the quantification of errors of categories A and D above. Errors in category C have been quantified through direct experimental measurement of the depletion characteristics of the detectors being used including the precision of the in-core instrumentation systems measurement of the current detector depletion. The description of the experimental measurement of detector depletion can be found in EPRI-NP-3814 (Reference 16).

WCAP-7308-L-P-A (Reference 7) describes critical experiments performed at the Westinghouse Reactor Evaluation Center and measurements taken on two Westinghouse plants with movable fission chamber in-core instrumentation systems. The measurement aspects of the movable fission chamber share the previous uncertainty categories less category C which is independent of the other sources of uncertainty. WCAP-7308-L-P-A (Reference 7) concludes that the uncertainty associated with peak linear heat rate (F_Q*P) is less than five percent at the 95 percent confidence level with only five percent of the measurements greater than the inferred value.

In comparing measured power distributions (or detector currents) with calculations for the same operating conditions, it is not possible to isolate the detector reproducibility. Thus, a comparison between measured and predicted power distributions includes some measurement error. Such a comparison is given in Figure 4.3-15 for one of the maps used in WCAP-7308-L-P-A (Reference 7). Since the first publication of WCAP-7308-L-P-A, hundreds of measurements have been taken on reactors all over the world. These results confirm the adequacy of the five percent uncertainty allowance on the calculated peak linear heat rate (ALHR*F_Q*P).

A similar analysis for the uncertainty in hot rod integrated power $F_{\Delta H}$*P measurements results in an allowance of four percent at the equivalent of a 95 percent confidence level.

A measurement in the fourth cycle of a 157-assembly, 12-foot core is compared with a simplified one-dimensional core average axial calculation in Figure 4.3-16. This calculation does not give explicit representation to the fuel grids.

The accumulated data on power distributions in actual operation are basically of three types:

- Much of the data is obtained in steady-state operation at constant power in the normal operating configuration.
- Data with unusual values of axial offset are obtained as part of the ex-core detector calibration exercise performed monthly.
- Special tests have been performed in load follow and other transient xenon conditions which have yielded useful information on power distributions.

These data are presented in detail in WCAP-7912-P-A (Reference 14). Figure 4.3-17 contains a summary of measured values of F_Q as a function of axial offset for five plants from that report.

4.3.2.2.8 Testing

A series of physics tests are planned to be performed on the first core. These tests and the criteria for satisfactory results are described in Chapter 14. Since not all limiting situations can be created at beginning of life, the main purpose of the tests is to provide a check on the calculational methods used in the predictions for the conditions of the test. Tests performed at the beginning of each reload cycle are limited to verification of the selected safety-related parameters of the reload design.

4.3.2.2.9 Monitoring Instrumentation

The adequacy of instrument numbers, spatial deployment, required correlations between readings and peaking factors, calibration, and errors are described in WCAP-12472-P (Reference 4). The relevant conclusions are summarized in Subsection 4.3.2.2.7 and Subsection 4.4.6.

Provided the limitations given in Subsection 4.3.2.2.6 on rod insertion and flux difference are observed, the in-core and ex-core detector systems provide adequate monitoring of power distributions when the online monitoring system is out of service. Further details of specific limits on the observed rod positions and flux difference are given in the technical specifications, together with a discussion of their bases.

Limits for alarms and reactor trip are given in the technical specifications. Descriptions of the systems provided are given in Section 7.7.

4.3.2.3 Reactivity Coefficients

The kinetic characteristics of the reactor core determine the response of the core to changing plant conditions or to operator adjustments made during normal operation, as well as the core response during abnormal or accidental transients. These kinetic characteristics are quantified in reactivity coefficients. The reactivity coefficients reflect the changes in the neutron multiplication due to varying plant conditions, such as thermal power, moderator and fuel temperatures, coolant pressure, or void conditions, although the latter are relatively unimportant. Since reactivity coefficients change during the life of the core, ranges of coefficients are employed in transient analysis to determine the response of the plant throughout life. The results of such simulations and the reactivity coefficients used are presented in Chapter 15.

The reactivity coefficients are calculated with approved nuclear methods. The effect of radial and axial power distribution on core average reactivity coefficients is implicit in those calculations and is not significant under normal operating conditions. For example, a skewed xenon distribution which results in changing axial offset by five percent typically changes the moderator and Doppler temperature coefficients by less than 0.01 pcm/°F. An artificially skewed xenon distribution which results in changing the radial $F^{N}_{\Delta H}$ by three percent typically changes the moderator and Doppler temperature coefficients by less than 0.03 pcm/°F and 0.001 pcm/°F, respectively. The spatial effects are accentuated in some transient conditions, for example, in postulated rupture of the main steam line and rupture of a rod cluster control assembly mechanism housing described in Subsections 15.1.5 and 15.4.8, and are included in these analyses.

The analytical methods and calculational models used in calculating the reactivity coefficients are given in Subsection 4.3.3. These models have been confirmed through extensive qualification efforts performed for core and lattice designs.

Quantitative information for calculated reactivity coefficients including fuel-Doppler coefficient, moderator coefficients (density, temperature, pressure, and void), and power coefficient, is given in the following sections.

4.3.2.3.1 Fuel Temperature (Doppler) Coefficient

The fuel temperature (Doppler) coefficient is defined as the change in reactivity per degree change in effective fuel temperature and is primarily a measure of the Doppler broadening of U-238 and Pu-240 resonance absorption peaks. Doppler broadening of other isotopes is also considered, but their contribution to the Doppler effect is small. An increase in fuel temperature increases the effective resonance absorption cross sections of the fuel and produces a corresponding reduction in reactivity.

The fuel temperature coefficient is calculated using approved nuclear methods. Moderator temperature is held constant, and the power level is varied. Spatial variation of fuel temperature is taken into account by calculating the effective fuel temperature as a function of power density, as discussed in Subsection 4.3.3.1.

A typical Doppler temperature coefficient is shown in Figure 4.3-18 as a function of the effective fuel temperature (at beginning of life and end of life conditions). The effective fuel temperature is lower than the volume-averaged fuel temperature, since the neutron flux distribution is non-uniform through the pellet and gives preferential weight to the surface temperature. A typical Doppler-only contribution to the power coefficient, defined later, is shown in Figure 4.3-19 as a function of relative core power. The integral of the differential curve in Figure 4.3-19 is the Doppler contribution to the power defect and is shown in Figure 4.3-20 as a function of relative power. The Doppler temperature coefficient becomes more negative as a function of life as the Pu-240 content increases, thus increasing the Pu-240 resonance absorption. The upper and lower limits of Doppler coefficient used in accident analyses are given in Chapter 15.

4.3.2.3.2 Moderator Coefficients

The moderator coefficient is a measure of the change in reactivity due to a change in specific coolant parameters, such as density/temperature, pressure, or void. The coefficients obtained are moderator density/temperature, pressure, and void coefficients.

4.3.2.3.2.1 Moderator Density and Temperature Coefficients

The moderator temperature (density) coefficient is defined as the change in reactivity per degree change in the moderator temperature. Generally, the effects of the changes in moderator density and the temperature are considered together.

The soluble boron used in the reactor as a means of reactivity control also has an effect on the moderator density coefficient, since the soluble boron density and the water density are decreased when the coolant temperature rises. A decrease in the soluble boron density introduces a positive component in the moderator coefficient. If the concentration of soluble boron is large enough, the net value of the coefficient may be positive.

The initial core hot boron concentration is sufficiently low that the moderator temperature coefficient is negative at operating temperatures with the burnable absorber loading specified. Discrete or integral fuel burnable absorbers can be used in reload cores to confirm the moderator temperature coefficient is negative over the range of power operation. The effect of control rods is to make the moderator coefficient more negative, since the thermal neutron mean free path, and hence the volume affected by the control rods, increase with an increase in temperature.

With burnup, the moderator coefficient becomes more negative, primarily as a result of boric acid dilution, but also to a significant extent from the effects of the buildup of plutonium and fission products.

The moderator coefficient is calculated for a range of plant conditions by performing two group two- or three-dimensional calculations, in which the moderator temperature is varied by about ±5°F about each of the mean temperatures, resulting in density changes consistent with the temperature change. The moderator temperature coefficient is shown as a function of core temperature and boron concentration for the core in Figures 4.3-21 through 4.3-23. The temperature range covered is from cold, about 70°F, to about 550°F. The contribution due to Doppler coefficient (because of change in moderator temperature) has been subtracted from these results. Figure 4.3-24 shows the unrodded hot, full-power moderator temperature coefficient plotted as a function of burnup for the initial cycle. The temperature coefficient corresponds to the unrodded critical boron concentration present at hot full power operating conditions.

The moderator coefficients presented here are calculated to describe the core behavior in normal and accident situations when the moderator temperature changes can be considered to affect the entire core.

4.3.2.3.2.2 Moderator Pressure Coefficient

The moderator pressure coefficient relates the change in moderator density, resulting from a reactor coolant pressure change, to the corresponding effect on neutron production. This coefficient is of much less significance than the moderator temperature coefficient. A change of 50 psi in pressure has approximately the same effect on reactivity as a one half degree change in moderator temperature. This coefficient can be determined from the moderator temperature coefficient by relating change in pressure to the corresponding change in density. The typical moderator pressure coefficient may be negative over a portion of the moderator temperature range at beginning of life (BOL) (-0.004 pcm/psi) but is always positive at operating conditions and becomes more positive during life (+0.3 pcm/psi, at end of life).

4.3.2.3.2.3 Moderator Void Coefficient

The moderator void coefficient relates the change in neutron multiplication to the presence of voids in the moderator. In a PWR, this coefficient is not very significant because of the low void content in the coolant. The core void content is less than one-half of one percent and is due to local or statistical boiling. The typical void coefficient varies from 50 pcm/percent void at BOL and at low temperatures to minus 250 pcm/percent void at EOL and at operating temperatures. The void coefficient at operating temperature becomes more negative with fuel burnup.

4.3.2.3.3 Power Coefficient

The combined effect of moderator temperature and fuel temperature change as the core power level changes is called the total power coefficient and is expressed in terms of reactivity change per percent power change. Since a three-dimensional calculation is performed in determining total power coefficients and total power defects, the axial redistribution reactivity component described in Subsection 4.3.2.4.3 is implicitly included. A typical power coefficient at beginning of life (BOL) and end of life (EOL) conditions is given in Figure 4.3-25.

The total power coefficient becomes more negative with burnup, reflecting the combined effect of moderator and fuel temperature coefficients with burnup. The power defect (integral reactivity effect) at BOL and EOL is given in Figure 4.3-26.

4.3.2.3.4 Comparison of Calculated and Experimental Reactivity Coefficients

Subsection 4.3.3 describes the comparison of calculated and experimental reactivity coefficients in detail.

Experimental evaluation of the reactivity coefficients will be performed during the physics startup tests described in Chapter 14.

4.3.2.3.5 Reactivity Coefficients Used in Transient Analysis

Table 4.3-2 gives the limiting values as well as the best-estimate values for the reactivity coefficients for the initial cycle. The limiting values are used as design limits in the transient analysis. The exact values of the coefficient used in the analysis depend on whether the transient of interest is examined at the BOL or EOL, whether the most negative or the most positive (least negative) coefficients are appropriate, and whether spatial non-uniformity must be considered in the analysis. Conservative values of coefficients, considering various aspects of analysis, are used in the transient analysis. This is described in Chapter 15.

The reactivity coefficients shown in Figures 4.3-18 through 4.3-26 are typical best-estimate values calculated for the initial cycle. Limiting values are chosen to encompass the best-estimate reactivity coefficients, including the uncertainties given in Subsection 4.3.3.3 over appropriate operating conditions. The most positive, as well as the most negative, values are selected to form the design basis range used in the transient analysis. A direct comparison of the best-estimate and design limit values for the initial cycle is shown in Table 4.3-2. In many instances the most conservative combination of reactivity coefficients is used in the transient analysis even though the extreme coefficients assumed may not simultaneously occur at the conditions assumed in the analysis. The need for a reevaluation of any accident in a subsequent cycle is contingent upon whether the coefficients for that cycle fall within the identified range used in the analysis presented in Chapter 15 with due allowance for the calculational uncertainties given in Subsection 4.3.3.3. Control rod requirements are given in Table 4.3-3 for the initial cycle and for a hypothetical equilibrium cycle, since these are markedly different. These latter numbers are provided for information only.

4.3.2.4 Control Requirements

To establish the required shutdown margin stated in the COLR under conditions where a cooldown to ambient temperature is required, concentrated soluble boron is added to the coolant. Boron concentrations for several core conditions are listed in Table 4.3-2 for the initial cycle. For core conditions including refueling, the boron concentration is well below the solubility limit. The rod cluster control assemblies are employed to bring the reactor to the shutdown condition. The minimum required shutdown margin is given in the COLR.

The ability to accomplish the shutdown for hot conditions is demonstrated in Table 4.3-3 by comparing the difference between the rod cluster control assembly reactivity available with an allowance for the worst stuck rod with that required for control and protection purposes. The shutdown margin includes an allowance of seven percent for analytic uncertainties which assumes the use of silver-indium-cadmium rod cluster control assemblies. Use of a seven percent uncertainty allowance on rod cluster control assembly worth is discussed and shown to be acceptable in WCAP-9217 (Reference 17). The largest reactivity control requirement appears at the EOL when the moderator temperature coefficient reaches its peak negative value as reflected in the larger power defect.

The control rods are required to provide sufficient reactivity to account for the power defect from full power to zero power and to provide the required shutdown margin. The reactivity addition resulting from power reduction consists of contributions from Doppler effect, moderator temperature, flux redistribution, and reduction in void content as discussed below.

4.3.2.4.1 Doppler Effect

The Doppler effect arises from the broadening of U-238 and Pu-240 resonance cross-sections with an increase in effective pellet temperature. This effect is most noticeable over the range of zero power to full power due to the large pellet temperature increase with power generation.

4.3.2.4.2 Variable Average Moderator Temperature

When the core is shut down to the hot zero-power condition, the average moderator temperature changes from the equilibrium full-load value determined by the steam generator and turbine characteristics (such as steam pressure, heat transfer, tube fouling) to the equilibrium no-load value, which is based on the steam generator shell side design pressure. The design change in temperature is conservatively increased to account for the control system dead band and measurement errors.

When the moderator coefficient is negative, there is a reactivity addition with power reduction. The moderator coefficient becomes more negative as the fuel depletes because the boron concentration is reduced. This effect is the major contributor to the increased requirement at EOL.

4.3.2.4.3 Redistribution

During full-power operation, the coolant density decreases with core height. This, together with partial insertion of control rods, results in less fuel depletion near the top of the core. Under steady-state conditions, the relative power distribution will be slightly asymmetric toward the bottom of the core. On the other hand, at hot zero-power conditions, the coolant density is uniform up the core, and there is no flattening due to Doppler effect. The result will be a flux distribution which at zero power can be skewed toward the top of the core. Since a three-dimensional calculation is performed in determining total power defect, flux redistribution is implicitly included in this calculation. An additional redistribution allowance for adversely skewed xenon distributions is included in the determination of the total control requirement specified in Table 4.3-3.

4.3.2.4.4 Void Content

A small void content in the core is due to nucleate boiling at full power. The void collapse coincident with power reduction makes a small positive reactivity contribution.

4.3.2.4.5 Rod Insertion Allowance

At full power, the MSHIM and AO banks are operated within a prescribed band of travel to compensate for small changes in boron concentration, changes in temperature, and very small changes in the xenon concentration not compensated for by a change in boron concentration. When the MSHIM banks reach a predetermined insertion or withdrawal, a change in boron concentration would be required to compensate for additional reactivity changes. Use of soluble boron is limited to fuel depletion and shutdown considerations. Since the insertion limit is set by rod travel limit, a conservatively high calculation of the inserted worth is made, which exceeds the normally inserted reactivity.

4.3.2.4.6 Installed Excess Reactivity for Depletion

Excess reactivity is installed at the beginning of each cycle to provide sufficient reactivity to compensate for fuel depletion and fission product buildup throughout the cycle. This reactivity is controlled by the addition of soluble boron to the coolant and by burnable absorbers when necessary. The soluble boron concentration for several core configurations and the unit boron worth are given in Tables 4.3-1 and 4.3-2 for the initial cycle. Since the excess reactivity for burnup is controlled by soluble boron and/or burnable absorbers, it is not included in control rod requirements.

4.3.2.4.7 Xenon and Samarium Poisoning

Changes in xenon and samarium concentrations in the core occur at a sufficiently slow rate, even following rapid power level changes, that the resulting reactivity change can be controlled by changing the gray and/or control rod insertion. (Also see Subsection 4.3.2.4.16).

4.3.2.4.8 pH Effects

Changes in reactivity due to a change in coolant pH, if any, are sufficiently small in magnitude and occur slowly enough to be controlled by the boron system WCAP-3896-8 (Reference 18).

4.3.2.4.9 Experimental Confirmation

Following a normal shutdown, the total core reactivity change during cooldown with a stuck rod has been measured on a 121-assembly, 10-foot-high core and a 121-assembly, 12-foot-high core. In each case, the core was allowed to cool down until it reached criticality simulating the steam line break accident. For the 10-foot core, the total reactivity change associated with the cooldown is over predicted by about 0.3-percent $\Delta\rho$ with respect to the measured result. This represents an error of about five percent in the total reactivity change and is about half the uncertainty allowance for this quantity. For the 12-foot core, the difference between the measured and predicted reactivity change is an even smaller 0.2 percent $\Delta\rho$. These measurements and others demonstrate the capability of the methods described in Subsection 4.3.3.

4.3.2.4.10 Control

Core reactivity is controlled by means of a chemical poison dissolved in the coolant, rod cluster control assemblies, gray rod cluster assemblies and burnable absorbers as described below.

4.3.2.4.11 Chemical Shim

Boron in solution as boric acid is used to control relatively slow reactivity changes associated with:

- The moderator temperature defect in going from cold shutdown at ambient temperature to the hot operating temperature at zero power
- The transient xenon and samarium poisoning, such as that following power changes to levels below 30 percent rated thermal power
- The reactivity effects of fissile inventory depletion and buildup of long-life fission products
- The depletion of the burnable absorbers

The boron concentrations for various core conditions are presented in Table 4.3-2 for the initial cycle.

4.3.2.4.12 Rod Cluster Control Assemblies

The number of rod cluster control assemblies is shown in Table 4.3-1. The rod cluster control assemblies are used for shutdown and control purposes to offset fast reactivity changes associated with:

- The required shutdown margin in the hot zero power, stuck rod condition
- The reactivity compensation as a result of an increase in power above hot zero power (power defect, including Doppler and moderator reactivity changes)

- Unprogrammed fluctuations in boron concentration, coolant temperature, or xenon concentration (with rods not exceeding the allowable rod insertion limits)

- Reactivity changes resulting from load changes

The allowed control bank reactivity insertion is limited at full power to maintain shutdown capability. As the power level is reduced, control rod reactivity requirements are also reduced, and more rod insertion is allowed. The control bank position is monitored, and the operator is notified by an alarm if the limit is approached. The determination of the insertion limit uses conservative xenon distributions and axial power shapes. In addition, the rod cluster control assembly withdrawal pattern determined from the analyses is used in determining power distribution factors and in determining the maximum worth of an inserted rod cluster control assembly ejection accident. For further discussion, refer to the technical specifications on rod insertion limits.

Power distribution, rod ejection, and rod misalignment analyses are based on the arrangement of the shutdown and control groups of the rod cluster control assemblies shown in Figure 4.3-27. Shutdown rod cluster control assemblies are withdrawn before withdrawal of the control and AO banks is initiated. The approach to critical is initiated by using the chemical and volume control system to establish an appropriate boron concentration based upon the estimated critical condition then withdrawing the AO bank above the zero power insertion limit and finally withdrawing the control banks sequentially. The limits of rod insertion and further discussion on the basis for rod insertion limits are provided in the COLR and technical specifications.

4.3.2.4.13 Gray Rod Cluster Assemblies

The rod cluster control assembly control banks include four gray rod banks consisting of gray rod cluster assemblies (GRCAs). Gray rod cluster assemblies consist of 24 rodlets fastened at the top end to a common hub or spider. Geometrically, it is the same as a rod cluster control assembly except that 12 of the 24 rodlets are comprised of stainless steel while the remaining 12 rodlets are reduced diameter silver-indium-cadmium clad with stainless steel. The term gray rod refers to the reduced reactivity worth relative to that of a rod cluster control assembly consisting of 24 silver-indium-cadmium rodlets. The gray rod cluster assemblies are used in load follow maneuvering and provide a mechanical shim reactivity mechanism to eliminate the need for changes to the concentration of soluble boron (that is, chemical shim).

4.3.2.4.14 Burnable Absorbers

Discrete burnable absorber rods or integral fuel burnable absorber rods or both may be used to provide partial control of the excess reactivity available during the fuel cycle. In doing so, the burnable absorber loading controls peaking factors and prevents the moderator temperature coefficient from being positive at normal operating conditions. The burnable absorbers perform this function by reducing the requirement for soluble boron in the moderator at the beginning of the fuel cycle, as described previously. For purposes of illustration, the initial cycle burnable absorber pattern is shown in Figure 4.3-5. Figures 4.3-4a and 4.3-4b show the burnable absorber distribution within a fuel assembly for several burnable absorber patterns used in the 17 x 17 array. The boron in the rods is depleted with burnup but at a slow rate so that the peaking factor limits are not exceeded and the resulting critical concentration of soluble boron is such that the moderator temperature coefficient remains within the limits stated above for power operating conditions.

4.3.2.4.15 Peak Xenon Startup

Compensation for the peak xenon buildup may be accomplished using the boron control system. Startup from the peak xenon condition is accomplished with a combination of rod motion and boron

dilution. The boron dilution can be made at any time, including during the shutdown period, provided the shutdown margin is maintained.

4.3.2.4.16 Load Follow Control and Xenon Control

During load follow maneuvers, power changes are primarily accomplished using control rod motion alone, as required. Control rod motion is limited by the control rod insertion limits as provided in the COLR and discussed in Subsections 4.3.2.4.12 and 4.3.2.4.13. The power distribution is maintained within acceptable limits through limitations on control rod insertion. Reactivity changes due to the changing xenon concentration are also controlled by rod motion.

Rapid power increases (five percent/min) from part power during load follow operation are accomplished with rod motion.

The rod control system is designed to automatically provide the power and temperature control described above 30 percent rated power for most of the cycle length without the need to change boron concentration as a result of the load maneuver. The automated mode of operation is referred to as mechanical shim (MSHIM) because of the usage of mechanical means to control reactivity and power distribution simultaneously. MSHIM operation allows load maneuvering without boron change because of the degree of allowed insertion of the control banks in conjunction with the independent power distribution control of the axial offset (AO) control bank. The worth and overlap of the MA, MB, MC, MD, M1, and M2 control banks are designed such that the AO control bank insertion will always result in a monotonically decreasing axial offset. MSHIM operation uses the MA, MB, MC, MD, M1, and M2 control banks to maintain the programmed coolant average temperature throughout the operating power range. The AO control bank is independently modulated by the rod control system to maintain a nearly constant axial offset throughout the operating power range. The degree of control rod insertion under MSHIM operation allows rapid return to power without the need to change boron concentration.

The target axial offset used during MSHIM load follow and base load operation is established at a more negative value than the axial offset associated with the all rods out of condition. The negative bias is necessary to maintain both positive and negative axial offset control effectiveness by the AO control bank. Extended base load operation is performed by controlling axial offset to the target value using the AO control bank, and by controlling the coolant average temperature to the programmed value with the M-banks. Boron concentration changes are made periodically as the fuel depletes to reposition the M-banks and allow for a periodic exchange of the gray rod bank insertion sequence. MSHIM load follow and base load operations (including the gray rod bank insertion sequence exchanges) are considered Condition I normal operations.

4.3.2.4.17 Burnup

Control of the excess reactivity for burnup is accomplished using soluble boron and/or burnable absorbers. The boron concentration is limited during operating conditions to maintain the moderator temperature coefficient within its specified limits. A sufficient burnable absorber loading is installed at the beginning of a cycle to give the desired cycle lifetime, without exceeding the boron concentration limit. The end of a fuel cycle is reached when the soluble boron concentration approaches the practical minimum boron concentration in the range of 0 to 10 ppm.

4.3.2.4.18 Rapid Power Reduction System

The reactor power control system is designed with the capability of responding to full load rejection without initiating a reactor trip using the normal rod control system, reactor control system, and the rapid power reduction system. Load rejections requiring greater than a fifty percent reduction of rated thermal power initiate the rapid power reduction system. The rapid power reduction system utilizes

preselected control rod groups and/or banks which are intentionally tripped to rapidly reduce reactor power into a range where the rod control and reactor control systems are sufficient to maintain stable plant operation. The consequences of accidental or inappropriate actuation of the rapid power reduction system is included in the cycle specific safety analysis and licensing process.

4.3.2.5 Control Rod Patterns and Reactivity Worth

The rod cluster control assemblies are designated by function as the control groups and the shutdown groups. The terms group and bank are used synonymously to describe a particular grouping of control assemblies. The rod cluster control assembly patterns are displayed in Figure 4.3-27. The control banks are labeled MA, MB, MC, MD, M1, M2, and AO with the MA, MB, MC, and MD banks comprised of gray rod cluster assemblies; and the shutdown banks are labeled SD1, SD2, SD3, and SD4. Each bank of more than four rod cluster control assemblies, although operated and controlled as a unit, is composed of two or more subgroups. The axial position of the rod cluster control assemblies may be controlled manually or automatically. The rod cluster control assemblies are dropped into the core following actuation of reactor trip signals.

Two criteria have been employed for selection of the control groups. First, the total reactivity worth must be adequate to meet the requirements specified in Table 4.3-3. Second, in view of the fact that these rods may be partially inserted at power operation, the total power peaking factor should be low enough to meet the power capability requirements. Analyses indicate that the first requirement can be met either by a single group or by two or more banks whose total worth equals at least the required amount. The axial power shape is more peaked following movement of a single group of rods worth three to four percent $\Delta\rho$. Therefore, control bank rod cluster control assemblies have been separated into several bank groupings. Typical control bank worth for the initial cycle are shown in Table 4.3-2.

The position of control banks for criticality under any reactor condition is determined by the concentration of boron in the coolant. On an approach to criticality, boron is adjusted so that criticality will be achieved with control rods above the insertion limit set by shutdown and other considerations. (See the technical specifications and COLR). Early in the cycle, there may also be a withdrawal limit at low power to maintain the moderator temperature coefficient within the specified limits for that power level.

Ejected rod worths for several different conditions are given in Subsection 15.4.8.

Allowable deviations due to misaligned control rods are discussed in the technical specifications.

A representative differential rod worth calculation for two banks of control rods withdrawn simultaneously (rod withdrawal accident) is given in Figure 4.3-28.

Calculation of control rod reactivity worth versus time following reactor trip involves both control rod velocity and differential reactivity worth. The rod position versus time of travel after rod release assumed is given in Figure 4.3-29. For nuclear design purposes, the reactivity worth versus rod position is calculated by a series of steady-state calculations at various control positions, assuming the rods out of the core as the initial position in order to minimize the initial reactivity insertion rate. Also, to be conservative, the rod of highest worth is assumed stuck out of the core, and the flux distribution (and thus reactivity importance) is assumed to be skewed to the bottom of the core. The result of these calculations is shown in Figure 4.3-30.

The shutdown groups provide additional negative reactivity to establish adequate shutdown margin. Shutdown margin is the amount by which the core would be subcritical at hot shutdown if the rod cluster control assemblies were tripped, but assuming that the highest worth assembly remained fully

withdrawn and no changes in xenon or boron took place. The loss of control rod worth due to the depletion of the absorber material is negligible.

The values given in Table 4.3-3 show that the available reactivity in withdrawn rod cluster control assemblies provides the design bases minimum shutdown margin, allowing for the highest worth cluster to be at its fully withdrawn position. An allowance for the uncertainty in the calculated worth of N-1 rods is made before determination of the shutdown margin.

4.3.2.6 Criticality of the Reactor During Refueling

The basis for maintaining the reactor subcritical during refueling is presented in Subsection 4.3.1.5, and a discussion of how control requirements are met is given in Subsections 4.3.2.4 and 4.3.2.5.

4.3.2.6.1 Criticality Design Method Outside the Reactor

Criticality of fuel assemblies outside the reactor is precluded by adequate design of fuel transfer, shipping, and storage facilities and by administrative control procedures. The two principal methods of preventing criticality are limiting the fuel assembly array size and limiting assembly interaction by fixing the minimum separation between assemblies and/or inserting neutron poisons between assemblies. The details of the methodology used for the new fuel rack and spent fuel rack criticality analysis are included in the Chapter 9.1 references.

The design criteria are consistent with General Design Criterion (GDC) 62, Reference 19, and NRC guidance given in Reference 20. The applicable 10 CFR Part 50.68 requirements are as follows:

1. The maximum K-effective value, including all biases and uncertainties, must be less than 0.95 with soluble boron credit and less than 1.0 with full density unborated water. Note this design criterion is provided in 10 CFR Part 50.68, Item 4 of Paragraph b. Note that the specific terminology is:

   “If no credit for soluble boron is taken, the k-effective of the spent fuel storage racks loaded with fuel of the maximum fuel assembly reactivity must not exceed 0.95, at a 95 percent probability, 95 percent confidence level, if flooded with unborated water. If credit is taken for soluble boron, the k-effective of the spent fuel storage racks loaded with fuel of the maximum fuel assembly reactivity must not exceed 0.95, at a 95 percent probability, 95 percent confidence level, if flooded with borated water, and the k-effective must remain below 1.0 (subcritical), at a 95 percent probability, 95 percent confidence level, if flooded with unborated water.”

2. The maximum enrichment of fresh fuel assemblies must be less than or equal to 5.0 weight-percent U-235. Note this design criterion is provided in 10 CFR Part 50.68, Item 7 of Paragraph b. Note that the specific terminology is:

   “The maximum nominal U–235 enrichment of the fresh fuel assemblies is limited to five (5.0) percent by weight.”

The following conditions are assumed in meeting this design bases:

- The fuel assembly contains the highest enrichment authorized without any control rods or non-integral burnable absorber(s) and is at its most reactive point in life.

- For flooded conditions, the moderator is pure water at the temperature within the design limits which yields the largest reactivity.

- The array is either infinite in lateral extent or is surrounded by a conservatively chosen reflector, whichever is appropriate for the design.

- Mechanical uncertainties are treated by combining both the worst-case bounding value and sensitivity study approaches.

- Credit is taken for the neutron absorption in structural materials and in solid materials added specifically for neutron absorption.

Fuel depletion analyses during core operation were performed with CASMO-4 (using the 70-group cross-section library), a two-dimensional multigroup transport theory code based on capture probabilities (Reference 53). CASMO-4 is used to determine the isotopic composition of the spent fuel. In addition, the CASMO-4 calculations are restarted in the storage rack geometry, yielding the two-dimensional infinite multiplication factor (k_{inf}) for the storage rack to determine the reactivity effect of fuel and rack tolerances, temperature variation, and to perform various studies.

The design method which determines the criticality safety of fuel assemblies outside the reactor uses the MCNP4a code (Reference 21), with continuous energy cross-sections based on ENDF/B-V and ENDF/B-VI.

A set of 62 critical experiments has been analyzed using the above method to demonstrate its applicability to criticality analysis and to establish the method bias and uncertainty. The benchmark experiments cover a wide range of geometries, materials, and enrichments, all of them adequate for qualifying methods to analyze light water reactor lattices (References 22 to 28, and 65 to 68).

The analysis of the 62 critical experiments results in an average K_{eff} of 0.9991. Comparison with the measured values results in a method bias of 0.0009. The standard deviation of the set of reactivities is 0.0011. The 95/95 tolerance factor is conservatively set to 2.0.

The analytical methods employed herein conform with ANSI N18.2 (Reference 3), Section 5.7, Fuel Handling System; ANSI N16.9 (Reference 29), NRC Standard Review Plan, Subsection 9.1.2, the NRC guidance, “OT Position for Review and Acceptance of Spent Fuel Storage and Handling Applications” (Reference 30).

4.3.2.6.2 Soluble Boron Credit Methodology

The minimum soluble boron requirement under normal and accident conditions must be determined to show that the reactivity of the spent fuel racks remains below 0.95. This is achieved by crediting a discrete amount of soluble boron and then determining by linear interpolation the appropriate amount of soluble boron necessary to reduce the maximum K_{eff} to 0.95 with all uncertainties and biases included.

4.3.2.7 Stability

4.3.2.7.1 Introduction

The stability of the PWR cores against xenon-induced spatial oscillations and the control of such transients are discussed extensively in References 11, 31, 32, and 33. A summary of these reports is given in the following discussion, and the design bases are given in Subsection 4.3.1.6.

In a large reactor core, xenon-induced oscillations can take place with no corresponding change in the total power of the core. The oscillation may be caused by a power shift in the core which occurs rapidly by comparison with the xenon-iodine time constants. Such a power shift occurs in the axial

direction when a plant load change is made by control rod motion and results in a change in the moderator density and fuel temperature distributions. Such a power shift could occur in the diametral plane of the core as a result of abnormal control action.

Due to the negative power coefficient of reactivity, PWR cores are inherently stable to oscillations in total power. Protection against total power instabilities is provided by the control and protection system, as described in Section 7.7. Hence, the discussion on the core stability will be limited to xenon-induced spatial oscillations.

4.3.2.7.2 Stability Index

Power distributions, either in the axial direction or in the X-Y plane, can undergo oscillations due to perturbations introduced in the equilibrium distributions without changing the total core power. The harmonics and the stability of the core against xenon-induced oscillations can be determined in terms of the eigenvalue of the first flux harmonics. Writing the eigenvalue ξ of the first flux harmonic as:

$$\xi = b + ic \tag{1}$$

Then b is defined as the stability index and $T = 2\pi/c$ as the oscillation period of the first harmonic. The time dependence of the first harmonic $\delta\phi$ in the power distribution can now be represented as:

$$\delta\phi(t) = A e^{\xi t} = a e^{bt} \cos ct \tag{2}$$

where A and a are constants. The stability index can also be obtained approximately by:

$$b = \frac{1}{T} \ln \frac{A_{n+1}}{A_n} \tag{3}$$

where A_n and A_{n+1} are the successive peak amplitudes of the oscillation and T is the time period between the successive peaks.

4.3.2.7.3 Prediction of the Core Stability

The core described in this report has an active fuel length that is 24 inches longer (nominal) than that for previous Westinghouse PWRs licensed in the U.S. with 157 fuel assemblies. For this reason, it is expected that this core will be as stable as the 12-foot designs with respect to radial and diametral xenon oscillations since the radial core dimensions have not changed. This core will be slightly less stable than the 12-foot, 157 assembly cores with respect to axial xenon oscillations because the active core height has been increased by 24 inches. The effect of this increase will be to decrease the burnup at which the axial stability index becomes zero (Subsection 4.3.2.7.4 below). The moderator temperature coefficients and the Doppler temperature coefficients of reactivity will be similar to those of previous designs. Control banks included in the core design are sufficient to dampen any xenon oscillations that may occur. Free axial xenon oscillations are not allowed to occur for a core of any height, except during special tests as described in Subsection 4.3.2.7.4.

4.3.2.7.4 Stability Measurements

4.3.2.7.4.1 Axial Measurements

Two axial xenon transient tests conducted in a PWR with a core height of 12 feet and 121 fuel assemblies are reported in WCAP-7964 (Reference 34) and are discussed here. The tests were performed at approximately 10 percent and 50 percent of cycle life.

Both a free-running oscillation test and a controlled test were performed during the first test. The second test at mid-cycle consisted of a free-running oscillation test only. In each of the free-running oscillation tests, a perturbation was introduced to the equilibrium power distribution through an impulse motion of the lead control bank and the subsequent oscillation period was monitored. In the controlled test conducted early in the cycle, the part-length rods were used to follow the oscillations to maintain an axial offset within the prescribed limits. The axial offset of power was obtained from the ex-core ion chamber readings (which had been calibrated against the in-core flux maps) as a function of time for both free-running tests, as shown in Figure 12 of WCAP-7964 (Reference 34).

The total core power was maintained constant during these spatial xenon tests, and the stability index and the oscillation period were obtained from a least-square fit of the axial offset data in the form of equation 2. The axial offset of power is the quantity that properly represents the axial stability in the sense that it essentially eliminates any contribution from even-order harmonics, including the fundamental mode. The conclusions of the tests follow:

- The core was stable against induced axial xenon transients, at the core average burnups of both 1550 MWD/MTU and 7700 MWD/MTU. The measured stability indices are -0.041 h^{-1} for the first test and - 0.014 h^{-1} for the second test. The corresponding oscillation periods are 32.4 and 27.2 hours, respectively.

- The reactor core becomes less stable as fuel burnup progresses, and the axial stability index is essentially zero at 12,000 MWD/MTU. However, the movable control rod systems can control axial oscillations, as described in Subsection 4.3.2.7.

4.3.2.7.4.2 Measurements in the X-Y Plane

Two X-Y xenon oscillation tests were performed at a PWR plant with a core height of 12 feet and 157 fuel assemblies. The first test was conducted at a core average burnup of 1540 MWD/MTU and the second at a core average burnup of 12,900 MWD/MTU. Both of the X-Y xenon tests show that the core was stable in the X-Y plane at both burnups. The second test shows that the core became more stable as the fuel burnup increased, and Westinghouse PWRs with 121 and 157 assemblies are stable throughout their burnup cycles. The results of these tests are applicable to the 157-assembly AP1000 core, as discussed in Subsection 4.3.2.7.3.

In each of the two X-Y tests, a perturbation was introduced to the equilibrium power distribution through an impulse motion of one rod cluster control unit located along the diagonal axis. Following the perturbation, the uncontrolled oscillation was monitored, using the movable detector and thermocouple system and the ex-core power range detectors. The quadrant tilt difference (QTD) is the quantity that properly represents the diametral oscillation in the X-Y plane of the reactor core in that the differences of the quadrant average powers over two symmetrically opposite quadrants essentially eliminates the contribution to the oscillation from the azimuthal mode. The quadrant tilt difference data were fitted in the form of equation 2 of Subsection 4.3.2.7.2 through a least-square method. A stability index of - 0.076 hr^{-1} (per hour) with a period of 29.6 hr was obtained from the thermocouple data shown in Figure 4.3-31.

It was observed in the second X-Y xenon test that the PWR core with 157 fuel assemblies had become more stable due to an increased fuel depletion, and the stability index was not determined.

4.3.2.7.5 Comparison of Calculations with Measurements

The direct simulation of axial offset data was carried out using a licensed one-dimensional code (WCAP-7084-P-A Reference 35). The analysis of the X-Y xenon transient tests was performed in an X-Y geometry, using a licensed few group two-dimensional code (WCAP-7213-A Reference 36). Both of these codes solve the two-group, time-dependent neutron diffusion equation with time-

dependent xenon and iodine concentrations. The fuel temperature and moderator density feedback is limited to a steady-state model. The X-Y calculations were performed in an average enthalpy plane.

The detailed experimental data during the tests, including the reactor power level, the enthalpy rise, and the impulse motion of the control rod assembly, as well as the plant follow burnup data, were closely simulated in the study.

The results of the stability calculation for the axial tests are compared with the experimental data in Table 4.3-5. The calculations show conservative results for both of the axial tests with a margin of approximately 0.01 hr^{-1} in the stability index.

An analytical simulation of the first X-Y xenon oscillation test shows a calculated stability index of - 0.081 hr^{-1}, in good agreement with the measured value of - 0.076 hr^{-1}. As indicated earlier, the second X-Y xenon test showed that the core had become more stable compared to the first test, and no evaluation of the stability index was attempted. This increase in the core stability in the X-Y plane due to increased fuel burnup is due mainly to the increased magnitude of the negative moderator temperature coefficient.

Previous studies of the physics of xenon oscillations, including three-dimensional analysis, are reported in a series of topical reports (References 31, 32, and 33). A more detailed description of the experimental results and analysis of the axial and X-Y xenon transient tests is presented in WCAP-7964 (Reference 34) and Section 1 of WCAP-8768 (Reference 37).

4.3.2.7.6 Stability Control and Protection

The online monitoring system provides continuous indication of current power distributions and provides guidance to the plant operator as to the timing and most appropriate action(s) to maintain stable axial power distributions. In the event the online monitoring system is out of service, the ex-core detector system is utilized to provide indications of xenon-induced spatial oscillations. The readings from the ex-core detectors are available to the operator and also form part of the protection system.

4.3.2.7.6.1 Axial Power Distribution

The rod control system automatically maintains axial power distribution within very tight axial offset bands as part of normal operation. The AO control bank is specifically designed with sufficient worth to be capable of maintaining essentially constant axial offset over the power operating range. The rod control system is also allowed to be operated in manual control in which case the operator is instructed to maintain an axial offset within a prescribed operating band, based on the ex-core detector readings. Should the axial offset be permitted to move far enough outside this band, the protection limit is encroached, and the turbine power is automatically reduced or a reactor trip signal generated, or both.

As fuel burnup progresses, PWR cores become less stable to axial xenon oscillations. However, free xenon oscillations are not allowed to occur, except for special tests. The AO control bank is sufficient to dampen and control any axial xenon oscillations present. Should the axial offset be inadvertently permitted to move far enough outside the allowed band due to an axial xenon oscillation or for any other reason, the OTΔT and/or OPΔT protection setpoint including the axial offset compensation is reached and the turbine power is automatically reduced and/or a reactor trip signal is generated.

4.3.2.7.6.2 Radial Power Distribution

The core described herein is calculated to be stable against X-Y xenon-induced oscillations during the core life.

The X-Y stability of large PWRs has been further verified as part of the startup physics test program for PWR cores with 193 fuel assemblies. The measured X-Y stability of the cores with 157 and 193 assemblies was in close agreement with the calculated stability, as discussed in Subsections 4.3.2.7.4 and 4.3.2.7.5. In the unlikely event that X-Y oscillations occur, backup actions are possible and would be implemented, if necessary, to increase the natural stability of the core. This is based on the fact that several actions could be taken to make the moderator temperature coefficient more negative, which would increase the stability of the core in the X-Y plane.

Provisions for protection against non-symmetric perturbations in the X-Y power distribution that could result from equipment malfunctions are made in the protection system design. This includes control rod drop, rod misalignment, and asymmetric loss of coolant flow.

A more detailed discussion of the power distribution control in PWR cores is presented in WCAP-7811 (Reference 11) and WCAP-8385 (Reference 12).

4.3.2.8 Vessel Irradiation

A review of the methods and analyses used in the determination of neutron and gamma ray flux attenuation between the core and the pressure vessel is provided below. A more complete discussion on the pressure vessel irradiation and surveillance program is given in Section 5.3.

The materials that serve to attenuate neutrons originating in the core and gamma rays from both the core and structural components consist of the core shroud, core barrel and associated water annuli. These are within the region between the core and the pressure vessel.

In general, few group neutron diffusion theory codes are used to determine fission power density distributions within the active core, and the accuracy of these analyses is verified by in-core measurements on operating reactors. Region and rodwise power-sharing information from the core calculations is then used as source information in two-dimensional transport calculations which compute the flux distributions throughout the reactor.

The neutron flux distribution and spectrum in the various structural components vary significantly from the core to the pressure vessel. Representative values of the neutron flux distribution and spectrum are presented in Table 4.3-6.

As discussed in Section 5.3, the irradiation surveillance program utilizes actual test samples to verify the accuracy of the calculated fluxes at the vessel.

4.3.3 Analytical Methods

Calculations required in nuclear design consist of three distinct types, which are performed in sequence:

1. Determination of effective fuel temperatures

2. Generation of microscopic few-group parameters

3. Space-dependent, few-group diffusion calculations

These calculations are carried out by computer codes which can be executed individually. Most of the codes required have been linked to form an automated design sequence which minimizes design time, avoids errors in transcription of data, and standardizes the design methods.

4.3.3.1 Fuel Temperature (Doppler) Calculations

Temperatures vary radially within the fuel rod, depending on the heat generation rate in the pellet; the conductivity of the materials in the pellet, gap, and clad; and the temperature of the coolant.

The fuel temperatures for use in most nuclear design Doppler calculations are obtained from a simplified version of the Westinghouse fuel rod design model described in Subsection 4.2.1.3, which considers the effect of radial variation of pellet conductivity, expansion coefficient and heat generation rate, elastic deflection of the clad, and a gap conductance which depends on the initial fill gas, the hot open gap dimension, and the fraction of the pellet over which the gap is closed. The fraction of the gap assumed closed represents an empirical adjustment used to produce close agreement with observed reactivity data at beginning of life. Further gap closure occurs with burnup and accounts for the decrease in Doppler defect with burnup which has been observed in operating plants. For detailed calculations of the Doppler coefficient, such as for use in xenon stability calculations, a more sophisticated temperature model is used, which accounts for the effects of fuel swelling, fission gas release, and plastic clad deformation.

Radial power distributions in the pellet as a function of burnup are obtained from LASER (WCAP-6073, Reference 38) calculations.

The effective U-238 temperature for resonance absorption is obtained from the radial temperature distribution by applying a radially dependent weighing function. The weighing function was determined from REPAD (WCAP-2048, Reference 39) Monte Carlo calculations of resonance escape probabilities in several steady-state and transient temperature distributions. In each case, a flat pellet temperature was determined which produced the same resonance escape probability as the actual distribution. The weighing function was empirically determined from these results.

The effective Pu-240 temperature for resonance absorption is determined by a convolution of the radial distribution of Pu-240 densities from LASER burnup calculations and the radial weighing function. The resulting temperature is burnup dependent, but the difference between U-238 and Pu-240 temperatures, in terms of reactivity effects, is small.

The effective pellet temperature for pellet dimensional change is that value which produces the same outer pellet radius in a virgin pellet as that obtained from the temperature model. The effective clad temperature for dimensional change is its average value.

The temperature calculational model has been validated by plant Doppler defect data, as shown in Table 4.3-7, and Doppler coefficient data, as shown in Figure 4.3-32. Stability index measurements also provide a sensitive measure of the Doppler coefficient near full power (Subsection 4.3.2.7).

4.3.3.2 Macroscopic Group Constants

PHOENIX-P (WCAP-11596-P-A, Reference 40) has been used for generating the macroscopic cross sections needed for the spatial few group codes. PHOENIX-P or other NRC approved lattice codes will be used for reload designs.

PHOENIX-P has been approved by the NRC as a lattice code for the generation of macroscopic and microscopic few group cross sections for PWR analysis. (See WCAP-11596-P-A, Reference 40). PHOENIX-P is a two-dimensional, multigroup, transport-based lattice code capable of providing necessary data for PWR analysis. Since it is a dimensional lattice code, PHOENIX-P does not rely on

pre-determined spatial/spectral interaction assumptions for the heterogeneous fuel lattice and can provide a more accurate multigroup spatial flux solution than versions (ARK) of LEOPARD/CINDER.

The solution for the detailed spatial flux and energy distribution is divided into two major steps in PHOENIX-P (See References 40 and 41). First, a two-dimensional fine energy group nodal solution is obtained, coupling individual subcell regions (e.g., pellet, clad and moderator) as well as surrounding pins, using a method based on Carlvik's collision probability approach and heterogeneous response fluxes which preserve the heterogeneous nature of the pin cells and their surroundings. The nodal solution provides an accurate and detailed local flux distribution, which is then used to homogenize the pin cells spatially to few groups.

Then, a standard S_4 discrete ordinates calculation solves for the angular distribution, based on the group-collapsed and homogenized cross sections from the first step. These S_4 fluxes normalize the detailed spatial and energy nodal fluxes, which are then used to compute reaction rates, power distributions and to deplete the fuel and burnable absorbers. A standard B1 calculation evaluates the fundamental mode critical spectrum, providing an improved fast diffusion coefficient for the core spatial codes.

PHOENIX-P employs either a 42 or 70 energy group library derived mainly from the ENDF/B-V files (Reference 21). This library was designed to capture the integral properties of the multigroup data properly during group collapse and to model important resonance parameters properly. It contains neutronics data necessary for modelling fuel, fission products, cladding and structural materials, coolant, and control and burnable absorber materials present in PWRs.

Group constants for burnable absorber cells, control rod cells, guide thimbles and instrumentation thimbles, or other non-fuel cells, can be obtained directly from PHOENIX-P without any adjustments such as those required in the cell or 1D lattice codes.

PHOENIX-P has been validated through an extensive qualification effort which includes calculation-measurement comparison of the Strawbridge-Barry critical experiments (See References 42 and 43), the KRITZ high temperature criticals (Reference 44), the AEC sponsored B&W criticals (References 45 through 47) and measured actinide isotopic data from fuel pins irradiated in the Saxton and Yankee Rowe cores (References 48 through 52). In addition, calculation-measurement comparisons have been made to operating reactor data measured during startup tests and during normal power operation.

Validation of the cross section method is based on analysis of critical experiments, isotopic data, plant critical boron concentration data, and control rod worth measurement data such as that shown in Table 4.3-8.

Confirmatory critical experiments on burnable absorber rods are described in WCAP-7806 (Reference 42).

4.3.3.3 Spatial Few-Group Diffusion Calculations

The 3D ANC code (see WCAP-10965-P-A, Reference 57) permits the introduction of advanced fuel designs with axial heterogeneities, such as axial blankets and part-length burnable absorbers, and allows such features to be modeled explicitly. The three dimensional nature of this code provides both radial and axial power distribution. For some applications, the updated version APOLLO (see WCAP-13524 Reference 60) of the PANDA code (see WCAP-7084-P-A Reference 35) will continue to be used for axial calculations, and a two-dimensional collapse of 3D ANC that properly accounts for the three-dimensional features of the fuel is used for X-Y calculations.

Spatial few group calculations are carried out to determine the critical boron concentrations and power distributions. The moderator coefficient is evaluated by varying the inlet temperature in the same kind of calculations as those used for power distribution and reactivity predictions.

Validation of the reactivity calculations is associated with validation of the group constants themselves, as discussed in Subsection 4.3.3.2. Validation of the Doppler calculations is associated with the fuel temperature validation discussed in Subsection 4.3.3.1. Validation of the moderator coefficient calculations is obtained by comparison with plant measurements at hot zero power conditions, similar to that shown in Table 4.3-9.

Axial calculations are used to determine differential control rod worth curves (reactivity versus rod insertion) and to demonstrate load follow capability. Group constants are obtained from the three-dimensional nodal model by flux-volume weighing on an axial slicewise basis. Radial bucklings are determined by varying parameters in the buckling model while forcing the one-dimensional model to reproduce the axial characteristics (axial offset, midplane power) of the three-dimensional model.

Validation of the spatial codes for calculating power distributions involves the use of in-core and ex-core detectors and is discussed in Subsection 4.3.2.2.7.

As discussed in Subsection 4.3.3.2, calculation-measurement comparisons have been made to operating reactor data measured during startup tests and during normal power operation. These comparisons include a variety of core geometries and fuel loading patterns, and incorporate a reasonable extreme range of fuel enrichment, burnable absorber loading, and cycle burnup. Qualification data identified in Reference 40 indicate small mean and standard deviations relative to measurement which are equal to or less than those found in previous reviews of similar or parallel approved methodologies. For the reload designs the spatial codes described above, other NRC approved codes, or both are used.

4.3.4 Combined License Information

Changes to the reference design of the fuel, burnable absorber rods, rod cluster assemblies, or initial core design from that presented in the DCD are addressed in APP-GW-GLR-059 (Reference 64).

4.3.5 References

1. Bordelon, F. M, et al., “Westinghouse Reload Safety Evaluation Methodology,” WCAP-9272-P-A (Proprietary) and WCAP-9273-NP-A (Nonproprietary), July 1985.

2. [*Davidson, S. L. (Ed.), “Fuel Criteria Evaluation Process,” WCAP-12488-P-A (Proprietary) and WCAP-14204-A - (Nonproprietary), October 1994.*]*

3. ANSI N18.2-1973, “Nuclear Safety Criteria for the Design of Stationary Pressurized Water Reactor Plants.”

4. Beard, C. L. and Morita, T., “BEACON: Core Monitoring and Operations Support System,” WCAP-12472-P-A (Proprietary) and WCAP-12473-A (Nonproprietary), August 1994; Addendum 1, May 1996; and Addendum 2, March 2001.

5. Gangloff, W. C. and Loftus, W. D., “Westinghouse Anticipated Transients Without Reactor Trip Analysis,” WCAP-8330, August 1974.

6. Not used.

*NRC Staff approval is required prior to implementing a change in this information.

7. Spier, E. M., “Evaluation of Nuclear Hot Channel Factor Uncertainties,” WCAP-7308-L-P-A (Proprietary) and WCAP-7308-L-A, (Nonproprietary), June 1988.

8. Hellman, J. M., ed. “Fuel Densification Experimental Results and Model for Reactor Application,” WCAP-8218-P-A (Proprietary) and WCAP-8219-A (Nonproprietary), March 1975.

9. Meyer, R. O., “The Analysis of Fuel Densification,” Division of Systems Safety, U.S. Nuclear Regulatory Commission, NUREG-0085, July 1976.

10. Hellman, J. M., Olson, C. A., and Yang, J. W., “Effects of Fuel Densification Power Spikes on Clad Thermal Transients,” WCAP-8359; July 1974.

11. Moore, J. S., “Power Distribution Control of Westinghouse Pressurized Water Reactors,” WCAP-7811, December 1971.

12. Morita, T., et al., “Power Distribution Control and Load Following Procedures,” WCAP-8385 (Proprietary) and WCAP-8403 (Nonproprietary), September 1974.

13. Miller, R. W., et al., “Relaxation of Constant Axial Offset Control, FQ Surveillance Technical Specification,” WCAP-10216-P-A, (Proprietary) and WCAP-10217-A, (Nonproprietary) Revision 1A, February 1994.

14. McFarlane, A. F., “Power Peaking Factors,” WCAP-7912-P-A (Proprietary) and WCAP-7912-A (Nonproprietary), January 1975.

15. Meyer, C. E., and Stover, R. L., “Incore Power Distribution Determination in Westinghouse Pressurized Water Reactors,” WCAP-8498, July 1975.

16. Warren, H. D., “Rhodium In-Core Detector Sensitivity Depletion, Cycles 2-6,” EPRI-NP-3814, December 1984.

17. Henderson, W. B., “Results of the Control Rod Worth Program,” WCAP-9217 (Proprietary) and WCAP-9218 (Nonproprietary), October 1977.

18. Cermak, J. O., et al., “Pressurized Water Reactor pH - Reactivity Effect Final Report,” WCAP-3696-8 (EURAEC-2074), October 1968.

19. USNRC Code of Federal Regulations, Title 10, Part 50, Appendix A, Criterion 62, “Prevention of Criticality in Fuel Storage and Handling.”

20. Kopp, L. (NRC), “Guidance on the Regulatory Requirements for Criticality Analysis of Fuel Storage at Light-Water Reactor Power Plants,” February 1998.

21. Briesmeister, J. F., Editor, “MCNP – A General Monte Carlo N-Particle Transport Code, Version 4A,” LA-12625, Los Alamos National Laboratory (1993).

22. Baldwin, M. N., et al., “Critical Experiments Supporting Close Proximity Water Storage of Power Reactor Fuel,” BAW-1484-7, Babcock & Wilcox Company, July 1979.

23. Hoovier, G. S., et al., “Critical Experiments Supporting Underwater Storage of Tightly Packed Configurations of Spent Fuel Pins,” BAW-1645-4, Babcock & Wilcox Company, November 1991.

24. Newman, L. W., et al., “Urania Gadolinia: Nuclear Model Development and Critical Experiment Benchmark,” BAW-1810, Babcock & Wilcox Company, April 1984.

25. Manaranche, J. C., et al., “Dissolution and Storage Experimental Program with 4.75 w/o Enriched Uranium-Oxide Rods,” Trnas. Am. Nucl. Soc. 33:362-364 (1979).

26. Bierman, S. R. and Clayton, E. D., “Criticality Experiments with Subcritical Clusters of 2.35 w/o and 4.31 w/o 235U Enriched UO_2 Rods in Water with Steel Reflecting Walls,” PNL-3602, Batelle Pacific Northwest Laboratory, April 1981.

27. Bierman, S. R., et al., “Criticality Experiments with Subcritical Clusters of 2.35 w/o and 4.31 w/o 235U Enriched UO_2 Rods in Water with Uranium or Lead Reflecting Walls,” PNL-3926, Batelle Pacific Northwest Laboratory, December 1981.

28. Bierman, S. R., et al., “Criticality Experiments with Subcritical Clusters of 2.35 w/o and 4.31 w/o 235U Enriched UO_2 Rods in Water with Fixed Neutron Poisons,” PNL-2615, Batelle Pacific Northwest Laboratory, October 1977.

29. ANSI N16.9-1975, “Validation of Calculational Methods for Nuclear Criticality Safety.”

30. NRC Letter “OT Position for Review and Acceptance of Spent Fuel Storage and Handling Applications,” from Grimes, B. K., to all power reactor licenses, April 14, 1978.

31. Poncelet, C. G., and Christie, A. M., “Xenon-Induced Spatial Instabilities in Large Pressurized Water Reactors,” WCAP-3680-20 (EURAEC-1974), March 1968.

32. Skogen, F. B., and McFarlane, A. F., “Control Procedures for Xenon-Induced X-Y Instabilities in Large Pressurized Water Reactors,” WCAP-3680-21 (EURAEC-2111), February 1969.

33. Skogen, F. B., and McFarlane, A. F., “Xenon-Induced Spatial Instabilities in Three Dimensions,” WCAP-3680-22 (EURAEC-2116), September 1969.

34. Lee, J. C., et al., “Axial Xenon Transient Tests at the Rochester Gas and Electric Reactor,” WCAP-7964, June 1971.

35. Barry, R. F., and Minton, G., “The PANDA Code,” WCAP-7048-P-A (Proprietary) and WCAP-7757-A (Nonproprietary), February 1975.

36. Barry, R. F., and Altomare, S., “The TURTLE 24.0 Diffusion Depletion Code,” WCAP-7213-A (Proprietary) and WCAP-7758-A (Non-Proprietary), February 1975.

37. Eggleston, F. T., “Safety-Related Research and Development for Westinghouse Pressurized Water Reactors, Program Summaries - Winter 1977 - Summer 1978,” WCAP-8768, Revision 2, October 1978.

38. Poncelet, C. G., “LASER - A Depletion Program for Lattice Calculations Based on MUFT and THERMOS,” WCAP-6073, April 1966.

39. Olhoeft, J. E., “The Doppler Effect for a Non-Uniform Temperature Distribution in Reactor Fuel Elements,” WCAP-2048, July 1962.

40. Nguyen, T. Q., et al., “Qualification of the PHOENIX-P/ANC Nuclear Design System for Pressurized Water Reactor Cores,” WCAP-11596-P-A (Proprietary) and WCAP-11597-A (Nonproprietary), June 1988.

41. Mildrum, C. M., Mayhue, L. T., Baker, M. M., and Isaac, P. G., “Qualification of the PHOENIX/POLCA Nuclear Design and Analysis Program for Boiling Water Reactors,” WCAP-10841 (Proprietary), and WCAP-10842 (Nonproprietary), June 1985.

42. Barry, R. F., “Nuclear Design of Westinghouse Pressurized Water Reactors with Burnable Poison Rods,” WCAP-7806, December 1971.

43. Strawbridge, L. E., and Barry, R. F., “Criticality Calculation for Uniform Water-Moderated Lattices,” Nuclear Science and Engineering 23, p. 58, 1965.

44. Persson, R., Blomsjo, E., and Edenius, M., “High Temperature Critical Experiments with H_2O Moderated Fuel Assemblies in KRITZ,” Technical Meeting No. 2/11, NUCLEX 72, 1972.

45. Baldwin, M. N., and Stern, M. E., “Physics Verification Program Part III, Task 4: Summary Report,” BAW-3647-20, March 1971.

46. Baldwin, M. N., “Physics Verification Program Part III, Task 11: Quarterly Technical Report January-March 1974,” BAW-3647-30, July 1974.

47. Baldwin, M. N., “Physics Verification Program Part III, Task 11: Quarterly Technical Report July-September 1974,” BAW-3647-31, February 1975.

48. Nodvik, R. J., “Saxton Core II Fuel Performance Evaluation Part II: Evaluation of Mass Spectrometric and Radiochemical Analyses of Irradiated Saxton Plutonium Fuel,” WCAP-3385-56 Part II, July 1970.

49. Smalley, W. R., “Saxton Core II - Fuel Performance Evaluation Part I: Materials,” WCAP-3386-56 Part I, September 1971.

50. Goodspeed, R. C., “Saxton Plutonium Project - Quarterly Progress Report for the Period Ending June 20, 1973,” WCAP-3385-36, July 1973.

51. Crain, H. H., “Saxton Plutonium Project - Quarterly Progress Report for the Period Ending September 30, 1973,” WCAP-3385-37, December 1973.

52. Melehan, J. B., “Yankee Core Evaluation Program Final Report,” WCAP-3017-6094, January 1971.

53. APP-GW-GLR-029P, Revision 3, “AP1000 Spent Fuel Storage Racks Criticality Analysis,” Westinghouse Electric Company LLC (Westinghouse Proprietary).

54. Not used.

55. Not used.

56. Not used.

57. Davidson, S. L., (Ed.), et al., “ANC: A Westinghouse Advanced Nodal Computer Code,” WCAP-10965-P-A (Proprietary) and WCAP-10966-A (Nonproprietary), September 1986.

58. Leamer, R. D., et al., "PuO_2-U O_2 Fueled Critical Experiments," WCAP-3726-1, July 1967.

59. Davidson, S. L., et al., "Assessment of Clad Flattening and Densification Power Spike Factor Elimination in Westinghouse Nuclear Fuel," WCAP-13589-A (Proprietary) and WCAP-14297-A (Nonproprietary), March 1995.

60. Yarbrough, M. B., Liu, Y. S., Paterline, D. L., Hone, M. J., "APOLLO - A One Dimensional Neutron Theory Program," WCAP-13524, Revision 1 (Proprietary), August 1994 and WCAP-14952-NP-A, Revision 1A (Nonproprietary), September 1977.

61. Letter, Peralta, J. D. (NRC) to Maurer, B. F. (Westinghouse), "Approval for Increase in Licensing Burnup Limit to 62,000 MWD/MTU (TAC No. MD1486)," May 25, 2006.

62. Not used.

63. Not used.

64. APP-GW-GLR-059/WCAP-16652-NP, "AP1000 Core & Fuel Design Technical Report," Revision 0.

65. Bierman, S. R., "Criticality Experiments with Neutron Flux Traps Containing Voids," PNL-7167, Battelle Pacific Northwest Laboratory, April 1990.

66. Durst, B. M., et al., "Critical Experiments with 4.32 wt% 235U Enriched UO_2 Rods in Highly Borated Water Lattices," PNL-4267, Battelle Pacific Northwest Laboratory, August 1982.

67. Bierman, S. R., "Criticality Experiments with Fast Test Reactor Fuel Pins in Organic Moderator," PNL-5803, Battelle Pacific Northwest Laboratory, December 1981.

68. Taylor, E. G., et al., "Saxton Plutonium Program Critical Experiments for the Saxton Partial Plutonium Core," WCAP-3385-54, Westinghouse Electric Corp., Atomic Power Division, December 1965.

Table 4.3-1 (Sheet 1 of 3)
[*REACTOR CORE DESCRIPTION (FIRST CYCLE)*]*

Active core
Equivalent diameter (in.) *119.7*
Active fuel height first core (in.), cold *168*
Height-to-diameter ratio *1.40*
Total cross section area (ft^2) *78.14*
H_2O/U molecular ratio, cell, cold *2.40*
Reflector thickness and composition
Top - water plus steel (in.) ..... *~10*
Bottom - water plus steel (in.) ..... *~10*
Side - water plus steel (in.) ..... *~15*
Fuel assemblies
Number *157*
Rod array ..... *17 x 17*
Rods per assembly *264*
Rod pitch (in.) *0.496*
Overall transverse dimensions (in.) ..... *8.426 x 8.426*
Fuel weight, as UO_2 (lb) *211,588*
Zircaloy clad weight (lb) *43,105*
Number of grids per assembly
Top and bottom - (Ni-Cr-Fe Alloy 718) ..... *2[(a)]*
Intermediate ..... *8 ZIRLO™*
Intermediate flow mixing (IFM) ..... *4 ZIRLO™*
Number of guide thimbles per assembly *24*
Composition of guide thimbles ..... *ZIRLO™*
Diameter of guide thimbles, upper part (in.) ..... *0.442 ID x 0.482 OD*
Diameter of guide thimbles, lower part (in.) ..... *0.397 ID x 0.482 OD*
Diameter of instrument guide thimbles (in.) ..... *0.442 ID x 0.482 OD*

Note:
(a) The top grid will be fabricated of nickel-chromium-iron Alloy 718.

*NRC Staff approval is required prior to implementing a change in this information.

Table 4.3-1 (Sheet 2 of 3)
[*REACTOR CORE DESCRIPTION (FIRST CYCLE)*]*

Fuel rods	
Number	*41,448*
Outside diameter (in.)	*0.374*
Diameter gap (in.)	*0.0065*
Clad thickness (in.)	*0.0225*
Clad material	*ZIRLO™*
Fuel pellets	
Material	*UO_2 sintered*
Density (% of theoretical) (nominal)	*95.5*
Fuel enrichments (weight %)	
Region 1	*2.35*
Region 2	*3.40*
Region 3	*4.45*
Diameter (in.)	*0.3225*
Length (in.)	*0.387*
Mass of UO_2 per ft of fuel rod (lb/ft)	*0.366*
Rod Cluster Control Assemblies	
Neutron absorber	*Ag-In-Cd*
Diameter (in.)	*0.341*
Density (lb/in.^{3})	*Ag-In-Cd 0.367*
Cladding material	*Type 304, cold-worked SS*
Clad thickness (in.)	*0.0185*
Number of clusters, full-length	*53*
Number of absorber rods per cluster	*24*
Gray Rod Cluster Assemblies	
Neutron absorber	*Ag-In-Cd/304SS*
Diameter (in.)	*0.160*
Density (lb/in.^{3})	*Ag-In-Cd 0.367 / 304SS 0.285*
Cladding material	*Type 304, cold-worked SS*
Clad thickness (in.)	*0.0185*
Number of clusters, full-length	*16*
Number of absorber rods per cluster	*12 Ag-In-Cd / 12 304SS*

*NRC Staff approval is required prior to implementing a change in this information.

Table 4.3-1 (Sheet 3 of 3)
[*REACTOR CORE DESCRIPTION (FIRST CYCLE)*]*

Discrete Burnable absorber rods (first core)
Number 1558
Material ..... Borosilicate Glass
OD (in.) 0.381
Inner tube, OD (in.) 0.1815
Clad material ..... Stainless Steel
Inner tube material ..... Stainless Steel
B_{10} content (Mg/cm) 6.24
Absorber length (in.) 145
Integral Fuel Burnable Absorbers (first core)
Number 8832
Type ..... IFBA
Material ..... Boride Coating
B_{10} Content (Mg/cm) 0.772
Absorber length (in.) 152
Excess reactivity
Maximum fuel assembly K_∞ (cold, clean, unborated water) 1.328
Maximum core reactivity K_{eff} (cold, zero power, beginning of cycle, zero soluble boron) 1.205

*NRC Staff approval is required prior to implementing a change in this information.

Table 4.3-2 (Sheet 1 of 2)
[*NUCLEAR DESIGN PARAMETERS (FIRST CYCLE)*]*

Core average linear power, including densification effects (kW/ft)		*5.72*
Total heat flux hot channel factor, F_Q		*2.60*
Nuclear enthalpy rise hot channel factor, $F^N_{\Delta H}$		*1.65*
Reactivity coefficients [(a)]	*Design Limits*	*Best Estimate*
Doppler-only power coefficients (see Figure 15.0.4-1) (pcm/% power)[(b)]		
Upper curve	*-19.4 to -12.6*	*-13.3 to -8.7*
Lower curve	*-10.2 to -6.7*	*-11.3 to -8.4*
Doppler temperature coefficient (pcm/°F)[(b)]	*-3.5 to -1.0*	*-2.1 to -1.3*
Moderator temperature coefficient (pcm/°F)[(b)]	*0 to -40*	*0 to -35*
Boron coefficient (pcm/ppm)[(b)]	*-13.5 to -5.0*	*-10.5 to -6.9*
Rodded moderator density (pcm/g/cm^3)[(b)]	*≤ 0.47x10^5*	*≤ 0.45x10^5*
Delayed neutron fraction and lifetime, β_{eff}		*0.0075(0.0044)[(c)]*
Prompt Neutron Lifetime, ℓ^*, μs		*19.8*
Control rods		
Rod requirements		*See Table 4.3-3*
Maximum ejected rod worth		*See Chapter 15*
Bank worth HZP no overlap (pcm)[(b)]	*BOL, Xe Free*	*EOL, Eq. Xe*
MA Bank	*299*	*205*
MB Bank	*195*	*250*
MC Bank	*139*	*218*
MD Bank	*312*	*198*
M1 Bank	*856*	*632*
M2 Bank	*933*	*1405*
AO Bank	*2027*	*1571*

*NRC Staff approval is required prior to implementing a change in this information.

Table 4.3-2 (Sheet 2 of 2)
[*NUCLEAR DESIGN PARAMETERS (FIRST CYCLE)*]*

Typical Hot Channel Factors $F^N_{\Delta H}$	*BOL*	*EOL*
Unrodded	*1.40*	*1.33*
MA bank	*1.46*	*1.38*
MA + MB banks	*1.46*	*1.33*
MA + MB + MC banks	*1.50*	*1.31*
MA + MB + MC + MD banks	*1.50*	*1.37*
MA + MB + MC + MD + M1 banks	*1.52*	*1.45*
AO bank	*1.60*	*1.52*
Boron concentrations (ppm)		
Zero power, k_{eff} = 0.99, cold[(d)] RCCAs out		*1574*
Zero power, k_{eff} = 0.99, hot[(e)] RCCAs out		*1502*
Design basis refueling boron concentration		*2700*
Zero power, $k_{eff} \leq 0.95$, cold[(d)] RCCAs in		*1179*
Zero power, k_{eff} = 1.00, hot[(e)] RCCAs out		*1382*
Full power, no xenon, k_{eff} = 1.0, hot RCCAs out		*1184*
Full power, equilibrium xenon, k = 1.0, hot RCCAs out		*827*
Reduction with fuel burnup		
First cycle (ppm/(GWD/MTU))[(f)]		*See Figure 4.3-3*
Reload cycle (ppm/(GWD/MTU))		*~40*

Notes:

(a) Uncertainties are given in Subsection 4.3.3.3.
(b) 1 pcm = 10^{-5} Δρ where Δρ is calculated form two statepoint values of k_{eff} by ln (k_1/k_2).
(c) Bounding lower value used for safety analysis.
(d) *Cold means 68°F, 1 atm.*
(e) *Hot means 557°F, 2250 psia.*
(f) 1 GWD = 1000 MWD. During the first cycle, a large complement of burnable absorbers is present which significantly reduce the boron depletion rate compared to reload cycles.

*NRC Staff approval is required prior to implementing a change in this information.

Table 4.3-3
[*REACTIVITY REQUIREMENTS FOR ROD CLUSTER CONTROL ASSEMBLIES*]*

Reactivity Effects (Percent)	***BOL (First Cycle)***	***EOL (First Cycle)***	***EOL Representative (Equilibrium Cycle)***
1. Control requirements			
Total power defect (%Δρ)[(a)]	*1.89*	*2.54*	*3.02*
Redistribution (adverse xenon only) (%Δρ)	*0.27*	*0.40*	*0.32*
Rod insertion allowance (%Δρ)	*2.00*	*2.00*	*2.00*
2. Total control (%Δρ)	*4.16*	*4.94*	*5.34*
3. Estimated RCCA worth (69 rods)			
a. All full-length assemblies inserted (%Δρ)	*12.69*	*10.89*	*10.64*
b. All assemblies but one (highest worth inserted (%Δρ)	*10.49*	*9.27*	*9.35*
4. Estimated RCCA credit with 7 percent adjustment to accommodate uncertainties, item 3b minus 7 percent (%Δρ)	*9.76*	*8.62*	*8.70*
5. Shutdown margin available, item 4 minus item 2 (%Δρ)[(b)]	*5.60*	*3.68*	*3.36*

Notes:
(a) Includes void effects.
(b) The design basis minimum shutdown is 1.60 percent.

*NRC Staff approval is required prior to implementing a change in this information.

Table 4.3-4 Not Used

Table 4.3-5
Stability Index for Pressurized Water Reactor Cores with a 12-Foot Height

Burnup (MWD/MTU)	F_Z	C_B (ppm)	Axial Stability Index (h^{-1})	
			Experiment	Calculated
1550	1.34	1065	-0.0410	-0.0320
7700	1.27	700	-0.0140	-0.0060
5090[(a)]			-0.0325	-0.0255
			Radial Stability Index (h^{-1})	
			Experiment	Calculated
2250[(b)]			-0.0680	-0.0700

Notes:
(a) Four-loop plant, 12-foot core in cycle 1, axial stability test
(b) Four-loop plant, 12-foot core in cycle 1, radial (X-Y) stability test

Table 4.3-6
Typical Neutron Flux Levels (n/cm^2/s) at Full Power

	E ≥ 1.0 MeV	**1.00 MeV > E ≥5.53 KeV**	**5.53 KeV > E ≥0.625 eV**	**E < 0.625 eV**
Core center	1.12×10^{14}	1.76×10^{14}	1.28×10^{14}	5.47×10^{13}
Core outer radius at midheight	3.86×10^{13}	6.08×10^{13}	4.42×10^{13}	1.83×10^{13}
Core top, on axis	3.02×10^{13}	4.75×10^{13}	3.46×10^{13}	2.17×10^{13}
Core bottom, on axis	2.92×10^{13}	4.59×10^{13}	3.34×10^{13}	2.40×10^{13}
Pressure vessel ID azimuthal peak	4.71×10^{10}	8.4×10^{10}	5.56×10^{10}	5.32×10^{10}

Table 4.3-7
Comparison of Measured and Calculated Doppler Defects

Plant	Fuel	Core Burnup (MWD/MTU)	Measured (pcm)[(a)]	Calculated (pcm)
1	Air filled	1800	1700	1710
2	Air filled	7700	1300	1440
3	Air and helium filled	8460	1200	1210

Note:
(a) $pcm = 10^5 \times \ln (k_2/k_1)$

Table 4.3-8
Comparison of Measured and Calculated AG-in-CD Rod Worth

2-Loop Plant, 121 Assemblies, 10-ft Core		Measured (pcm)	Calculated (pcm)
Group B		1885	1893
Group A		1530	1649
Shutdown group		3050	2917
ESADA critical, 0.69-in. pitch[(a)] 2 w/o PuO_2, 8% Pu-240, 9 control rods			
6.21-in. rod separation		2250	2250
2.07-in. rod separation		4220	4160
1.38-in. rod separation		4100	4019
Benchmark Critical Experiment Hafnium Control Rod Worth			
Control Rod Configuration	**No. of Fuel Rods**	**Measured[(b)] Worth (Δppm B-10)**	**Calculated[(b)] Worth (Δppm B-10)**
9 hafnium rods	1192	138.3	141.0

Notes:
(a) Report in WCAP-3726-1 (Reference 58).
(b) Calculated and measured worth are given in terms of an equivalent charge in B-10 concentration.

Table 4.3-9
Comparison of Measured and Calculated Moderator Coefficients at HZP, BOL

Plant Type/ Control Bank Configuration	Measured α_{iso} [(a)] (pcm/°F)	Calculated α_{iso} (pcm/°F)
3-loop, 157-assembly, 12-ft core		
D at 160 steps	-0.50	-0.50
D in, C at 190 steps	-3.01	-2.75
D in, C at 28 steps	-7.67	-7.02
B, C, and D in	-5.16	-4.45
2-loop, 121-assembly, 12-ft core		
D at 180 steps	+0.85	+1.02
D in, C at 180 steps	-2.40	-1.90
C and D in, B at 165 steps	-4.40	-5.58
B, C, and D in, A at 174 steps	-8.70	-8.12
4-loop, 193-assembly, 12-ft core		
ARO	-0.52	-1.2
D in	-4.35	-5.7
D and C in	-8.59	-10.0
D, C, and B in	-10.14	-10.55
D, C, B, and A in	-14.63	-14.45

Note:
(a) Isothermal coefficients, which include the Doppler effect in the fuel

$$\alpha_{iso} = 10^5 \ln \frac{k_2}{k_1} / \Delta T\,^{\circ}F$$

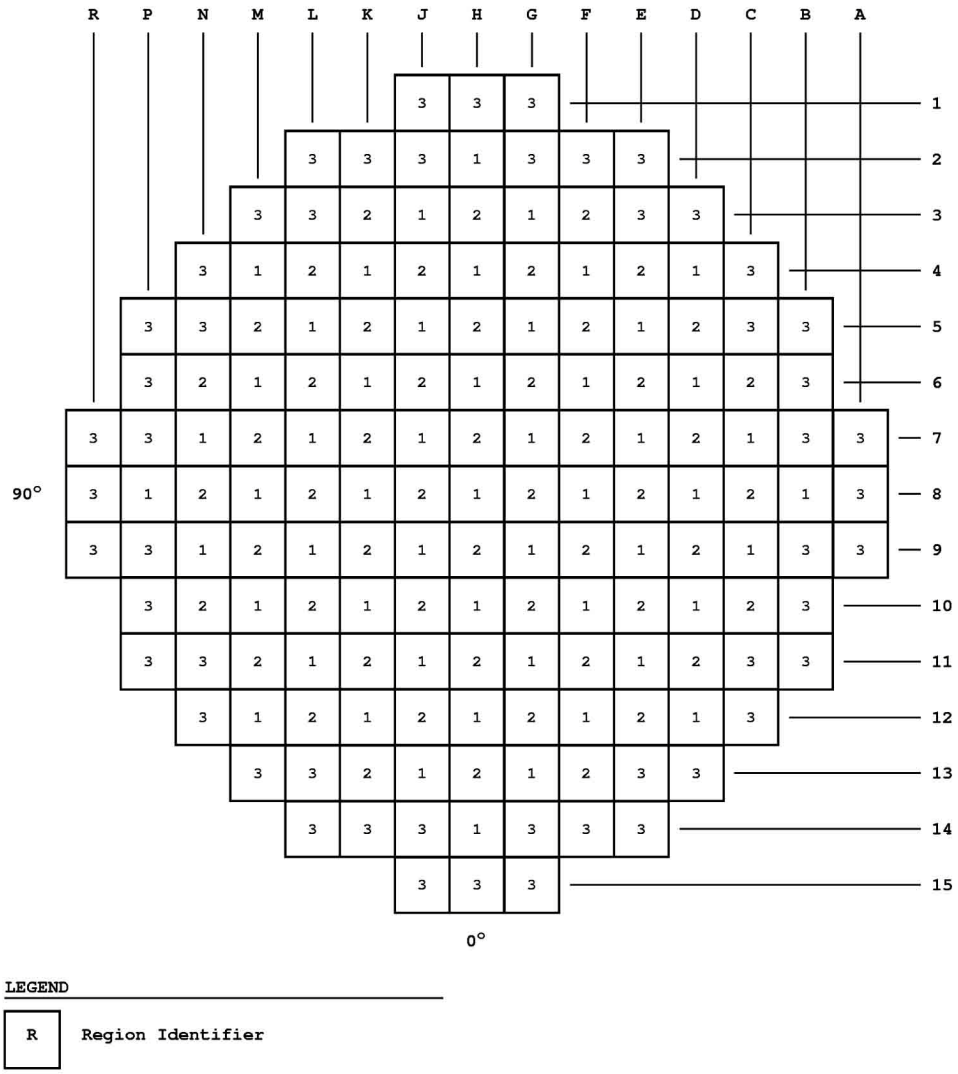

Region	Enrichment
1	2.35 w/o
2	3.40 w/o
3	4.45 w/o

Figure 4.3-1
Fuel Loading Arrangement

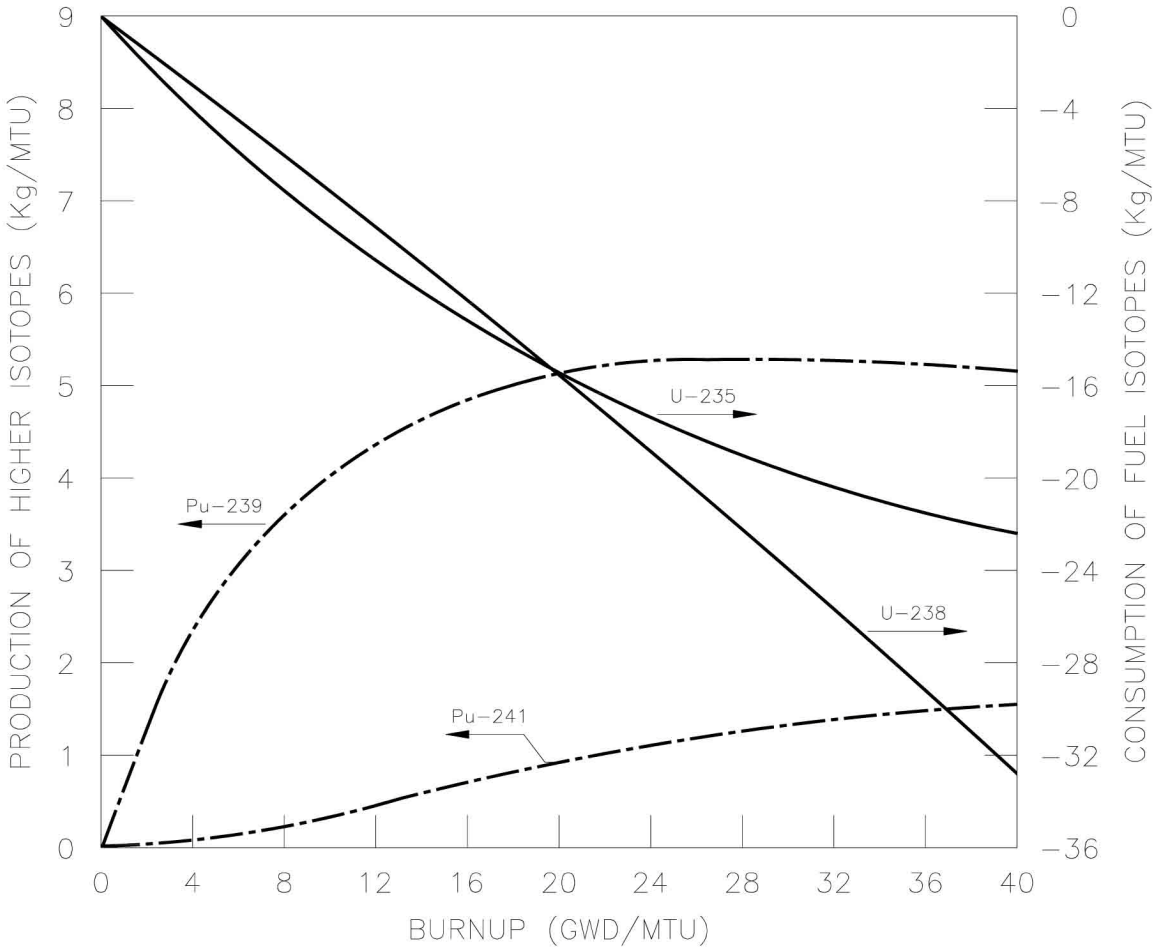

Figure 4.3-2
Typical Production and Consumption of Higher Isotopes

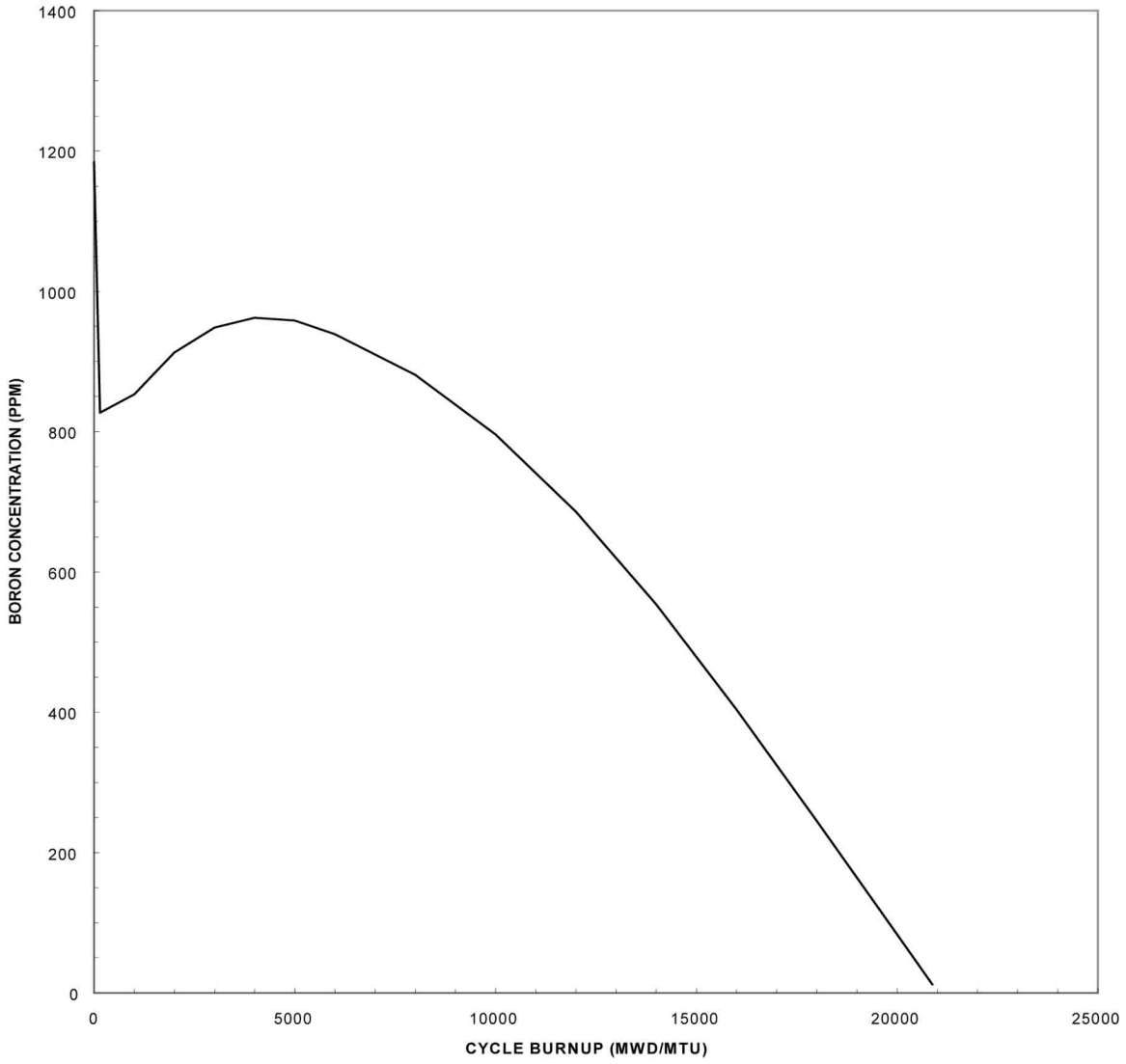

Figure 4.3-3
Cycle 1 Soluble Boron Concentration Versus Burnup

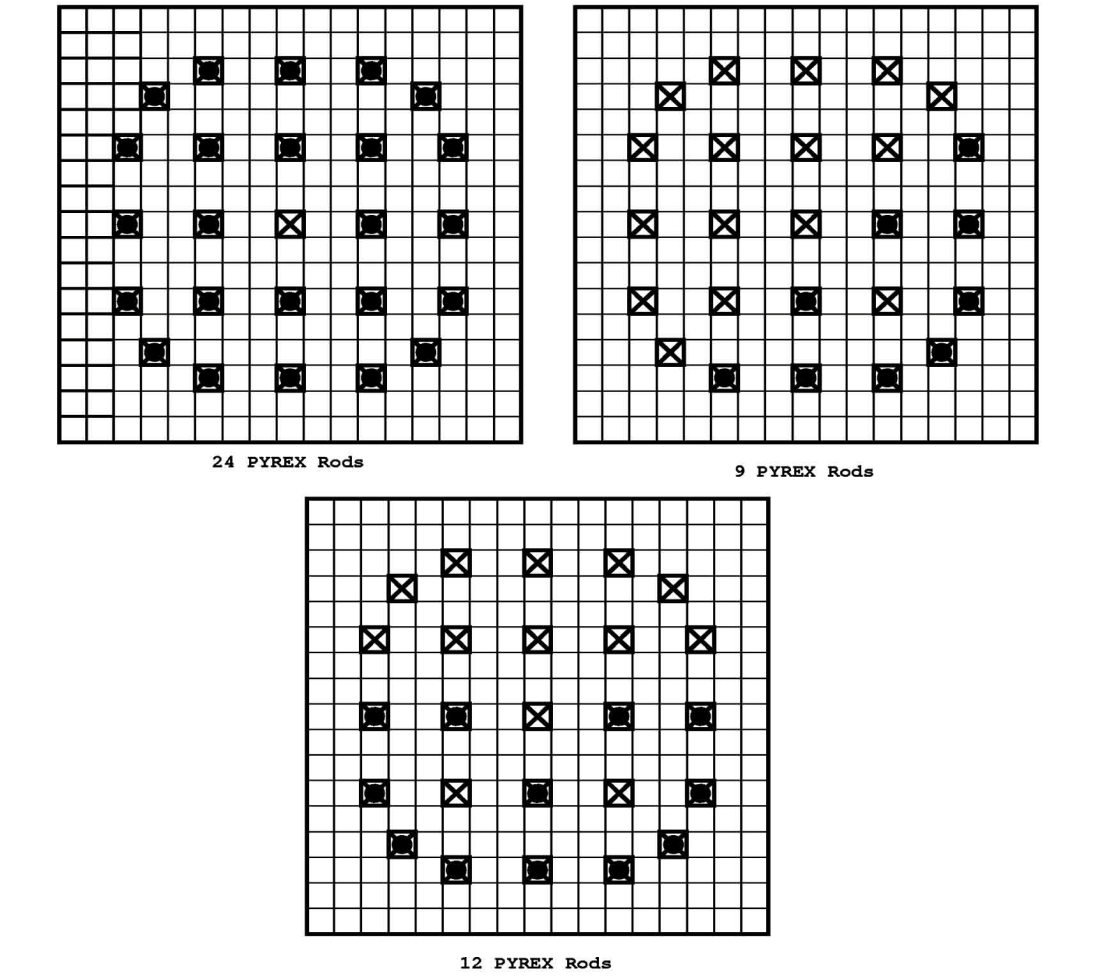

Figure 4.3-4a
Cycle 1 Assembly Burnable Absorber Patterns

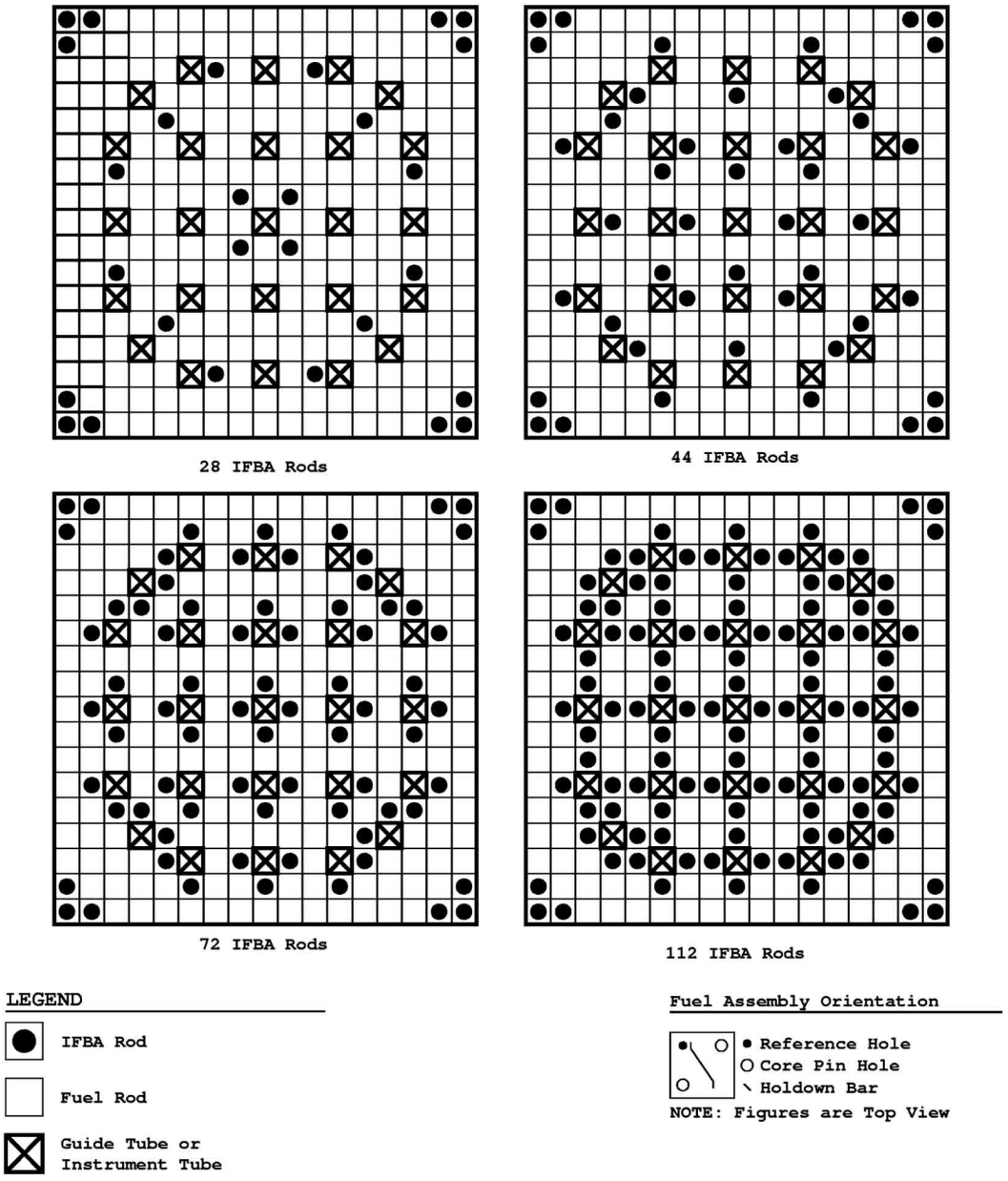

Figure 4.3-4b (Sheet 1 of 2)
Cycle 1 Assembly Burnable Absorber Patterns

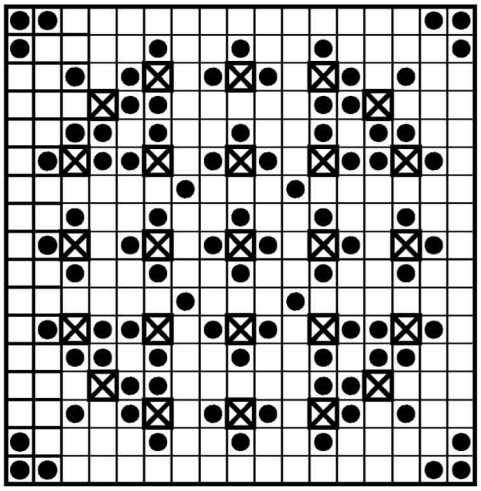

88 IFBA Rods

LEGEND

IFBA Rod

Fuel Rod

Guide Tube or
Instrument Tube

Fuel Assembly Orientation

● Reference Hole
○ Core Pin Hole
\ Holdown Bar

NOTE: Figures are Top View

Figure 4.3-4b (Sheet 2 of 2)
Cycle 1 Assembly Burnable Absorber Patterns

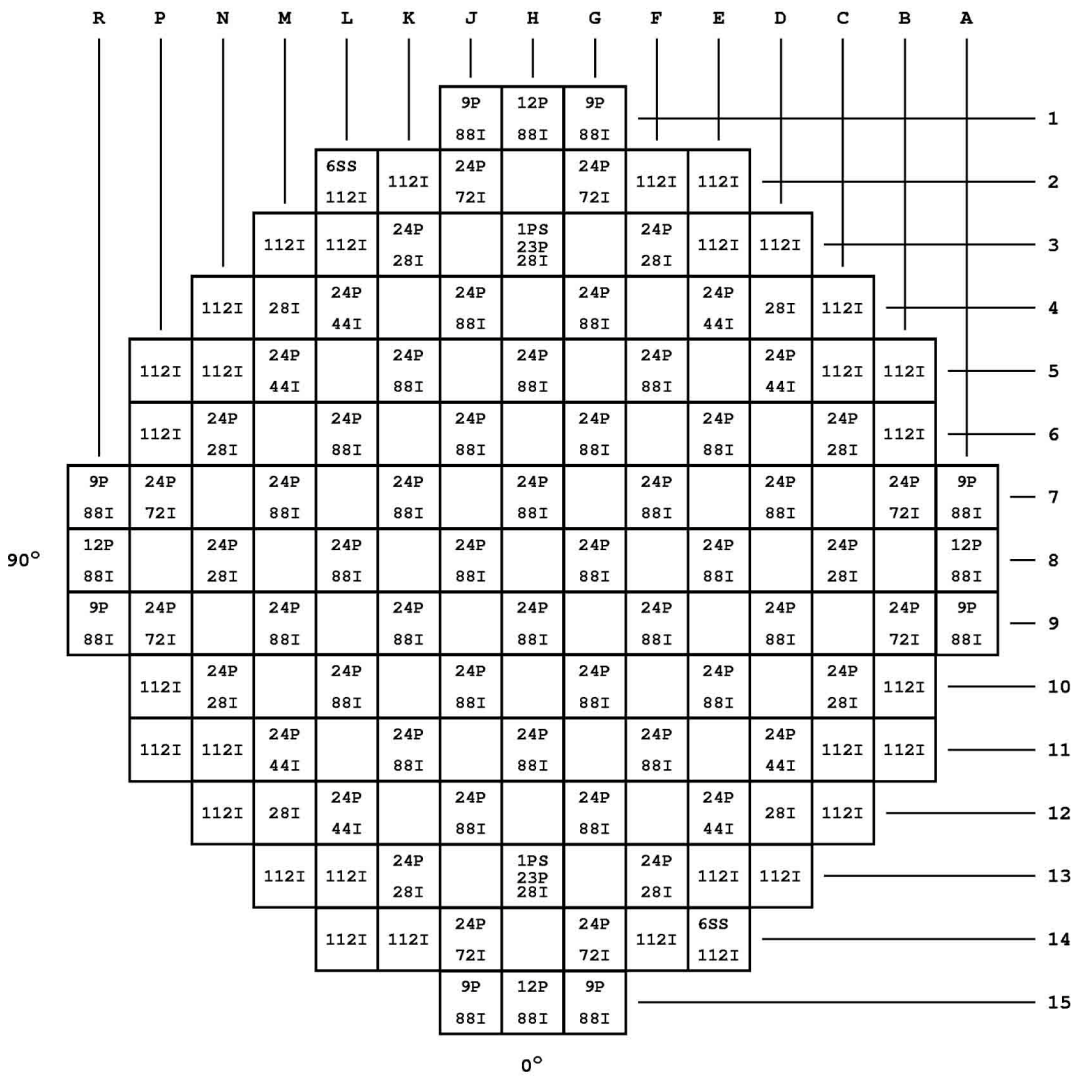

TYPE	TOTAL
##P...(NUMBER OF PYREX RODLETS).....	1558
##I...(TOTAL NUMBER OF FRESH IFBA RODS).....	8832
#PS...(NUMBER OF PRIMARY SOURCE RODLETS).....	2
#SS...(NUMBER OF SECONDARY SOURCE RODLETS).....	12

Figure 4.3-5
Burnable Absorber, Primary, and Secondary Source Assembly Locations

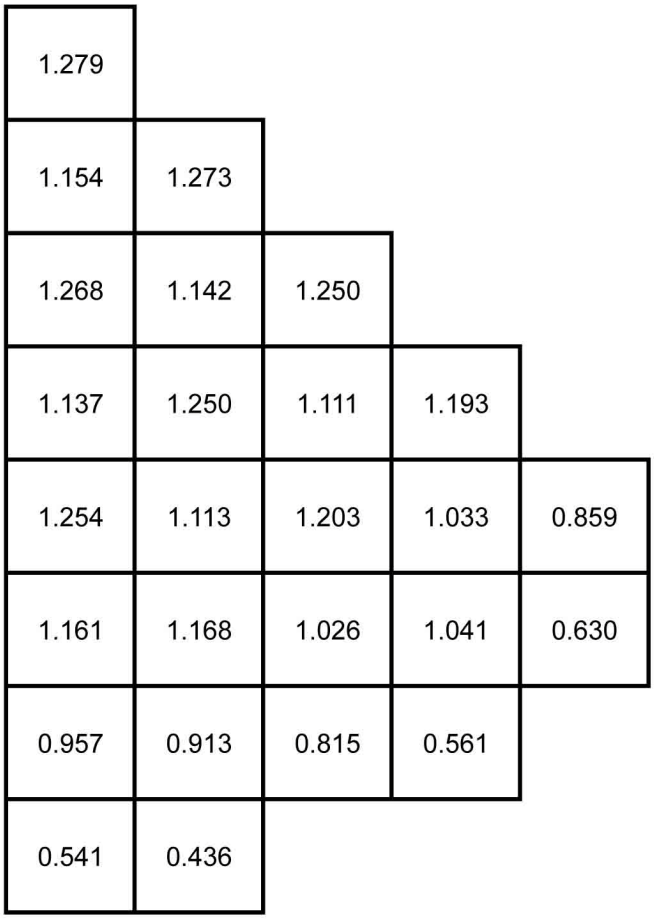

CALCULATED F-DELTA-H = 1.406

KEY: VALUE REPRESENTS ASSEMBLY
RELATIVE POWER

Figure 4.3-6
Normalized Power Density Distribution
Near Beginning of Life, Unrodded Core,
Hot Full Power, No Xenon

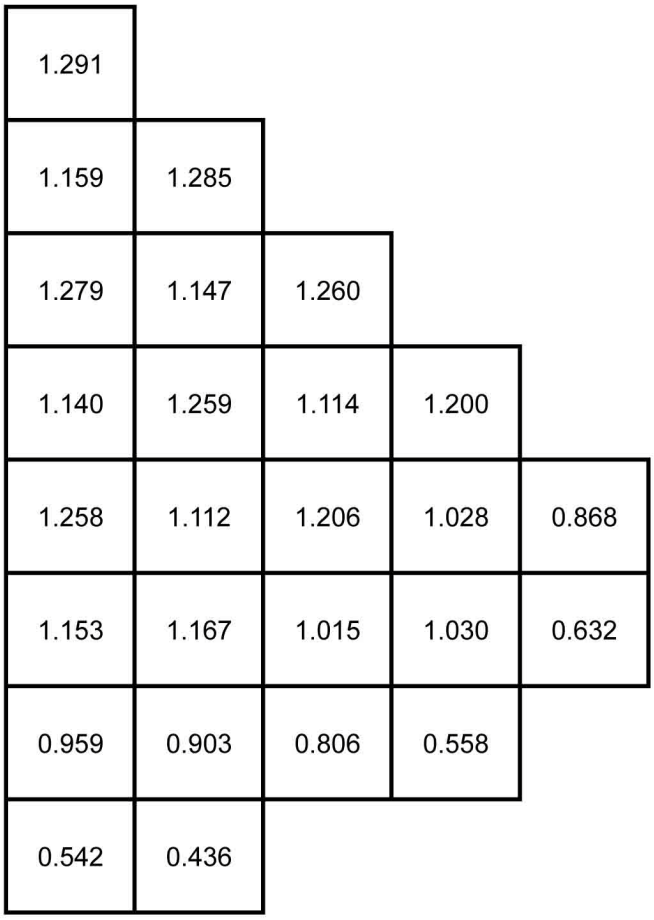

CALCULATED F-DELTA-H = 1.403

KEY: VALUE REPRESENTS ASSEMBLY
RELATIVE POWER

Figure 4.3-7
Normalized Power Density Distribution
Near Beginning of Life, Unrodded Core,
Hot Full Power, Equilibrium Xenon

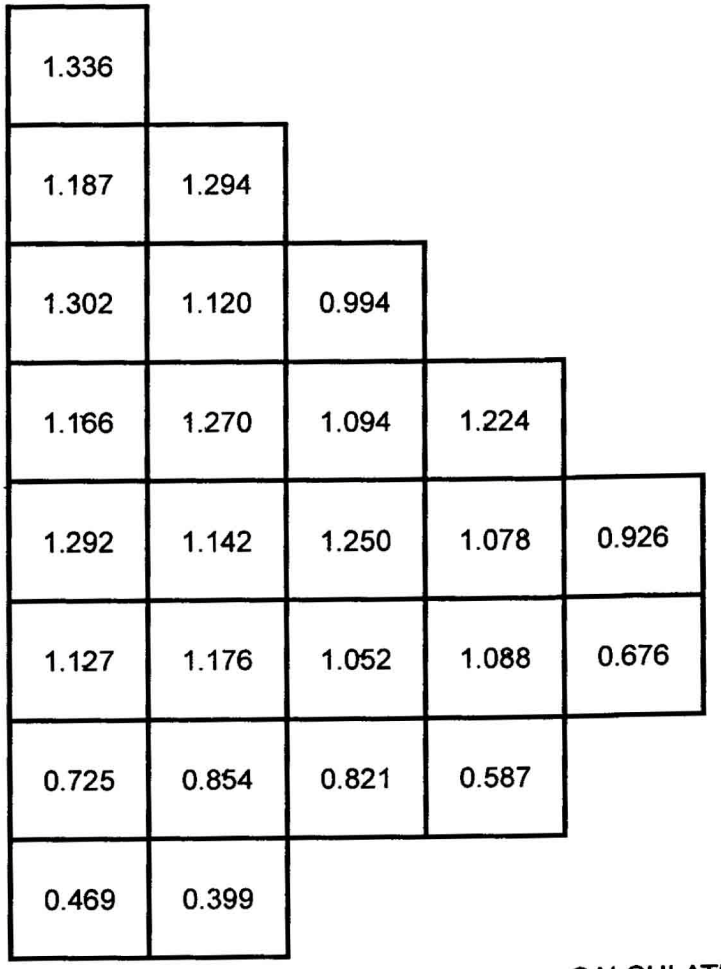

Figure 4.3-8
Normalized Power Density Distribution
Near Beginning of Life, Gray Bank MA+MB Inserted,
Hot Full Power, Equilibrium Xenon

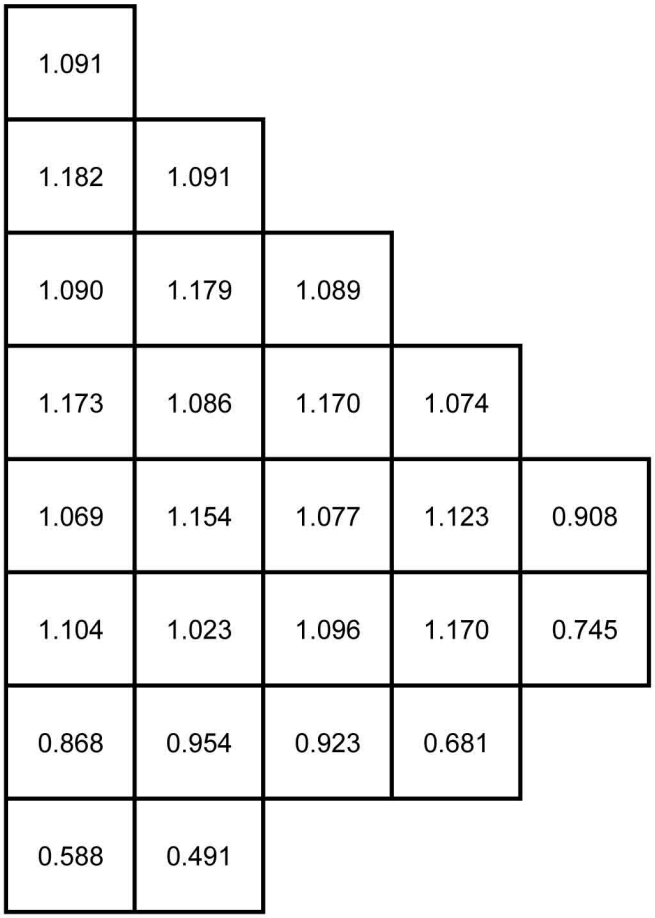

CALCULATED F-DELTA-H = 1.333

KEY: VALUE REPRESENTS ASSEMBLY
RELATIVE POWER

Figure 4.3-9
Normalized Power Density Distribution
Near Middle of Life, Unrodded Core,
Hot Full Power, Equilibrium Xenon

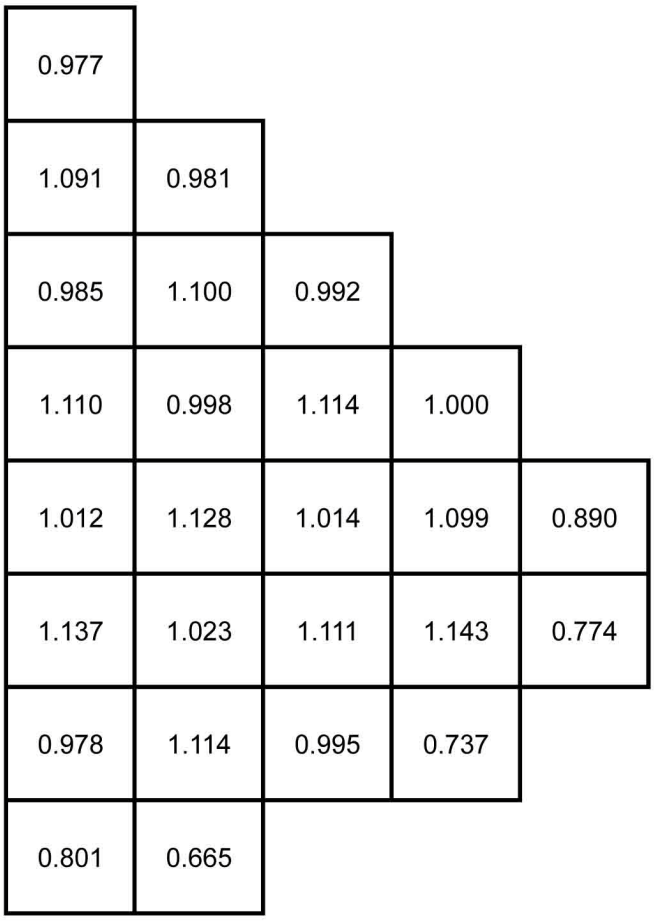

Figure 4.3-10
Normalized Power Density Distribution
Near End of Life, Unrodded Core,
Hot Full Power, Equilibrium Xenon

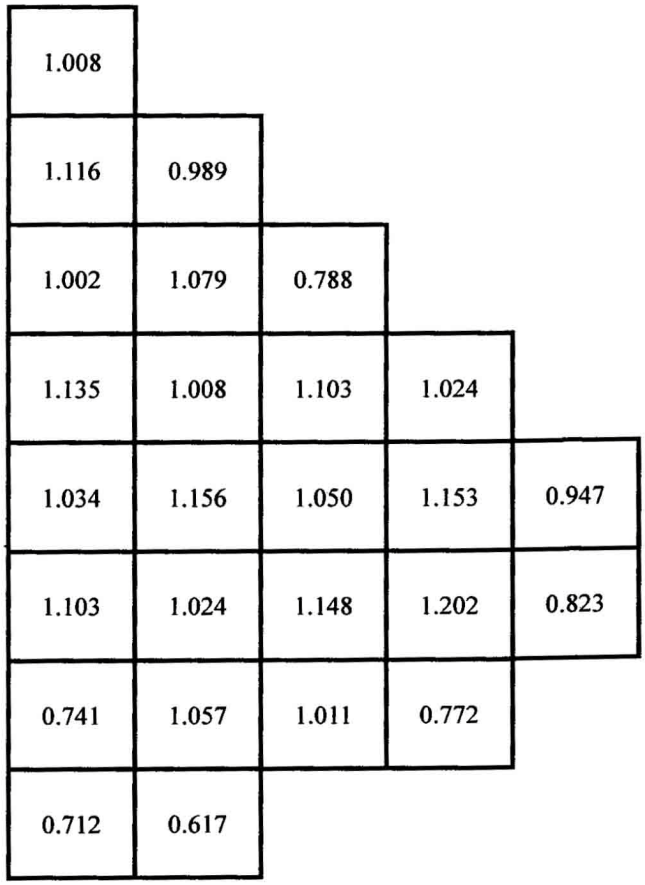

CALCULATED F-DELTA-H = 1.328

KEY: VALUE REPRESENTS ASSEMBLY RELATIVE POWER

Figure 4.3-11
Normalized Power Density Distribution
Near End of Life, Gray Bank MA+MB Inserted,
Hot Full Power, Equilibrium Xenon

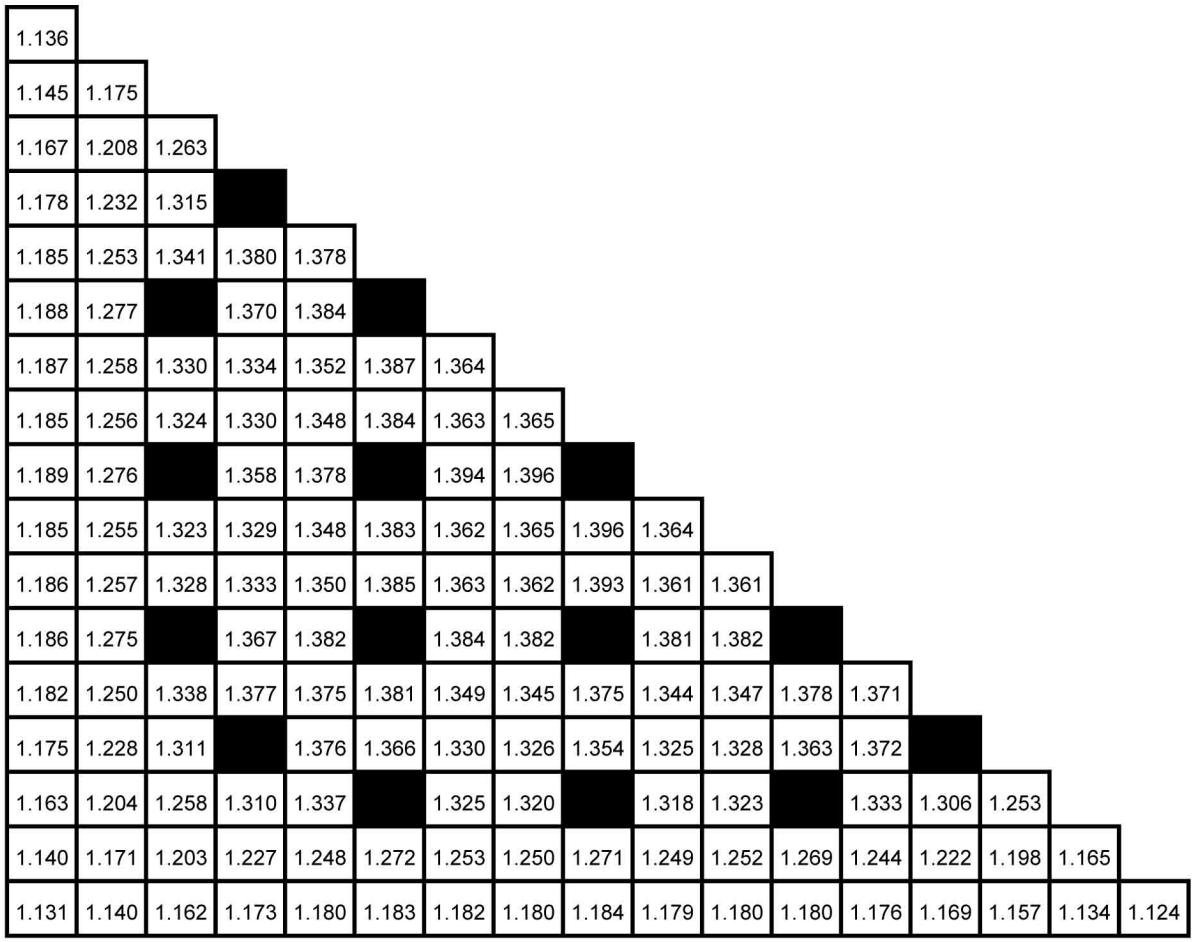

Figure 4.3-12
Rodwise Power Distribution in a Typical Assembly (G-9)
Near Beginning of Life
Hot Full Power, Equilibrium Xenon, Unrodded Core

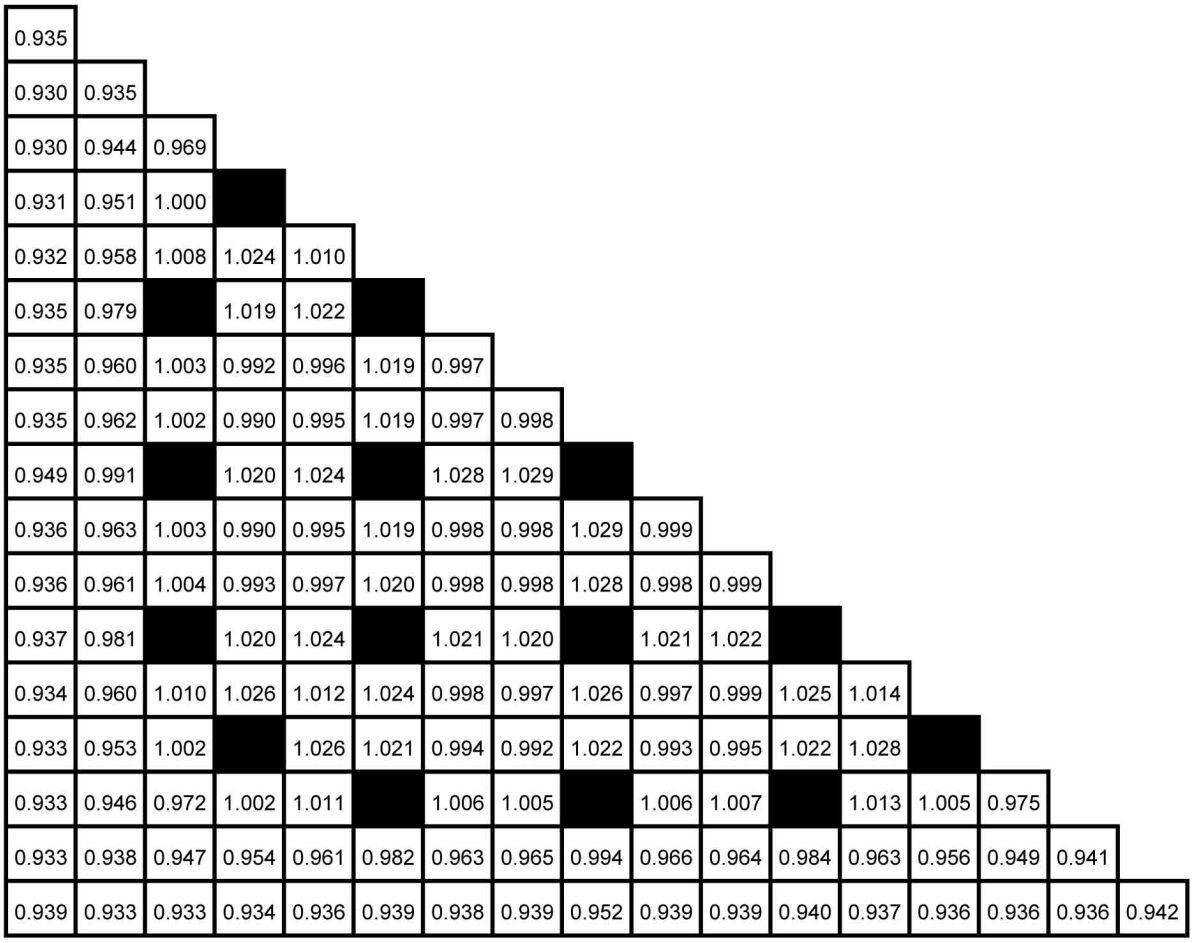

Figure 4.3-13
Rodwise Power Distribution in a Typical Assembly (G-9)
Near End of Life
Hot Full Power, Equilibrium Xenon, Unrodded Core

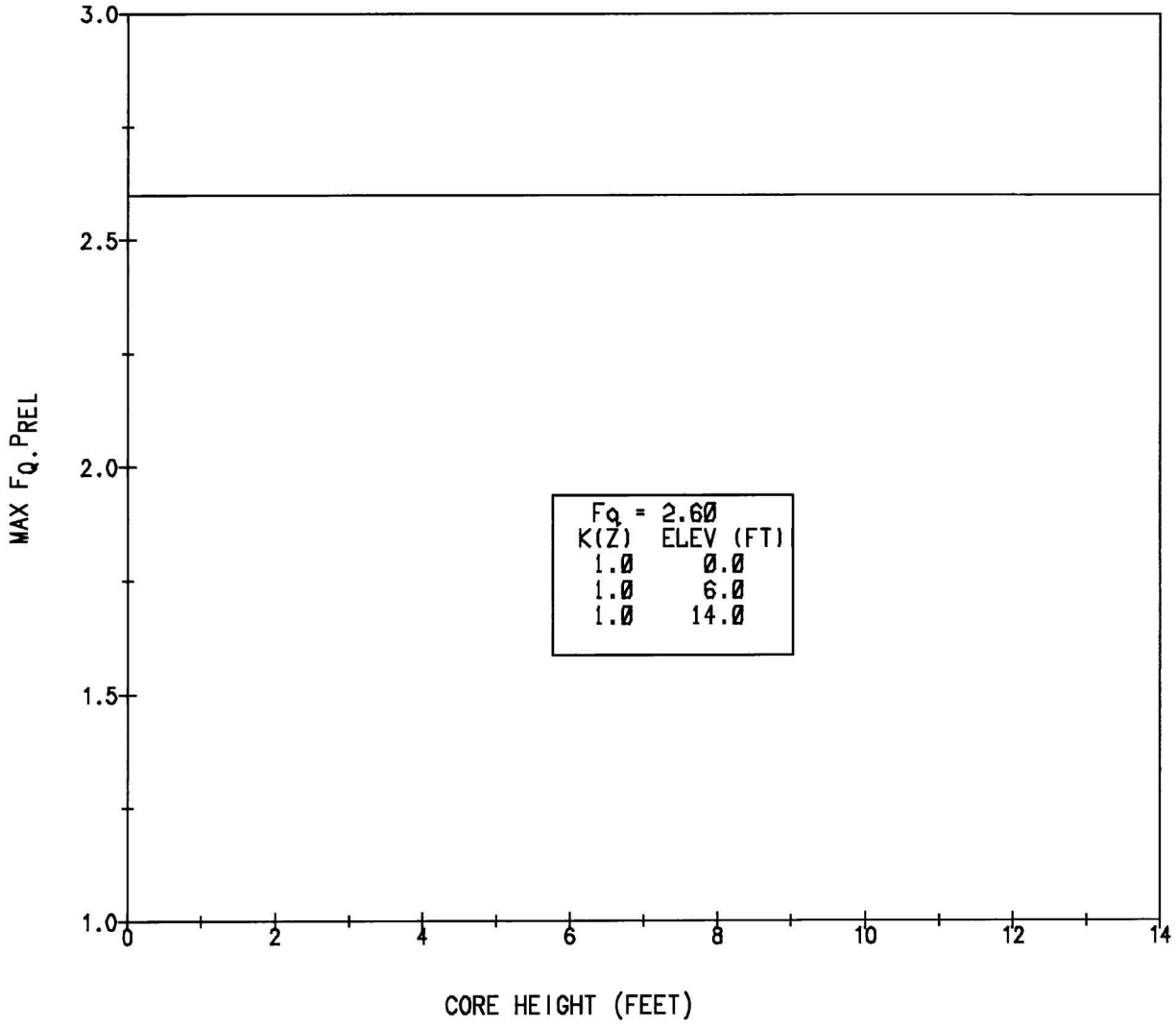

Figure 4.3-14
Maximum F_Q x Power Versus Axial Height
During Normal Operation

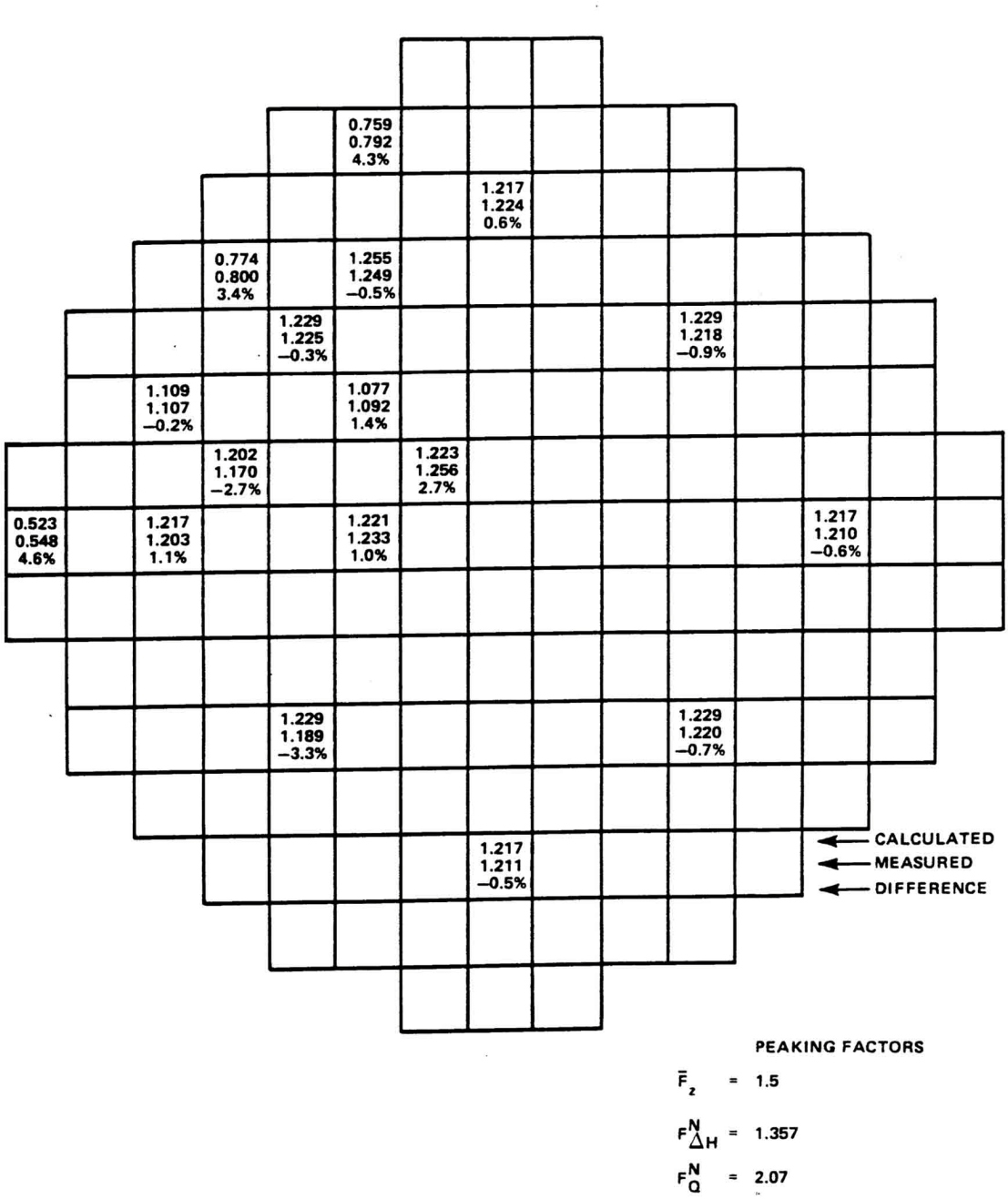

Figure 4.3-15
Typical Comparison Between Calculated and Measured Relative Fuel Assembly Power Distribution

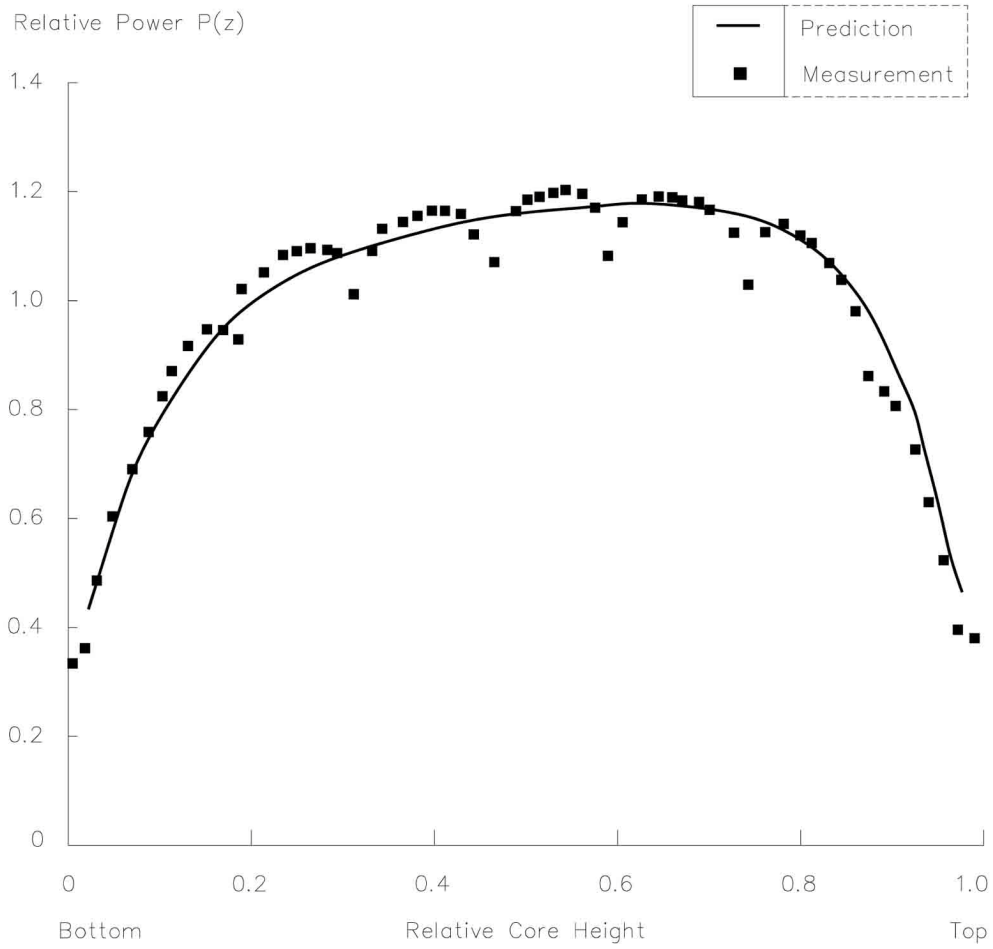

Figure 4.3-16
Typical Calculated Versus Measured Axial Power Distribution

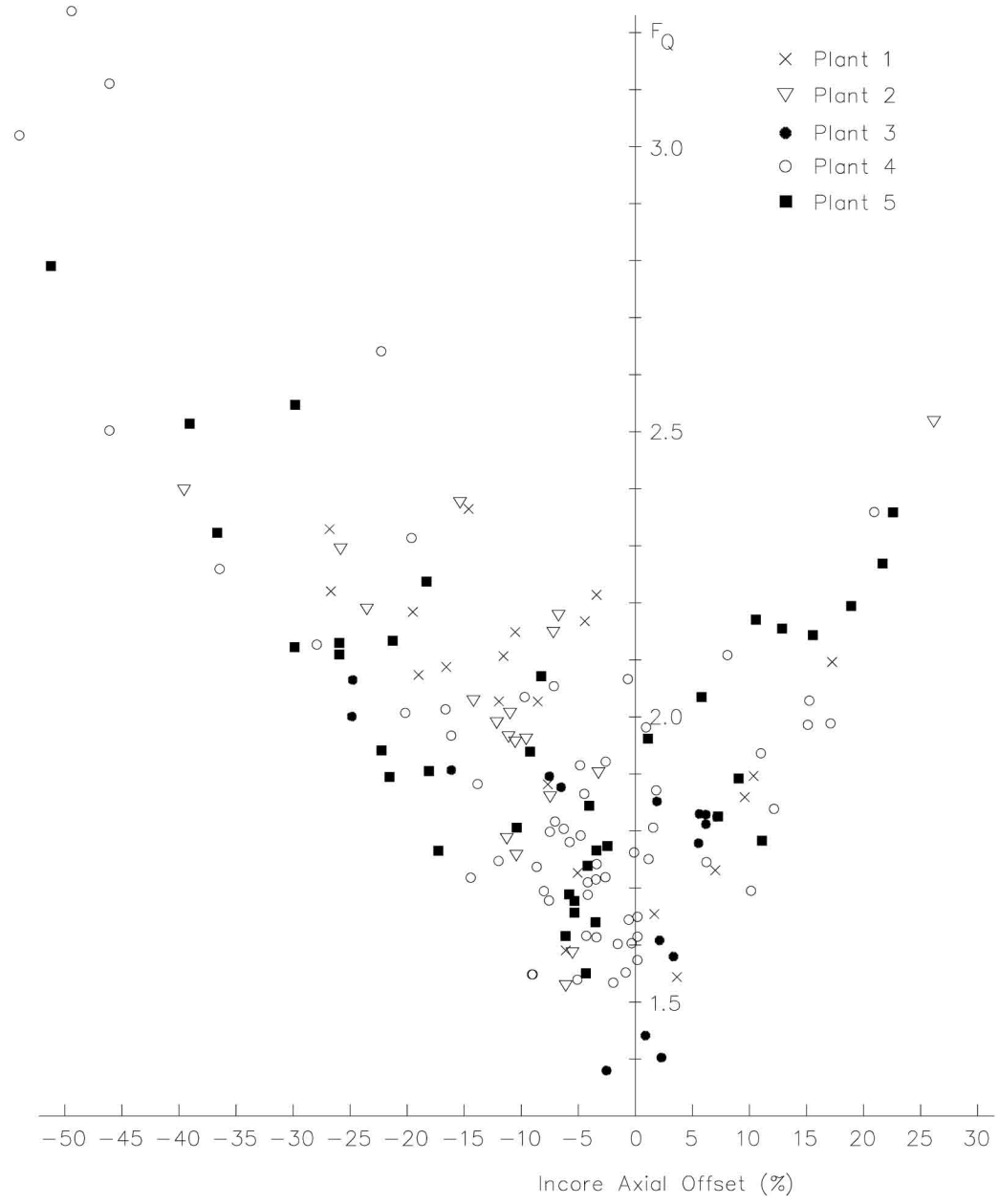

Figure 4.3-17
Measured F_Q Values Versus Axial Offset for Full Power Rod Configurations

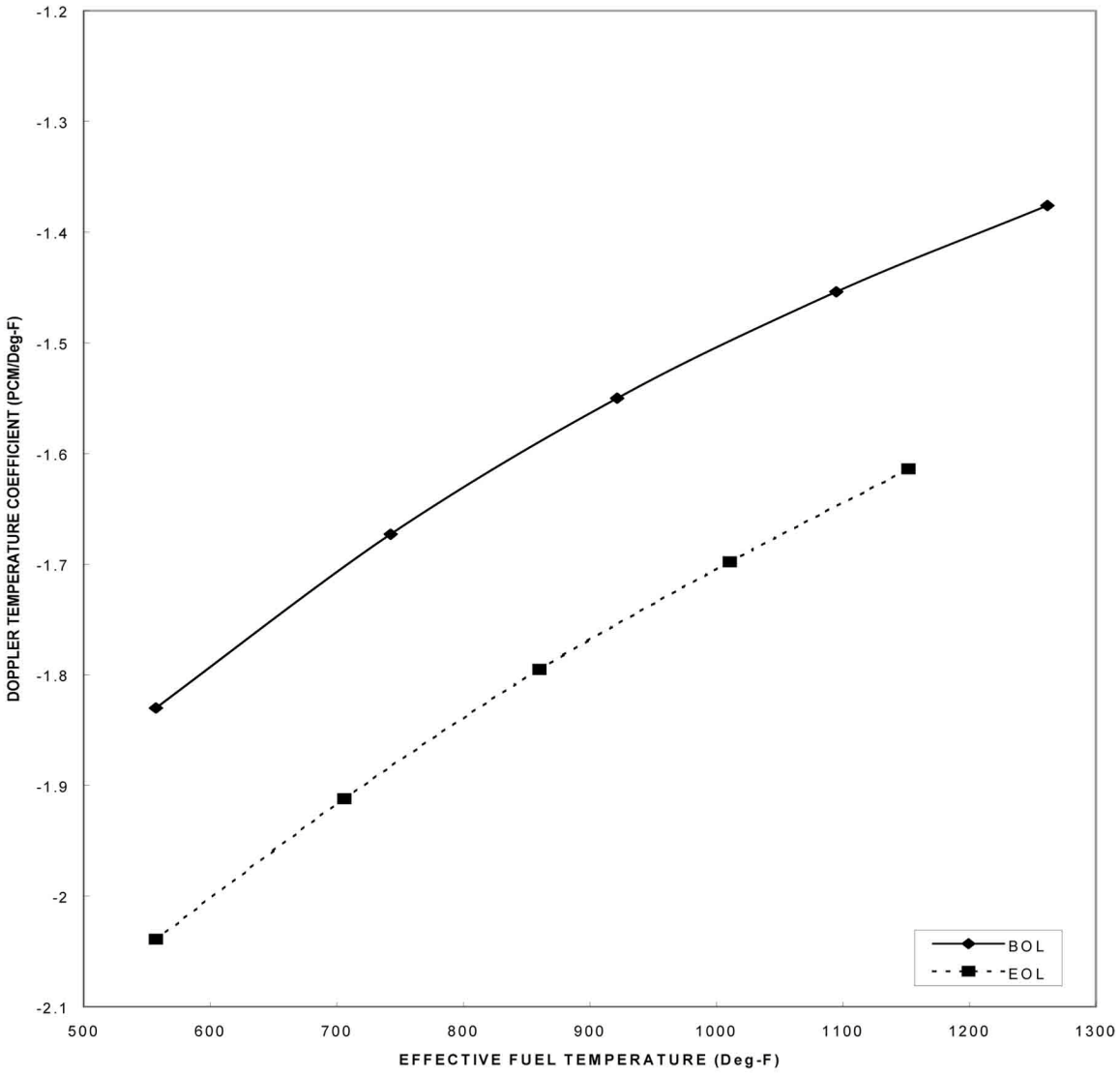

Figure 4.3-18
Typical Doppler Temperature Coefficient at BOL and EOL

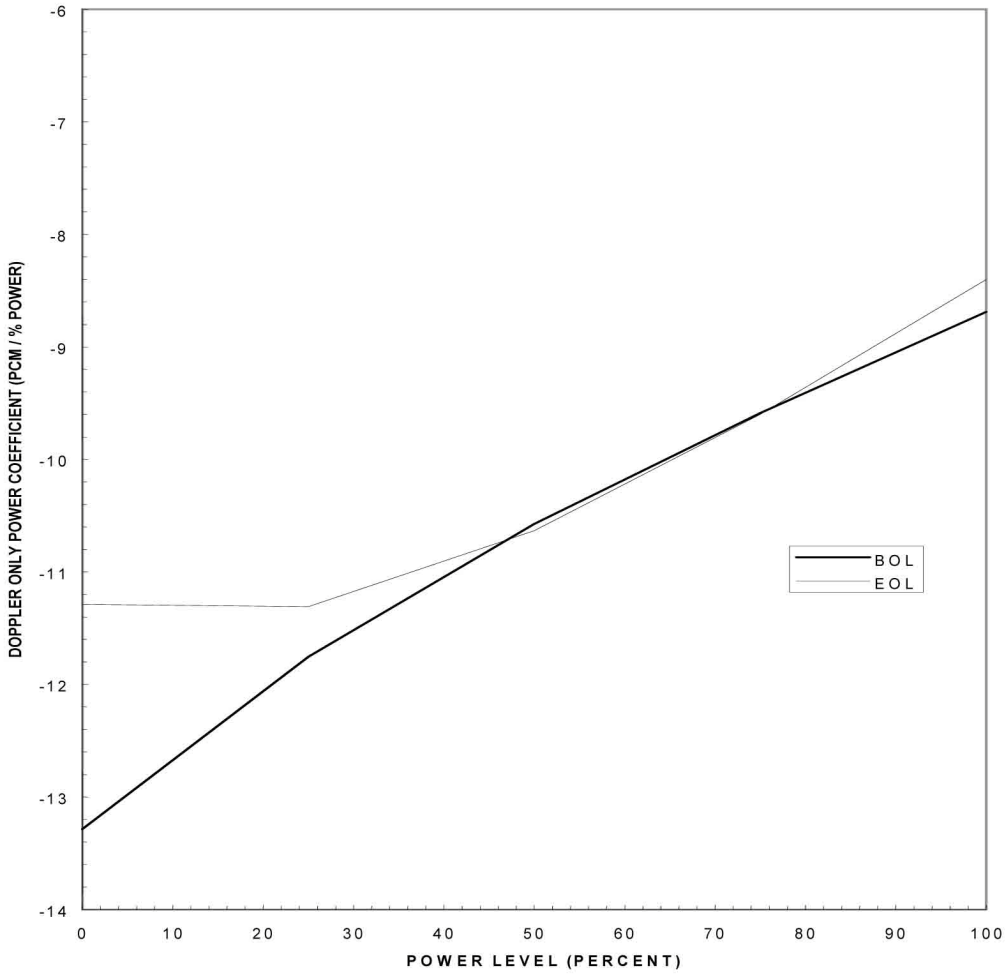

Figure 4.3-19
Typical Doppler-Only Power Coefficient at BOL and EOL

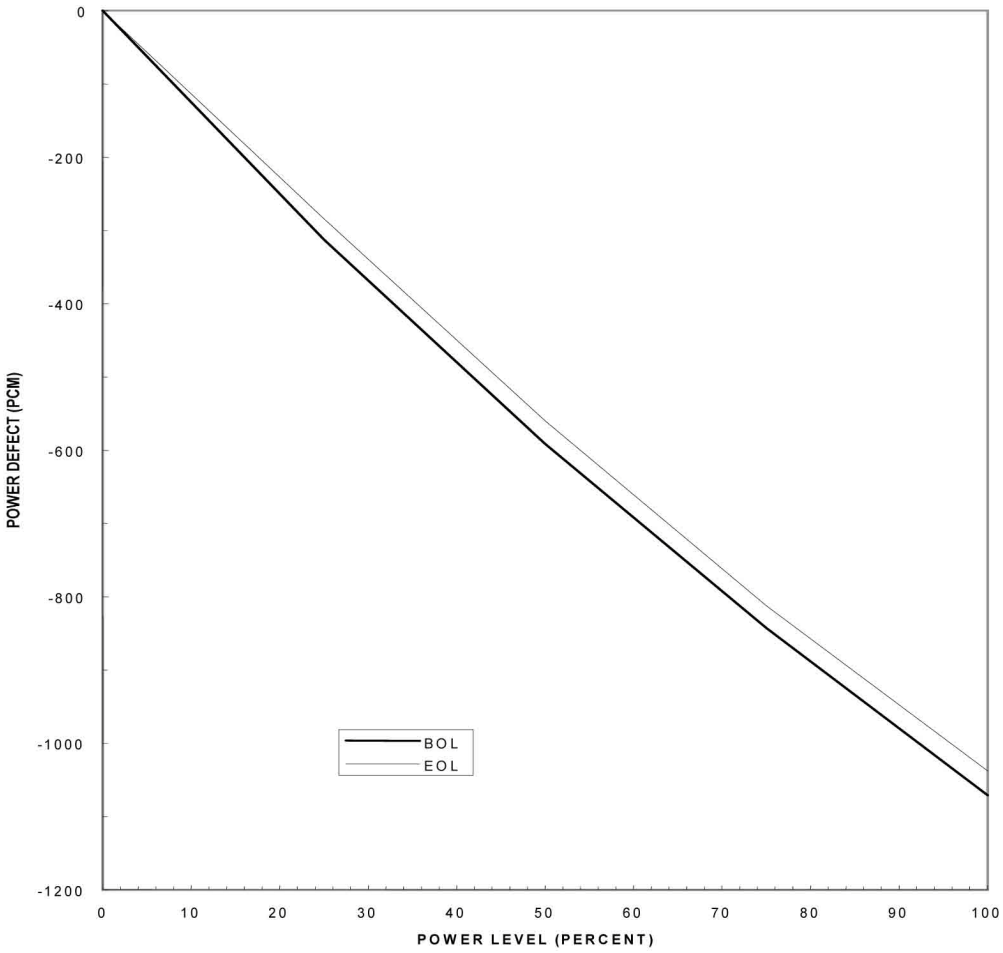

Figure 4.3-20
Typical Doppler-Only Power Defect at BOL and EOL

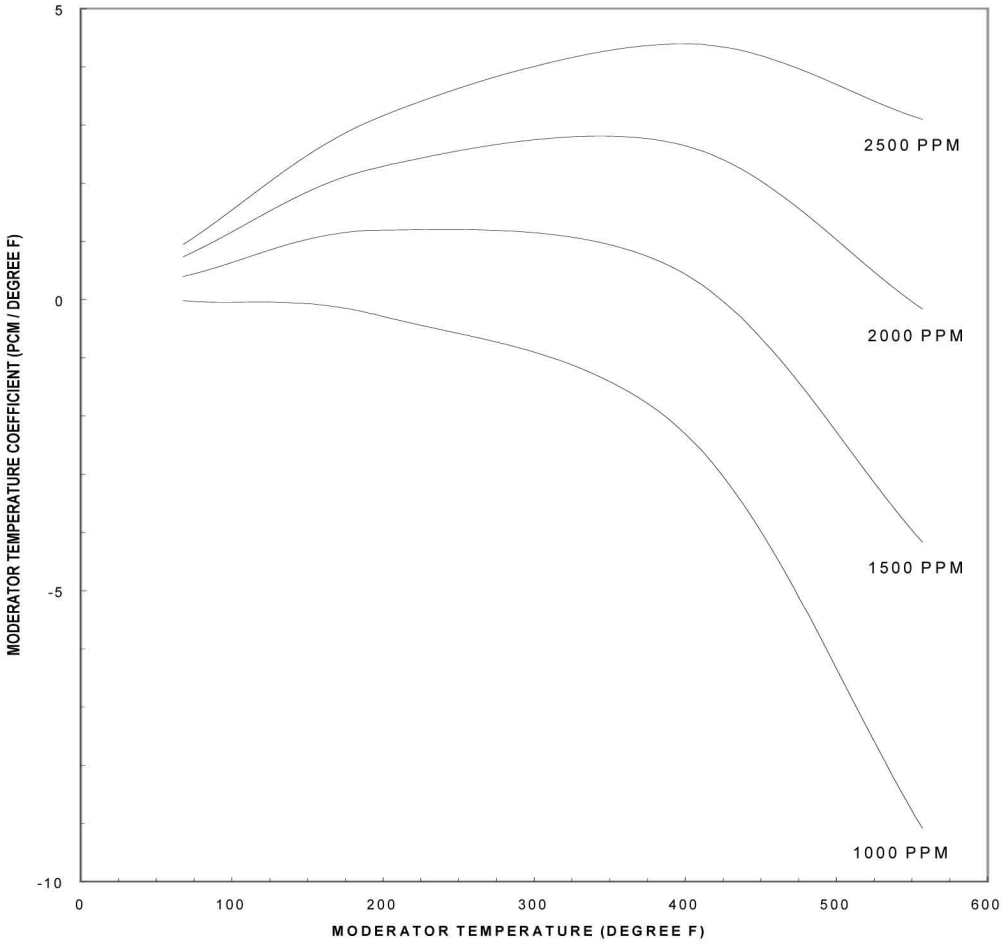

Figure 4.3-21
Typical Moderator Temperature Coefficient at BOL, Unrodded

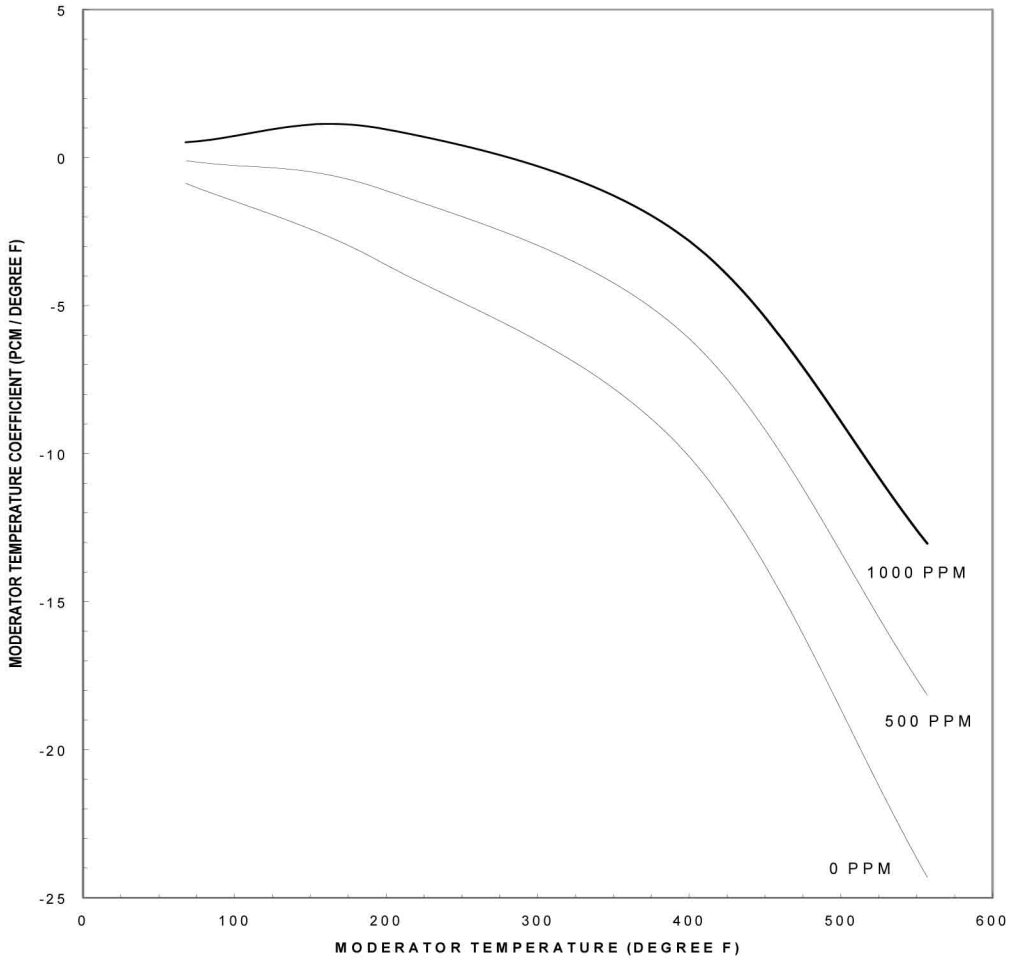

Figure 4.3-22
Typical Moderator Temperature Coefficient at EOL

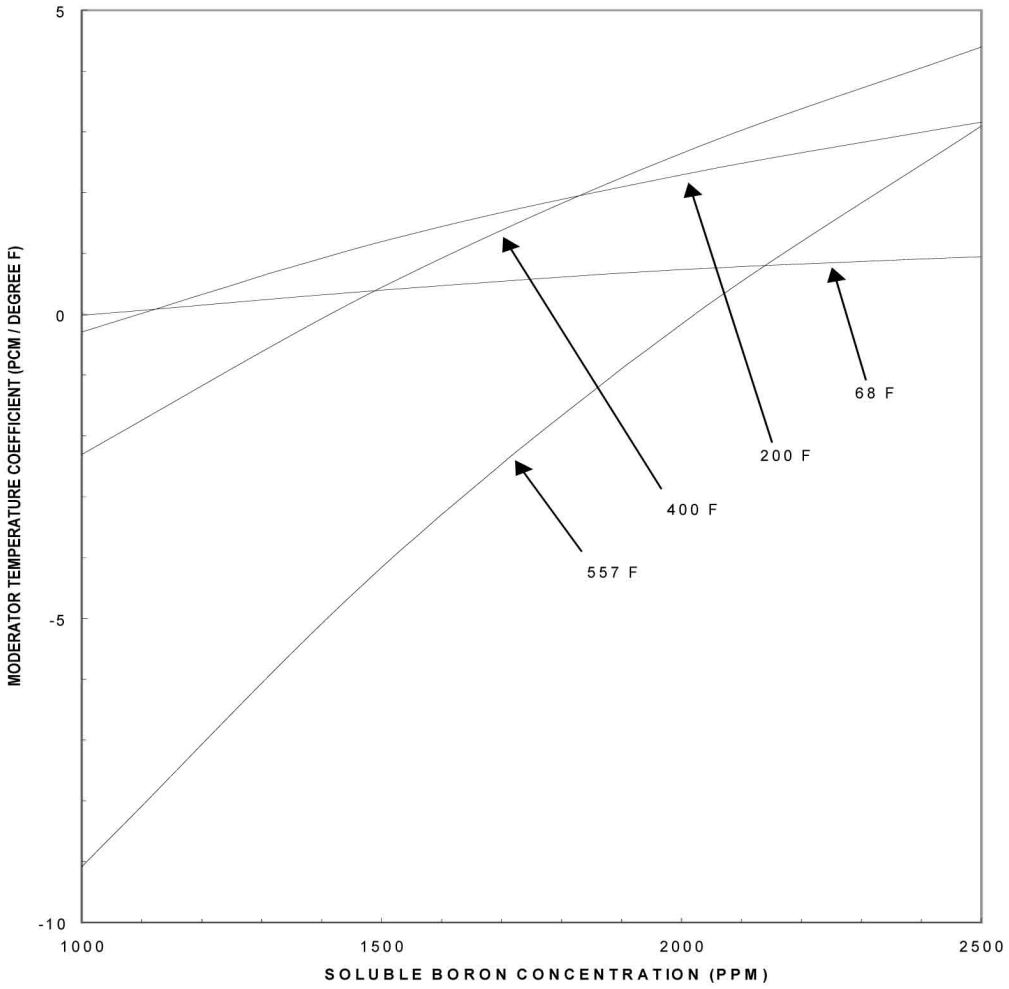

Figure 4.3-23
Typical Moderator Temperature Coefficient as a Function of Boron Concentration at BOL, Unrodded

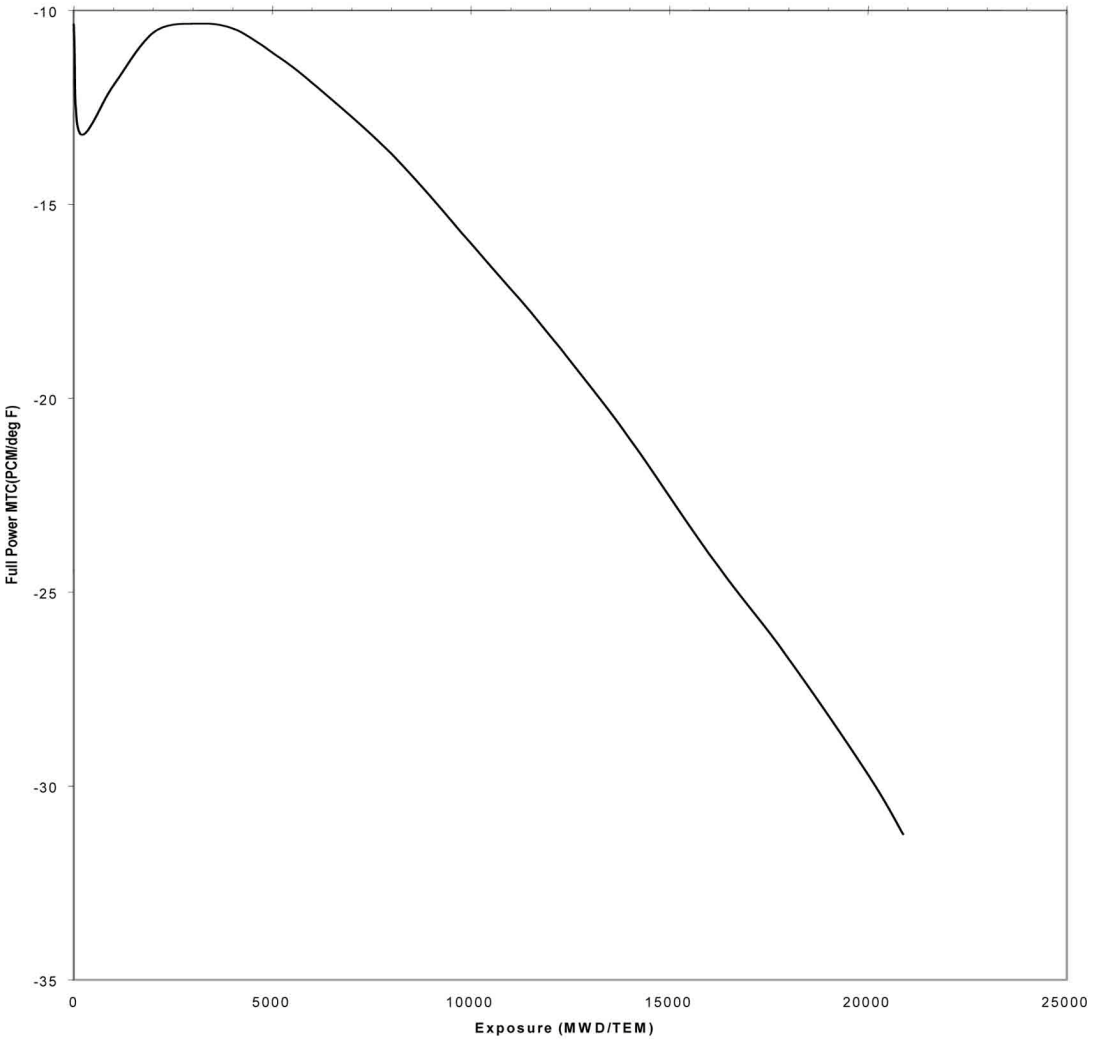

Figure 4.3-24
Typical Hot Full Power Temperature Coefficient Versus Cycle Burnup

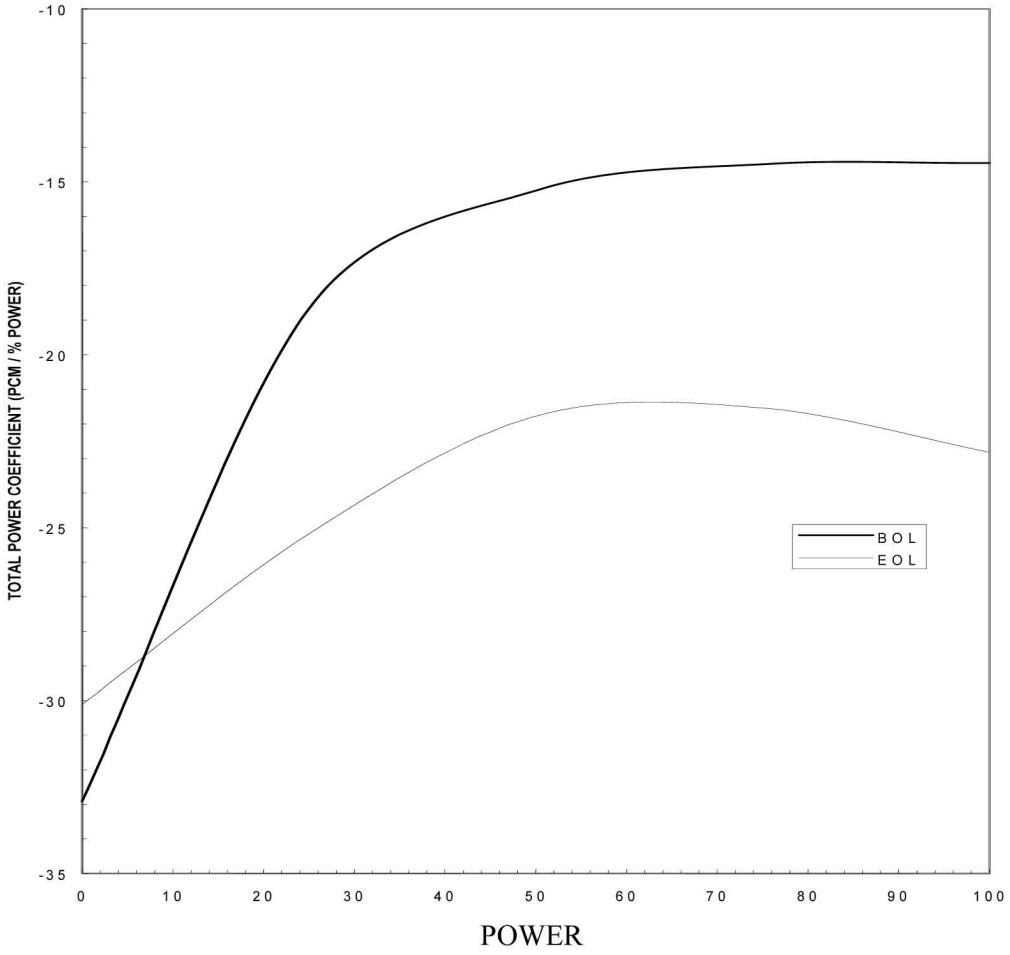

Figure 4.3-25
Typical Total Power Coefficient at BOL and EOL

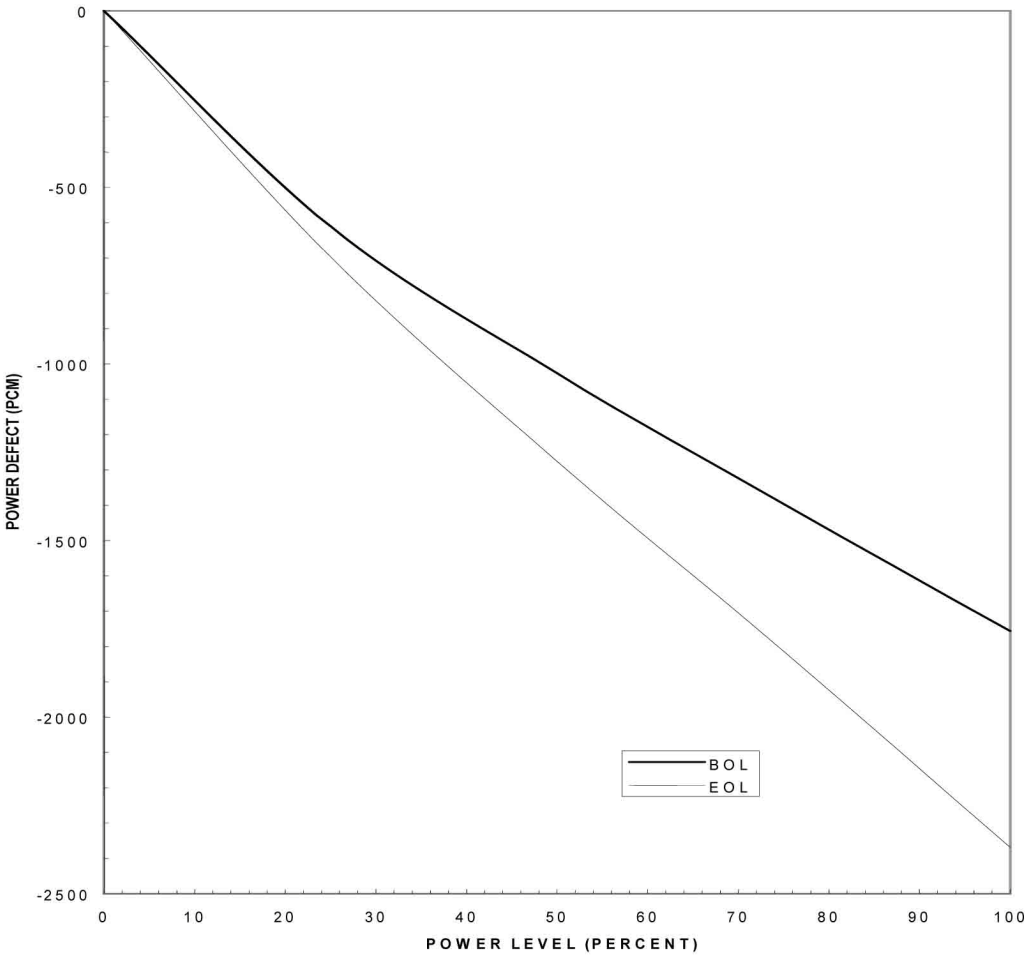

Figure 4.3-26
Typical Total Power Defect at BOL and EOL

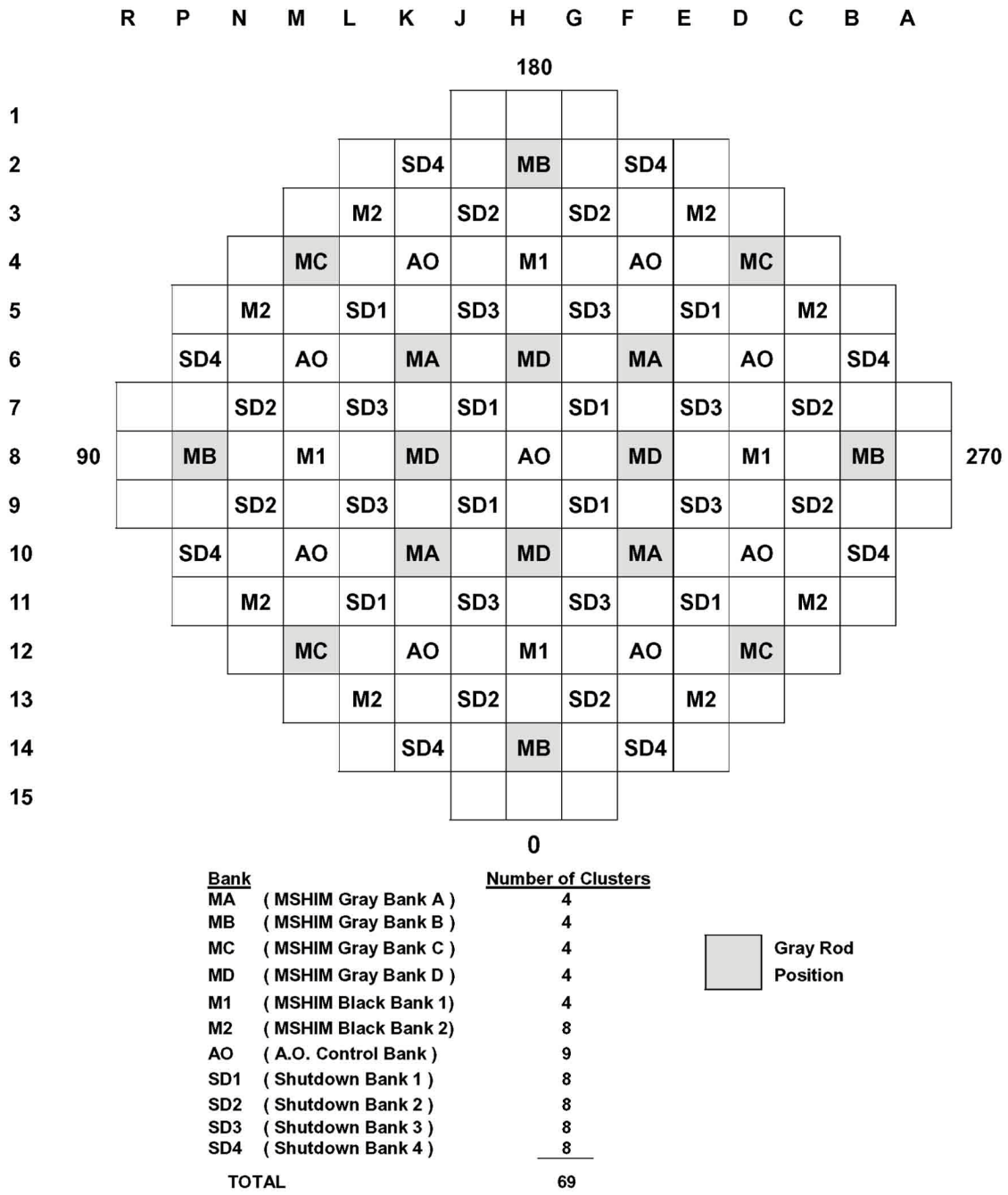

Bank		Number of Clusters
MA	(MSHIM Gray Bank A)	4
MB	(MSHIM Gray Bank B)	4
MC	(MSHIM Gray Bank C)	4
MD	(MSHIM Gray Bank D)	4
M1	(MSHIM Black Bank 1)	4
M2	(MSHIM Black Bank 2)	8
AO	(A.O. Control Bank)	9
SD1	(Shutdown Bank 1)	8
SD2	(Shutdown Bank 2)	8
SD3	(Shutdown Bank 3)	8
SD4	(Shutdown Bank 4)	8
TOTAL		69

Figure 4.3-27
Rod Cluster Control Assembly Pattern

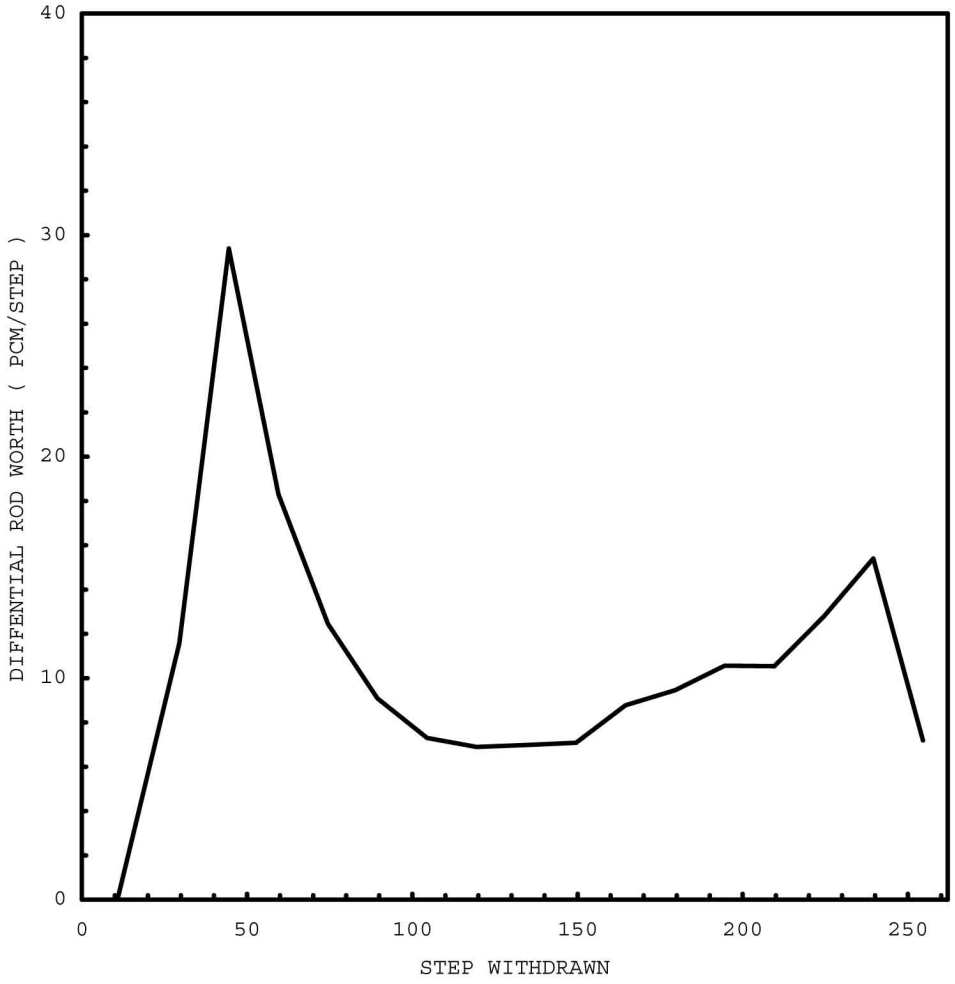

Figure 4.3-28
Typical Accidental Simultaneous Withdrawal of Two Control Banks at EOL, HZP, Moving in the Same Plane

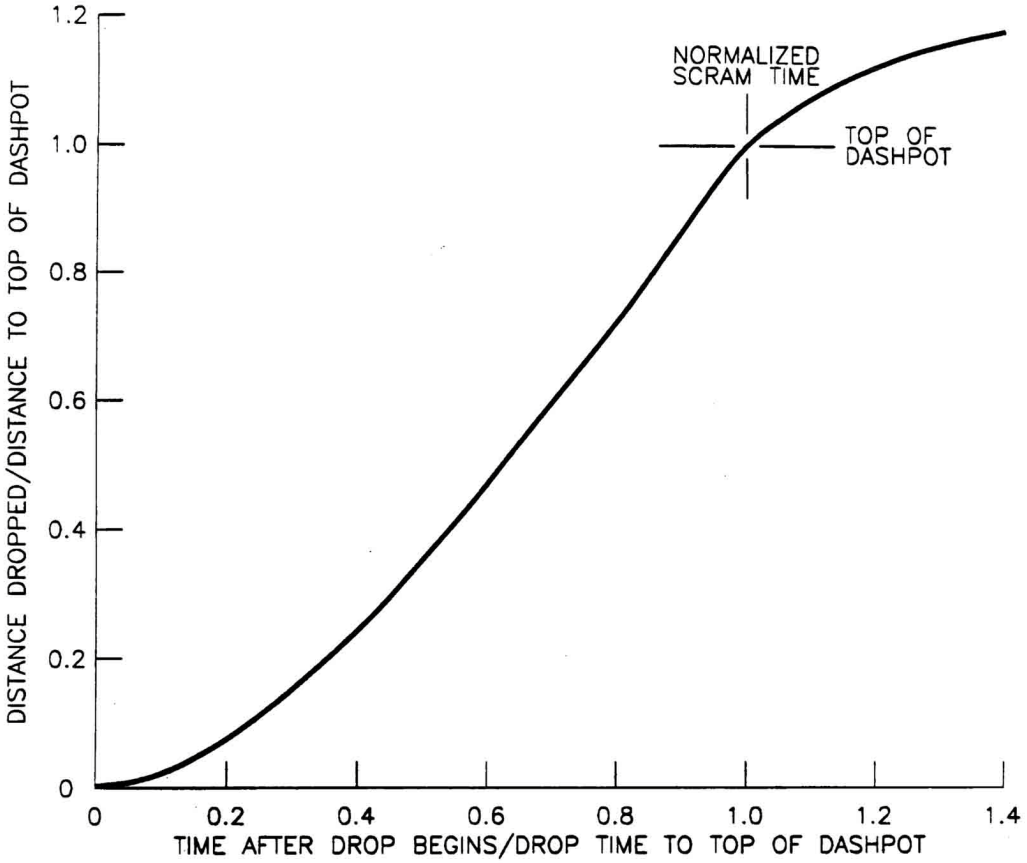

Figure 4.3-29
Typical Design Trip Curve

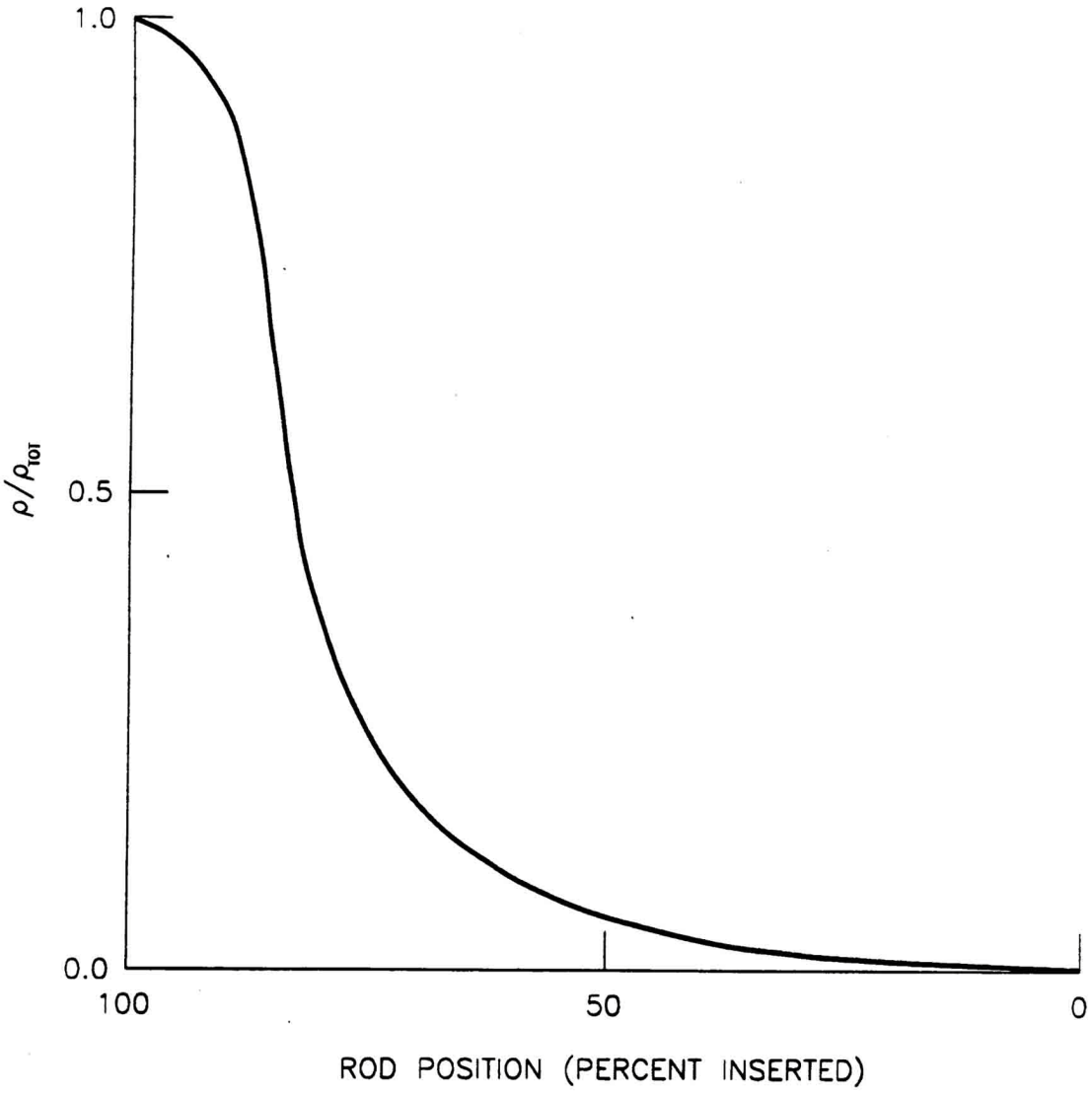

Figure 4.3-30
Typical Normalized Rod Worth Versus Percent Insertion
All Rods Inserting Less Most Reactive Stuck Rod

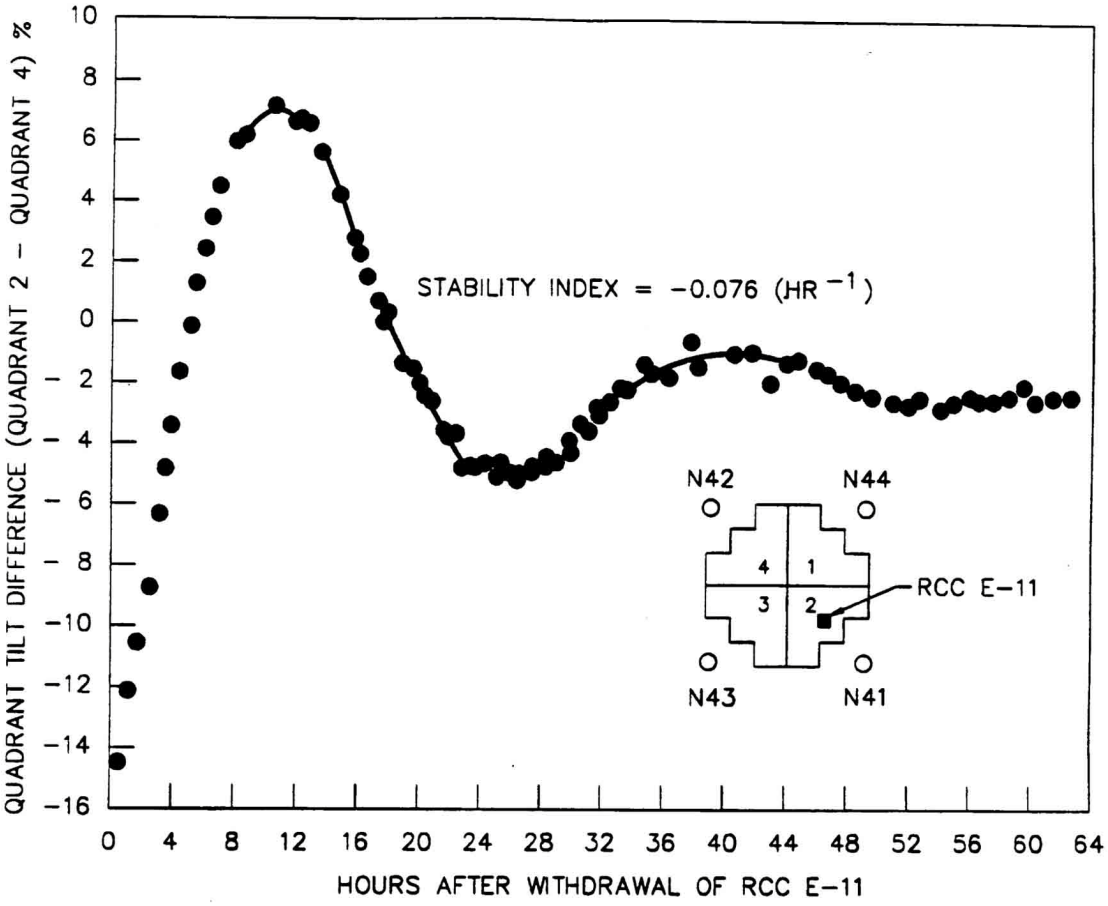

Figure 4.3-31
X-Y Xenon Test Thermocouple Response
Quadrant Tilt Difference Versus Time

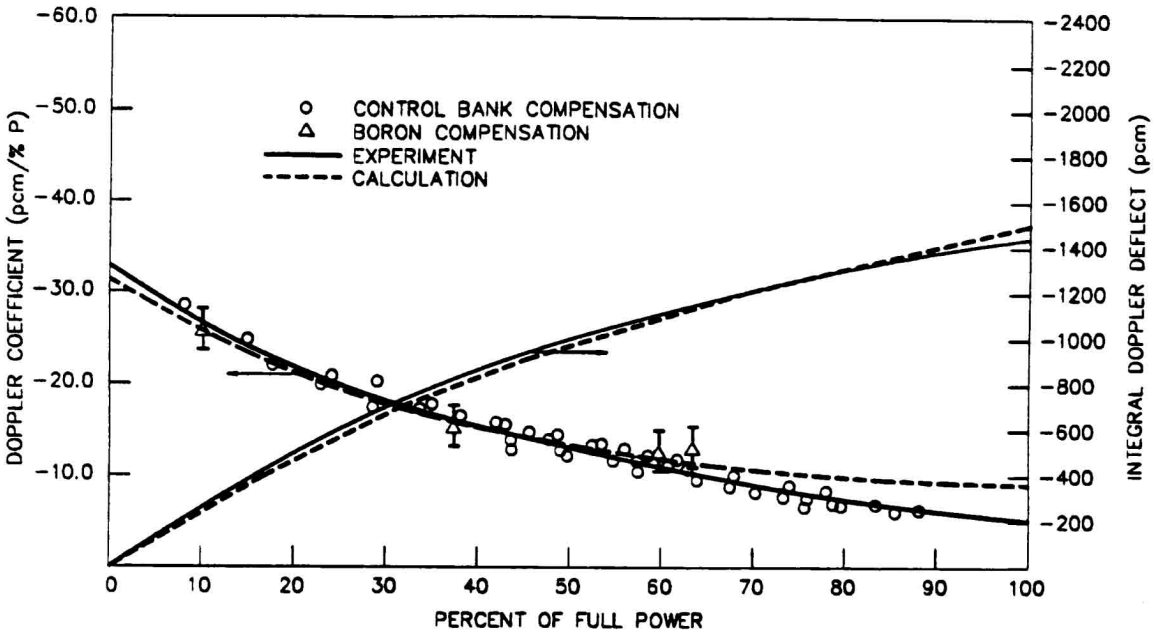

Figure 4.3-32
Calculated and Measured Doppler Defect and Coefficients at BOL, 2-Loop Plant, 121 Assemblies, 12-foot Core

4.4 Thermal and Hydraulic Design

The thermal and hydraulic design of the reactor core provides adequate heat transfer compatible with the heat generation distribution in the core. This provides adequate heat removal by the reactor coolant system, the normal residual heat removal system, or the passive core cooling system.

4.4.1 Design Basis

The following performance and safety criteria requirements are established for the thermal and hydraulic design of the fuel. Condition I, II, III, and IV transients and events through out this section are as defined in ANSI N18.2a-75 (Reference 1).

- Fuel damage (defined as penetration of the fission product barrier; that is, the fuel rod clad) is not expected during normal operation and operational transients (Condition I) or any transient conditions arising from faults of moderate frequency (Condition II). It is not possible, however, to preclude a very small number of rod failures. These are within the capability of the plant cleanup system and are consistent with the plant design bases.

- The reactor can be brought to a safe state following a Condition III event with only a small fraction of fuel rods damaged (as defined in the above definition), although sufficient fuel damage might occur to preclude resumption of operation without considerable outage time.

- The reactor can be brought to a safe state and the core can be kept subcritical with acceptable heat transfer geometry following transients arising from Condition IV events.

To satisfy these requirements, the following design bases have been established for the thermal and hydraulic design of the reactor core.

4.4.1.1 Departure from Nucleate Boiling Design Basis

4.4.1.1.1 Design Basis

There is at least a 95-percent probability at a 95-percent confidence level that departure from nucleate boiling (DNB) does not occur on the limiting fuel rods during normal operation and operational transients and any transient conditions arising from faults of moderate frequency (Condition I and II events).

4.4.1.1.2 Discussion

The design method employed to meet the DNB design basis for the AP1000 fuel assemblies is the Revised Thermal Design Procedure, WCAP-11397-P-A (Reference 2). With the Revised Thermal Design Procedure methodology, uncertainties in plant operating parameters, nuclear and thermal parameters, fuel fabrication parameters, computer codes, and DNB correlation predictions are considered statistically to obtain DNB uncertainty factors. Based on the DNB uncertainty factors, Revised Thermal Design Procedure design limits departure from nucleate boiling ratio (DNBR) values are determined such that there is at least a 95-percent probability at a 95-percent confidence level that DNB will not occur on the most limiting fuel rod during normal operation and operational transients and during transient conditions arising from faults of moderate frequency (Condition I and II events).

Assumed uncertainties in the plant operating parameters (pressurizer pressure, primary coolant temperature, reactor power, and reactor coolant system flow) are evaluated. Only the random portion of the plant operating parameter uncertainties is included in the statistical combination. Instrumentation bias is treated as a direct DNBR penalty. Since the parameter uncertainties are

considered in determining the Revised Thermal Design Procedure design limit DNBR values, the plant safety analyses are performed using input parameters at their nominal values.

For those transients that use the VIPRE-01 computer program (Subsection 4.4.4.5.2) and the WRB-2M correlation (Subsection 4.4.2.2.1), the Revised Thermal Design Procedure design limits are 1.25 for the typical cell and 1.25 for the thimble cell for Core and Axial Offset Limits and 1.22 for the typical cell and 1.21 for the thimble cell for all other RTDP transients. These values may be revised (slightly) when plant specific uncertainties are available.

To maintain DNBR margin to offset DNB penalties such as those due to fuel rod bow (as described in Subsection 4.4.2.2.5), the safety analyses are performed to DNBR limits higher than the design limit DNBR values. The difference between the design limit DNBRs and the safety analysis limit DNBRs results in DNBR margin. A portion of this margin is used to offset rod bow and unanticipated DNBR penalties.

The Standard Thermal Design Procedure is used for those analyses where the Revised Thermal Design Procedure is not applicable. In the Standard Thermal Design Procedure method the parameters used in analysis are treated in a conservative way from a DNBR standpoint. The parameter uncertainties are applied directly to the plant safety analyses input values to give the lowest minimum DNBR. The DNBR limit for Standard Thermal Design Procedure is the appropriate DNB correlation limits increased to give sufficient margins to cover any DNBR penalties associated with the analysis.

By preventing DNB, adequate heat transfer is provided from the fuel clad to the reactor coolant, thereby preventing clad damage as a result of inadequate cooling. Maximum fuel rod surface temperature is not a design basis, since it is within a few degrees of coolant temperature during operation in the nucleate boiling region. Limits provided by the nuclear control and protection systems are such that this design basis is met for transients associated with Condition II events including overpower transients. There is an additional large DNBR margin at rated power operation and during normal operating transients.

4.4.1.2 Fuel Temperature Design Basis

4.4.1.2.1 Design Basis

During modes of operation associated with Condition I and Condition II events, there is at least a 95-percent probability at a 95-percent confidence level that the peak kW/ft fuel rods will not exceed the uranium dioxide melting temperature. The melting temperature of uranium dioxide is 5080°F (Reference 3) unirradiated and decreasing 58°F per 10,000 MWD/MTU. By precluding uranium dioxide melting, the fuel geometry is preserved and possible adverse effects of molten uranium dioxide on the cladding are eliminated. Design evaluations for Condition I and II events have shown that fuel melting will not occur for achievable local burnups up to 75,000 MWD/MTU (Reference 81). The NRC has approved design evaluations up to 60,000 MWD/MTU in Reference 81 and up to 62,000 MWD/MTU in References 9 and 88.

4.4.1.2.2 Discussion

Fuel rod thermal evaluations are performed at rated power, at maximum overpower, and during transients at various burnups. These analyses confirm that this design basis and the fuel integrity design bases given in Section 4.2 are met. They also provide input for the evaluation of Condition III and IV events given in Chapter 15.

The center-line temperature limit has been applied to reload cores with a lead rod average burnup of up to 60,000 MWD/MTU. For higher burnups, the peak kilowatt-per-foot experienced during

Condition I and II events is limited to that maximum value which is sufficient to provide that the fuel center-line temperatures remain below the melting temperature for the fuel rods. Thus, the fuel rod design basis that fuel rod damage not occur due to fuel melting continues to be met.

4.4.1.3 Core Flow Design Basis

4.4.1.3.1 Design Basis

Typical minimum value of 94.1 percent of the thermal flow rate is assumed to pass through the fuel rod region of the core and is effective for fuel rod cooling. Coolant flow through the thimble and instrumentation tubes and the leakage between the core barrel and core shroud, head cooling flow, and leakage to the vessel outlet nozzles are not considered effective for heat removal.

4.4.1.3.2 Discussion

Core cooling evaluations are based on the thermal flow rate (minimum flow) entering the reactor vessel. A typical maximum value of 5.9 percent of this value is allotted as bypass flow. This includes rod cluster control guide thimble and instrumentation tube cooling flow, leakage between the core barrel and the core shroud, head cooling flow, and leakage to the vessel outlet nozzles. The shroud core cavity flow is considered as active flow that is effective for fuel rod cooling.

The maximum bypass flow fraction of 5.9 percent assumes the use of thimble plugging devices in the rod cluster control guide thimble tubes that do not contain any other core components.

4.4.1.4 Hydrodynamic Stability Design Basis

Modes of operation associated with Condition I and II events do not lead to hydrodynamic instability.

4.4.1.5 Other Considerations

The design bases described in Subsections 4.4.1 through 4.4.1.4 together with the fuel clad and fuel assembly design bases given in Subsection 4.2.1 are sufficiently comprehensive that additional limits are not required.

Fuel rod diametral gap characteristics, moderator coolant flow velocity and distribution, and moderator void are not inherently limiting. Each of these parameters is incorporated into the thermal and hydraulic models used to confirm that the above-mentioned design criteria are met. For instance, the fuel rod diametral gap characteristics change with time, as described in Subsection 4.2.3, and the fuel rod integrity is evaluated on that basis. The effect of the moderator flow velocity and distribution described in Subsection 4.4.2.2 and the moderator void distribution described in Subsection 4.4.2.4 are included in the core thermal evaluation and thus affect the design basis.

Meeting the fuel clad integrity criteria covers the possible effects of clad temperature limitations. Clad surface temperature limits are imposed on Condition I and Condition II operation to preclude conditions of accelerated oxidation. A clad temperature limit is applied to the loss-of-coolant accident described in Subsection 15.6.5; control rod ejection accident described in Subsection 15.4.8; and locked rotor accident described in Subsection 15.3.3.

4.4.2 Description of Thermal and Hydraulic Design of the Reactor Core

4.4.2.1 Summary Comparison

Table 4.4-1 provides a comparison of the design parameters for the AP1000, the AP600, and a licensed Westinghouse-designed plant using XL Robust fuel. For the comparison with a plant

containing XL Robust fuel, a 193 fuel assembly plant is used, since no domestic Westinghouse designed 157 fuel assembly plants use 17x17 fuel XL Robust fuel.

4.4.2.2 Critical Heat Flux Ratio or DNBR and Mixing Technology

The minimum DNBRs for the rated power and anticipated transient conditions are given in Table 4.4-1. The minimum DNBR in the limiting flow channel is typically downstream of the peak heat flux location (hotspot) due to the increased downstream enthalpy rise.

DNBRs are calculated by using the correlation and definitions described in Subsections 4.4.2.2.1 and 4.4.2.2.2. The VIPRE-01 computer code described in Subsection 4.4.4.5, is used to determine the flow distribution in the core and the local conditions in the hot channel for use in the DNB correlation. The use of hot channel factors is described in Subsections 4.4.4.3.1 (nuclear hot channel factors) and 4.4.2.2.4 (engineering hot channel factors).

4.4.2.2.1 DNB Technology

The primary DNB correlation used for the analysis of the AP1000 fuel is the WRB-2M correlation (References 82 and 82a). The WRB-2M correlation applies to the Robust Fuel Assemblies, which are planned to be used in the AP1000 core. This correlation applies to most AP1000 conditions.

A correlation limit of 1.14 is applicable for the WRB-2M correlation.

The applicable range of parameters for the WRB-2M correlation is:

Pressure	$1495 \le P \le 2425$ psia
Local mass velocity	$0.97 \le G_{loc}/10^6 \le 3.1$ lb/ft^2-hr
Local quality	$-0.1 \le X_{loc} \le 0.29$
Heated length, inlet to CHF location	$L_H \le 14$ feet
Grid spacing	$10 \le g_{sp} \le 20.6$ inches
Equivalent hydraulic diameter	$0.37 \le D_e \le 0.46$ inches
Equivalent heated hydraulic diameter	$0.46 \le D_h \le 0.54$ inches

The WRB-2 (Reference 4) or W-3 (References 5 and 6) correlation is used wherever the WRB-2M correlation is not applicable. The WRB-2 correlation limit is 1.17.

The applicable range of parameters for the WRB-2 correlation is:

Pressure	$1440 \le P \le 2490$ psia
Local mass velocity	$0.9 \le G_{loc}/10^6 \le 3.7$ lb/ft^2-hr
Local quality	$-0.1 \le X_{loc} \le 0.3$
Heat length, inlet to DNB location	$L_h \le 14$ feet
Grid spacing	$10 \le g_{sp} \le 26$ inches
Equivalent hydraulic diameter	$0.37 \le D_e \le 0.51$ inches
Equivalent heated hydraulic diameter	$0.46 \le D_h \le 0.59$ inches

The WRB-2 correlation was developed based on mixing vane data and, therefore, is only applicable in the heated rod spans above the first mixing vane grid.

In the heated region below the first mixing vane grid the W-3 correlation (see References 5 and 6), which does not take credit for mixing vane grids, is used to calculate DNBR values. In addition, the W-3 correlation is applied in the analysis of accident conditions where the system pressure is below the range of the primary correlation. For system pressures in the range of 500 to 1000 psia, the W-3 correlation limit is 1.45 (Reference 7). For system pressures greater than 1000 psia, the W-3 correlation limit is 1.30. The pressures associated with some of the steam line break statepoints are in the range of 300 to 500 psia. Using additional information, the W-3 correlation is shown to be applicable with these pressures and a correlation limit of 1.45.

A cold wall factor, described in WCAP-7695-L (Reference 8), is applied to the W-3 DNB correlation to conservatively account for the presence of the unheated thimble surfaces.

4.4.2.2.2 Definition of DNBR

The DNB heat flux ratio, DNBR, as applied to typical cells (flow cells with all walls heated) and thimble cells (flow cells with heated and unheated walls) is defined as:

$$DNBR = \frac{q''_{DNB,\ predicted}}{q''actual}$$

where:

$$q''_{DNB,\ predicted} = \frac{q''_{WRB-2M}}{F} \quad \text{or} \quad q''_{DNB,\ predicted} = \frac{q''_{WRB-2}}{F}$$

q''_{WRB-2M} = the uniform DNB heat flux as predicted by the WRB-2M DNB correlation

q''_{WRB-2} = the uniform DNB heat flux as predicted by the WRB-2 DNB correlation

F = the flux shape factor to account for nonuniform axial heat flux distributions (Reference 10) with the term “C” modified as in Reference 5

$q''actual$ = the actual local heat flux

The DNBR as applied to the W-3 DNB correlation is:

$$DNBR = \frac{q''_{predicted}}{q''_{actual}}$$

where:

$$q''_{predicted} = \frac{q''_{EU-W-3}\ x\ CWF}{F}$$

q''_{EU-W-3} = the uniform DNB heat flux as predicted by the W-3 DNB correlation (Reference 5)

$$CWF = 1.0\text{-}Ru\ [T]$$

where:

$$T = 13.76 - 1.372e^{1.78x} - 4.732 \left(\frac{G}{10^6}\right)^{-0.0535} - 0.0619 \left(\frac{P}{1000}\right)^{0.14} - 8.509\, D_h^{0.017}$$

$Ru = 1-D_e/D_h$

If the cold wall factor is used (thimble cell), D_h is used in evaluating $q''_{EU\text{-}W\text{-}3}$. If the CWF is not used (typical cells), set CWF = 1.0.

4.4.2.2.3 Mixing Technology

The rate of heat exchange by mixing between flow channels is proportional to the difference in the local mean fluid enthalpy of the respective channels, the local fluid density, and the flow velocity. The proportionality is expressed by the dimensionless thermal diffusion coefficient (TDC) which is defined as:

$$TDC = \frac{w'}{\rho V a}$$

where:

w′ = flow exchange rate per unit length (lbm/ft-s)

ρ = fluid density (lbm/ft^3)

V = fluid velocity (ft/s)

a = lateral flow area between channels per unit length (ft^2/ft)

The application of the thermal diffusion coefficient in the VIPRE-01 analysis for determining the overall mixing effect or heat exchange rate is presented in Reference 83.

As discussed in WCAP-7941-P-A (Reference 12) those series of tests, using the “R” mixing vane grid design on 13-, 26-, and 32-inch grid spacing, were conducted in pressurized water loops at Reynolds numbers similar to that of a pressurized water reactor core under the following single- and two-phase (subcooled boiling) flow conditions:

- Pressure — 1500 to 2400 psia
- Inlet temperature — 332 to 642°F
- Mass velocity — 1.0 to 3.5 x 10^6 lbm/hr-ft^2
- Reynolds number — 1.34 to 7.45 x 10^5
- Bulk outlet quality — -52.1 to -13.5 percent

The thermal diffusion coefficient is determined by comparing the THINC code predictions with the measured subchannel exit temperatures. Data for 26-inch axial grid spacing are presented in Figure 4.4-1, where the thermal diffusion coefficient is plotted versus the Reynolds number. The thermal diffusion coefficient is found to be independent of the Reynolds number, mass velocity, pressure, and quality over the ranges tested. The two-phase data (local, subcooled boiling) falls

within the scatter of the single-phase data. The effect of two-phase flow on the value of the thermal diffusion coefficient is demonstrated in WCAP-7941-P-A (Reference 12), by Rowe and Angle (References 13 and 14), and Gonzalez-Santalo and Griffith (Reference 15). In the subcooled boiling region, the values of the thermal diffusion coefficient are indistinguishable from the single-phase values. In the quality region, Rowe and Angle show that in the case with rod spacing similar to that in pressurized water reactor core geometry, the value of the thermal diffusion coefficient increased with quality to a point and then decreased, but never below the single-phase value. Gonzalez-Santalo and Griffith show that the mixing coefficient increased as the void fraction increased.

The data from these tests on the R-mixing vane grid show that a design thermal diffusion coefficient value of 0.038 (for 26-inch grid spacing) can be used in determining the effect of coolant mixing in the THINC analysis. An equivalent value of the mixing coefficient is used in the VIPRE-01 evaluations (Reference 83). A mixing test program similar to the one just described was conducted for the current 17 x 17 geometry and mixing vane grids on 26-inch spacing, as described in WCAP-8298-P-A (Reference 16). The mean value of the thermal diffusion coefficient obtained from these tests is 0.059.

The inclusion of intermediate flow mixer grids in the upper spans of the fuel assembly results in a grid spacing of approximately 10 inches giving higher values of the thermal diffusion coefficient. A conservative value of the thermal diffusion coefficient, .038, is used to determine the effect of coolant mixing in the core thermal performance analysis.

4.4.2.2.4 Hot Channel Factors

The total hot channel factors for heat flux and enthalpy rise are defined as the maximum-to-core-average ratios of these quantities. The heat flux hot channel factor considers the local maximum linear heat generation rate at a point (the hotspot), and the enthalpy rise hot channel factor involves the maximum integrated value along a channel (the hot channel).

Each of the total hot channel factors is composed of a nuclear hot channel factor, Subsection 4.4.4.3, describing the neutron power distribution and an engineering hot channel factor, which allows for variations in flow conditions and fabrication tolerances. The engineering hot channel factors are made up of subfactors which account for the influence of the variations of fuel pellet diameter, density, enrichment, and eccentricity; inlet flow distribution; flow redistribution; and flow mixing.

Heat Flux Engineering Hot Channel Factor, F_Q^E

The heat flux engineering hot channel factor is used to evaluate the maximum linear heat generation rate in the core. This subfactor is determined by statistically combining the fabrication variations for fuel pellet diameter, density, and enrichment. As shown in WCAP-8174 (Reference 17), no DNB penalty needs be taken for the short, relatively low-intensity heat flux spikes caused by variations in the above parameters, as well as fuel pellet eccentricity and fuel rod diameter variation.

Enthalpy Rise Engineering Hot Channel Factor, $F_{\Delta H}^E$

The effect of variations in flow conditions and fabrication tolerances on the hot channel enthalpy rise is directly considered in the VIPRE-01 core thermal subchannel analysis, described in Subsection 4.4.4.5.1 under any reactor opening condition. The following items are considered as contributors to the enthalpy rise engineering hot channel factor:

- Pellet diameter, density, and enrichment

  Variations in pellet diameter, density, and enrichment are considered statistically in establishing the limit DNBRs, described in Subsection 4.4.1.1.2, for the Revised Thermal Design Procedure

(Reference 2). Uncertainties in these variables are determined from sampling of manufacturing data.

- Inlet flow maldistribution

  The consideration of inlet flow maldistribution in core thermal performances is described in Subsection 4.4.4.2.2. A design basis of five-percent reduction in coolant flow to the hot assembly is used in the VIPRE-01 analyses.

- Flow redistribution

  The flow redistribution accounts for the reduction in flow in the hot channel resulting from the high flow resistance in the channel due to the local or bulk boiling. The effect of the nonuniform power distribution is inherently considered in the VIPRE-01 analyses for every operating condition evaluated.

- Flow mixing

  The subchannel mixing model incorporated in the VIPRE-01 code and used in reactor design is based on experimental data, as detailed in WCAP-7667-P-A (Reference 18) and discussed in Subsections 4.4.2.2.3 and 4.4.4.5.1. The mixing vanes incorporated in the spacer grid design induce additional flow mixing between the various flow channels in a fuel assembly as well as between adjacent assemblies. This mixing reduces the enthalpy rise in the hot channel resulting from local power peaking or unfavorable mechanical tolerances. The VIPRE-01 mixing model is discussed in Reference 83.

4.4.2.2.5 Effects of Rod Bow on DNBR

The phenomenon of fuel rod bowing, as described in WCAP-8691 (Reference 19), is accounted for in the DNBR safety analysis of Condition I and Condition II events for each plant application. Applicable generic credits for margin resulting from retained conservatism in the evaluation of DNBR and/or margin obtained form measured plant operating parameters (such as $F^N_{\Delta H}$ or core flow), which are less limiting than those required by the plant safety analysis, can be used to offset the effect of rod bow.

For the safety analysis of the AP1000, sufficient DNBR margin was maintained, as described in Subsection 4.4.1.1.2, to accommodate the full and low flow rod bow DNBR penalties identified in Reference 20. The referenced penalties are applicable to the analyses using the WRB-2M or WRB-2 DNB correlations.

The maximum rod bow penalties (less than about 2 percent DNBR) accounted for in the design safety analysis are based on an assembly average burnup of 24,000 MWD/MTU. At burnups greater than 24,000 MWD/MTU, credit is taken for the effect of $F^N_{\Delta H}$ burndown, due to the decrease in fissionable isotopes and the buildup of fission product inventory, and no additional rod bow penalty is required (Reference 21).

In the upper spans of the fuel assembly, additional restraint is provided with the intermediate flow mixer grids such that the grid-to-grid spacing in those spans with intermediate flow mixer grids is approximately 10 inches compared to approximately 20 inches in the other spans. Using the NRC approved scaling factor [see WCAP 8691 (Reference 19) and Reference 21], results in predicted channel closure in the limiting 10 inch spans of less than 50 percent closure. Therefore, no rod bow DNBR penalty is required in the 10 inch spans in the safety analyses.

4.4.2.3 Linear Heat Generation Rate

The core average and maximum linear heat generation rates are given in Table 4.4-1. The method of determining the maximum linear heat generation rate is given in Subsection 4.3.2.2.

4.4.2.4 Void Fraction Distribution

The calculated core average and the hot subchannel maximum and average void fractions are presented in Table 4.4-2 for operation at full power. The void models used in the VIPRE-W code are described in Subsection 4.4.2.7.3.

4.4.2.5 Core Coolant Flow Distribution

The VIPRE-01 code is used to calculate the flow and enthalpy distribution in the core for use in safety analysis. Extensive experimental verification of VIPRE-01 is presented in Reference 84.

4.4.2.6 Core Pressure Drops and Hydraulic Loads

4.4.2.6.1 Core Pressure Drops

The analytical model and experimental data used to calculate the pressure drops shown in Table 4.4-1 are described in Subsection 4.4.2.7. The core pressure drop includes the fuel assembly, lower core plate, and upper core plate pressure drops. The full-power operation pressure drop values shown in Table 4.4-1 are the unrecoverable pressure drops across the vessel, including the inlet and outlet nozzles, and across the core. These pressure drops are based on the best-estimate flow for actual plant operating conditions as described in Subsection 5.1.4. This subsection also defines and describes the thermal design flow (minimum flow) that is the basis for reactor core thermal performance and the mechanical design flow (maximum flow) that is used in the mechanical design of the reactor vessel internals and fuel assemblies. Since the best-estimate flow is that flow which is most likely to exist in an operating plant, the calculated core pressure drops in Table 4.4-1 are based on this best-estimate flow rather than the thermal design flow.

The uncertainties associated with the core pressure drop values are presented in Subsection 4.4.2.9.2.

4.4.2.6.2 Hydraulic Loads

Figure 4.2-2 shows the fuel assembly hold-down springs. These springs are designed to keep the fuel assemblies in contact with the lower core plate under Condition I and II events, except for the turbine overspeed transient associated with a loss of external load. The hold-down springs are designed to tolerate the possibility of an overdeflection associated with fuel assembly lift-off for this case and to provide contact between the fuel assembly and the lower core plate following this transient. More adverse flow conditions occur during a loss-of-coolant accident. These conditions are presented in Subsection 15.6.5.

Hydraulic loads at normal operating conditions are calculated considering the best-estimate flow, described in Section 5.1, and accounting for the minimum core bypass flow based on manufacturing tolerances. Core hydraulic loads at cold plant startup conditions are based on the cold best-estimate flow, but are adjusted to account for the coolant density difference. Conservative core hydraulic loads for a pump overspeed transient, which could possibly create a flow rate 18-percent greater than the best estimate flow, are evaluated to be approximately twice the fuel assembly weight.

Hydraulic verification tests for the fuel assembly are described in Reference 86.

4.4.2.7 Correlation and Physical Data

4.4.2.7.1 Surface Heat Transfer Coefficients

Forced convection heat transfer coefficients are obtained from the Dittus-Boelter correlation (Reference 24), with the properties evaluated at bulk fluid conditions:

$$\frac{hD_e}{K} = 0.023\left(\frac{D_eG}{\mu}\right)^{0.8}\left(\frac{C_p\mu}{K}\right)^{0.4}$$

where:

h = heat transfer coefficient (btu/h-ft^2-°F)

D_e = equivalent diameter (ft)

K = thermal conductivity (Btu/h-ft-°F)

G = mass velocity (lbm/h-ft^2)

μ = dynamic viscosity (lbm/ft-h)

C_p = heat capacity (Btu/lb-°F)

This correlation has been shown to be conservative (Reference 25) for rod bundle geometries with pitch-to-diameter ratios in the range used by pressurized water reactors.

The onset of nucleate boiling occurs when the clad wall temperature reaches the amount of superheat predicted by Thom's correlation (Reference 26). After this occurrence, the outer clad wall temperature is determined by:

$$\Delta T_{sat} = [0.072\exp(-P/1260)](q'')^{0.5}$$

where:

ΔT_{sat} = wall superheat, $T_W - T_{sat}$ (°F)

q″ = wall heat flux (Btu/h-ft^2)

P = pressure (psia)

T_w = outer clad wall temperature (°F)

T_{sat} = saturation temperature of coolant at pressure P (°F)

4.4.2.7.2 Total Core and Vessel Pressure Drop

Unrecoverable pressure losses occur as a result of viscous drag (friction) and/or geometry changes (form) in the fluid flow path. The flow field is assumed to be incompressible, turbulent, single-phase water. Those assumptions apply to the core and vessel pressure drop calculations for the purpose of establishing the primary loop flow rate. Two-phase considerations are neglected in the vessel

pressure drop evaluation because the core average void is negligible, as shown in Table 4.4-2. Two-phase flow considerations in the core thermal subchannel analysis are considered and the models are described in Subsection 4.4.4.2.3. Core and vessel pressure losses are calculated by equations of the form:

$$\Delta P_L = (K + f \frac{L}{D_e}) \frac{\rho V^2}{2 g_c (144)}$$

where:

ΔP_L = unrecoverable pressure drop (lb/in.^{2})

ρ = fluid density (lbm/ft^3)

L = length (ft)

D_e = equivalent diameter (ft)

V = fluid velocity (ft/s)

g_c = 32.174 (lbm-ft/lbf p-s^2)

K = form loss coefficient (dimensionless)

f = friction loss coefficient (dimensionless)

Fluid density is assumed to be constant at the appropriate value for each component in the core and vessel. Because of the complex core and vessel flow geometry, precise analytical values for the form and friction loss coefficients are not available. Therefore, experimental values for these coefficients are obtained from geometrically similar models.

Values are quoted in Table 4.4-1 for unrecoverable pressure loss across the reactor vessel, including the inlet and outlet nozzles, and across the core. The results of full-scale tests of core components and fuel assemblies are used in developing the core pressure loss characteristic.

Tests of the primary coolant loop flow rates are made prior to initial criticality as described in Subsection 4.4.5.1, to verify that the flow rates used in the design, which are determined in part from the pressure losses calculated by the method described here, are conservative. See Section 14.2 for preoperational testing.

4.4.2.7.3 Void Fraction Correlation

VIPRE-01 considers two-phase flow in two steps. First, a quality model is used to compute the flowing vapor mass fraction (true quality) including the effects of subcooled boiling. Then, given the true void quality, a bulk void model is applied to compute the vapor volume fraction (void fraction).

VIPRE-01 uses a profile fit model (Reference 83) for determining subcooled quality. It calculates the local vapor volumetric fraction in forced convection boiling by: 1) predicting the point of bubble departure from the heated surface and 2) postulating a relationship between the true local vapor fraction and the corresponding thermal equilibrium value.

The void fraction in the bulk boiling region is predicted by using homogeneous flow theory and assuming no slip. The void fraction in this region is therefore a function only of the thermodynamic quality.

4.4.2.8 Thermal Effects of Operational Transients

DNB core safety limits are generated as a function of coolant temperature, pressure, core power, and axial power imbalance. Steady-state operation within these safety limits provides that the DNB design basis is met. Subsection 15.0.6 discusses the overtemperature ΔT trip (based on DNBR limit) versus T_{avg}. This system provides protection against anticipated operational transients that are slow with respect to fluid transport delays in the primary system. In addition, for fast transients (such as uncontrolled rod bank withdrawal at power incident as described in Subsection 15.4.2), specific protection functions are provided as described in Section 7.2. The use of these protection functions is described in Chapter 15.

4.4.2.9 Uncertainties in Estimates

4.4.2.9.1 Uncertainties in Fuel and Clad Temperatures

As described in Subsection 4.4.2.11, the fuel temperature is a function of crud, oxide, clad, pellet-clad gap, and pellet conductances. Uncertainties in the fuel temperature calculation are essentially of two types: fabrication uncertainties, such as variations in the pellet and clad dimensions and the pellet density; and model uncertainties, such as variations in the pellet conductivity and the gap conductance. These uncertainties have been quantified by comparison of the thermal model to the in-pile thermocouple measurements (References 30 through 36), by out-of-pile measurements of the fuel and clad properties (References 37 through 48), and by measurements of the fuel and clad dimensions during fabrication. The resulting uncertainties are then used in the evaluations involving the fuel temperature. The effect of densification on fuel temperature uncertainties is also included in the calculation of the total uncertainty.

In addition to the temperature uncertainty described above, the measurement uncertainty in determining the local power and the effect of density and enrichment variations on the local power are considered in establishing the heat flux hot channel factor. These uncertainties are described in Subsection 4.3.2.2.1.

Reactor trip setpoints, as specified in the technical specifications, include allowance for instrument and measurement uncertainties such as calorimetric error, instrument drift and channel reproducibility, temperature measurement uncertainties, noise, and heat capacity variations.

Uncertainty in determining the cladding temperature results from uncertainties in the crud and oxide thicknesses. Because of the excellent heat transfer between the surface of the rod and the coolant, the film temperature drop does not appreciably contribute to the uncertainty.

4.4.2.9.2 Uncertainties in Pressure Drops

Core and vessel pressure drops based on the best-estimate flow, as described in Section 5.1, are quoted in Table 4.4-1. The uncertainties quoted are based on the uncertainties in both the test results and the analytical extension of these values to the reactor application.

A major use of the core and vessel pressure drops is to determine the primary system coolant flow rates, as described in Section 5.1. In addition, as described in Subsection 4.4.5.1, tests on primary system prior to initial criticality, are conducted to verify that a conservative primary system coolant flow rate has been used in the design and analysis of the plant.

4.4.2.9.3 Uncertainties Due to Inlet Flow Maldistribution

The effects of uncertainties in the inlet flow maldistribution criteria used in the core thermal analyses are described in Subsection 4.4.4.2.2.

4.4.2.9.4 Uncertainty in DNB Correlation

The uncertainty in the DNB correlation described in Subsection 4.4.2.2, is written as a statement on the probability of not being in DNB based on the statistics of the DNB data. This is described in Subsection 4.4.2.2.2.

4.4.2.9.5 Uncertainties in DNBR Calculations

The uncertainties in the DNBRs calculated by the VIPRE-01 analyses, discussed in Subsection 4.4.4.5.1, due to uncertainties in the nuclear peaking factors are accounted for by applying conservatively high values of the nuclear peaking factors. Measurement error allowances are included in the statistical evaluation of the limit DNBR described in Subsection 4.4.1.1 using the Revised Thermal Design Procedure. More information is provided in WCAP-11397-P-A (Reference 2). In addition, conservative values for the engineering hot channel factors are used as presented in Subsection 4.4.2.2.4. The results of a sensitivity study, WCAP-8054-P-A (Reference 22), with THINC-IV, a VIPRE-01 equivalent code, show that the minimum DNBR in the hot channel is relatively insensitive to variations in the core-wide radial power distribution (for the same value of $F_{\Delta H}^{N}$).

The ability of the VIPRE-01 computer code to accurately predict flow and enthalpy distributions in rod bundles is discussed in Subsection 4.4.4.5.1 and in Reference 83. Studies (Reference 84) have been performed to determine the sensitivity of the minimum DNBR to the void fraction correlation (see also Subsection 4.4.2.7.3) and the inlet flow distributions. The results of these studies show that the minimum DNBR is relatively insensitive to variation in these parameters. Furthermore, the VIPRE-01 flow field model for predicting conditions in the hot channels is consistent with that used in the derivation of the DNB correlation limits including void/quality modeling, turbulent mixing and crossflow and two phase flow (Reference 83).

4.4.2.9.6 Uncertainties in Flow Rates

The uncertainties associated with reactor coolant loop flow rates are discussed in Section 5.1. A thermal design flow is defined for use in core thermal performance evaluations accounting for both prediction and measurement uncertainties. In addition, another 5.9 percent of the thermal design flow is assumed to be ineffective for core heat removal capability because it bypasses the core through the various available vessel flow paths described in Subsection 4.4.4.2.1.

4.4.2.9.7 Uncertainties in Hydraulic Loads

As described in Subsection 4.4.2.6.2, hydraulic loads on the fuel assembly are evaluated for a pump overspeed transient which creates flow rates 18 percent greater than the best estimate flow. The best estimate flow is the most likely flow rate value for the actual plant operating condition.

4.4.2.9.8 Uncertainty in Mixing Coefficient

A conservative value of the mixing coefficient, that is, the thermal diffusion coefficient, is used in the VIPRE-01 analyses.

4.4.2.10 Flux Tilt Considerations

Significant quadrant power tilts are not anticipated during normal operation since this phenomenon is caused by some asymmetric perturbation. A dropped or misaligned rod cluster control assembly could cause changes in hot channel factors. These events are analyzed separately in Chapter 15.

Other possible causes for quadrant power tilts include X-Y xenon transients, inlet temperature mismatches, enrichment variations within tolerances, and so forth.

In addition to unanticipated quadrant power tilts as described above, other readily explainable asymmetries may be observed during calibration of the ex-core detector quadrant power tilt alarm. During operation, in-core maps are taken at least one per month and additional maps are obtained periodically for calibration purposes. Each of these maps is reviewed for deviations from the expected power distributions.

Asymmetry in the core, from quadrant to quadrant, is frequently a consequence of the design when assembly and/or component shuffling and rotation requirements do not allow exact symmetry preservation. In each case, the acceptability of an observed asymmetry, planned or otherwise, depends solely on meeting the required accident analyses assumptions. In practice, once acceptability has been established by review of the incore maps, the quadrant power tilt alarms and related instrumentation are adjusted to indicate zero quadrant power tilt ratio as the final step in the calibration process. This action confirms that the instrumentation is correctly calibrated to alarm in the event an unexplained or unanticipated change occurs in the quadrant-to-quadrant relationships between calibration intervals.

Proper functioning of the quadrant power tilt alarm is significant. No allowances are made in the design for increased hot channel factors due to unexpected developing flux tilts, since likely causes are presented by design or procedures or are specifically analyzed.

Finally, in the event that unexplained flux tilts do occur, the Technical Specifications provide appropriate corrective actions to provide continued safe operation of the reactor.

4.4.2.11 Fuel and Cladding Temperatures

Consistent with the thermal-hydraulic design bases described in Subsection 4.4.1, the following discussion pertains mainly to fuel pellet temperature evaluation. A description of fuel clad integrity is presented in Subsection 4.2.3.1.

The thermal-hydraulic design provides that the maximum fuel temperature is below the melting point of uranium dioxide, Subsection 4.4.1.2. To preclude center melting and to serve as a basis for overpower protection system setpoints, a calculated center-line fuel temperature of 4700°F is selected as the overpower limit. This provides sufficient margin for uncertainties in the thermal evaluations, as described in Subsection 4.4.2.9.1. The temperature distribution within the fuel pellet is predominantly a function of the local power density and the uranium dioxide thermal conductivity. However, the computation of radial fuel temperature distributions combines crud, oxide, clad gap, and pellet conductances. The factors which influence these conductances, such as gap size (or contact pressure), internal gas pressure, gas composition, pellet density, and radial power distribution within the pellet, have been combined into a semi-empirical thermal model, discussed in Subsection 4.2.3.3, that includes a model for time-dependent fuel densification, as given in WCAP-10851-P-A (Reference 49) and WCAP-15063-P-A, Revision 1 (Reference 85). This thermal model enables the determination of these factors and their net effects on temperature profiles. The temperature predictions have been compared to in-pile fuel temperature measurements (References 30 through 36, 50 and 85) and melt radius data (References 51 and 52) with good results.

Fuel rod thermal evaluations (fuel centerline, average and surface temperatures) are performed at several times in the fuel rod lifetime (with consideration of time-dependent densification) to determine the maximum fuel temperatures.

The principal factors employed in the determination of the fuel temperature follow.

4.4.2.11.1 Uranium Dioxide Thermal Conductivity

The thermal conductivity of uranium dioxide was evaluated from data reported in References 37 through 48 and 53. At the higher temperatures, thermal conductivity is best obtained by using the integral conductivity to melt. From an examination of the data, it has been concluded that the best estimate is:

$$\int_{o}^{2800} K dt = 93 \text{ W/cm}$$

This conclusion is based on the integral values reported in References 51 and 53 through 57.

The design curve for the thermal conductivity is shown in Figure 4.4-2. The section of the curve at temperatures between 0° and 1300°C is in agreement with the recommendation of the International Atomic Energy Agency (IAEA) panel (Reference 58). The section of the curve above 1300°C is derived for an integral value of 93 W/cm. (References 51, 53, and 57).

Thermal conductivity for uranium dioxide at 95-percent theoretical density can be represented by the following equation:

$$K = \frac{1}{11.8 + 0.0238\,T} + 8.775 \text{ x } 10^{-13}\,T^3$$

where:

K = W/cm-°C

T = °C.

4.4.2.11.2 Radial Power Distribution in Uranium Dioxide Fuel Rods

An accurate description of the radial power distribution as a function of burnup is needed for determining the power level for incipient fuel melting and other important performance parameters, such as pellet thermal expansion, fuel swelling, and fission gas release rates. Radial power distribution in uranium dioxide fuel rods is determined with the neutron transport theory code, LASER. The LASER code has been validated by comparing the code predictions on radial burnup and isotopic distributions with measured radial microdrill data, as detailed in WCAP-6069 (Reference 59) and WCAP-3385-56 (Reference 60). A radial power depression factor, f, is determined using radial power distributions predicted by LASER. The factor, f, enters into the determination of the pellet centerline temperature, T_c, relative to the pellet surface temperature, T_g, through the expression:

$$\int_{T_i}^{T_c} K(T)\, dT = \frac{q'' f}{4\pi}$$

where:

K(T) = the thermal conductivity for uranium dioxide with a uniform density distribution

q″ = the linear power generation rate

4.4.2.11.3 Gap Conductance

The temperature drop across the pellet-clad gap is a function of the gap size and the thermal conductivity of the gas in the gap. The gap conductance model is selected so that when combined with the uranium dioxide thermal conductivity model, the calculated fuel center-line temperature reflect the in-pile temperature measurements. A more detailed description of the gap conductance model is presented in WCAP-10851-P-A (Reference 49) and WCAP-15063-P-A (Reference 85).

4.4.2.11.4 Surface Heat Transfer Coefficients

The fuel rod surface heat transfer coefficients during subcooled forced convection and nucleate boiling are presented in Subsection 4.4.2.7.1.

4.4.2.11.5 Fuel Clad Temperatures

The outer surface of the fuel rod at the hotspot operates at a temperature a few degrees above fluid temperature for steady-state operation at rated power throughout core life due to the onset of nucleate boiling. At beginning of life this temperature is the same as the clad metal outer surface.

During operation over the life of the core, the buildup of oxides and crud on the fuel rod surface causes the clad surface temperature to increase. Allowance is made in the fuel center melt evaluation for this temperature rise. Since the thermal-hydraulic design basis limits DNB, adequate heat transfer is provided between the fuel clad and the reactor coolant so that the core thermal output is not limited by considerations of clad temperature.

4.4.2.11.6 Treatment of Peaking Factors

The total heat flux hot channel factor, F_Q, is defined by the ratio of the maximum-to-core-average heat flux. The design value of F_Q, as presented in Table 4.3-2 and described in Subsection 4.3.2.2.6, is 2.6 for normal operation.

As described in Subsection 4.3.2.2.6, the peak linear power resulting from overpower transients/ operator errors (assuming a maximum overpower of 118 percent) is less than or equal to 22.45 kW/ft. The centerline fuel temperature must be below the uranium dioxide melt temperature over the lifetime of the rod, including allowances for uncertainties. The fuel temperature design basis is described in Subsection 4.4.1.2 and results in a maximum allowable calculated center-line temperature of 4700°F. The peak linear power for prevention of center-line melt is 22.5 kW/ft. The center-line temperature at the peak linear power resulting from overpower transients/operator errors (assuming a maximum overpower of 118 percent) is below that required to produce melting.

4.4.3 Description of the Thermal and Hydraulic Design of the Reactor Coolant System

4.4.3.1 Plant Configuration Data

Plant configuration data for the thermal-hydraulic and fluid systems external to the core are provided as appropriate in Chapters 5, 6, and 9. Areas of interest are as follows:

- Total coolant flow rates for the reactor coolant system and each loop are provided in Table 5.1-3. Flow rates employed in the evaluation of the core are presented throughout Section 4.4.
- Total reactor coolant system volume including pressurizer and surge line and reactor coolant system liquid volume, including pressurizer water at steady-state power conditions, are given in Table 5.1-2.
- The flow path length through each volume may be calculated from physical data provided in Table 5.1-2.
- Line lengths and sizes for the passive core cooling system are determined to provide a total system resistance which will provide, as a minimum, the fluid delivery rates assumed in the safety analyses described in Chapter 15.
- The parameters for components of the reactor coolant system are presented in Section 5.4.
- The steady-state pressure drops and temperature distributions through the reactor coolant system are presented in Table 5.1-1.

4.4.3.2 Operating Restrictions on Pumps

The minimum net positive suction head is established before operating the reactor coolant pumps. The operator verifies that the system pressure satisfies net positive suction head requirements prior to operating the pumps.

4.4.3.3 Power-Flow Operating Map (Boiling Water Reactor BWR)

This subsection is not applicable to AP1000.

4.4.3.4 Temperature-Power Operating Map (PWR)

The relationship between reactor coolant system temperature and power is a linear relationship between zero and 100-percent power.

The effects of reduced core flow due to inoperative pumps is described in Subsections 5.4.1 and 15.2.6 and Section 15.3. The AP1000 does not include power operation with one pump out of service. Natural circulation capability of the system is described in Subsection 5.4.2.3.2.

4.4.3.5 Load Following Characteristics

Load follow using control rod and gray rod motion is described in Subsection 4.3.2.4.16. The reactor power is controlled to maintain average coolant temperature at a value which is a linear function of load, as described in Section 7.7.

4.4.3.6 Thermal and Hydraulic Characteristics Summary Table

The thermal and hydraulic characteristics are given in Tables 4.1-1, 4.4-1, and 4.4-2.

4.4.4 Evaluation

4.4.4.1 Critical Heat Flux

The critical heat flux correlations used in the core thermal analysis are explained in Subsection 4.4.2.

4.4.4.2 Core Hydraulics

4.4.4.2.1 Flow Paths Considered in Core Pressure Drop and Thermal Design

The following flow paths for core bypass are considered:

A. Flow through the spray nozzles into the upper head for head cooling purposes

B. Flow entering into the rod cluster control and gray rod cluster guide thimbles

C. Leakage flow from the vessel inlet nozzle directly to the vessel outlet nozzle through the gap between the vessel and the barrel

D. Flow introduced through the core shroud for the purpose of cooling and not considered available for core cooling

The above contributions are evaluated to confirm that the design value of the core bypass flow is met.

Of the total allowance, one part is associated with the core and the remainder is associated with the internals (items A, C, and D above). Calculations have been performed using drawing tolerances in the worst direction and accounting for uncertainties in pressure losses. Based on these calculations, the core bypass is no greater than the 5.9 percent design value.

Flow model test results for the flow path through the reactor are described in Subsection 4.4.2.7.2.

4.4.4.2.2 Inlet Flow Distributions

A core inlet flow distribution reduction of five percent to the hot assembly inlet is used in the VIPRE-01 analyses of DNBR in the AP1000 core. Studies shown in WCAP-8054-P-A (Reference 22), made with THINC-IV, a VIPRE-01 equivalent code, show that flow distributions significantly more nonuniform than five percent have a very small effect on DNBR, which is accounted for in the DNB analysis.

4.4.4.2.3 Empirical Friction Factor Correlations

The friction factor for VIPRE-01 in the axial direction, parallel to the fuel rod axis, is evaluated using a correlation for a smooth tube (Reference 83). The effect of two-phase flow on the friction loss is expressed in terms of the single-phase friction pressure drop and a two-phase friction multiplier. The multiplier is calculated using the homogenous equilibrium flow model.

The flow in the lateral directions, normal to the fuel rod axis, views the reactor core as a large tube bank. Thus, the lateral friction factor proposed by Idel'chik (Reference 64) is applicable. This correlation is of the form:

$$F_L = A\, Re_L^{-0.2}$$

where:

A = a function of the rod pitch and diameter as given in Idel'chik (Reference 64)

Re_L = the lateral Reynolds number based on the rod diameter

The comparisons of predictions to data given in Reference 83 verify the applicability of the VIPRE-01 correlations in PWR design.

4.4.4.3 Influence of Power Distribution

The core power distribution, which is largely established at beginning of life by fuel enrichment, loading pattern, and core power level, is also a function of variables such as control rod worth and position, and fuel depletion through lifetime. Radial power distributions in various planes of the core are often illustrated for general interest. However, the core radial enthalpy rise distribution, as determined by the integral of power up each channel, is of greater importance for DNBR analyses. These radial power distributions, characterized by $F_N^{\Delta H}$ (defined in Subsection 4.3.2.2.1), as well as axial heat flux profiles are discussed in the Subsections 4.4.4.3.1 and 4.4.4.3.2

4.4.4.3.1 Nuclear Enthalpy Rise Hot Channel Factor, $F_{\Delta H}^N$

Given the local power density q′ (kW/ft) at a point x, y, z in a core with N fuel rods and height H, then:

$$F_{\Delta H}^N = \frac{\text{hot rod power}}{\text{average rod power}} = \frac{\text{Max} \int_o^H q'(x_o, y_o, z_o)\, dz}{\frac{1}{N} \sum_{\text{all rods}} \int_o^H q'(x, y, z)\, dz}$$

The way in which $F_{\Delta H}^N$ is used in the DNBR calculation is important. The location of minimum DNBR depends on the axial profile, and the value of DNBR depends on the enthalpy rise to that point. Basically, the maximum value of the rod integral power is used to identify the most likely rod for minimum DNBR. An axial power profile is obtained that, when normalized to the design value of $F_{\Delta H}^N$, recreates the axial heat flux along the limiting rod. The surrounding rods are assumed to have the same axial profile with rod average powers which are typical distributions found in hot assemblies. In this manner, worst-case axial profiles can be combined with worst-case radial distributions for reference DNBR calculations.

It should be noted again that $F_{\Delta H}^N$ is an integral and is used as such in DNBR calculations. Local heat fluxes are obtained by using hot channel and adjacent channel explicit power shapes which take into account variations in horizontal power shapes throughout the core.

For operation at a fraction of full power, the design $F_{\Delta H}^N$ used is given by:

$$F_{\Delta H}^N = F_{\Delta H}^{RTP}\,[1 + 0.3(1 - P)]$$

where:

$F^N_{\Delta H}$ is the limit at rated thermal power (RTP):

P is the fraction of rated thermal power and $F^{RTP}_{\Delta H}$ = 1.59.

The permitted relaxation of $F^N_{\Delta H}$ is included in the DNB protection setpoints and allows radial power shape changes with rod insertion to the insertion limits, as detailed in WCAP-7912-P-A (Reference 65). This allows greater flexibility in the nuclear design.

4.4.4.3.2 Axial Heat Flux Distributions

As described in Subsection 4.3.2.2, the axial heat flux distribution can vary as a result of rod motion or power change or as a result of a spatial xenon transient which may occur in the axial direction. The ex-core nuclear detectors, as described in Subsection 4.3.2.2.7, are used to measure the axial power imbalance. The information from the ex-core detectors is used to protect the core from excessive axial power imbalance. The reference axial shape used in establishing core DNB limits (that is, overtemperature ΔT protection system setpoints) is a chopped cosine with a peak-to-average value of 1.61. The reactor trip system provides automatic reduction of the trip setpoints on excessive axial power imbalance. To determine the magnitude of the setpoint reduction, the reference shape is supplemented by other axial shapes skewed to the bottom and top of the core.

The course of those accidents in which DNB is a concern is analyzed in Chapter 15 assuming that the protection setpoints have been set on the basis of these shapes. In many cases, the axial power distribution in the hot channel changes throughout the course of the accident due to rod motion, coolant temperature, and power level changes.

The initial conditions for the accidents for which DNB protection is required are assumed to be those permissible within the specified axial offset control limits described in Subsection 4.3.2.2. In the case of the loss-of-flow accident, the hot channel heat flux profile is very similar to the power density profile in normal operation preceding the accident. It is therefore possible to illustrate the calculated minimum DNBR for conditions representative of the loss-of-flow accident as a function of the flux difference initially in the core. The power shapes are evaluated with a full-power radial peaking factor ($F^N_{\Delta H}$) of 1.59. The radial contribution to the hot rod power shape is conservative both for the initial condition and for the condition at the time of minimum DNBR during the loss-of-flow transient. The minimum DNBR is calculated for the design power shape for non-overpower/overtemperature DNB events. This design shape results in calculated DNBR that bounds the normal operation shapes.

4.4.4.4 Core Thermal Response

A general summary of the steady-state thermal-hydraulic design parameters including thermal output and flow rates is provided in Table 4.4-1.

As stated in Subsection 4.4.1, the design bases of the application are to prevent DNB and to prevent fuel melting for Condition I and II events. The protective systems described in Chapter 7 are designed to meet these bases. The response of the core to Condition II transients is given in Chapter 15.

4.4.4.5 Analytical Methods

4.4.4.5.1 Core Analysis

The objective of reactor core thermal design is to determine the maximum heat removal capability in all flow subchannels and to show that the core safety limits, as presented in the technical

specifications, are not exceeded while combining engineering and nuclear effects. The thermal design takes into account local variations in dimensions, power generation, flow redistribution, and mixing. The Westinghouse version of VIPRE-01, a three-dimensional subchannel code that has been developed to account for hydraulic and nuclear effects on the enthalpy rise in the core and hot channels, is described in Reference 83, VIPRE-01 modeling of a PWR core is based on a one-pass modeling approach (Reference 83). In the one-pass modeling, hot channels and their adjacent channels are modeled in detail, while the rest of the core is modeled simultaneously on a relatively coarse mesh. The behavior of the hot assembly is determined by superimposing the power distribution upon the inlet flow distribution while allowing for flow mixing and flow distribution between flow channels. Local variations in fuel rod power, fuel rod and pellet fabrication, and turbulent mixing are also considered in determining conditions in the hot channels. Conservation equations of mass, axial and lateral momentum, and energy are solved for the fluid enthalpy, axial flow rate, lateral flow, and pressure drop.

4.4.4.5.2 Steady State Analysis

The VIPRE-01 core model as approved by the NRC (Reference 83) is used with the applicable DNB correlations to determine DNBR distributions along the hot channels of the reactor core under all expected operating conditions. The VIPRE-01 code is described in detail in Reference 84, including discussions on code validation with experimental data. The VIPRE-01 modeling method is described in Reference 83, including empirical models and correlations used. The effect of crud on the flow and enthalpy distribution in the core is not directly accounted for in the VIPRE-01 evaluations. However, conservative treatment by the Westinghouse VIPRE-01 modeling method has been demonstrated to bound this effect in DNBR calculations (Reference 83).

Estimates of uncertainties are discussed in Subsection 4.4.2.9.

4.4.4.5.3 Experimental Verification

Extensive additional experimental verification of VIPRE-01 is presented in Reference 84.

The VIPRE-01 analysis is based on a knowledge and understanding of the heat transfer and hydrodynamic behavior of the coolant flow and the mechanical characteristics of the fuel elements. The use of the VIPRE-01 analysis provides a realistic evaluation of the core performance and is used in the thermal hydraulic analyses as described above.

4.4.4.5.4 Transient Analysis

VIPRE-01 is capable of transient DNB analysis. The conservation equations in the VIPRE-01 code contain the necessary accumulation terms for transient calculations. The input description can include one or more of the following time dependent arrays:

1. Inlet flow variation
2. Core heat flux variation
3. Core pressure variation
4. Inlet temperature or enthalpy variation

At the beginning of the transient, the calculation procedure is carried out as in the steady state analysis. The time is incremented by an amount determined either by the user of by the time step control options in the code itself. At each new time step the calculations are carried out with the

addition of the accumulation terms which are evaluated using the information from the previous time step. This procedure is continued until a preset maximum time is reached.

At time intervals selected by the user, a complete description of the coolant parameter distributions as well as DNBR is printed out. In this manner the variation of any parameter with time can be readily determined.

4.4.4.6 Hydrodynamic and Flow Power Coupled Instability

Boiling flow may be susceptible to thermohydrodynamic instabilities (Reference 68). These instabilities are undesirable in reactors, since they may cause a change in thermohydraulic conditions that may lead to a reduction in the DNB heat flux relative to that observed during a steady flow condition or to undesired forced vibrations of core components. Therefore, a thermo-hydraulic design criterion was developed which states that modes of operation under Condition I and II events shall not lead to thermohydrodynamic instabilities.

Two specific types of flow instabilities are considered for AP1000 operation. These are the Ledinegg (or flow excursion) type of static instability and the density wave type of dynamic instability.

A Ledinegg instability involves a sudden change in flow rate from one steady state to another. This instability occurs (Reference 68) when the scope of the reactor coolant system pressure drop-flow rate curve:

$$\left(\frac{\partial \Delta P}{\partial G} \mid \text{internal}\right)$$

becomes algebraically smaller than the loop supply (pump head) pressure drop-flow rate curve:

$$\left(\frac{\partial \Delta P}{\partial G} \mid \text{external}\right)$$

The criterion for stability is thus:

$$\left(\frac{\partial \Delta P}{\partial G}\Big|_{\text{internal}} \geq \frac{\partial \Delta P}{\partial G}\Big|_{\text{external}}\right)$$

The reactor coolant pump head curve has a negative slope ($\partial\Delta P/\partial G$ external less than zero), whereas the reactor coolant system pressure drop-flow curve has a positive slope ($\partial\Delta P/\partial G$ internal greater than zero) over the Condition I and Condition II operational ranges. Thus, the Ledinegg instability does not occur.

The mechanism of density wave oscillations in a heated channel has been described by R. T. Lahey and F. J. Moody (Reference 69). Briefly, an inlet flow fluctuation produces an enthalpy perturbation. This perturbs the length and the pressure drop of the single-phase region and causes quality or void perturbations in the two-phase regions that travel up the channel with the flow. The quality and length perturbations in the two-phase region create two-phase pressure drop perturbations. However, since the total pressure drop across the core is maintained by the characteristics of the fluid system

external to the core, then the two-phase pressure drop perturbation feeds back to the single-phase region. These resulting perturbations can be either attenuated or self-sustained.

A simple method has been developed by M. Ishii (Reference 70) for parallel closed-channel systems to evaluate whether a given condition is stable with respect to the density wave type of dynamic instability. This method had been used to assess the stability of typical Westinghouse reactor designs, including the design outlined in References 71, 72, and 73, under Condition I and II operation. The results indicate that a large margin-to-density wave instability exists. Increases on the order of 150 percent of rated reactor power would be required for the predicted inception of this type of instability.

The application of the Ishii method (Reference 70) to Westinghouse reactor designs is conservative due to the parallel open-channel feature of Westinghouse pressurized water reactor cores. For such cores, there is little resistance to lateral flow leaving the flow channels of high-power density. There is also energy transfer from channels of high-power density to lower power density channels. This coupling with cooler channels leads to the conclusion that an open-channel configuration is more stable than the above closed-channel analysis under the same boundary conditions.

Flow stability tests (Reference 74) have been conducted where the closed channel systems were shown to be less stable than when the same channels were cross-connected at several locations. The cross-connections were such that the resistance to channel cross-flow and enthalpy perturbations would be greater than would exist in a pressurized water reactor core which has a relatively low resistance to cross-flow.

Flow instabilities that have been observed have occurred almost exclusively in closed-channel systems operating at low pressures relative to the Westinghouse pressurized water reactor operating pressures. H. S. Kao, T. D. Morgan, and W. B. Parker (Reference 75) analyzed parallel closed-channel stability experiments simulating a reactor core flow. These experiments were conducted at pressures up to 2200 psia. The results showed that, for flow and power levels typical of power reactor conditions, no flow oscillations could be induced above 1200 psia.

Additional evidence that flow instabilities do not adversely affect thermal margin is provided by the data from the rod bundle DNB tests. Many Westinghouse rod bundles have been tested over wide ranges of operating conditions with no evidence of premature DNB or inconsistent data which might be indicative of flow instabilities in the rod bundle.

In summary, it is concluded that thermohydrodynamic instabilities will not occur under Condition I and II for Westinghouse pressurized water reactor designs. A large power margin, greater than 150 percent of rated power, exists to predicted inception of such instabilities. Analysis has been performed which shows that minor plant-to-plant differences in Westinghouse reactor designs such as fuel assembly arrays, power-to-flow ratios, and fuel assembly length do not result in gross deterioration of the above power margins.

4.4.4.7 Fuel Rod Behavior Effects from Coolant Flow Blockage

Coolant flow blockages can occur within the coolant channels of a fuel assembly or external to the reactor core. The effects of fuel assembly blockage within the assembly on fuel rod behavior are more pronounced than external blockages of the same magnitude. In both cases, the flow blockages cause local reductions in coolant flow. The amount of local flow reduction, where the reduction occurs in the reactor, and how far along the flow stream the reduction persists are considerations which will influence the fuel rod behavior. The effects of coolant flow blockages in terms of maintaining rated core performance are determined both by analytical and experimental methods. The experimental data are usually used to augment analytical tools such as computer programs similar to the VIPRE-

01 program. Inspection of the DNB correlation (Subsection 4.4.2.2 and References 4, 5, and 6) shows that the predicted DNBR is dependent upon the local values of quality and mass velocity.

The VIPRE-01 code is capable of predicting the effects of local flow blockages on DNBR within the fuel assembly on a subchannel basis, regardless of where the flow blockage occurs. Reference 84 shows that, for a fuel assembly similar to the Westinghouse design, VIPRE-01 accurately predicts the flow distribution within the fuel assembly when the inlet nozzle is completely blocked. Full recovery of the flow was found to occur about 30 inches downstream of the blockage. With the reactor operating at the nominal full-power conditions specified in Table 4.4-1, the effects of an increase in enthalpy and decrease in mass velocity in the lower portion of the fuel assembly would not result in the fuel rods reaching the DNBR limit.

The open literature supports the conclusion that flow blockage in open-lattice cores, similar to the Westinghouse cores, causes flow perturbations which are local to the blockage. For example, A. Ohstubo and S. Uruwashi (Reference 76) show that the mean bundle velocity is approached asymptomatically about four inches downstream from the flow blockage in a single flow cell. Similar results were also found for two and three cells completely blocked. P. Basmer, et al., (Reference 77) tested an open-lattice fuel assembly in which 41 percent of the subchannels were completely blocked in the center of the test bundle between spacer grids. Their results show that the stagnant zone behind the flow blockage essentially disappears after 1.65 L/De or about five inches for their test bundle. They also found that leakage flow through the blockage tended to shorten the stagnant zone or, in essence, the complete recovery length. Thus, local flow blockages within a fuel assembly have little effect on subchannel enthalpy rise. In reality, a local flow blockage would be expected to promote turbulence and, therefore would not likely affect DNBR at all.

Coolant flow blockages induce local cross-flows as well as promote turbulence. Fuel rod behavior is changed under the influence of a sufficiently high cross-flow component. Fuel rod vibration could occur, caused by this cross-flow component, through vortex shedding or turbulent mechanisms. If the cross-flow velocity exceeds the limit established for fluid elastic stability, large amplitude whirling results. The limits for a controlled vibration mechanism are established from studies of vortex shedding and turbulent pressure fluctuations. The cross-flow velocity required to exceed fluid elastic stability limits is dependent on the axial location of the blockage and the characterization of the cross-flow (jet flow or not). These limits are greater than those for vibratory fuel rod wear. Cross-flow velocity above the established limits can lead to mechanical wear of the fuel rods at the grid support locations. Fuel rod wear due to flow-induced vibration is considered in the fuel rod fretting evaluation as discussed in Section 4.2.

4.4.5 Testing and Verification

4.4.5.1 Tests Prior to Initial Criticality

A reactor coolant flow test is performed, as discussed in Chapter 14, following fuel loading but prior to initial criticality. Coolant loop pressure data is obtained in this test. This data allows determination of the coolant flow rates at reactor operating conditions. This test verifies that proper coolant flow rates have been used in the core thermal and hydraulic analysis.

4.4.5.2 Initial Power and Plant Operation

Core power distribution measurements are made at several core power levels, as discussed in Chapter 14. These tests are used to confirm that conservative peaking factors are used in the core thermal and hydraulic analysis.

Additional demonstration of the overall conservatism of the THINC analysis was obtained by comparing THINC predictions to in-core thermocouple measurements, as detailed WCAP-8453-A

(Reference 78). VIPRE-01 has been confirmed to be as conservative as the THINC code in Reference 83.

4.4.5.3 Component and Fuel Inspections

Inspections performed on the manufactured fuel are described in Subsection 4.2.4. Fabrication measurements critical to thermal and hydraulic analysis are obtained to verify that the engineering hot channel factors in the design analyses (Subsection 4.4.2.2.4) are met.

4.4.6 Instrumentation Requirements

4.4.6.1 Incore Instrumentation

The primary function of the incore instrumentation system is to provide a three-dimensional flux map of the reactor core. This map is used to calibrate neutron detectors used by the protection and safety monitoring system as well as to optimize core performance. A secondary function of the incore instrumentation system is to provide the protection and safety monitoring system with the signals necessary for monitoring core exit temperatures. This secondary function is the result of the mechanical design that groups the detectors used for generating the flux map in the same thimble as the core exit thermocouples.

The incore instrumentation system consists of incore instrument thimble assemblies, which house fixed incore detectors, core exit thermocouple assemblies contained within an inner and outer sheath assembly, and associated signal processing and data processing equipment. There are 42 incore instrument thimble assemblies: each is composed of multiple fixed incore detectors and one thermocouple.

The thimbles are inserted into the active core through the upper head and internals of the reactor vessel. The signals output from the fixed incore detectors are digitized inside containment and multiplexed out of the containment. The signal processing software integral to the incore instrumentation system allows the fixed incore detector signals to be used to calculate an accurate three-dimensional core power distribution suitable for developing calibration information for the excore nuclear instrumentation input to the overtemperature and overpower ΔT reactor trip setpoints. The system is also capable of accurately determining whether the reactor power distribution is currently within the operating limits defined in the technical specifications while the reactor is operating above approximately 20 percent of rated thermal power.

The incore instrument system data processor receives the transmitted digitized fixed incore detector signals from the signal processor and combines the measured data with analytically-derived constants, and certain other plant instrumentation sensor signals, to generate a full three-dimensional indication of nuclear power distribution in the reactor core. It also edits the three-dimensional indication of power distribution to extract pertinent power distribution parameters outputs for use by the plant operators and engineers. The data processor also generates hardcopy representations of the detailed three-dimensional nuclear power indications.

The hardware and software which performs the three-dimensional power distribution calculation are capable of executing the calculation algorithms and constructing graphical and tabular displays of core conditions at intervals of less than one minute. The software provides information to enable the reactor operator to ascertain how the measured peaking factor performance agrees with the peaking factor performance predicted by the design model used to determine the acceptability of the fuel loading pattern. The analysis software provides information required to activate a visual alarm display to alert the reactor operator about the current existence of, or the potential for, reactor operating limit violations. The calculation algorithms are capable of determining the core average axial offset using a minimum set of the total 42 incore monitor assemblies. A minimum set of incore monitor assemblies

is at least 30 operating assemblies, with at least two operating assemblies in each quadrant, prior to nuclear model calibration; and at least 21 operating assemblies, with at least two operating assemblies in each quadrant, after nuclear model calibration. The nuclear model calibration is performed after each new core load. The hardware which performs the online power distribution monitoring is configured such that a single hardware failure will not necessitate a reactor maximum power reduction or restrict normal reactor operations.

During plant operation, the incore instrument thimble assembly is positioned within the fuel assembly and exits through the top of the reactor vessel QuickLoc seal connection. The fixed incore detector and core exit thermocouple signal exit the detector through a multipin connector to the incore instrument thimble tube cables. The fixed incore detector and core exit thermocouple cables are then routed to different data conditioning and processing stations. The data is processed and the results are available for display in the main control room.

4.4.6.2 Overtemperature and Overpower ΔT Instrumentation

The overtemperature ΔT trip protects the core against low DNBR. The overpower ΔT trip protects against excessive power (fuel rod rating protection).

As described in Subsection 7.2.1.1.3, factors included in establishing the overtemperature ΔT and overpower ΔT trip setpoints include the reactor coolant temperature in each loop and the axial distribution of core power as seen by excore neutron detectors.

4.4.6.3 Instrumentation to Limit Maximum Power Output

The signals from the three ranges (source, intermediate, and power) of neutron flux detectors, are used to limit the maximum power output of the reactor within their respective ranges.

There are eight radial locations containing a total of twelve neutron flux detectors installed around the reactor between the vessel and the primary shield. Four proportional counters for the source range are located at the highest fluence portions of the core containing the primary startup sources at an elevation approximately one-fourth of the core height. Four pulse fission chambers for the intermediate range, located in the same instrument wells as the source range detectors, are positioned at an elevation corresponding to one-half of the core height. Four uncompensated ionization chamber assemblies for the power range are installed vertically at the four corners of the core. These assemblies are located equidistant from the reactor vessel along the length and, to minimize neutron flux pattern distortions, within approximately one foot of the reactor vessel. Each power range detector provides two signals corresponding to the neutron flux in the upper and in the lower sections of a core quadrant. The three ranges of detectors are used as inputs to monitor neutron flux from a completely shutdown condition to 120 percent of full power, with the capability of recording overpower excursions up to 200 percent of full power.

The output of the power range channels is used for:

- Protecting the core against the consequences of rod ejection accidents
- Protecting the core against the consequences of adverse power distributions resulting from dropped rods
- The rod speed control function
- Alerting the operator to an excessive power imbalance between the quadrants

The intermediate range detectors also provide signals for the post-accident monitoring system.

Details of the neutron detectors and nuclear instrumentation design and the control and trip logic are given in Chapter 7. The limits on neutron flux operation and trip setpoints are given in the technical specifications.

4.4.6.4 Digital Metal Impact Monitoring System

The digital metal impact monitoring system is a nonsafety-related system that monitors the reactor coolant system for metallic loose parts. It consists of several active instrumentation channels, each comprising a piezoelectric accelerometer (sensor), signal conditioning, and diagnostic equipment. The digital impact monitoring system conforms with Regulatory Guide 1.133.

The digital metal impact monitoring system is designed to detect a loose parts that weigh from 0.25 to 30 pounds, and can also detect impact with a kinetic energy of 0.5 foot-pounds on the inside surface of the reactor coolant system pressure boundary within three feet of a sensor.

The digital impact monitoring system consists of several redundant instrumentation channels, each comprised of a piezoelectric accelerometer (sensor), preamplifier, and signal conditioning equipment. The output signal from each accelerometer is amplified by the preamplifier and signal conditioning equipment before it is processed by a discriminator to eliminate noise and signals which are not indicative of loose part impacts. The system starts up and operates automatically.

The system facilitates performance tests, hardware integrity tests, and the recognition, location, replacement, repair and adjustment of malfunctioning components. System performance tests are made using a hammer as a tool to simulate an impact. Additional system performance testing is performed using special test modules. These modules simulate impacts and test performance of the signal processing equipment. Hardware integrity tests are also performed to verify equipment operation.

The impact detect algorithm, used by the signal processing equipment, is designed to minimize the number of false alarms. False impact detection, attributable to normal hydraulic, mechanical and electrical noise, is minimized by a number of techniques including:

- Utilizing a floating level within the impact detection algorithm. The floating level is based on signal levels not characteristic of an impact, and is generally a function of the background noise level.

- Comparing the impact event with the times and type of normally occurring plant operation events received from plant control system such as a control rod stepping.

- Comparing the number of events detected within a given time interval.

The sensors of the impact monitoring system are fastened mechanically to the reactor coolant system at potential loose part collection regions including the upper and lower head region of the reactor pressure vessel, and the reactor coolant inlet region of each steam generator.

The equipment inside the containment is designed to remain functional through an earthquake of a magnitude equal to 50 percent of the calculated safe shutdown earthquake and normal environments (radiation, vibration, temperature, humidity) anticipated during the operating lifetime. The instrument channels associated with the sensors at each reactor coolant system location are physically separated from each other starting at the sensor locations to a point in the plant that is always accessible for maintenance during full-power operation.

The digital metal impact monitoring system is calibrated prior to plant startup. Capabilities exist for subsequent periodic online channel checks and channel functional tests and for offline channel calibrations at refueling outages.

4.4.7 Combined License Information

4.4.7.1 Changes to the reference design of the fuel, burnable absorber rods, rod cluster control assemblies, or initial core design from that presented in the DCD are addressed in APP-GW-GLR-059 (Reference 87).

4.4.7.2 Following selection of the actual plant operating instrumentation and calculation of the instrumentation uncertainties of the operating plant parameters as discussed in Subsection 7.1.6, the design limit DNBR values will be calculated. The calculations will be completed using the RTDP with these instrumentation uncertainties and confirm that either the design limit DNBR values as described in this section remain valid or that the safety analysis minimum DNBR bounds the new design limit DNBR values plus DNBR penalties, such as rod bow penalty. This will be completed prior to fuel load.

4.4.8 References

1. ANSI N18.2a-75, “Nuclear Safety Criteria for the Design of Stationary Pressurized Water Reactor Plants.”

2. Friedland, A. J. and Ray, S., “Revised Thermal Design Procedure,” WCAP-11397-P-A (Proprietary) and WCAP-11397-A (Non-Proprietary), April 1989.

3. Christensen, J. A., Allio, R. J., and Biancheria, A., “Melting Point of Irradiated UO_2,” WCAP-6065, February 1965.

4. Davidson, S. L. and Kramer, W. R. (Ed.), “Reference Core Report VANTAGE 5 Fuel Assembly,” WCAP-10444-P-A (Proprietary) and WCAP-10445-NP-A (Non-Proprietary), September 1985.

5. Tong, L. S., “Boiling Crisis and Critical Heat Flux,” AEC Critical Review Series, TID-25887, 1972.

6. Tong, L. S., “Critical Heat Fluxes in Rod Bundles, Two Phase Flow and Heat Transfer in Rod Bundles,” Annual Winter Meeting ASME, November 1968, p. 3146.

7. Letter from A. C. Thadani (NRC) to W. J. Johnson (Westinghouse), January 31, 1989, Subject: Acceptance for Referencing of Licensing Topical Report, WCAP-9226-P/9227-NP, “Reactor Core Response to Excessive Secondary Steam Releases.”

8. Motley, F. E., Cadek, F. F., “DNB Test Results for R-Grid Thimble Cold Wall Cells,” WCAP-7695-L Addendum 1, October 1972.

9. [*Davidson, S. L. (Ed.), “Westinghouse Fuel Criteria Evaluation Process,” WCAP-12488-A, October 1994.*]*

10. Tong, L. S., “Prediction of Departure from Nucleate Boiling for an Axially Nonuniform Heat Flux Distribution,” Journal of Nuclear Energy 21, pp 241-248, 1967.

11. Not used.

*NRC Staff approval is required prior to implementing a change in this information.

12. Cadek, F. F., Motley, F. E., and Dominicis, D. P., “Effect of Axial Spacing on Interchannel Thermal Mixing with the R Mixing Vane Grid,” WCAP-7941-P-A (Proprietary) and WCAP-7959-A (Non-Proprietary), January 1975.

13. Rowe, D. S., and Angle, C. W., “Crossflow Mixing Between Parallel Flow Channels During Boiling, Part II Measurements of Flow and Enthalpy in Two Parallel Channels,” BNWL-371, Part 2, December 1967.

14. Rowe, D. S., and Angle, C. W., “Crossflow Mixing Between Parallel Flow Channels During Boiling, Part III Effect of Spacers on Mixing Between Two Channels,” BNWL-371, Part 3, January 1969.

15. Gonzalez-Santalo, J. M., and Griffith, P., “Two-Phase Flow Mixing in Rod Bundle Subchannels,” ASME Paper 72-WA/NE-19.

16. Motley, F. E., Wenzel, A. H., and Cadek, F. F., “The Effect of 17 x 17 Fuel Assembly Geometry on Interchannel Thermal Mixing,” WCAP-8298-P-A (Proprietary) and WCAP-8290A (Non-Proprietary), January 1975.

17. Hill, K. W., Motley, F. E., and Cadek, F. F., “Effect of Local Heat Flux Spikes on DNB in Non Uniform Heated Rod Bundles,” WCAP-8174 (Proprietary), August 1973, and WCAP-8202 (Non-Proprietary), August 1973.

18. Cadek, F. F., “Interchannel Thermal Mixing with Mixing Vane Grids,” WCAP-7667-P-A (Proprietary) and WCAP-7755-A (Non-Proprietary), January 1975.

19. Skaritka, J., Ed, “Fuel Rod Bow Evaluation,” WCAP-8691, Revision 1 (Proprietary) and WCAP-8692, Revision 1 (Non-Proprietary), July 1979.

20. “Partial Response to Request Number 1 for Additional Information on WCAP-8691, Revision 1,” Letter from E. P. Rahe, Jr. (Westinghouse) to J. R. Miller (NRC), NS-EPR-2515, October 9, 1981; “Remaining Response to Request Number 1 for Additional Information on WCAP-8691, Revision 1,” Letter from E. P. Rahe, Jr. (Westinghouse) to R. J. Miller (NRC), NS-EPR-2572, March 16, 1982.

21. Letter from C. Berlinger (NRC) to E. P. Rahe, Jr. (Westinghouse), Subject: “Request for Reduction in Fuel Assembly Burnup Limit for Calculations of Maximum Rod Bow Penalty,” June 18, 1986.

22. Hochreiter, L. E., “Applications of the THINC-IV Program to PWR Design,” WCAP-8054-P-A (Proprietary), February 1989 and WCAP-8195 (Non-Proprietary), October 1973.

23. Hochreiter, L. E., Chelemer, H., and Chu, P. T., “THINC-IV, An Improved Program for Thermal-Hydraulic Analysis of Rod Bundle Cores,” WCAP-7956-P-A, February 1989.

24. Dittus, F. W., and Boelter, L. M. K., “Heat Transfer in Automobile Radiators of the Tubular Type,” California University Publication in Engineering 2, No. 13, 443461, 1930.

25. Weisman, J., “Heat Transfer to Water Flowing Parallel to Tube Bundles,” Nuclear Science Engineering 6, pp 78-79, 1959.

26. Thom, J. R. S., et al., “Boiling in Subcooled Water During Flowup Heated Tubes or Annuli,” Proceedings of the Institution of Mechanical Engineers 180, Part C, pp 226-246, 1955-1966.

27. Not used.

28. Not used.

29. Not used.

30. Kjaerheim, G., and Rolstad, E., “In-Pile Determination of UO_2, Thermal Conductivity, Density Effects, and Gap Conductance,” HPR-80, December 1967.

31. Kjaerheim, G., In-Pile Measurements of Center Fuel Temperatures and Thermal Conductivity Determination of Oxide Fuels, Paper IFA-175 Presented at the European Atomic Energy Society Symposium on Performance Experience of Water-Cooled Power Reactor Fuel, Stockholm, Sweden, October 1969.

32. Cohen, I., Lustman, B., and Eichenberg, D., “Measurement of the Thermal Conductivity of Metal-Glad Uranium Oxide Rods During Irradiation,” WAPD-228, 1960.

33. Clough, D. J., and Sayers, J. B., “The Measurement of the Thermal Conductivity of UO_2, under Irradiation in the Temperature Range 150 to 1600°C,” AERE-4690, UKAEA Research Group, Harwell, December 1964.

34. Stora, J. P., et al., “Thermal Conductivity of Sintered Uranium Oxide under In-Pile Conditions,” EURAEC-1095, 1964.

35. Devold, I., “A Study of the Temperature Distribution in UO_2, Reactor Fuel Elements,” AE-318, Aktiebolaget Atomenergi, Stockholm, Sweden, 1968.

36. Balfour, M. G., Christensen, J. A., and Ferrari, H. M., “In-Pile Measurement of UO_2 Thermal Conductivity,” WCAP-2923, 1966.

37. Howard, V. C., and Gulvin, T. G., “Thermal Conductivity Determinations on Uranium Dioxide by a Radial Flow Method,” UKAEA IG-Report 51, November 1960.

38. Lucks, C. F., and Deem, H. W., “Thermal Conductivity and Electrical Conductivity of UO_2,” in Progress Reports Relating to Civilian Applications, BMI-1448 (Revised) for June 1960, BMI-1489 (Revised) for December 1960, and BMI-1518 (Revised) for May 1961.

39. Daniel, J. L., Matolich, J. Jr., and Deem, H. W., “Thermal Conductivity of UO_2,” HW-69945, September 1962.

40. Feith, A. D., “Thermal Conductivity of UO_2 by a Radial Heat Flow Method,” TID-21668, 1962.

41. Vogt, J., Grandel, L., and Runfors, U., “Determination of the Thermal Conductivity of Unirradiated Uranium Dioxide,” AB Atomenergi Report RMB-527, 1964, Quoted by IAEA Technical Report Series No. 59, “Thermal Conductivity of Uranium Dioxide.”

42. Nishijima, T., Kawada, T., and Ishihata, A., “Thermal Conductivity of Sintered UO_2 and $4Al_2O_3$ at High Temperatures,” Journal of the American Ceramic Society 48, pp 31-44, 1965.

43. Ainscough, J. B., and Wheeler, M. J., "Thermal Diffusivity and Thermal Conductivity of Sintered Uranium Dioxide," Proceedings of the Seventh Conference of Thermal Conductivity, National Bureau of Standards, Washington, p 467, 1968.

44. Godfrey, T. G., et al., "Thermal Conductivity of Uranium Dioxide and Armco Iron by an Improved Radial Heat Flow Technique," ORNL-3556, June 1964.

45. Stora, J. P., et al., "Thermal Conductivity of Sintered Uranium Oxide Under In-Pile Conditions," EURAEC-1095, August 1964.

46. Bush, A. J., "Apparatus for Measuring Thermal Conductivity to 2500°C," Reporting 64-1P6-401-43 (Proprietary), Westinghouse Research Laboratories, February 1965.

47. Asamoto, R. R., Anselin, F. L., and Conti, A. E., "The Effect of Density on the Thermal Conductivity of Uranium Dioxide," GEAP-5493, April 1968.

48. Kruger, O. L., Heat Transfer Properties of Uranium and Plutonium Dioxide, Paper 11-N-68F, presented at the Fall Meeting of Nuclear Division of the American Ceramic Society, Pittsburgh, September 1968.

49. Weiner, R. A., et al., "Improved Fuel Performance Models for Westinghouse Fuel Rod Design and Safety Evaluations," WCAP-10851-P-A (Proprietary) and WCAP-11873-A (Non-Proprietary), August 1988.

50. Leech, W. J. et al., "Revised PAD Code Thermal Safety Model," WCAP-8720, Addendum 2, October 1982.

51. Duncan, R. N., "Rabbit Capsule Irradiation of UO_2," CVTR Project, CVNA Project, CVNA-142, June 1962.

52. Nelson, R. G., et al., "Fission Gas Release from UO_2 Fuel Rods with Gross Central Melting," GEAP-4572, July 1964.

53. Gyllander, J. A., "In-Pile Determination of the Thermal Conductivity of UO_2 in the Range 500 to 2500°C," AE-411, January 1971.

54. Lyons, M. F., et al., "UO_2 Powder and Pellet Thermal Conductivity During Irradiation," GEAP-5100-1, March 1966.

55. Coplin, D. H., et al., "The Thermal Conductivity of UO_2 by Direct In-Reactor Measurements," GEAP-5100-6, March 1968.

56. Bain, A. S., "The Heat Rating Required to Produce Center Melting in Various UO_2 Fuels," ASTM Special Technical Publication No. 306, Philadelphia, pp 30-46, 1962.

57. Stora, J. P., "In-Reactor Measurements of the Integrated Thermal Conductivity of UO_2 - Effect of Porosity," Transactions of the American Nuclear Society 13, pp 137-138, 1970.

58. International Atomic Energy Agency, "Thermal Conductivity of Uranium Dioxide," Report of the Panel Held in Vienna, April 1965, IAEA Technical Reports Series, No. 59, Vienna, 1966.

59. Poncelet, C. G., "Burnup Physics of Heterogeneous Reactor Lattices," WCAP-6069, June 1965.

60. Nodvick, R. J., “Saxton Core II Fuel Performance Evaluation,” WCAP-3385-56, Part II, “Evaluation of Mass Spectrometric and Radiochemical Analyses of Irradiated Saxton Plutonium Fuel,” July 1970.

61. Not used.

62. Not used.

63. Not used.

64. Idel'chik, I. E., “Handbook of Hydraulic Resistance,” 2nd Edition, Hemisphere Publishing Corp., 1986.

65. McFarlane, A. F., “Power Peaking Factors,” WCAP-7912-P-A (Proprietary) and WCAP-7912-A (Non-Proprietary), January 1975.

66. Not used.

67. Not used.

68. Boure, J. A., Bergles, A. E., and Tong, L. S., “Review of Two-Phase Flow Instability,” Nuclear Engineering Design 25, pp 165-192, 1973.

69. Lahey, R. T., and Moody, F. J., The Thermal Hydraulics of a Boiling Water Reactor, American Nuclear Society, 1977.

70. Saha, P., Ishii, M., and Zuber, N., “An Experimental Investigation of the Thermally Induced Flow Oscillations in Two-Phase Systems,” Journal of Heat Transfer, pp 616-622, November 1976.

71. Virgil C. Summer Nuclear Station FSAR, Chapter 4, South Carolina Electric & Gas Company, Docket No. 50-395.

72. Byron/Braidwood Stations FSAR, Chapter 4, Commonwealth Edison Company, Docket No. 50-456.

73. South Texas Project Electric Generating Station FSAR, Chapter 4, Houston Lighting and Power Company, Docket No. 50-498.

74. Kakac, S., et al., “Sustained and Transient Boiling Flow Instabilities in a Cross-Connected Four-Parallel-Channel Upflow System,” Proceedings of Fifth International Heat Transfer Conference, Tokyo, September 1974.

75. Kao, H. S., Morgan, T. D., and Parker, W. B., “Prediction of Flow Oscillation in Reactor Core Channel,” Transactions of the American Nuclear Society 16, pp 212-213, 1973.

76. Ohtsubo, A., and Uruwashi, S., “Stagnant Fluid Due to Local Flow Blockage,” Journal of Nuclear Science Technology, No. 7, pp 433-434, 1972.

77. Basmer, P., Kirsh, D., and Schultheiss, G. F., “Investigation of the Flow Pattern in the Recirculation Zone Downstream of Local Coolant Blockages in Pin Bundles,” Atomwirtschaft 17, No. 8, pp 416-417, 1972 (in German).

78. Burke, T. M., Meyer, G. E., and Shefcheck, J., “Analysis of Data from the Zion (Unit 1) THINC Verification Test,” WCAP-8453-A, May 1976.

79. Not used.

80. Not used.

81. Davidson, S. L., and Ryan, T. L., “VANTAGE+ Fuel Assembly Reference Core Report,” WCAP-12610-P-A (Proprietary) and WCAP-14342-A (Non-Proprietary), April 1995.

82. Smith, L. D., et al., “Modified WRB-2 Correlation, WRB-2M, for Predicting Critical Heat Flux in 17x17 Rod Bundles with Modified LPD Mixing Vane Grids,” WCAP-15025-P-A (Proprietary) and WCAP-15026-NP (Non-Proprietary), April 1999.

82a. Letter from D. S. Collins (USNRC) to J. A. Gresham (Westinghouse), “Modified WRB-2 Correlation WRB-2M for Predicting Critical Heat Flux in 17x17 Rod Bundles with Modified LPD Mixing Vane Grids,” February 3, 2006.

83. Sung, Y. X., et al., “VIPRE-01 Modeling and Qualification for Pressurized Water Reactor Non-LOCA Thermal-Hydraulic Safety Analysis,” WCAP-14565-P-A and WCAP-15306-NP-A, October 1999.

84. Stewart, C. W., et al., “VIPRE-01: A Thermal-Hydraulic Code for Reactor Core,” Volume 1-3 (Revision 3, August 1989), Volume 4 (April 1987), NP-2511-CCM-A, Electric Power Research Institute.

85. Slagle, W. H. (ed.) et al., “Westinghouse Improved Performance Analysis and Design Model (PAD 4.0),” WCAP-15063-P-A, Revision 1 (Proprietary) and WCAP-15064-NP-A, Revision 1 (Non-Proprietary), July 2000.

86. Kitchen, T. J., “Generic Safety Evaluation for 17x17 Standard Robust Fuel Assembly (17x17 STD RFA),” SECL-98-056, Revision 0, September 30, 1998.

87. APP-GW-GLR-059/WCAP-16652-NP, “AP1000 Core & Fuel Design Technical Report,” Revision 0.

88. Letter, Peralta, J. D. (NRC) to Maurer, B. F. (Westinghouse), “Approval for Increase in Licensing Burnup Limit to 62,000 MWD/MTU (TAC No. MD1486),” May 25, 2006.

Table 4.4-1 (Sheet 1 of 2)
Thermal and Hydraulic Comparison Table
(AP1000, AP600 and a Typical Westinghouse XL Plant)

Design Parameters	AP1000[a]	AP600	Typical XL Plant
Reactor core heat output (MWt)	3400	1933	3800
Reactor core heat output (10^6 BTU/hr)	11601	6596	12,969
Heat generated in fuel (%)	97.4	97.4	97.4
System pressure, nominal (psia)	2250	2250	2250
System pressure, minimal (psia)	2190	2200	2204
Minimum DNBR at nominal conditions			
Typical flow channel	2.80	3.48	2.20
Thimble (cold wall) flow channel)	2.74	3.33	2.12
Minimum DNBR for design transients			
Typical flow channel	>1.25[b] >1.22[b]	>1.23	>1.26
Thimble (cold wall)flow channel	>1.25[b] >1.21[b]	>1.22	>1.24
DNB correlation[c]	WRB-2M	WRB-2	WRB-1
Coolant conditions[d]			
Vessel minimum measured flow rate (MMF)			
10^6 lbm/hr	115.55	74.4	148.9
gpm	301,670	193,200	403,000
Vessel thermal design flow rate (TDF)			
10^6 lbm/hr	113.5	72.9	145.0
gpm	296,000	189,600	392,000
Effective flow rate for heat transfer[e]			
10^6 lbm/hr	106.8	66.3	132.7
gpm	278,500	172,500	358,700
Effective flow area for heat transfer (ft^2)	41.8	38.5	51.1
Average velocity along fuel rods (ft/s)[e]	15.8	10.6	16.6
Average mass velocity, 10^6 lbm/hr-ft^2[e]	2.55	1.72	2.60
Coolant temperature[d][e]			
Nominal inlet (°F)	535.0	532.8	561.2
Average rise in vessel (°F)	77.2	69.6	63.6
Average rise in core (°F)	81.4	75.8	68.7
Average in core (°F)	578.1	572.6	597.8
Average in vessel (°F)	573.6	567.6	593.0

Table 4.4-1 (Sheet 2 of 2)
Thermal and Hydraulic Comparison Table
(AP1000, AP600 and a Typical Westinghouse XL Plant)

Design Parameters	AP1000[a]	AP600	Typical XL Plant
Heat transfer			
Active heat transfer surface area (ft^2)[f]	56,700	44,884	69,700
Average heat flux (BTU/hr-ft^2)	199,300	143,000	181,200
Maximum heat flux for normal operation (BTU/hr-ft^2)[g]	518,200	372,226	498,200
Average linear power (kW/ft)[f][m]	5.72	4.11	5.20
Peak linear power for normal operation (kW/ft)[g,h]	14.9	10.7	14.0
Peak linear power resulting from overpower transients/operator errors, assuming a maximum overpower of 118% (kW/ft)[h]	≤22.45	22.5	≤22.45
Peak Linear power for prevention of center-line melt (kW/ft)[i]	22.5	22.5	22.45
Power density (kW/liter of core)[j]	109.7	78.82	98.8
Specific power (kW/kg uranium)[j]	40.2	28.89	36.6
Fuel central temperature			
Peak at peak linear power for prevention of centerline melt (°F)	4700	4,700	4700
Pressure drop[k]			
Across core (psi)	39.9 ± 4.0[l]	17.5 ± 1.7	38.8 ± 3.9
Across vessel, including nozzle (psi)	62.3 ± 6.2[l]	45.3 ± 4.5	59.7 ± 6.0

Notes:

(a) Robust Fuel Assembly.
(b) 1.25 applies to Core and Axial Offset limits; 1.22 and 1.21 apply to all other RTDP transients.
(c) WRB-2M is used for AP1000. WRB-2 or W-3 is used for AP1000 where WRB-2M is not applicable. See Subsection 4.4.2.2.1 for use of W-3, WRB-2 and WRB-2M correlations.
(d) Based on vessel average temperature equal to 573.6°F. Flow rates and temperatures based on 10 percent steam generator tube plugging.
(e) Based on thermal design flow and 5.9 percent bypass flow.
(f) Based on densified active fuel length. The value for AP1000 is rounded to 5.72 kW/ft.
(g) Based on 2.60 F_Q peaking factor.
(h) See Subsection 4.3.2.2.6.
(i) See Subsection 4.4.2.11.6.
(j) Based on cold dimensions and 95.5 percent of theoretical density fuel for AP1000; 95 percent for others.
(k) These are typical values based on best-estimate reactor flow rate as discussed in Section 5.1.
(l) Inlet temperature = 536.8°F.
(m) The value for AP1000 is rounded to 5.72 kW/ft.

Table 4.4-2
Void Fractions At Nominal Reactor Conditions
With Design Hot Channel Factors
(Based On VIPRE-01)

	Average	Maximum
Core, %	0.0	-
Hot Subchannel, %	0.1	0.9

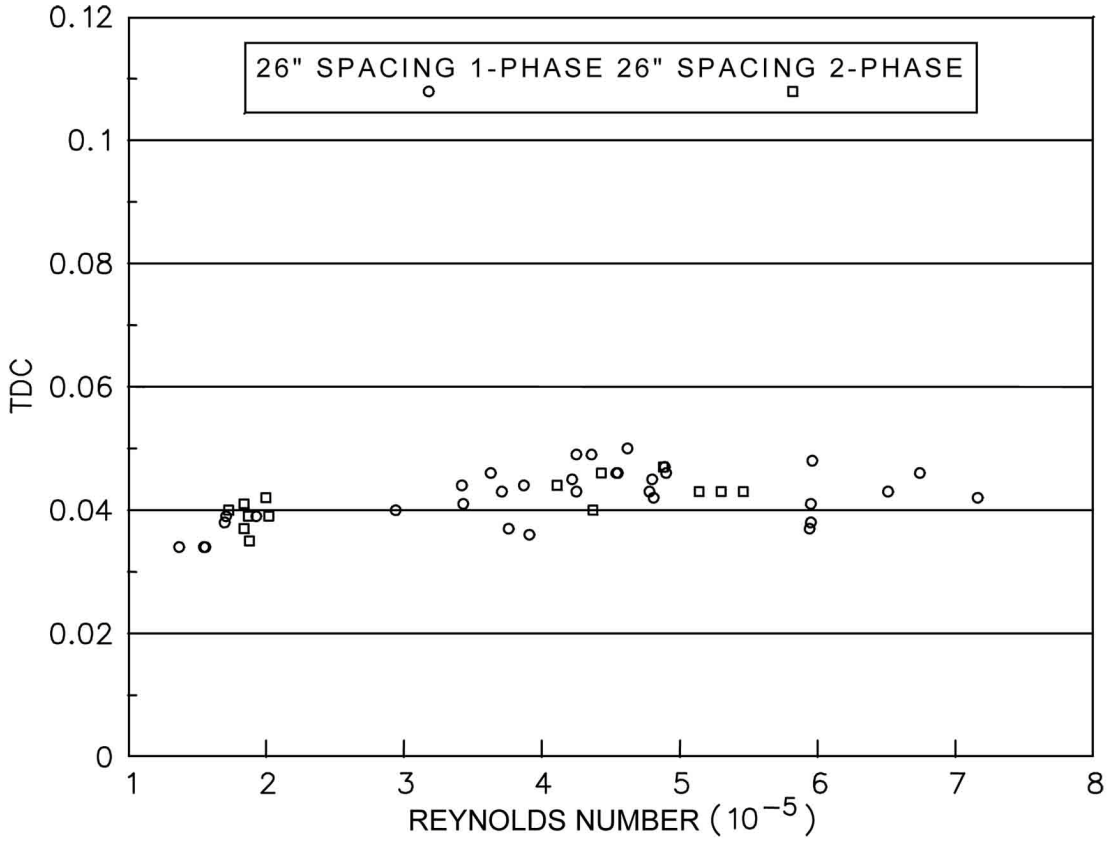

Figure 4.4-1
Thermal Diffusion Coefficient (TDC)
as a Function of Reynolds Number

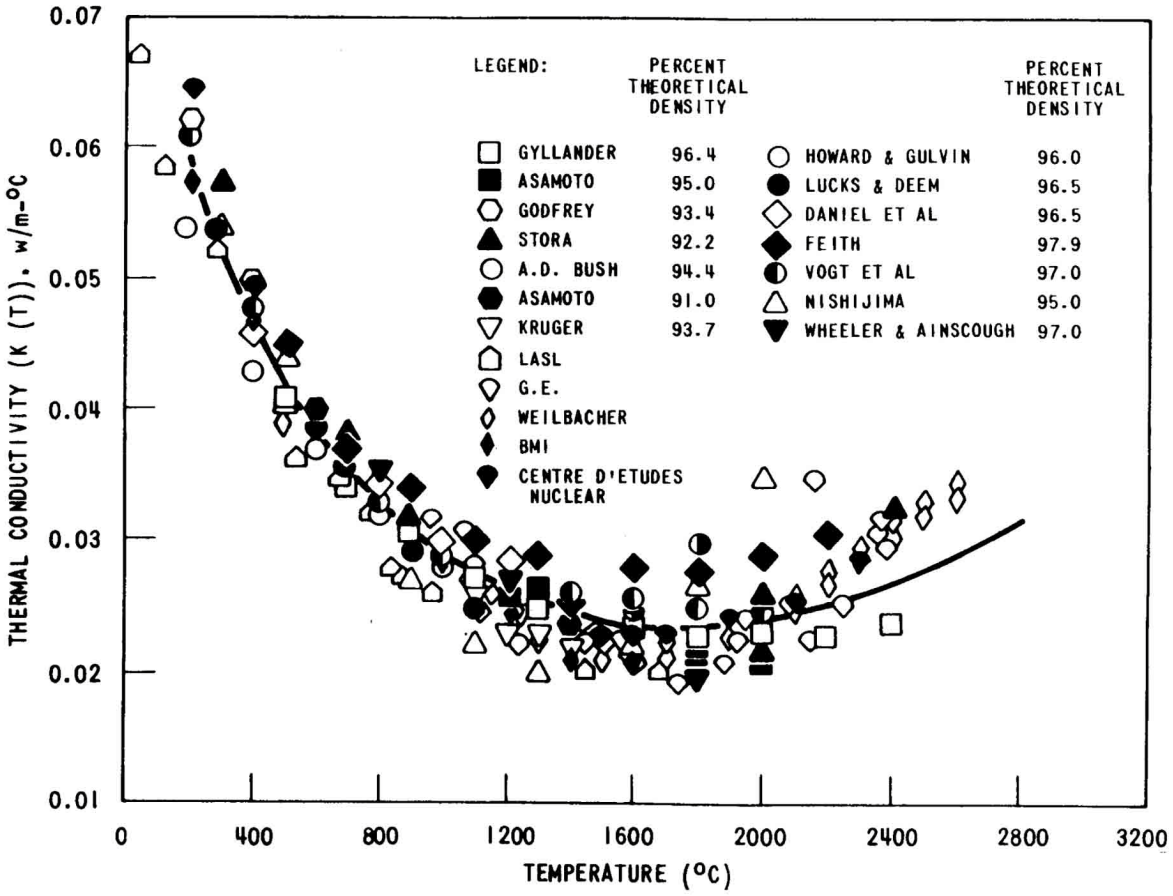

Figure 4.4-2
Thermal Conductivity of Uranium Dioxide
(Data Corrected to 95% Theoretical Density)

4.5 Reactor Materials

4.5.1 Control Rod and Drive System Structural Materials

4.5.1.1 Materials Specifications

The parts of the control rod drive mechanisms and control rod drive line exposed to reactor coolant are made of metals that resist the corrosive action of the coolant. Three types of metals are used exclusively: stainless steels, nickel-chromium-iron alloys, and, to a limited extent, cobalt-based alloys. These materials have provided many years of successful operation in similar control rod drive mechanisms. In the case of stainless steels, only austenitic and martensitic stainless steels are used. Where low or zero cobalt alloys are substituted for cobalt-based alloy pins, bars, or hard facing, the substitute material is qualified by evaluation or test.

Pressure-containing materials comply with the ASME Code, Section III. The material specifications for portions of the control rod drive mechanism that are reactor coolant pressure boundary are included in Table 5.2-1. These parts are fabricated from austenitic (Type 316, 316L, 316LN and Type 304, 304L, 304LN) stainless steel. Nickel-chromium-iron alloy (Alloy 690) is used for the reactor vessel head penetration. For pressure boundary parts, austenitic stainless steels are not used in the heat-treated conditions which can cause susceptibility to stress-corrosion cracking or accelerated corrosion in pressurized water reactor coolant chemistry and temperature environments. Pressure boundary parts and components made of stainless steel do not have specified minimum yield strength greater than 90,000 psi.

The material selection is based in part on the duty cycle specified for the control rod drive mechanisms and control rods. The materials are specified so that the components do not suffer adverse effects, such as excessive wear or galling, as a result of a minimum 300 trips from full power and 60 coupling and decoupling cycles of the drive rod coupling assembly. The material for the control rod drive mechanisms and the control rod assemblies are selected for acceptable performance. That is, the design goal is to achieve a service life of 9×10^6 full-step cycles. Inspection or changes in operation indicate the need for replacement or refurbishment. The worst case result of undetected wear of a control rod drive mechanism or drive rod is a rod assembly drop or a failure to drop an assembly during a trip. Both events are accounted for in safety analyses. The pressure boundary components are not subject to significant wear due to stepping cycles.

Internal latch assembly parts are fabricated of heat-treated martensitic and austenitic stainless steel. Heat treatment is such that stress-corrosion cracking is not initiated. Components and parts made of stainless steel do not have specified minimum yield strength greater than 90,000 psi. Magnetic pole pieces are immersed in the reactor coolant and are fabricated from Type 410 stainless steel. Nonmagnetic parts, except shims, pins, and springs, are fabricated from Type 304 stainless steel. A cobalt alloy or qualified substitute is used to fabricate the latch, link, and link pins. Springs and shims are made from nickel-chromium-iron alloy (Alloy X-750 and Alloy 625). Lock screws are fabricated of Type 316 stainless steel. Latch arm tips fabricated of stainless steel may be surfaced with a suitable hard facing material to provide improved resistance to wear. Hard chrome plate is used selectively for bearing and wear surfaces.

The drive rod assembly is also immersed in the reactor coolant and uses a Type 410 stainless steel drive rod. The drive rod coupling is machined from Type 403 or 410 stainless steel. The protective sleeve and disconnect button are also Type 410 stainless steel. The remaining parts are Type 304 or Type 304L stainless steel with the exception of the springs, button retainer, and locking button, which are fabricated of nickel-chromium-iron alloy.

The absorber rodlets in the rod control cluster assemblies and the gray rod cluster assemblies are closed stainless steel tubes (cladding) containing absorber material. The other rodlets in the gray rod

cluster assemblies are constructed of a material similar to the stainless steel cladding of the absorber rods. The stainless steel cladding isolates from the reactor coolant, the absorber material, and other substances inside the tubes. The containment function of the control rod cladding and the effects of neutron flux in the control rod materials are addressed in Section 4.2. The outside surface of the absorber and other rodlets is chromium plated to enhance resistance to wear due to the stepping motion and vibration of the rods. The rods included in one rod control cluster assembly or gray rod cluster assembly are attached at the top to a common hub which connects with the drive rod of the control rod drive mechanism. The hub is fabricated of type 316 stainless steel.

The coil housing is exposed to containment atmosphere and requires a magnetic material. Low carbon cast steel and ductile iron are qualified by tests or other evaluations for this application. The finished housings are electroless nickel plated to provide resistance against general corrosion.

Coils are wound on composite bobbins, with double glass-insulated copper wire. Coils are vacuum impregnated with silicone varnish. A wrapping of mica sheet is secured to the coil outside diameter. The result is a well-insulated coil capable of sustained operation at 392°F (200°C).

4.5.1.2 Fabrication and Processing of Austenitic Stainless Steel Components

The discussions provided in Subsection 5.2.3.4 concerning the processes, inspections, and tests on austenitic stainless steel components to prevent increased susceptibility to intergranular corrosion caused by sensitization are applicable to the austenitic stainless steel pressure-housing components of the control rod drive mechanism. The discussions provided in Subsection 5.2.3.4, concerning the control of welding of austenitic stainless steels especially control of delta ferrite are also applicable. Subsection 5.2.3.4 discusses the compliance with the guidelines of Regulatory Guides 1.31, 1.34, and 1.44. The welded control rod drive mechanism austenitic stainless steels that come into contact with the primary reactor coolant meet the guidance of Regulatory Guide 1.44.

4.5.1.3 Other Materials

For the cobalt alloy used to fabricate the latch, link, and link pins in latch assemblies, stress-corrosion cracking has not been observed in this application. Where hardfacing material is used in the latch assembly, a cobalt base alloy equivalent to Stellite-6 or qualified low or zero cobalt substitute is used. Low or zero cobalt alloys used for hardfacing or other applications where cobalt alloys have been previously used are qualified using wear and corrosion tests. The corrosion tests qualify the corrosion resistance of the alloy in reactor coolant. Low cobalt or cobalt free wear resistant alloys considered for this application include those developed and qualified in industry programs.

The springs in the control rod drive mechanism are made from nickel-chromium-iron alloy (Alloy 750), ordered to Aerospace Material Specification (AMS) 5698 or AMS 5699 with additional restrictions on prohibited materials. Operating experience has shown that springs made of this material are not subject to stress-corrosion cracking in pressurized water reactor primary water environments. Alloy 750 is not used for bolting applications in the control rod drive mechanisms.

4.5.1.4 Contamination Protection and Cleaning of Austenitic Stainless Steel

The control rod drive mechanisms are cleaned prior to delivery in accordance with the guidance provided in NQA-1 (see Chapter 17). Process specifications in packaging and shipment are discussed in Subsection 5.2.3. Westinghouse personnel conduct surveillance of these operations to verify that manufacturers and installers adhere to appropriate requirements as described in Subsection 5.2.3.

Tools used in abrasive work operations on austenitic stainless steel, such as grinding or wire brushing, do not contain and are not contaminated with ferritic carbon steel or other materials that could contribute to intergranular cracking or stress-corrosion cracking.

4.5.2 Reactor Internal and Core Support Materials

4.5.2.1 Materials Specifications

The major core support material for the reactor internals is SA-182, SA-336, SA-376, SA-479, or SA-240 Types 304, 304L, 304LN, or 304H stainless steels. Fabricators performing welding of any of these materials are required to qualify the welding procedures for maximum carbon content and heat input for each welding process in accordance with Regulatory Guide 1.44. For threaded structural fasteners the material used is strain hardened Type 316 stainless steel and for the clevis insert-to-vessel bolts either UNS N07718 or N07750. Remaining internals parts not fabricated from Types 304, 304L, 304LN, or 304H stainless steels typically include wear surfaces such as hardfacing on the radial keys, clevis inserts, alignment pins (Stellite™ 6 or 156 or low cobalt hardfaces); dowel pins (Type 316); hold down spring (Type 403 stainless steel (modified)); clevis inserts (UNS N06690); and irradiation specimen springs (UNS N07750).Instrument guide assembly materials that are not Types 304, 304L, 304LN, or 304H stainless steel are the guide bushings and guide stud tip (UNS S21800) and the instrument guide tube spring (UNS N07718). Core support structure and threaded structural fastener materials are specified in the ASME Code, Section III, Appendix I as supplemented by Code Cases N-60 and N-4. The qualification of cobalt free wear resistant alloys for use in reactor coolant is addressed in Subsection 4.5.1.3.

The use of cast austenitic stainless steel (CASS) is minimized in the AP1000 reactor internals. If used, CASS will be limited in carbon (low carbon grade: L grade) and ferrite contents and will be evaluated in terms of thermal aging effects.

The estimated peak neutron fluence for the AP1000 reactor internals has been considered in the design. Susceptibility to irradiation-assisted stress corrosion cracking or void swelling in reactor internals identified in the current pressurized water reactor fleet are being addressed in reactor internals material reliability programs. The selection of materials for the AP1000 reactor internals considers information developed by these programs. Ni-Cr-Fe Alloy 600 is not used in the AP1000 reactor internals.

4.5.2.2 Controls on Welding

The discussions provided in Subsection 5.2.3.4 are applicable to the welding of reactor internals and core support components.

4.5.2.3 Nondestructive Examination of Tubular Products and Fittings

The nondestructive examination of wrought seamless tubular products and fittings is in accordance with ASME Code, Section III, Article NG-2500. The acceptance standards are in accordance with the requirements of ASME Code, Section III, Article NG-5300.

4.5.2.4 Fabrication and Processing of Austenitic Stainless Steel Components

The discussions provided in Subsection 5.2.3.4 and Section 1.9 describes the conformance of reactor internals and core support structures with Regulatory Guides 1.31 and 1.44.

The discussion provided in Section 1.9 describes the conformance of reactor internals with Regulatory Guides 1.34 and 1.71.

4.5.2.5 Contamination Protection and Cleaning of Austenitic Stainless Steel

The discussions provided in Subsection 5.2.3 and Section 1.9 are applicable to the reactor internals and core support structures describe the conformance of the process specifications with Regulatory Guide 1.37. The process specifications follow the guidance of NQA-1 (Reference 1).

4.5.3 Combined License Information

This section contained no requirement for additional information.

4.6 Functional Design of Reactivity Control Systems

4.6.1 Information for Control Rod Drive System

The control rod drive mechanism (CRDM) and operation of the control rod drive system are described in Subsection 3.9.4. Figure 3.9.4 provides the details of the control rod drive mechanisms. Figure 4.2-8 provides the configuration of the driveline, including the control rod drive mechanism. No hydraulic system is associated with the functioning of the control rod drive system. The instrumentation and controls for the reactor trip system are described in Section 7.2. The reactor control system is described in Section 7.7.

The control rod drive mechanisms are contained within an integrated head package located on top of the reactor vessel head as described in Subsection 3.9.7. This assembly provides the support required for seismic restraint in conjunction with the attachment of the control rod drive mechanisms to the reactor vessel head. An outer shroud and the seismic restraint structure isolate the control rod drive mechanisms from the effects of ruptures of high-energy lines outside the shroud, and from missiles. The shroud also is used to direct air from the cooling fans past the control rod drive mechanisms. The cooling system maintains the temperatures of the coils in the control rod drive mechanisms below the design operating temperature. The integrated head package provides the proper support and required separation for electrical lines providing power to the control rod drive mechanisms and signals from the rod position sensors.

The line for the reactor head vent system is located among the control rod drive mechanisms and is supported by the integrated head package. This line is pressurized to reactor coolant system pressure and considered to be a high-energy line. This line is constructed to the appropriate requirements of the ASME Code. Figure 3.9-7 shows elements of the integrated head package surrounding the control rod drive mechanisms.

4.6.2 Evaluations of the Control Rod Drive System

Rod control systems of the type used in the AP1000 have been analyzed in detailed reliability studies. These studies include fault tree analysis and failure mode and effects analyses. These studies, and the analyses presented in Chapter 15, demonstrate that the control rod drive system performs its intended safety-related function – a reactor trip. The control rod drive system puts the reactor in a subcritical condition when a safety-related system setting is reached with an assumed credible failure of a single active component.

The essential elements of the control rod drive system (those required to provide reactor trip) are isolated from nonessential portions of the rod control system by the reactor trip switchgear, as described in Section 7.2. The essential portion of the control rod drive system is shielded from the direct effects of postulated moderate- and high-energy line breaks by the integrated head package. The dynamic effects of pipe ruptures do not have to be considered for those pipes that satisfy the requirements for mechanistic pipe break, as outlined in Subsection 3.6.3.

The reactor vessel head vent lines and instrumentation conduits are one inch nominal diameter or smaller. Breaks in lines of this size do not have to be postulated for dynamic effects, pressurization, and spray wetting. The pressure boundary housing of the control rod drive mechanisms is constructed to the requirements of the ASME Code and a break in this pressure boundary is not credible.

The only instrumentation required of the control rod drive mechanism and supporting systems to operate safely is the rod position indicator. A break in the cables connected to the rod position indicators would neither preclude a reactor trip, nor would it result in an unplanned withdrawal of a rod assembly. A break in the power cable to the control rod drive mechanism coils results in a drop of

the rod assembly. Information on the pressure and temperature of the control rod drive mechanisms and surrounding areas is not required for safe operation. The design pressure and temperature of the control rod drive mechanism housing is the same as the reactor coolant system, which is protected by safety valves. Overheating of the control rod drive mechanism coils due to a failure of the cooling system would in the worst case result in a drop of one or more rod assemblies. The reactor and reactor protection system is designed to accommodate and protect against rod drop events. Additional information is provided in Subsection 3.9.1, and Sections 7.2, and 15.4.

4.6.3 Testing and Verification of the Control Rod Drive System

The control rod drive system is extensively tested prior to its operation. These tests may be subdivided into five categories:

- Prototype tests of components
- Prototype control rod drive system tests
- Production tests of components following manufacture and prior to installation
- Onsite pre-operational and initial startup tests
- Periodic in-service tests

These tests, which are described in Subsection 3.9.4.4 and Sections 4.2 and 14.2, are conducted to verify the operability of the control rod drive system when called upon to function.

4.6.4 Information for Combined Performance of Reactivity Systems

As indicated in Chapter 15, there are only three postulated events that assume credit for reactivity control systems, other than a reactor trip to render the plant subcritical. These events are the steam-line break, feedwater line break, and small break loss of coolant accident. The reactivity control systems in these accidents are the reactor trip system and the passive core cooling system (PXS). Additional information on the control rod drive system is presented in Subsection 3.9.4. The passive core cooling system is discussed further in Section 6.3.

No credit is taken for the boration capabilities of the chemical and volume control system (CVS) as a system in the analysis of transients presented in Chapter 15. Information on the capabilities of the chemical and volume control system is provided in Subsection 9.3.6. The adverse boron dilution possibilities due to the operation of the chemical and volume control system are investigated in Subsection 15.4.6. Prior proper operation of the chemical and volume control system has been presumed as an initial condition to evaluate transients. Appropriate technical specifications promote the correct operation or remedial action.

The AP1000 instrumentation and control system includes a diverse actuation system (DAS). This system provides for automatic control rod insertion, turbine trip, passive residual heat removal heat exchanger start, core makeup tank start, isolation of critical containment penetrations, and start of the passive containment cooling system as appropriate upon conditions indicative of an anticipated transient without scram or other failure of the plant control and reactor protection system. This system is diverse and independent from the reactor trip system from the sensor through actuation devices.

In addition to the above, the AP1000 plant systems provide for operator response to an anticipated transient without scram (ATWS) event that includes core reactivity control followed by core decay heat removal. Core reactivity control is provided by a manual trip of the control rods, insertion of the

control rods, the chemical and volume control system, or by the core makeup tank injection. The decay heat removal can be performed by the startup feedwater system or the passive residual heat removal system.

4.6.5 Evaluation of Combined Performance

The evaluations of the steam-line break, the feedwater line break, and the small break loss of coolant accident, which presume the combined actuation of the reactor trip system and the control rod drive system and the passive safety injection, are presented in Subsections 15.1.5 and 15.2.8 and Section 15.6. Reactor trip signals and signals to actuate passive safety features for these events are generated from functionally diverse sensors. These signals actuate diverse means of reactivity control; that is, control rod insertion and injection of soluble neutron absorber.

Non-diverse but redundant types of equipment are used only in the processing of the incoming sensor signals into appropriate logic which initiates the protective action. This equipment is described in Sections 7.2 and 7.3. In particular, protection from equipment failures is provided by redundant equipment and periodic testing. Effects of failures of this equipment have been extensively investigated. Reliability studies, including failure mode and effects analysis for this type of equipment verify that a single failure does not have an adverse effect upon the engineered safety features actuation system. Adequacy of the passive core cooling system performance under faulted conditions is verified in Section 6.3.

In addition to the automatic actuations provided for by the diverse actuation system, that system also provides for manual actuation of the reactor trip.

The probability of a common mode failure impairing the ability of the reactor trip system to perform its safety-related function is extremely low. However, analyses are performed to demonstrate compliance with the requirements of 10 CFR 50.62. These analyses demonstrate that safety criteria would not be exceeded even if the control rod drive system were rendered incapable of functioning during anticipated transients for which its function would normally be expected. The evaluation demonstrates that borated water from the core makeup tank shuts down the reactor with no rods required, and the passive residual heat removal system provides sufficient core heat removal.

4.6.6 Combined License Information

This section contained no requirement for additional information.